Ryerson University
Digital Commons @ Ryerson

Theses and dissertations

1-1-2013

Theoretical and Experimental Study of Single-Needle Thermal Conductivity Probe

Lam Dang
Ryerson University

Follow this and additional works at: http://digitalcommons.ryerson.ca/dissertations

Part of the [Applied Mechanics Commons](http://network.bepress.com/hgg/discipline/295?utm_source=digitalcommons.ryerson.ca%2Fdissertations%2F2064&utm_medium=PDF&utm_campaign=PDFCoverPages)

Recommended Citation

Dang, Lam, "Theoretical and Experimental Study of Single-Needle Thermal Conductivity Probe" (2013). *Theses and dissertations.* Paper 2064.

This Thesis is brought to you for free and open access by Digital Commons @ Ryerson. It has been accepted for inclusion in Theses and dissertations by an authorized administrator of Digital Commons @ Ryerson. For more information, please contact bcameron@ryerson.ca.

THEORETICAL AND EXPERIMENTAL STUDY OF SINGLE-NEEDLE THERMAL CONDUCTIVITY PROBE

By

Lam Dang

Hon. B.Eng., Ryerson University, 2013

A thesis presented to Ryerson University in partial fulfilment of

the requirements for the degree of

Master of Applied Science (MASc)

in the program of

Mechanical Engineering

Toronto, Ontario, Canada, 2013

© Lam Dang 2013

AUTHOR'S DECLARATION

I hereby declare that I am the sole author of this thesis.

I authorize Ryerson University to lend this thesis to other institutions or individuals for the purpose of scholarly research.

I further authorize Ryerson University to reproduce this thesis by photocopying or by other means, in total or in part, at the request of other institutions or individuals for the purpose of scholarly research.

ABSTRACT

The thermal conductivities of materials (k_m) are important in many fields such as agriculture, mining and biomedical engineering. For example, better knowing the k_m values of biomaterials can be useful in radiofrequency ablation (RFA) to treat and/or cure tumor and cancer cells (Liu *et al.* [3]). Thermal conductivity probes (TCPs) have proven to be very attractive in obtaining relatively accurate k_m values due to their inline measurements, inexpensiveness, portability, and versatility.

However, due to the vast number of designs and applications of TCPs, sources of errors with using the probes are diverse. As a result, in this thesis, possible sources of errors in TCPs (single needle) were investigated. The sources include probe sizes, heating powers, sampling media, selection of TCP materials, location of the thermocouple, axial heat conduction, thermal contact resistance, initiating time t_0, decision to use heating or cooling period for k_m calculations and tolerance in the thermal properties of epoxy.

ACKNOWNLEDGEMENTS

I would like to express my special thanks to my supervisor Dr. Wey Leong who has been extremely patient and resourceful in guiding me through this thesis. I am also pleased to express my sincere appreciations to Dr. Vlodek Tarnawski and research staff at Saint Mary's University in Halifax, Nova Scotia, Canada for providing me the necessary experimental TCP data to complete a main part of this thesis.

The Natural Science and Engineering Research Council of Canada (NSERC) is greatly remembered for providing financial supports in this thesis.

Lastly, I would like to gratefully thank my family members who have been so closely and patiently supporting me during my years of post-secondary education.

TABLE OF CONTENTS

LIST OF TABLES

LIST OF FIGURES

NOMENCLATURE AND ABBREVIATIONS

c_p: specific heat capacity ($J/kg{\cdot}K$)

H: thermal conductance ($W/m^2{\cdot}K$)

I: electrical current (A)

k: thermal conductivity ($W/m{\cdot}K$)

L: TCP length (m)

LHW: length of heating wire (m)

q: heat flux (W/m^2)

$\dot{q}$: heating power per unit probe length (W/m)

r: radial location (m)

R: thermal resistance ($m^2{\cdot}K/W$)

R_{pr}: resistance of precision resistor (Ω)

Shunt_R: resistance of shunt resistor (Ω)

Sr: saturation ratio $= \frac{\forall_{water}}{\forall_{pores}} = \frac{\theta_{water}}{\phi}$

t: time (s)

$T(r,t_i)$: temperature at location r and time t_i (°C)

V: voltage across an element (V)

<u>Greek letters:</u>

α: thermal diffusivity (m^2/s)

Δ: difference between two points/parameters

$\Delta T(r,t)$: temperature rise/drop at location r after time t (°C)

γ: Euler constant = 0.577215665

ϕ: porosity of soil (m^3/m^3) $= \dfrac{\forall_{pores}}{\forall_{total}}$

π: pi = 3.141592654

ρ: density (kg/m^3)

θ_i: volumetric ratio of the i^{th} component = $\dfrac{\forall_i}{\forall_{total}}$

Subscripts:

c: contact or cooling

C109: Graded Ottawa sand

e: pertaining to epoxy

i: the i^{th} value

m: pertaining to medium being measured

p: pertaining to probe

PC: perfect contact

s: pertaining to steel

sen: pertaining to sensor

SR: pertaining to shunt resistor

TCR: thermal contact resistance

w: pertaining to heating wire

Mathematical functions:

exp(x): exponential function of *x*

$Ei(x)$: exponential integral function of x, $Ei(-x) = -\int_x^{\infty} \frac{e^{-t}dt}{t}$ for $x > 0$

$erf(x)$: error function of x

$J_0(x)$: Bessel function of x of the first kind, zeroth order

$I_0(x)$: Bessel function of x of the second kind, zeroth order

$J_1(x)$: Bessel function of x of the first kind, first order

$I_1(x)$: Bessel function of x of the second kind, first order

$ln(x)$: natural logarithmic function of x

W_0: zeroth order Neumann function

W_1: first order Neumann function

Abbreviations:

COMSOL: from COMSOL Multiphysics ® software

DAQ: data acquisition

DR: diameter ratio of TCP = r_e/r_s

FEHT: Finite Element Heat Transfer software by F-Chart

FS: Fully Saturated or Saturated (for C109 sand conditions)

GHPA: Guarded Hot Plate Apparatus

GSHP: Ground Source Heat Pump

PS: Partially Saturated or Unsaturated (for C109 sand conditions)

RFA: Radiofrequency Ablation

TCP: Thermal Conductivity Probe

TCR: Thermal Contact Resistance

TRR: Thermal Resistance Ratio

DIMENSIONLESS PARAMETERS

Thermal rates (Fourier number): $Fo = \frac{\alpha_m t}{r_s^2}$

Thermal resistance ratio (TRR): $\frac{R_c \cdot k_m}{r}$ or $\frac{\text{thermal contact resistance}}{\text{thermal conduction ressitance}}$

CHAPTER 1 - INTRODUCTION

1.1 - Background

According to Canadian Cancer Society [1], about 2 in 5 Canadians will develop cancer during their lifetime and about 1 in 4 Canadians will die of cancer. Also, 29.8% of the total deaths in Canada in 2009 was because of cancer. And radiofrequency ablation (RFA) is one method that can be used to treat certain types of cancers in the liver, bone, kidney, lung and other locations (Mayo Clinic [2]). In addition, Liu *et al.* [3] found that the thermal conductivity of biological tissues was important in understanding the performance of RFA on hepatic tumors.

Furthermore, energy loss due to underground transmission lines can be severe. The losses can result from the thermal conductivity of the ground where the transmission lines are buried. When electricity passes through the lines, heat is generated. If the thermal conductivity of the surrounding ground is too low to dissipate the heat, the insulating layers of the cables will be damaged and water from the surrounding ground can penetrate through the insulating layers of the cables. As indicated by Aras *et al*. [4], water getting into the cables is the major factor that damages the transmission lines in the long run. Therefore, there are shorter lifespans for the transmission lines, it is more costly to maintain for the owner, and electricity is more expensive for the normal and frequent electricity consumers.

Moreover, the thermal conductivity of the ground is important in designing the ground source heat pump (GSHP) systems. According to Lee *et al.* [5], GHSP systems can save 44% of energy consumption and corresponding greenhouse gas emissions from the air-source heat pumps and 72% of those from the electric resistance heating with standard air-conditioning equipment. And the more accurately the thermal conductivity of the surrounding ground can be estimated, the better the GHSP system can be designed.

Therefore, in order to obtain thermal conductivity of a material, there are many techniques to apply. Two of the most commonly used techniques are the guarded hot plate apparatus and needle probes as discussed below.

1.2 - Measuring techniques

1.2.1 - Guarded Hot Plate Apparatus (GHPA)

In 1910, the American Society of Refrigerating Engineers (currently known as American Society of Heating, Refrigerating, and Air-conditioning Engineers or ASHRAE) needed to understand more about heat transmission in insulation for designing purposes, so the quest to have a reliable method to measure thermal properties of insulating materials became popular. As a result, in 1910, Hobart Cutler Dickinson from the National Institute of Standards and Technology (NIST) of the U.S. Department of Commerce came up with the first GHPA for that purpose. Prior to the development of the GHPA, scientists and engineers used panels of insulation and passed warm air on one side and hot air on the other side of the panels, which exhibited many inconsistencies and errors. With the newly developed GHPA, Dickinson and Van Dusen in 1916 published the first important paper in the heat transmission field; the paper showed more accurate calculations of heat flow through air spaces and through 30 insulating materials [6]. In 1929, Van Dusen made the final version of the GHPA. In 1945, ASHRAE formally applied the GHPA as a standard testing technique. From the development of GHPA, data on thermal conductivities of insulating and building materials have significantly been more accurate in technical journals and handbooks, resulting in much better designs and reductions of operating costs of buildings and houses. Under the operating temperature range to which typical building insulation is exposed, inter-laboratory comparisons (which are measured from GHPA) agree to within ±3% of the values of thermal conductivity and thermal resistance of the insulating materials [7].

A GHPA is a measuring instrument that applies steady state conditions to obtain materials' thermal properties such as thermal conductivity and thermal resistance. This measuring method is known to be most accurate among other methods when very low thermal conductivity is to be measured [8]. There are many designs for a GHPA with different standards. One design of GHPA is shown in Fig. 1.1 below.

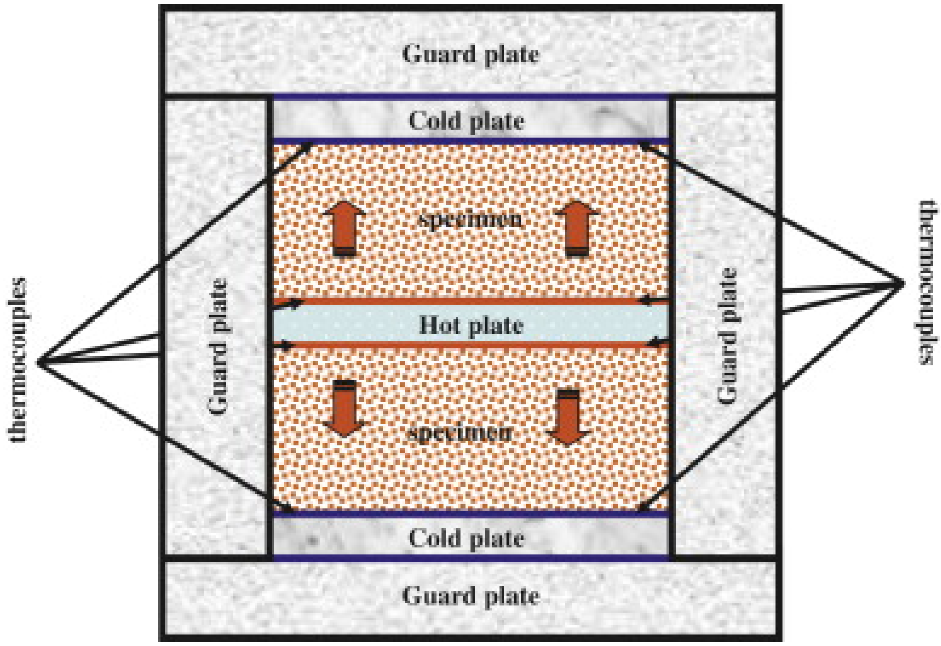

Figure 1.1. A GHPA design. (Adopted from [9])

In Fig. 1.1, the design follows the standards of ISO 8990:1994, EN 12939:2000, and EN 12664:2001. The specimens are covered by hot, cold, and guard plates. The hot plate in the middle of the figure is a flat plate that is heated by external electrical wires and heat source. Specimens to be measured and experimented are placed next to the hot plate. Two flat plates (cold plates) that are not heated are put adjacent to the specimens. Four more flat plates are used to completely cover the specimens and are made of insulating materials to provide adiabatic conditions for the GPHA during the experiment.

Thermocouples are placed on top of the hot and cold plates' surfaces that contact the specimens. Heat flows from hot to cold places. Under the conditions shown in Fig. 1.1, one dimensional heat flow is achieved. With known heat input Q (from the external energy source through the electrical wires), the exact thickness Δx and surface area A_s of the specimen, temperature change ΔT across the specimen (measured from the thermocouples), the thermal conductivity k_m of the specimen can be obtained from the following relationship from Fourier's law (p. 18 of Cengel [10]) for bi-directional heat conduction:

$$\frac{Q}{2A_s} = -k_m \frac{\Delta T}{\Delta x} \tag{1.1}$$

Fig. 1.2 shows another GHPA design. Similar to the design shown in Fig. 1.1, the specimen is positioned between the hot and cold plates while the insulating guard plates provide adiabatic conditions during the experiment. Thermocouples are placed on the surfaces where the hot and cold plates contact the specimen. However, instead of bi-directional heat flow as in Fig. 1.1, the design in Fig. 1.2 makes one directional heat flow. This design is not well-balanced because the heat at the interface between the guard plate and the hot plate can accumulate after the experiment has been run for a long time.

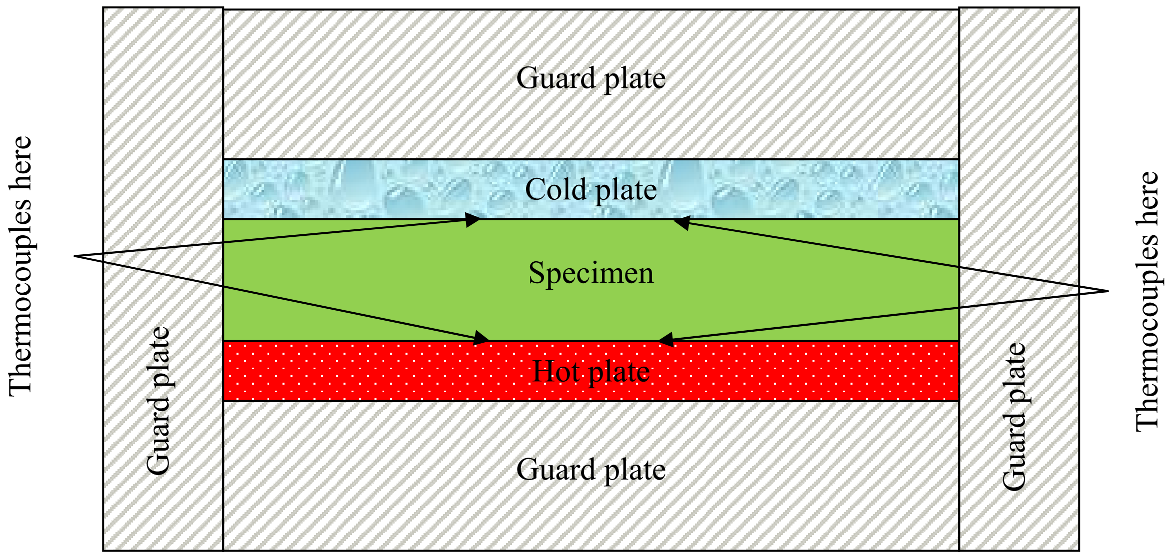

Figure 1.2. Another GHPA design.

With known heat input ΔQ (from the external energy source through the electrical wires), exact thickness Δx and surface area A_s of the specimen, temperature change ΔT across the specimen (measured from the thermocouples), the thermal conductivity k_m of the specimen can be obtained from the following relationship from Fourier's law (p. 18 of Cengel [10]):

$$\frac{\Delta Q}{A_s} = -k_m \frac{\Delta T}{\Delta x} \tag{1.2}$$

However, as indicated by Tarnawski *et al*. [11], the GHPA experiment is very time-consuming (to reach steady-state conditions) and requires a higher temperature difference between the surfaces of the hot and cold plates. In addition, the GHPA cannot be used on the field where soil samples are about to be measured *in-situ* because of its relatively long size.

1.2.2 - Thermal Conductivity Probe (TCP)

Thermal conductivity probes, derived from an idealized transient heat transfer model as shown in Appendix A, are also called needle probes, resulting from the probes' sizes being relatively negligible compared to the size of the material the probes are used to measure. This transient method, as stated by Nagasaka *et al*. [12] and Xie *et al*. [13], can experimentally eliminate convective error of the fluid flowing around the probe and the data obtained can be more reliable than those from the GHPA using steady-state conditions.

The TCP for measuring the thermal conductivity of materials was originated by Stalhane and Pyk in 1931 [14]. This method was further used by Van der Held and Van Drunen to obtain the thermal conductivities of many liquids. Generally, this method (as schematically shown in Fig. 1.3) contains a very small heating wire which is heated by passing electricity through it and acts as the central heating source. The heat from the wire is assumed to dissipate radially and is then sensed by thermocouples.

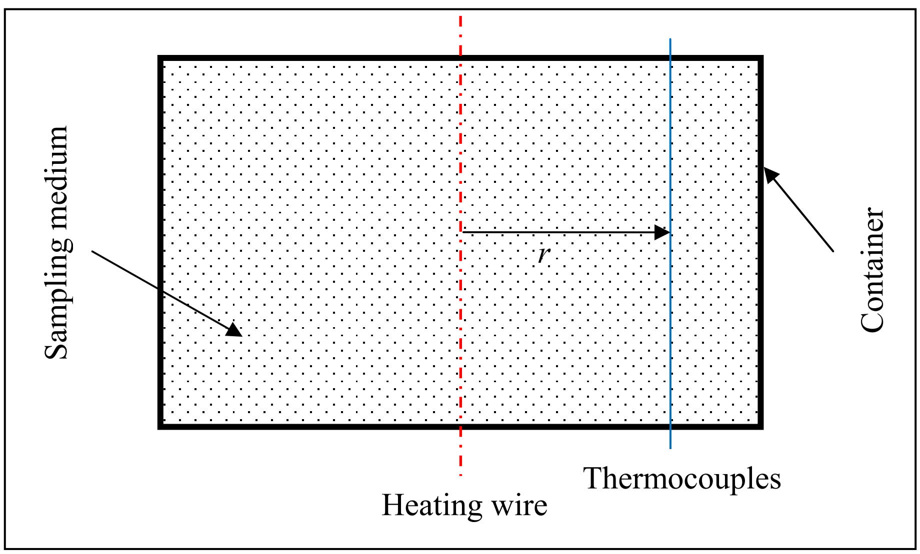

Figure 1.3. Schematic drawing of a TCP experiment.

Although the idea of the TCP appeared in 1931, the first relatively small probe (made of aluminum with dimensions of Ø3/16" × 19") started in 1953 by Hooper and Chang [15] with reproducibility within ±0.5%. After that, in 1959, Carslaw and Jaeger [16] developed a classical mathematical solution to obtain the thermal conductivity of the sample being measured as follows:

$$T(r,t) = \frac{-\dot{q}_w}{4\pi k_m} Ei\left(\frac{-r^2}{4\alpha_m t}\right) + T_i \tag{1.3a}$$

or

$$T(r,t) \approx \frac{\dot{q}_w}{4\pi k_m}\left[\ln\left(\frac{4\alpha_m t}{r^2}\right) - \gamma\right] + T_i \qquad \text{for } \frac{4\alpha_m t}{r^2} >> 1 \tag{1.3b}$$

For a chosen temperature *T(r,t)* at time t_0, the thermal conductivity of the sampling medium can be calculated from:

$$k_m = \frac{\dot{q}_w}{4\pi}\frac{1}{slope} \qquad \text{for } \frac{4\alpha_m t}{r_{sen}^2} >> 1 \text{ and } t \geq t_0 \tag{1.4}$$

where *slope* is the slope of linear portion that is typically as shown in Fig. 1.4.

Typically, the experimental results obtained from a TCP can be shown as in Fig. 1.4 where $\Delta T = T(r,t) - T(r,t_0)$ and $\ln(t/t_0)$, which are from readings of the thermocouple, make a relatively straight line. From the slope of the line, k_m can be calculated.

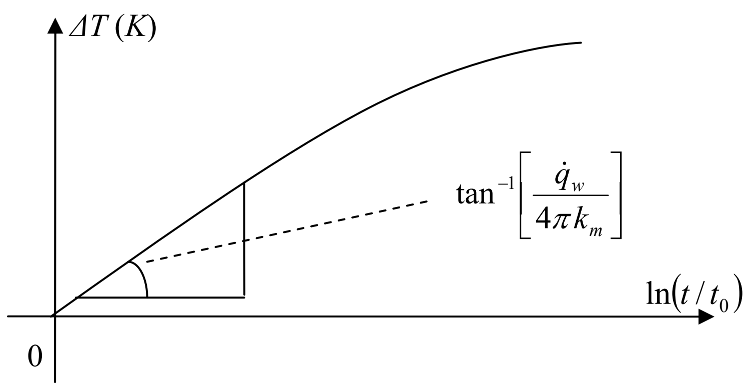

Figure 1.4. Typical graph (from TCP measurement) of temperature difference vs. natural logarithmic time ratio for line heat source theory.

Since the appearance of Eq. 1.3, many researchers have continued to further develop the concept of TCP to many different TCP designs.

1.2.2.1 -Single-Needle Probe

One design of the TCP by De Vries and Peck [17] is shown in Fig 1.5. A heating wire is covered by capillary glass. The glass is embedded in a paraffin wax. One side of the wax contains the constantan wire and copper wire. The wax is embedded in a Monel gauge. At one end of the gauge lie an insulating cover and a plastic socket to hold the gauge.

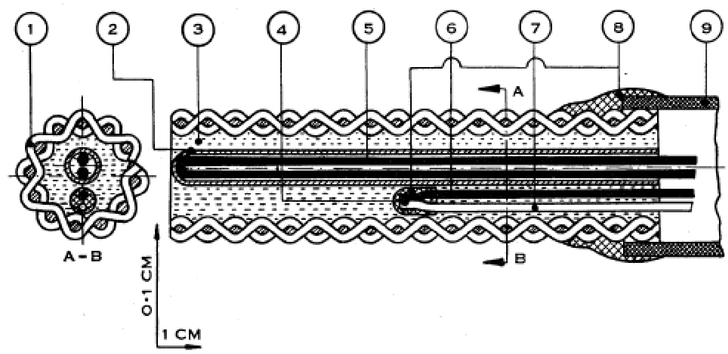

Figure 1.5. Radial and longitudinal cross sections of a TCP. 1, Monel gauze (filled with paraffin wax); 2, glass capillary; 3, paraffin wax; 4, thermojunction; 5, heating wire; 6, constantan wire; 7, copper wire; 8, insulating cover; 9, plastic socket. (Adopted from [17]*)*

Another TCP design is shown in Fig. 1.6. Eletrical heating coils are used. The coils surround a rod made by silicon and rubber. The coils are then sealed as shown in Fig 1.6. A thermistor temperature sensor is inserted in the middle of the silicon rubber rod. The rod is about 20 *cm* long.

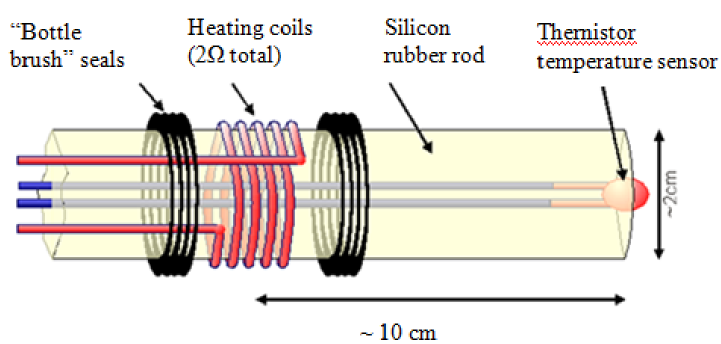

Figure 1.6. Another TCP design. [18]

In Fig. 1.7, a line heat source made of a heating wire is embedded in epoxy and steel. The heating wire has various heating powers and is about 5 *cm* long. The thermocouples are inserted in the epoxy layer.

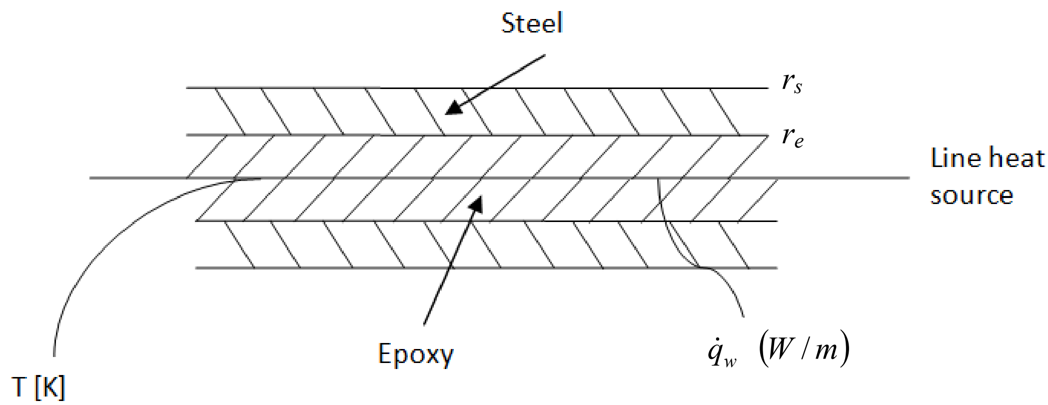

Figure 1.7. TCP used in this thesis.

1.2.2.2 - Multi-Needle Probe

A multi-needle probe is the probe mentioned in Section 1.2.1 but has more than one needle altogether as shown in Fig. 1.8 as an example. According to Bristow *et al*. [19], this type of TCP employs heat-pulse technology to obtain the thermal properties and water content. as well as the electrical conductivity of the sampling porous medium.

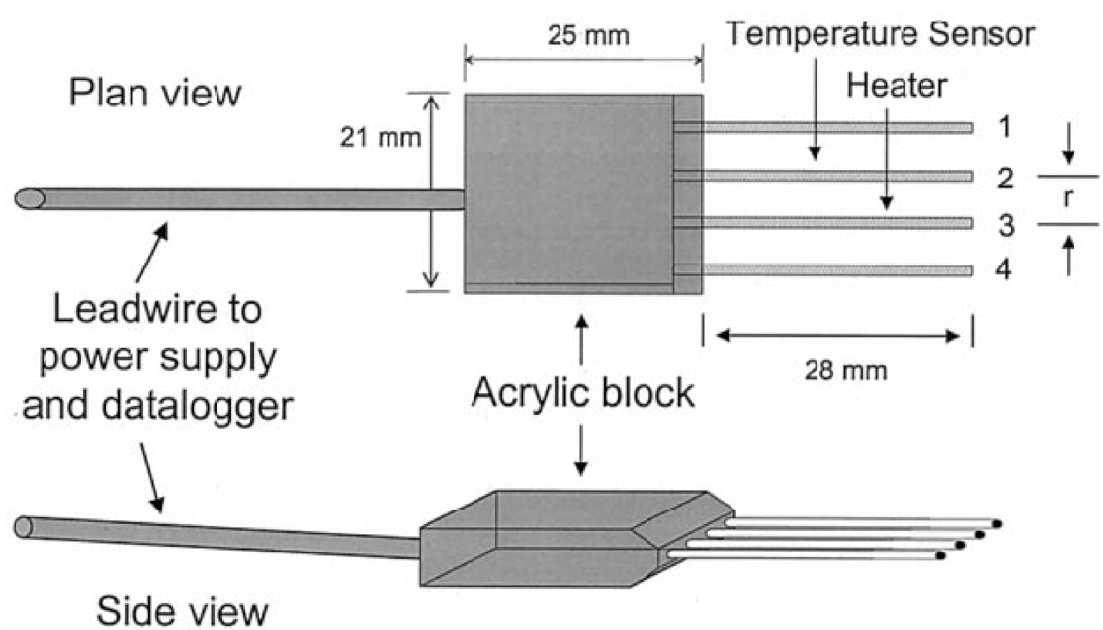

Figure 1.8. A multi-needle TCP design.(Adopted from [19]*)*

In Fig. 1.8, there are four needles in the TCP. Two needles are used for measuring the medium's thermal properties and water content while the other needles are for measurements of the electrical conductivity of the sampling porous medium. The sampling porous medium's thermal conductivity, thermal diffusivity, and heat capacity are obtained as in the case of single-needle probes. The water content of the sampling porous medium can be calculated from Eq. 1.5, assuming that the thermal properties and amount of the other constituents of the porous medium are known.

$$(\rho c_p)_m = (\rho c_p)_{air}\theta_{air} + (\rho c_p)_{water}\theta_{water} + (\rho c_p)_{minerals}\theta_{minerals} + ... \tag{1.5}$$

The TCP construction in Fig. 1.8 provides an equivalent 4-electrode Wenner array as shown Fig. 1.9. The bulk electrical conductivity of the sampling porous medium is can also be obtained [19].

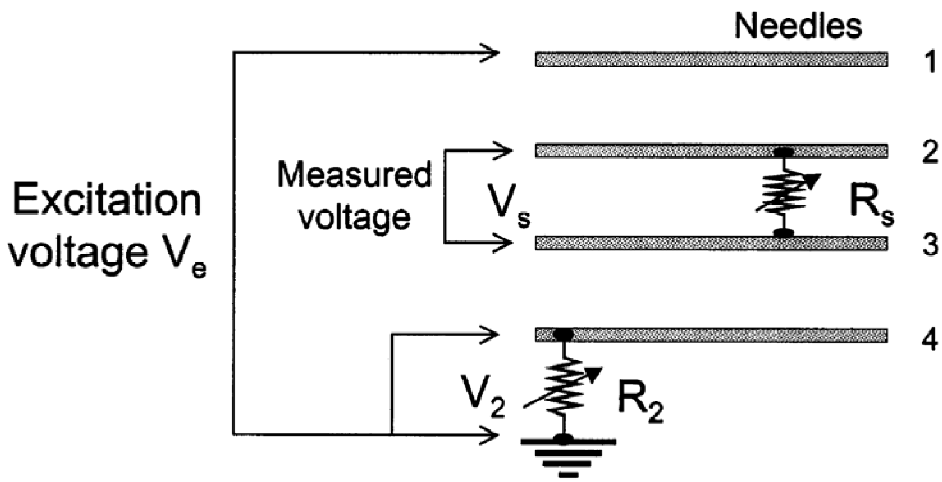

Figure 1.9. Schematic outline of Wenner array of TCP design in Fig. 1.8. [19]

Being cheaper and more portable than GHPA and able to measure granular/liquid materials *in-situ*, TCPs are selected. And the single-needle TCP shown in Fig. 1.7 is focused because it is cheaper to manufacture and more convenient to use and carry. Also mathematical models can be made to compare with the experimental data from Dr. Tarnawski and research staff in St. Mary's University in Halifax, Canada.

1.3 Objectives

The objectives of this research are:

1. To develop two new and improved equations to enhance the accuracy of Eq. 1.3a.
2. To theoretically study many possible sources of errors when a single-needle probe is used, such as probe sizes, the heating power, the TCP materials, the location of the thermocouple pair inside the TCP, and the sampling medium being measured.
3. To experimentally explore how t_0 can affect the calculated thermal conductivities and whether the heating or cooling period of TCP produces more accurate thermal conductivity values of the sampling media. Also, a method is developed to estimate the thermal contact resistance (TCR) between the TCP and the sampling medium.

Eq. 1.3 (or the classical solution by Carslaw and Jaeger [16]) has been reported as erroneous by many researchers. This thesis aims to improve the solution by removing many of the assumptions and simplifications that are used to derive Eq. 1.3.

There are many possible situations or designs that one can come up with for TCP measurements. First of all, the TCP can be made of many possible sizes as desired. Secondly, any material can be used to manufacture TCPs. Thirdly, the location of the thermocouple to sense the temperature rise of the probe can be put anywhere as wanted. Last but not least, any material (soft, granular, or liquid) can be taken to measure its thermal conductivity. All of the situations mentioned can have errors that the measurer may or may not be aware of. Due to the time, effort, and funding constraints of this research, the situations can only be studied theoretically and numerically to analyze possible errors that lie within each situation. As a result, this thesis explores possibilities that can improve the accuracy of TCPs using numerical analysis.

Traditionally, researchers have been applying Eq. 1.3 heavily by randomly picking a value of t_0 for their thermal conductivity calculations. The random selection of t_0 can cause errors without the knowledge of the researcher(s). In addition, researchers have had controversies over which period (heating or cooling of TCP) should be used to obtain more accurate k_m. This research will work on and help clarify the controversies. Moreover, the thermal contact resistance (TCR) has not been popularly studied yet. The literature has a limited amount of works on the TCR, so this research will add to literature more insights into the TCR.

1.4 - Thesis Outline

Chapter 2 provides insights to the possible errors that researchers have discovered. The errors include the assumption of isotropic materials, the neglect of the size and construction of the TCP, the lack of knowledge about bulk flow, radiation effect, and thermal contact resistance, and the approximation from Eq. 1.3a to Eq. 1.3b.

Chapter 3 shows the necessary equations that are used for possible errors mentioned in Section 1.3. The equations are the classical solution using line heat source theory, the inclusion of TCP materials but with perfect contact between TCP and sampling medium, and the equation that considers the TCP materials and the contact resistance layer. The first main important equation is the classical solution while the other two main equations are developed to improve the accuracy of the classical solution. As there are many equations in this research, the three main equations are grouped at the end of chapter 3 so that they can be referred to in subsequent chapters.

Chapter 4 contains numerical comparisons between the classical solution and the perfect contact equation with finite element heat transfer software packages such as FEHT and COMSOL. Simulations of the heating period of TCP are run in the software packages and the two equations are used to compute numbers. The results from simulations and the numbers are compared. The comparisons can become guidelines for future productions of TCPs or can be verified for better development of TCPs. This chapter explores the second objective in Section 1.3.

Chapter 5 lists the experimental apparatus and procedures that are used to produce data to be studied in chapter 6, which shows the third objective in Section 1.3.

Chapter 6 analyzes the experimental data which are used to experimentally study the errors and variations of the calculated k_m. Also, theoretical k_m errors are included.

Chapter 7 summarizes the contribution of this thesis, provides concluding remarks, and makes recommendations for future enhancements of TCP designs.

CHAPTER 2 - LITERATURE REVIEW

Thermal conductivity probes (TCPs) are currently very popular in many fields such as agriculture, mining and ground source heat pump systems in buildings. Much research has been undertaken to investigate as well as to improve TCPs. Because of the vast amount of information available, one may feel overwhelmed and find it difficult to start using or developing TCPs. Also, the applications of TCPs are so various that one may not realize that using TCPs can produce relatively more accurate results in many cases such as inline measurements. However, because designing and applying the TCPs are highly subjective and extensive, errors from the designs and applications of TCPs are numerous but not all reviewed and studied. Therefore, in this chapter, the major characteristics of TCPs are reviewed first. Secondly, the significance and importance of thermal conductivities of materials are briefly described. Thirdly, typical works from other researchers are mentioned. Fourthly, possible errors in TCP measurements from other researchers are reviewed. Finally, studies in the literatures that are found missing are mentioned.

2.1 - TCP Major Characteristics

As already briefly described in Subsection 1.2.2, a TCP is a transient method that has a hot-wire in the middle and has been widely used for determining the thermal conductivities of fluids with a relatively good accuracy [12], [13]. Because the probe generally does not produce high temperature differences during measurements, the convective error is eliminated and the experimental data obtained are more reliable than those from the steady-state GHPA (mentioned in Subsection 1.2.1) as Nagasaka *et al.* [12] and Rahman [20] realized.

The main characteristic of a TCP is from the thermocouple that is embedded inside the TCP and used to measure the temperature response of the probe as it is heated or cooled. Moreover, the heating time of a TCP can be varied as desired. Tarnawski *et al.* [21] heated their TCPs (whose outer diameter was ~1.06 *mm*) for 120 *s* while ASTM [22] indicates that heating small TCPs (whose outer diameters are < 2.5 *mm*) for 30 to 60 *s* is sufficient to accurately measure the thermal conductivity of the sampling medium. The discrepancies in the heating time of the TCP will be later investigated whether it is better to use shorter or longer heating time. In addition, the temperature responses from the heating and cooling periods can produce different thermal conductivity values. Hence, it is worth finding out why they are different and which one gives more accurate values of the thermal conductivities.

2.2 - TCP Applications

Due to its versatility, simplicity, and the fact that a TCP generally eliminates moisture loss and migration within the material, the TCP has gained much popularity in food and biomedical engineering applications (Murakami *et al.* [23] and Lund *et al.* [24]). Knowledge of the thermal conductivities of biological materials such as biotissues and foods is of great importance. In the food industry, the thermal conductivity of food is important to predict and control the heat flux during the processing of the food, such as cooking, frying, or drying, for higher qualities (Chaves and de Almeida [25]). In the biomedical field, the thermal conductivity of biological tissues is of great importance in treating and curing diseases such as tumors and cancers (Liu *et al.* [3]).

As a result, Yi *et al.* [26] applied the TCP method and measured the thermal conductivities of pig livers. The researchers first simulated the temperature rise of a TCP using COMSOL and calculated the theoretical thermal conductivity. They then bought two pig livers from a local slaughter house and measured their thermal conductivities with a TCP based on the line heat source theory (*i.e.* Eq. 1.3). A radio frequency (RF) ablation system, Cool-tip RF applicator (Valleylab, Boulder, CO), was applied to provide RF treatment to the biomaterials for 12 minutes. The thermal conductivities of the pig livers were re-measured to examine the influence of RF ablation on biomaterials. Yi *et al.* found that RF ablation slightly increased the thermal conductivities of the biomaterials, which means that RF ablation causes animal tissues to conduct more heat and warm up faster. Thus, the tissues can die because of excessive heat if the researchers provide a certain amount of RF ablation; an excellent technique to treat tumor and cancer cells in human bodies.

Furthermore, Liang *et al.* [27] applied the TCP method to get the thermal conductivities of fresh pig meat, pig liver, pig kidney, and snake heads before and after refrigeration. Again, the line heat source (or Eq. 1.3) was used to obtain the thermal conductivities of the biomaterials. Liang *et al.* noted that different structures of meat gave different thermal conductivities because of inconsistent lean/fat ratios. Also, the researchers realized that thermal conductivities of the materials at room temperature are not influenced by the refrigeration processes. In other words, freezing the materials and defrosting them to room temperature do not affect the biomaterials' thermal conductivities. In addition, the water content was found to be important for the thermal conductivities of the biological tissues, which, together with Yi *et al.*'s results [26], lead to better knowledge of how much RF ablation should be used on the individual basis.

Moreover, Chaves and de Almeida [25] obtained the thermal conductivities of cream milk, ketchup and condensed milk with a TCP which was a hypodermic needle with dimensions of Ø1.50 mm × 100 mm. The researchers developed a new TCP that was 10 times cheaper than the commercial ones in the Brazilian market. Chaves and de Almeida applied the microcontroller technology from BASICSTAMP ® for the internal processor of their TCP. The microcontrollers processed the temperature readings from the TCP using Eq. 1.3 and output the thermal conductivity value to a LCD screen. A piezo speaker was also included to alert the experimenters when the thermal conductivity was calculated. The researchers put the microcontrollers, LCD screen, and speaker inside a metal box. The whole TCP construction is shown in Fig. 2.1. The TCP was then calibrated in glycerin at 25 ± 0.01^{o}C and found to be in excellent agreement (from +1.4% to -2.1%) with the published data by a Brazilian certified lab.

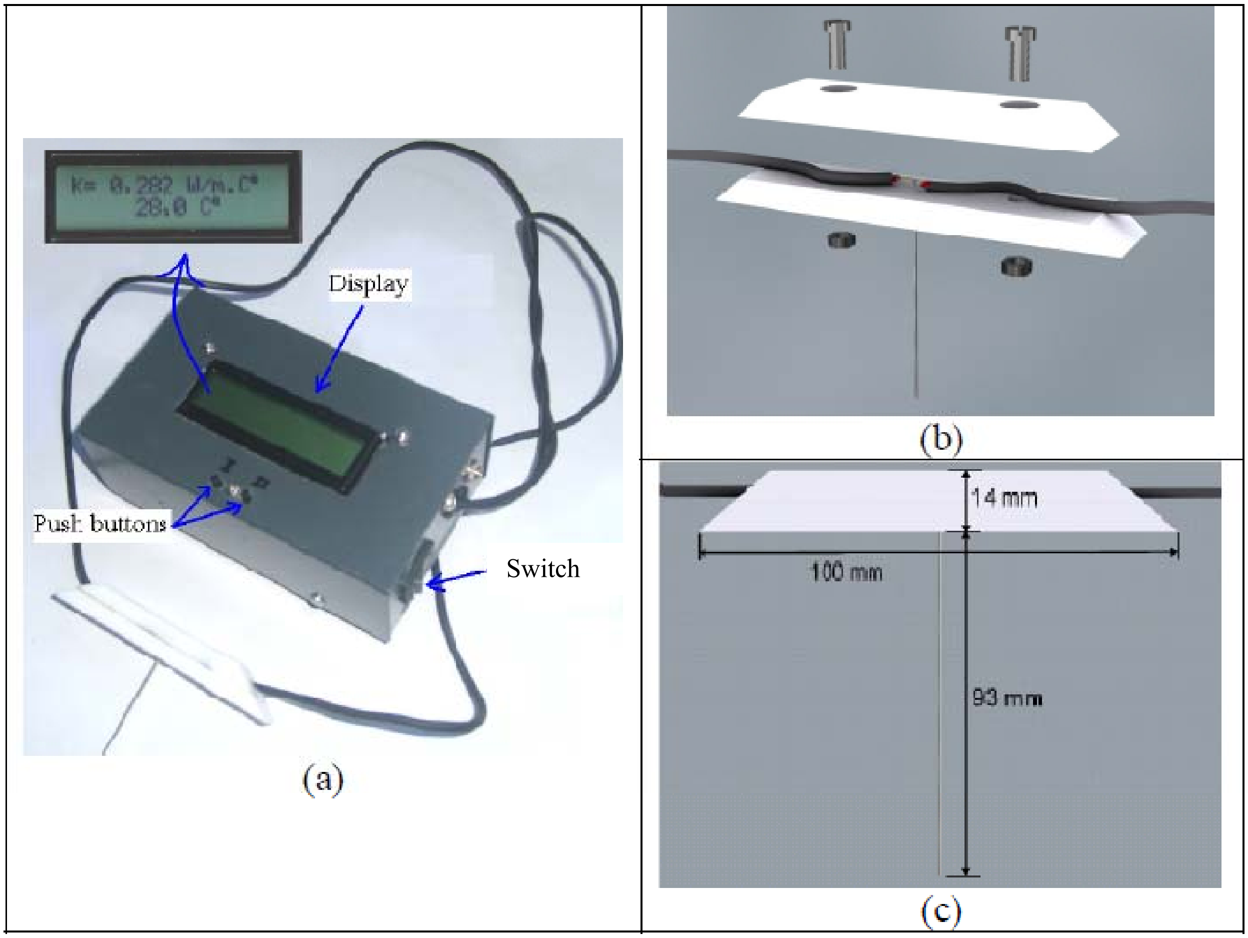

Figure 2.1. A TCP constructed by Chaves and de Almedia. (a): Device view, (b): Probe details, (c): Probe dimensions. (Adopted from [25]*).*

Another popular field for TCPs is with granular materials such as soils and sands. In recent years, the high consumption rate of non-renewable energy sources such as fossil fuels and natural gases has created a huge amount of green house gases and caused quick depletion of non-renewable energy sources. So renewable energies are being explored as alternative energies to reduce the green house gas effects. Ground source heat pump (GSHP) systems are so attractive being an alternative energy source of high efficiency that millions of them have been installed globally as indicated by Lund *et al.* [28]. In designing GSHP systems, the thermal conductivity of the surrounding ground plays a significant role because the thermal recovery of the ground is highly dependent on its *k*-value (Sufen and Shang [29]). The reason is GSHP systems take heat from or to the ground for heating or cooling purposes inside a building, which can create annual thermal imbalances in the ground (Trillat-Berdal *et al.* [30]). For example, drying of the ground surrounding the ground heat exchangers may happen if excessive heat is put into the ground, leading to low soil thermal conductivity and further deteriorating the performance of the GSHP systems. On the contrary, permafrost of the underground may occur if excessive heat is taken from the ground. To avoid such failures, appropriate sizing of the ground heat exchanger is important, which depends on the thermal conductivity in the ground. As a result, the more accurately the thermal conductivity of the ground is known, the better the GSHP system can be designed to sustain the surrounding environment.

Consequently, Tarnawski *et al.* [21] built TCPs and studied the thermal conductivities of soils with a wide range of saturation. The TCPs are Ø1.06 *mm* × 55.0 *mm* and were validated against agar gel (1% agar and 99% water). Ottawa sands (C190 and C109) and Toyoura sand with saturation ratios from 0.0 to 1.0 were measured and their corresponding thermal conductivities were calculated using the line heat source theory. The researchers found that the sands at fully dry and fully saturated conditions agreed with data from the steady state GHPA while sands in the partially saturated region exceeded the steady state data. Tarnawski *et al.* [21] also believed that the thermal conductivities obtained from the TCP measurements are more reliable than those from the steady state GHPA because of low heating and relatively much shorter heating time of the TCP; hence there is little moisture migration inside the sands.

Moreover, King *et al.* [31] with a TCP studied the variation of the thermal conductivities of the grounds in Central England on different days. The researchers went to Ecton, Staffordshire and Whatstandwell, Derbyshire to make field measurements by inserting a TCP (with different heating powers and a handle of 1.5 *m* long) into the grounds. While in the ground, the TCP was rested for 5 minutes and heated for 10 minutes. Because of geological variations of the grounds on different days, King *et al.* recommended using the geometric mean (as defined in Eq. 2.1) of the thermal conductivity (from different measurements) as the best estimate for GSHP system designs at small sites.

$$k_{GM} = \left(k_{m1} \cdot k_{m2} \cdot k_{m3} ... k_{mn}\right)^{1/n} \tag{2.1}$$

where k_{GM} is the geometric mean thermal conductivity and n is the number of measurements.

2.3 - Possible Errors with TCPs

The majority of thermal conductivity measurements using TCPs in the literatures is calculated from Eq. 1.3b and Eq. 1.4 (which has been referred to as the classical solution of TCP) with the following assumptions and simplifications (*A/S*):

1. Homogeneous material with constant properties.
2. TCP size is much smaller than the sampling medium's, so the medium can be treated as infinite.
3. TCP's construction is neglected.
4. No bulk flow in the medium and no radiation effects.
5. The length-to-diameter ratio of the TCP is greater than 50.
6. Thermal contact resistance is ignored.
7. $\frac{r_{probe}^2}{4\alpha_m t} << 1$ so that $-Ei\left(\frac{-r_{probe}^2}{4\alpha_m t}\right) \approx -\gamma + \ln\left(\frac{4\alpha_m t}{r_{probe}^2}\right)$. (Asymptotic approximation)

With the above assumptions and simplifications in the derivation of Eqs. 1.3b and 1.4, many researchers have reported errors and uncertainties. The coming Subsections will elaborate what have been reported as errors and uncertainties of using Eqs. 1.3b and 1.4 during TCP experiments.

2.3.1 - Error Associated with Homogeneous Material Assumption

The properties of a material are mildly to highly dependent on the temperature at which the material is. The greatest property changes can be easily observed in gaseous materials such as air. However, the properties of solids do not change as sharply as those of gases when the surrounding temperature varies. Cengel [10] showed that the thermal conductivity of AISI304 stainless steel is 12.6 *W/m·K* at 200 *K* while it is 16.6 *W/m·K* at 400 *K*. Also, Wu *et al.* [32] reported that his team's epoxy composite (Boron-free glass fiber reinforced isopropylidenebisphenol bis(2-glycidyyloxy-3n-butoxy)-1-propylether/triglycidyl-p-aminophenol) had a thermal conductivity of 0.425 *W/m·K* at 280 *K* and 0.440 *W/m·K* at 300 *K*. In addition, the densities and specific heat capacities of the solids do not vary much with temperature (below melting point). As a result, for a temperature change of up to about 4 *K* during TCP experiments, the thermal properties of the TCP materials (stainless steel and epoxy) can be assumed constant and *A/S* #1 (assumption/simplification #1) is almost completely true.

2.3.2 - Error Associated with Probe Size

Every TCP has finite dimensions with various sizes that have been used. Yi *et al.* [26] applied a TCP of 1.5 *mm* in diameter to measure pig livers' thermal conductivities while Teka Inc. [33] produced a TCP (Field VLQ) of 6.0 *mm* in diameter to make measurements of soils. With the use of Eqs. 1.3b and 1.4, the size of the TCP is ignored, *i.e.*, the TCP size is assumed to have insignificant effects in the measuring processes. However, as Bristow *et al.* [19] and Cheng *et al.* [24] indicated, bigger TCPs produce higher errors. Murakami *et al.* [23] even suggested making the TCP as small as the application and fabrication permits, which means making a customized probe for a particular measurement. But the suggestion poses high costs for manufacturing customized TCPs. Consequently, in the *A/S* #2 of using Eqs. 1.3b and 1.4, there lurks unknown uncertainties from the size of the TCP and may render the thermal conductivity of the sampling medium mildly to highly inaccurate.

Moreover, the diameter ratio of the TCP and the sampling medium (r_s/r_m) during a TCP experiment in a lab can produce edge effects that lower the accuracy of the calculated thermal conductivity. Murakami *et al.* [23] used a potato cylinder to clarify the possible error. Fresh potatoes were bought, peeled, and shaped into cylinders with diameter of 7.0 *mm* and length greater than 50 *mm.* The thermal conductivity of the potato cylinder was found to be 0.56 *W/m·K*. The cylinder was then exposed to environments of air (k_{air} = 0.0244 *W/m·K*) and stirred water (k >> 0.6 *W/m·K*). In the two environments, the heat reached the cylinder wall after 40 *s*. For the case of the air environment, the linear portion of the *t-T* plot (*e.g.* Fig. 1.4) shifted up and was 0.7^{o}C more than normal, indicating that convection started after 40 *s* and acted like an insulator to reduce the heat flow rate of the cylinder. Consequently, the calculated k_m would be lower than the case of an infinite sampling medium. Meanwhile, in the stirred water environment (engaged by a magnetic stirrer), the linear portion of the *t-T* plot moved downwards, causing calculated k_m to be higher than the case of an infinite sampling medium.

2.3.3 - Error Associated with Neglected TCP Construction

Regardless of which materials are used to make the TCP, Eq. 1.3 still treats them as insignificant in *A/S* #3. In other words, making the TCP from epoxy and steel would be as insignificant as from silica gel and copper or from any other combination of materials. This assumption and simplification of Eq. 1.3 may lead to inaccurate results. The reason is that when the thermal properties of the TCP materials are different from those of the sampling medium, the thermal conductivity of the sampling medium can become less accurate from the following error estimation equations (Elustondo *et al.* [34]):

$$\Delta T = \frac{\dot{q}_w}{4\pi k_m}\left\{4\pi k_m R_c + \left[1 + \frac{r^2}{2\alpha_m t}(1-\beta)\cdot\left(-\gamma - \ln\left(\frac{r^2}{4\alpha_m t}\right)\right)\right] + ...\right\} \tag{2.2a}$$

$$\zeta \approx -\frac{r^2}{2\alpha_m t}(1-\beta) + ... \tag{2.2b}$$

where $\beta = \frac{(\rho \cdot c_p)_{probe}}{(\rho \cdot c_p)_m}$ and ζ is the error of k_m.

The researchers [34] realized that β can be minimized if the materials to construct the TCP are appropriately selected. However, the selection criteria were not clearly mentioned.

2.3.4 - Error Associated with Bulk Flow and Radiation

When the thermal conductivities of soils with some degree of saturation (*i.e.,* soils that contain some water or liquid) are determined using Eq. 1.3, the water or liquid migration is not considered (*A/S* #4). However, the neglect has been reported problematic even though Hooper and Lepper [35] showed the TCP induces less moisture migration within the sampling medium than the GHPA. Brandon and Mitchell [36] mentioned that when the pores of the soil are several millimeters across (or the sand particles are of gravel size or larger), convection heat transfer can occur. The problem of moisture migration in soils and sands was also addressed by many other researchers such as Radhakrishma [37] and Adams and Baljet [38]. Nevertheless, because a TCP is usually heated up to 5^{o}C more than the ambient (or initial) temperature, the radiation effect can be ignored. Searches in the literatures provide no report on the problems caused by radiation in TCPs with low heating powers (10 *W/m* or less). As a result, *A/S* #4 may not be completely valid for a medium with moisture or convective flow.

2.3.5 - Error Associated with TCP Length-to-Diameter Ratio

When a TCP is heated along its axial direction, heat conduction can happen radially and/or axially inside the TCP and the sampling medium. So the assumption of sole radial heat conduction in deriving Eq. 1.3 may not be accurate. Blackwell [39] thought of the possible error with axial thermal conduction and came up with the following equation (where z is the height variation along the length of the TCP):

$$\left.\frac{\partial T_{probe}}{\partial(\ln t)}\right|_{z=0} = \frac{\dot{q}_w}{4\pi k_m} Y \tag{2.3}$$

where $Y = erf(X) - \frac{2}{e^{X^2}\sqrt{\pi}} C \cdot S \cdot X^3 + \frac{C^2}{\sqrt{\pi}}\left(3S^2 - \frac{\pi^2}{2}\right)\cdot\left(\frac{1}{2} + \frac{X}{2} - X^2\right)X^4 \cdot e^{X^2}$, $\quad X = \frac{L}{4\sqrt{\alpha_m t}}$,

$$C = 4\sigma \cdot r_s^2 \frac{(\varepsilon - \beta)}{L^2}, \quad S = \ln\left(\frac{4\alpha_m t}{r_s^2}\right) - \gamma + \frac{2k_m}{H_c r_s^2}, \quad \varepsilon = \frac{k_{probe}}{k_m}, \quad \beta = \varepsilon \frac{\alpha_m}{\alpha_{probe}}, \quad LR = \frac{L}{2r_s}$$

$\sigma = \frac{2r_t}{r_s}\left(1 + \frac{r_t}{2r_s}\right) \approx \frac{2r_t}{r_s}$ for hollow probes, $\quad r_t$: wall thickness of the hollow probe (m),

$z = 0$ is at the centroid of the TCP (m), and r_s: the radius of the TCP (m).

Eq. 2.3 shows how the temperature varies along the TCP. The heat conducted axially will appear in ΔY, the relative error due to axial flow, where $\Delta Y = 1 - Y$. Blackwell [39] then assumed some arbitrary values to estimate how long the TCP should be to have relatively small axial heat conduction. It is very unlikely that $\frac{\alpha_m t}{r_s^2}$ will be over 25, and assuming $\frac{2k_m}{H_c r_s} = 2$, $\varepsilon = 50$, $\beta = 1.5$, hollow brass probe of r_s = 1.25" and r_t = 0.125", and LR = 25, σ = 0.4, then the percentage change in the axial heat conduction $\Delta Y = 0.7\%$. If LR = 60, $\Delta Y = 0.051\%$. Because of the complexity and many unpredicted variables of Eq. 2.1, researchers, such as Tarnawski *et al.* [11] and Bilskie *et al.* [40] have believed that the length-to-diameter ratio of 50 of the TCP will produce axial heat conduction of less than 0.01%. The ratio is highly probable but not error free as in *A/S* #5.

2.3.6 - Error Associated with Neglected Thermal Contact Resistance

In practical situations when inserted into a soil sample, the TCP can make a big to very small gap between it and the sampling medium. The gap creates a thermal contact resistance (TCR). However, during the derivation of Eq. 1.3, the TCR was ignored. Using numerical simulations and theories, researchers have found out that there are differences in the temperature response at the thermal sensor location with the TCR being considered. Goto and Matsubayashi [41] mentioned the following equation for the inclusion of the TCR:

$$T = \frac{\dot{q}_w}{k_m} G(h, 2\beta, \tau) \tag{2.4}$$

where $G(h,2\beta,\tau) = \frac{8\beta^2}{\pi^3}\int_0^\infty \frac{1-\exp(-\tau \cdot u^2)}{u^3 \cdot \Delta(u)} du$, $\quad h = \frac{k_m}{H_c \cdot r_s}$, $\quad \tau = \frac{\alpha_m t}{r_s^2}$, $\quad \alpha_m = \frac{k_m}{(\rho \cdot cp)_m}$, and

$$\Delta(u) = \left[uJ_0(u) - (2\beta - h\cdot u^2)J_1(u)\right]^2 + \left[uW_0(u) - (2\beta - h\cdot u^2)W_1(u)\right]^2$$

With Eq. 2.4 and by varying the parameters in the equation, Goto and Matsubayashi [41] simulated temperature responses. The responses showed that the more the heat capacity of the sampling medium decreased, the less the temperature rise was. Also, when h was lowered, the temperature rise decreased. The researchers went on to experimentally explore how estimating k_m could affect h. Goto and Matsubayashi [41] found that a ±5.0% estimation error of k_m could lead to a ±100% error predicting h. In other words, the TCR had very little influence on obtaining the thermal conductivity of the sampling medium which agrees well with the TCR explored in this thesis.

Liu *et al.* [42] experimentally studied the thermal contact resistance of TCP by immersing a TCP to agar-water and inserting the TCP to air-dried Great Sand Hill sand. The heating power was 5 *W/m* and the following empirical formulas were applied to obtain H_c for very small time ($t \le r_s^2 / \alpha_m$):

$$T(t) \approx Z_1 t - Z_1 Z_2 t^2 + Z_1 Z_2 Z_3 t^{2.5} \tag{2.5}$$

$$H_c = \frac{\dot{q}_w}{\pi r_s} \frac{Z_2}{Z_1} \tag{2.6}$$

where Z_1, Z_2 and Z_3 are fitting parameters which are obtained by fitting Eq. 2.5 to the temperature response of the TCP.

By using Eq. 2.5 and 2.6 with experimental data and a TCP of Ø1.27 *mm*, Liu *et al.* obtained H_c = 113 $W/m^2 \cdot K$ for the sand and H_c = 1056 $W/m^2 \cdot K$ for the agar. With a TCP of Ø3.175 *mm*, H_c = 841 $W/m^2 \cdot K$ for the sand and H_c = 1196 $W/m^2 \cdot K$ for the agar. The thermal contact conductance values are intuitive. However, when the method used by Liu *et al.* [42] was applied to the TCP experimental data from Tarnawski *et al.* [21], no unique solution could be obtained. The reason can be that only some sampling materials and TCP designs would fit the empirical equations (Eqs. 2.5 and 2.6). Also, the TCP designs of Liu *et al.* [42] and of Tarnawski are quite different. In addition, the samples used by the two groups of researchers were not the same.

Moreover, Murakami *et al.* [23] showed that the TCR only causes the *t-T* plot (*e.g.* Fig. 1.4) to shift up but does not change the slope of the plot which is used to calculate k_m using Eq. 1.3. Consequently the k_m value is not affected or has few disturbances. The result from Murakami *et al.* [23] agrees well with Elustondo *et al.* [34] (Eq. 2.2a) and this thesis in terms of the TCR.

2.3.7 - Error Associated with Asymptotic Approximation

Besides the edge effects mentioned earlier, when approximating the exponential integral function to the natural logarithmic function in Eq. 1.4, there could be errors from the selection of "warm-up" heating time of TCP t_0. The parameter t_0 is the time where researchers initiate the calculation of the thermal conductivity of the sampling medium from the temperature response. This parameter has been subjective. ASTM [22] recommends ignoring the temperature data of the first 10 to 30 *s* with probes of diameters of 2.5 *mm* or less. No explanation was given to why the time interval was selected. Tarnawski *et al.* [11], [43], [21] started calculating the thermal conductivities for their temperature data from 20 *s* but did not elaborate why they chose the time. In addition, searching through the literatures did not provide any research on how choosing the t_0 can affect the accuracy of the calculated thermal conductivity.

2.3.8 - Other Reported Error Sources

In addition to the errors from the assumptions and simplifications during the derivation of Eq. 1.3, there have been many other reported sources of errors during a TCP experiment. Examples include the following studies from researchers:

1. For a larger TCP, longer heating time is suggested to reduce the errors (Strambu [44]).
2. In the study of Xie and Cheng [13], the thermocouples inside the TCP are error sources as they have a thermal mass and cause unavoidable heat loss and asymmetry. In addition, systematic errors of the TCP components can cause trouble. Because everything has a tolerance during the manufacturing processes, the components of the TCP do not always perform consistently. As a result, the TCP can sometimes malfunction.
3. Liang *et al.* [27] mentioned that for $r_s > 2\sqrt{\alpha_m t}$, the surface effect (due to factors such as dirt or stain from previous experiments or surface micro-corrosion) would be less than 0.1%. In addition, the TCR would be eliminated by $\Delta T - \Delta T_0$. ΔT_0 is the temperature rise at time t_0 while ΔT is the temperature rise after time t_0 as read by the thermocouple.
4. Yi *et al.* [26] indicated that ΔT is more sensitive to k_m than to α_m.
5. Asher *et al.* [45] found that nonlinear curvature in the *t-T* plot at early time was due to the heat capacity of the TCP while that at late time of the plot was because of the axial end effects and maybe convection. Also, lowering the power input and increasing the measuring time would make Eq. 1.3 more accurate for experiments with tertiary butyl alcohol.

2.4 - Summary

A typical construction of TCPs is shown in Figs 1.3 and 1.7. Basically, a TCP is made of a stainless steel hypodermic tube with epoxy filling the inner space. Within the epoxy layer, there lie an electrical heating wire and a thermocouple. The steel tube provides inserting strength while the epoxy acts as the buffer layer that protects the heating wire and the thermocouple from shocks during transportation of the TCP. During a TCP experiment, electricity is passed through the heating wire and the thermocouple senses the temperature response. The heating duration and strength are subjective. Using the temperature response, the thermal conductivity of the sampling medium can be calculated by Eq. 1.4.

Moreover, typical applications of the TCPs are briefly reviewed. The applications include measuring the thermal conductivities of:

1. Biomaterials such as pig livers and snake heads (Yi *et al.* [26] and Liang *et al.* [27]). Combining the results of Yi *et al.* [26] and Liang *et al.* [27], better treatments of tumors and cancers can be made to treat people on an individual basis when the thermal conductivities of the biomaterials are known more accurately.
2. Foods for better processing procedures and higher quality (Chaves and Almeida [25]).
3. Granular materials such as soils and sands (Tarnawski *et al.* [11] and King *et al.* [31]*)*. Better knowledge of the thermal conductivity of the ground results in better performance of ground source heat pump (GSHP) systems (Sufen and Shang [29]).

However, most TCP measurements apply the classical solution or line heat source theory (Eq. 1.3) to calculate the thermal conductivity. The extensive use of Eq. 1.3 for various TCP designs has made many researchers question the accuracy of the equation. From the seven basic assumptions and simplifications (*A/S*) for the derivation of Eq. 1.3, studies have been made to verify the validity of the *A/S*. The studies showed that:

1. The assumption of constant-property materials may be violated depending on the materials being used to construct the TCP. From Cengel [10] and Wu *et al.* [32], it can be seen that the thermal conductivities of AISI 304 stainless steel and an epoxy composite

vary weakly with temperature. In addition, because TCP experiments generally do not involve high heating power (usually less than 5^{o}C temperature rise), the *A/S* #1 can be safe to apply to stainless steel 304 and epoxy to TCP, according to AS1.

2. The TCP size may create troubles. Bigger probes produce higher errors (Bristow *et al.* [19], Cheng *et al.* [24] and Murakami *et al.* [23]). Also, when the sampling medium is put in a container whose radius is not big enough to mimic an infinite medium, edge effect can occur (Murakami *et al.* [23]), resulting in less accurate k_m measurements.
3. When the thermal properties of a TCP are different from those of the sampling medium, errors can happen. Elustondo *et al.* [34] indicated that with the proper selection of the TCP materials, the error of the calculated k_m can be reduced. However, the selection criteria were not clearly mentioned.
4. The assumption of no bulk flow inside the sampling medium may be violated for granular materials such as sands and fluids (Brandon and Mitchell [36], Radhakrishma [37], and Adams and Baljet [38]).
5. In reality, when a TCP is heated, there exist radial and axial heat conductions. Blackwell [39] realized that for probes with the length-to-diameter ratio greater than 25, the error of neglecting the axial heat conduction is less than 0.1%.
6. The thermal contact resistance (TCR) at the TCP-medium interface was neglected in Eq. 1.3, which may cause troubles. Fortunately, researchers found that the TCR does not have much effect on k_m (Elustondo *et al.* [34], Murakami *et al.* [23], and Liang *et al.* [27]). The results from the researchers agree well with the TCR studied in this thesis.
7. In order to calculate k_m with Eqs. 1.3 and 1.7, a starting time t_0 is used. The time may cause errors but has not been widely studied.

Other than the problems with the assumptions and simplifications in deriving Eq. 1.3, factors that can decrease the accuracy of the calculated k_m include:

1. Short heating duration for big TCPs (Strambu [44]),
2. Inappropriate size and location of the thermocouple (Xie and Cheng [13]),
3. The surface effects, such as dirt or stain on the outermost surface of the TCP from the previous experiment, with $r_s < 2\sqrt{\alpha_m t}$ (Liang *et al.* [27]), and

4. High heating power and short measuring duration (Asher *et al.* [45]).

Nevertheless, the author of this thesis realized that there was almost no prior study on whether measuring different sampling media would produce the same errors. In addition, the material selection criteria in *A/S* #3 were not clear. Also, the tolerance of the thermocouple location could not be found in the literatures. Moreover, arbitrary selection of t_0 can be subjected to errors. Furthermore, only a limited number of studies such as that of Hsieh [46] touch the cooling period of TCPs. Theoretically, both heating and cooling periods of TCPs can be used to determine the thermal conductivity of the sampling medium. However, there is no clear indication which period (cooling or heating) of TCPs can give more accurate k_m. Also, the wall thickness of the stainless steel tube of the TCP may cause errors but was not found in the literatures. In addition, searches through the literatures provided no prior study on the effect caused by various heating powers of the TCP.

As a result, this thesis aims to address the missing parts of the studies of TCPs in the literatures. Due to the immense possibilities of TCP designs and applications, this research investigates both theoretical and experimental errors of calculating k_m in TCP measurements as follow:

1. The theoretical studies (in Chapter 4 and Section 6.4) include the errors from:
    a. Probe sizes
    b. Heating powers
    c. Sampling media
    d. Selection for TCP materials
    e. Location of the thermocouple
    f. Boundary conditions of the sampling-medium container
    g. Axial heat conduction of the length-to-diameter ratio of 45
2. The experimental studies (in Chapter 6) include the errors from:
    a. Thermal contact resistance
    b. Initiating time t_0
    c. Decision to use heating or cooling period for k_m calculations
    d. Tolerance in the thermal properties of epoxy k_e and α_e within a TCP

CHAPTER 3 - THEOREICAL MODELS OF TCP

In this chapter, the most important equations are introduced. The classical solution from Carslaw and Jaeger [16] is shown first. Then two new equations are introduced. Within each equation, the heating and cooling periods are given. Due to the complexity and the length, the full derivations of the theoretical models are shown in Appendices A.1 - A.5. Also, to reduce the confusion by the vast number of equations in this thesis, the second last part of this chapter will gather the three most important equations that are often referred to in subsequent chapters. Finally, the main equations are non-dimensionalized in the last Section of this chapter.

3.1 - Line Heat Source Model

According to de Vries [47] and Liu *et al.* [42], the classical infinite line source model (which is illustrated in Fig. 3.1) is:

$$\Delta T(r_{sen},t)=\begin{cases} \dfrac{-\dot{q}_w}{4\pi k_m} Ei\left(\dfrac{-r_{sen}^2}{4\alpha_m t}\right) \quad for\ t<t_c & (\text{Eq. } 3.1a) \\ \left[\dfrac{-\dot{q}_w}{4\pi k_m} Ei\left(\dfrac{-r_{sen}^2}{4\alpha_m t}\right)\right]-\left[\dfrac{-\dot{q}_w}{4\pi k_m} Ei\left(\dfrac{-r_{sen}^2}{4\alpha_m (t-t_c)}\right)\right] \quad for\ t>t_c & (\text{heat sink model}) \end{cases} \tag{3.1}$$

where $\Delta T(r_{sen},t)=T(r_{sen},t)-T_i$. The first expression on the right hand side (RHS) (for $0 \leq t \leq t_c$) of Eq. 3.1 is for the heating period of the line heat source and derived in Appendix A1. The second expression on the RHS (for $t > t_c$) of Eq. 3.1 is the cooling period (*i.e.*, the line heat source is off) and can be thought of as the difference between the heating starting from the time the line heat source is first heated ($t_o = 0\ s$) and the heating starting from the time the electricity is cut from the line heat source (t_c), *i.e.*, $\Delta T(r_{sen},t)_{cool\_class.} = \Delta T(r_{sen},t)_{heat\_class.} - \Delta T(r_{sen},t-t_c)_{heat\_class.}$ for $t > t_c$.

Theoretically speaking, the $Ei(x)$ function blows up at $x = 0$. However, in reality, the thermocouple location is mostly set to be away from the TCP's axis. As a result, the function never blows up in general.

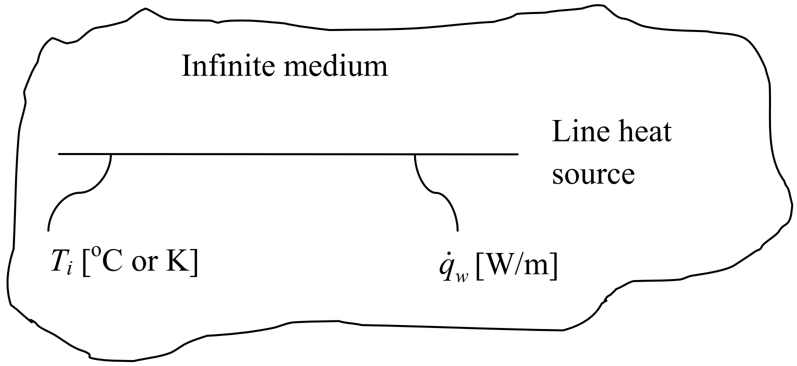

Figure 3.1. Infinite medium and a line heat source.

3.2 - TCP Model with Perfect Contact at the TCP-Medium Interface

Fig. 3.2 illustrates the Perfect Contact TCP Model. Refer to Appendix A.2. for the full derivation of the model in the heating period (*i.e.*, $t < t_c$) and difference observed in Eq. 3.1 for the cooling period (*i.e.*, $t > t_c$):

$$\Delta T(r_{sen},t)_{heat\_PC} = -\frac{\dot{q}_w}{4\pi k_m} Ei\left(-\frac{r_s^2}{4\alpha_m t}\right)\left[Term_1(t)\right] + Term_2(t) \qquad \text{for } t < t_c \tag{3.2}$$

where $\Delta T(r_{sen},t) = T(r_{sen},t) - T_i$, $Term_1(t) = e^{\frac{r_e^2}{4\alpha_s t}-\frac{r_e^2}{4\alpha_e t}+\frac{r_s^2}{4\alpha_m t}-\frac{r_s^2}{4\alpha_s t}}$, and

$$Term_2(t) = -\frac{\dot{q}_w}{4\pi k_e}\left[Ei\left(-\frac{r_{sen}^2}{4\alpha_e t}\right) - Ei\left(-\frac{r_e^2}{4\alpha_e t}\right)\right] - \frac{\dot{q}_w}{4\pi k_s} e^{\frac{r_e^2}{4\alpha_s t}-\frac{r_e^2}{4\alpha_e t}}\left[Ei\left(-\frac{r_e^2}{4\alpha_s t}\right) - Ei\left(-\frac{r_s^2}{4\alpha_s t}\right)\right]$$

$$\Delta T(r_{sen},t)_{cool\_PC} = \Delta T_{heat\_PC}(r_{sen},t) - \Delta T_{heat\_PC}(r_{sen},t-t_c) \qquad \text{for } t > t_c \tag{3.3}$$

where $\Delta T_{heat\_PC}(r_{sen},t)$ takes the form of Eq. 3.2 (with $t > t_c$) and

$$\Delta T_{heat\_PC}(r_{sen},t-t_c) = \frac{-\dot{q}_w}{4\pi k_m} Ei\left(\frac{-r_s^2}{4\alpha_m (t-t_c)}\right)\left[Term_3(t-t_c)\right] + Term_4(t-t_c) \text{ with}$$

$$Term_3(t-t_c) = exp\left(\frac{r_e^2}{4\alpha_s(t-t_c)} - \frac{r_e^2}{4\alpha_e(t-t_c)} + \frac{r_s^2}{4\alpha_m(t-t_c)} - \frac{r_s^2}{4\alpha_s(t-t_c)}\right) \text{ and}$$

$$Term_4(t-t_c) = \frac{-\dot{q}_w}{4\pi k_e}\left[Ei\left(\frac{-r_{sen}^2}{4\alpha_e(t-t_c)}\right) - Ei\left(\frac{-r_e^2}{4\alpha_e(t-t_c)}\right)\right]$$
$$-\frac{\dot{q}_w}{4\pi k_s} e^{\frac{r_e^2}{4\alpha_s(t-t_c)} - \frac{r_e^2}{4\alpha_e(t-t_c)}}\left[Ei\left(\frac{-r_e^2}{4\alpha_s(t-t_c)}\right) - Ei\left(\frac{-r_s^2}{4\alpha_s(t-t_c)}\right)\right]$$

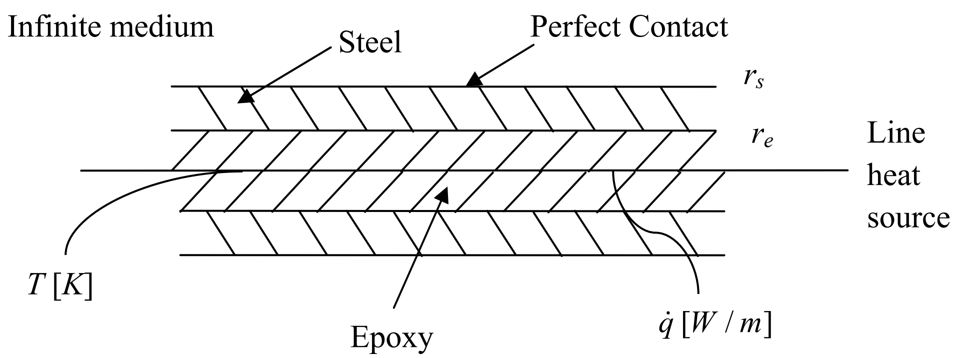

Figure 3.2. TCP containing line heat source.

3.3 - TCP Model with TCR at the TCP-Medium Interface

Referring to Appendices A.3 and A.4 for the full derivation of the model in the heating period:

$$\Delta T(r_{sen},t)_{heat\_TCR} = \frac{-\dot{q}_w}{4\pi k_m} Ei\left(\frac{-r_s^2}{4\alpha_m t}\right)[Term_1(t)] + Term_2(t) + TCR(t) \quad \text{for } 0 < t \le t_c \tag{3.4}$$

where $Term_1(t)$ and $Term_2(t)$ are those in Eq. 3.2; $TCR(t) = \frac{\dot{q}_w}{2\pi r_s} R_c \cdot exp\left(\frac{r_e^2}{4\alpha_s t} - \frac{r_e^2}{4\alpha_e t} - \frac{r_s^2}{4\alpha_s t}\right)$;

and R_c is the thermal contact resistance.

$$\Delta T_{cool\_TCR} = \Delta T_{heat\_PC}(r,t) - \Delta T_{heat\_PC}(r,t-t_c) + TCR(t) - TCR(t-t_c) \quad \text{for } t > t_c \tag{3.5}$$

where $\Delta T_{heat\_PC}(r,t)$ and $\Delta T_{heat\_PC}(r,t-t_c)$ are from Eq. 3.3, $TCR(t)$ is from Eq. 3.4, and

$$TCR(t-t_c) = \frac{\dot{q}_w}{2\pi r_s} R_c \cdot exp\left(\frac{r_e^2}{4\alpha_s(t-t_c)} - \frac{r_e^2}{4\alpha_e(t-t_c)} - \frac{r_s^2}{4\alpha_s(t-t_c)}\right).$$

Comparing Eq. 3.4 with Eq. 3.2, the only difference between the two equations is the *TCR(t)* term which is caused by the thermal contact resistance at the TCP-medium interface as shown in Fig. 3.3. The same holds true for the comparison between Eq. 3.5 and Eq. 3.3.

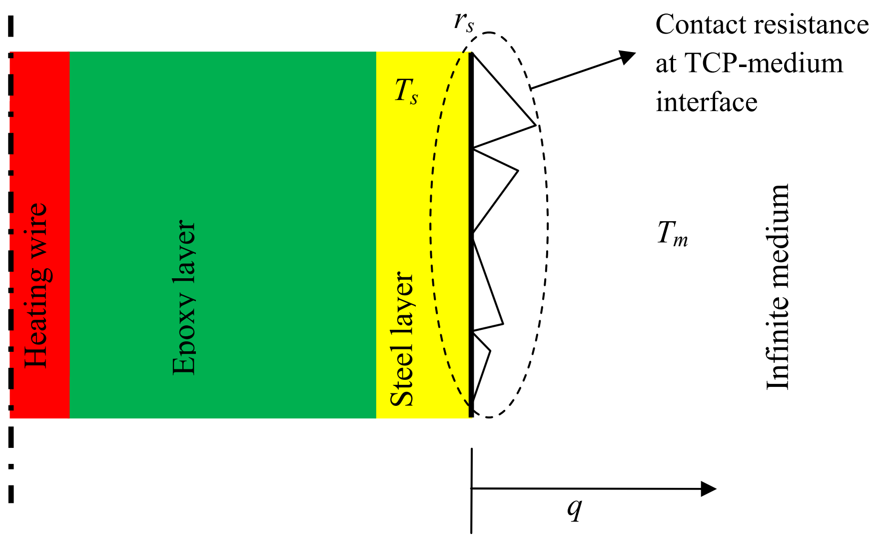

Figure 3.3. Schematic drawing for TCP model with TCR. (Picture not to scale)

3.4 - Grouping Equations

Since there are many equations in this thesis but only some are important for use in subsequent chapters, the following summarizes the most important equations for later analysis:

- Eq. 3.1 will be called **Eq. 1** in subsequent chapters as the line heat source model.
- Eqs. 3.2 and 3.3 are grouped as **Eq. 2** in subsequent chapters as the TCP model with perfect contact at the TCP-medium interface.
- Eqs. 3.4 and 3.5 are grouped as **Eq. 3** in future chapters as the TCP model with TCR at the TCP-medium interface.

3.5 - Non-dimensional Equations

Let $\vartheta = \dfrac{T - T_i}{\dot{q}_w / (4\pi k_m)}$, Eqs. 3.1a, 3.2, and 3.4 can be re-written as follow:

$$\vartheta_{Eq1} = -Ei\left[\frac{-1}{4Fo}\left(\frac{r_s}{r_{sen}}\right)^2\right] \tag{3.7}$$

$$\vartheta_{Eq2} = -Ei\left(\frac{-1}{4Fo}\right)\left[Term_{ND1}(t)\right] + \left[Term_{ND2}(t)\right] \tag{3.8}$$

$$\vartheta_{Eq3} = -Ei\left(\frac{-1}{4Fo}\right)\left[Term_{ND1}(t)\right] + \left[Term_{ND2}(t)\right] + TCR_{ND}(t) \tag{3.9}$$

where $Fo = \frac{\alpha_m t}{r_s^2}$, $Term_{ND1}(t) = exp\left[\frac{1}{4Fo}\left(\frac{r_e}{r_s}\right)^2\frac{\alpha_m}{\alpha_s} - \frac{1}{4Fo}\left(\frac{r_e}{r_s}\right)^2\frac{\alpha_m}{\alpha_e} + \frac{1}{4Fo} - \frac{1}{4Fo}\frac{\alpha_m}{\alpha_s}\right]$,

$$Term_{ND2}(t) = -\frac{k_m}{k_e}\cdot\left\{Ei\left[\frac{-1}{4Fo}\left(\frac{r_{sen}}{r_s}\right)^2\frac{\alpha_m}{\alpha_e}\right] - Ei\left[\frac{-1}{4Fo}\left(\frac{r_e}{r_s}\right)^2\frac{\alpha_m}{\alpha_e}\right]\right\}$$

$$-\frac{k_m}{k_s}\cdot exp\left[\frac{1}{4Fo}\left(\frac{r_e}{r_s}\right)^2\frac{\alpha_m}{\alpha_s} - \frac{1}{4Fo}\left(\frac{r_e}{r_s}\right)^2\frac{\alpha_m}{\alpha_e}\right]\cdot\left\{Ei\left[\frac{-1}{4Fo}\left(\frac{r_e}{r_s}\right)^2\frac{\alpha_m}{\alpha_s}\right] - Ei\left[\frac{-1}{4Fo}\frac{\alpha_m}{\alpha_s}\right]\right\},$$

and $TCR_{ND}(t) = \frac{TRR}{2}\cdot exp\left[\frac{1}{4Fo}\left(\frac{r_e}{r_s}\right)^2\frac{\alpha_m}{\alpha_s} - \frac{1}{4Fo}\left(\frac{r_e}{r_s}\right)^2\frac{\alpha_m}{\alpha_e} - \frac{1}{4Fo}\frac{\alpha_m}{\alpha_s}\right]$ with $TRR = \frac{R_c \cdot k_m}{r_s^2}$.

In other words, Eqs. 3.7, 3.8 and 3.9 can be written as:

$$\vartheta_{Eq1} = \vartheta_{Eq1}\left(Fo, \frac{r_s}{r_{sen}}\right) \tag{3.10}$$

$$\vartheta_{Eq2} = \vartheta_{Eq2}\left(Fo, \frac{k_e}{k_m}, \frac{k_s}{k_m}, \frac{k_e}{k_s}, \frac{r_s}{r_e}, \frac{r_s}{r_{sen}}, \frac{\alpha_e}{\alpha_m}, \frac{\alpha_s}{\alpha_m}, \frac{\alpha_e}{\alpha_s}\right) \tag{3.11}$$

$$\vartheta_{Eq3} = \vartheta_{Eq3}\left(Fo, \frac{k_e}{k_m}, \frac{k_s}{k_m}, \frac{k_e}{k_s}, \frac{r_s}{r_e}, \frac{r_s}{r_{sen}}, \frac{\alpha_e}{\alpha_m}, \frac{\alpha_s}{\alpha_m}, \frac{\alpha_e}{\alpha_s}, TRR\right) \tag{3.12}$$

TRR: Thermal resistance ratio.

CHAPTER 4 - COMPUTER SIMULATION

Before Eq. 1, Eq. 2, and Eq. 3 are compared, the first two equations (Eq. 1 and Eq. 2) are studied in the heating period to explore the differences the two equations make by using Finite Element Heat Transfer (FEHT) from F-Chart Software and COMSOL from COMSOL Multiphysics ® Software, which apply the general heat transfer equation for cylindrical objects. The reason for using FEHT and COMSOL is to reduce the computational time and power. FEHT is faster to arrive at the simulation results but has limited numbers of nodes (manually input) for the geometry and cells for the computation. Meanwhile, COMSOL can include all the nodes required for the geometry and cells for the computation but takes a long time to arrive at the simulation results. As a result, FEHT is used for 2D simulations and COMSOL is used for 3D simulations in this chapter. In addition, the cooling period is complicated, computer-power intensive, and time consuming to simulate using numerical software packages such as COMSOL or FEHT.

The heating period is studied first to see whether it is justifiable to further advance the newly developed equation (Eq. 2) to subsequent chapters. The analytical and numerical studies in this chapter include

1. various TCP sizes,
2. different heating powers of TCP,
3. diverse thermal conductivity and thermal diffusivity of the sampling medium,
4. different the thermal conductivities and thermal diffusivities of construction layers,
5. different radial and axial locations of the thermocouple inside the epoxy layer,
6. error analysis of the axial heat conduction for the TCP length-to-diameter ratio of 45.

COMSOL is used to explore how the radial and axial locations of the thermocouple can affect the temperature response of the TCP while FEHT is used for exploring other numerical studies mentioned.

The analytical and numerical studies can become guidelines for future designs of TCPs or comparisons with experimental studies. For example, based on the studies of changing probe sizes using FEHT, one can decide how large the TCP should be in order to have lower measuring errors. Or researchers can make different probe sizes and compare the results .

4.1 - Problem Descriptions and Study Parameters

Fig. 4.1 shows a typical TCP construction. The design has a piece of heating wire in the middle of the probe. The space between the wire and a stainless-steel hypodermic tube is filled in with epoxy to serve as a thermal conductor and an electric insulator.

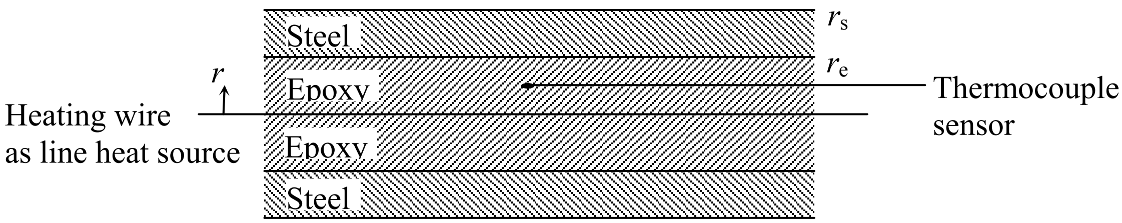

Figure 4.1. TCP design used in this thesis.

A thermocouple is placed in the epoxy layer. When the heating wire is heated up, the thermocouple is used to measure the temperature rise of the "probe". The TCP design in Fig. 4.1 is used to analyze the theoretical errors that may result from the design. Thermal contact resistance is neglected in this chapter but will be considered in Chapter 6. The values of the parameters used in the present study are tabulated in Table 4.1.

Table 4.1. Parameters and values used for the study in this chapter [17], [34], [48], [49], [50].

Parameter	k_e $(W/m{\cdot}K)$	α_e (m^2/s)	k_s $(W/m{\cdot}K)$	α_s (m^2/s)	k_m $(W/m{\cdot}K)$	α_m (m^2/s)
Value	0.682	3.80×10^{-7}	16.2	4.05×10^{-6}	0.502	1.30×10^{-7}
Parameter	r_e (μm)	r_s (μm)	r_w (μm)	r_{sen} (μm)	$\dot{q}_w$ (W/m)	T_i (ºC)
Value	450	550	20.0	275	3.00	15.0

Note: k_m and α_m of the sampling medium is of saturated organic soil [17].

4.2 - FEHT Setup

FEHT is used to produce the numerical solutions under many different conditions to compare the accuracies of the classical solution (Eq. 1) and Eq. 2 . The FEHT model is shown in Fig 4.2.

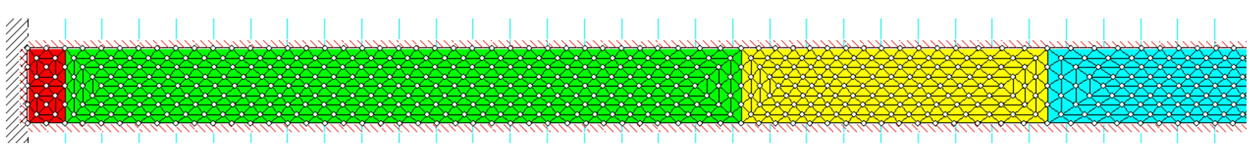
Figure 4.2. An axisymmetric sample FEHT model. Sections (with nodes) from left to right: heating wire (red), epoxy (green), steel (yellow), and medium (blue).

FEHT simulation conditions:

- Setup:
  - Scale and size: units: SI, grid spacing: 20 μm × 20 μm
  - Cylindrical coordinates and transient condition.
- Internal generation of the heating wire (red) section: 2.387 × 10^9 W/m^3, simulating *3 W/m* for the heating power of the actual wire.
- Model height: 40 μm or two cells high.
- Minimum radius of the medium (blue) section: 30,000 μm to simulate the infinite medium condition. (See Appendix A.5 for more details)
- Calculation setup: transient condition, start: 0 *s*, stop: 120 *s*, step: 0.01 *s*, solution method: Crank-Nicolson. Various small time steps were considered and their results are shown in Table 4.2. Although FEHT suggests using a smaller time step than the critical step time of 2×10^{-9} *s* based on the mesh of the model, it can be seen, from Table 4.2, that even if the step time is increased by three orders of magnitude (10^{-5} *s* vs. 0.01*s*), the results are within 0.06% difference after 0.10*s*. Because of limitations of time and computer power, the time step of 0.01*s* is deemed to be a suitable choice with enough accuracy for the present study.

Table 4.2. Simulated temperature rise (ºC) ΔT at the sensor location (r_{sen} = 275µm) by FEHT for different time steps at different times

TIME	TIME STEPS							
	10^{-5} s	10^{-4} s	3.125×10^{-3} s	1.25 ×10^{-3}s	2.50×10^{-3} s	5.0×10^{-3} s	0.01s	0.02s
0.02s	0.00838	0.00834	0.00834	0.00832	0.00828	0.00808	0.00804	0.00894
0.04s	0.05004	0.05004	0.05004	0.05003	0.04999	0.04984	0.04920	0.04448
0.10s	0.18773	0.18773	0.18773	0.18774	0.18774	0.18775	0.18783	0.18762
0.50s	0.52615	0.52615	0.52615	0.52615	0.52615	0.52616	0.52617	0.52620
1.0s	0.70080	0.70080	0.70080	0.70080	0.70080	0.70080	0.70080	0.70081
2.0s	0.90899	0.90899	0.90899	0.90899	0.90899	0.90899	0.90899	0.90899
5.0s	1.23413	1.23413	1.23413	1.23413	1.23413	1.23413	1.23413	1.23413
10s	1.51092	1.51092	1.51092	1.51092	1.51092	1.51092	1.51092	1.51092

The temperature responses in this chapter are taken from a point at a node inside the epoxy layer. The schematic of the cross section area where the thermocouple stays is shown in Fig. 4.3. The intersections of the white circle (representing the thermocouple) and the dashed line (representing a sample temperature profile) can be used to assign to the temperature responses. There are some differences at the intersection points. As a result of safety and accuracy, the average of the temperatures at the two points is assumed to be the temperature at the center of the white circle or the thermocouple. The center of the white circle can be treated as a node in the mesh of the FEHT models whose representative is shown in Fig. 4.2.

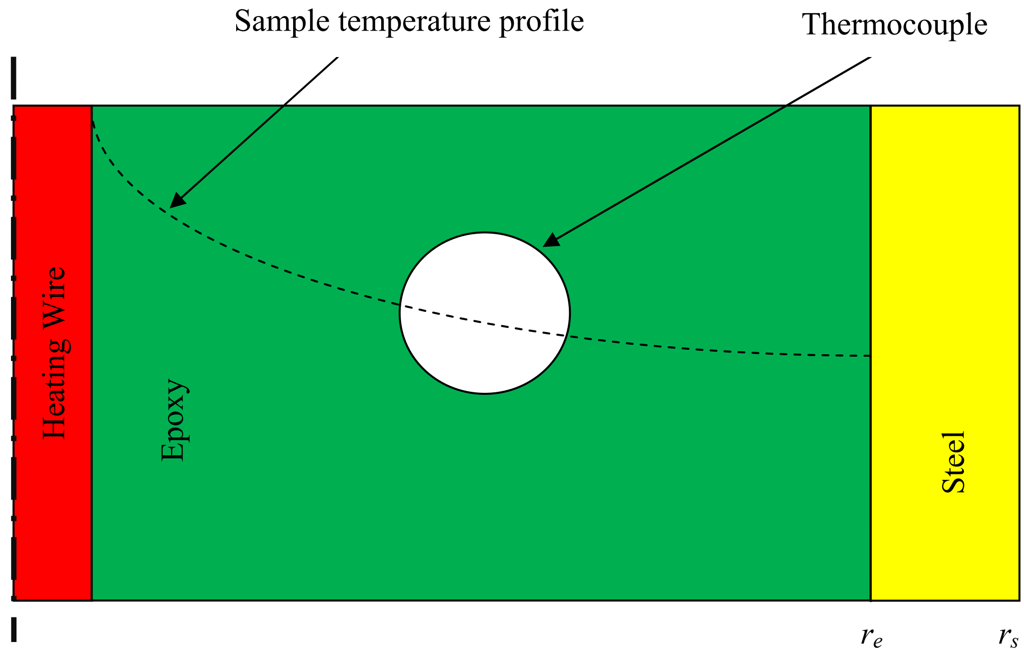

Figure 4.3. Schematic drawing of the temperature response across the epoxy layer. (Picture not to scale).

4.3 - Comparisons of Heat Transfer Models

In this Section, the following parameters are explored: r_{sen}, r_e, r_s, k_e, k_s, k_m, α_e, α_s, α_m in Eqs. 1 and 2 of Chapter 3. The effects of *Fo* (Fourier number as defined in Section 3.5) can be seen through the simulation time *t*. Although not shown in dimensionless forms, the figures in this Section are illustrated in the equivalent dimensional forms.

As shown in Fig. 4.4, when the numerical solution given by FEHT is compared with the analytical solutions of Eqs. 1 and 2, it is found that Eq. 2 yields a closer fit. The predicted and simulated temperatures at $r = r_{sen}$ are being compared here, and the errors are calculated as:

$$\%Error = \left(\frac{T_{Eq} - T_{FEHT}}{T_{FEHT}} \right) \times 100 \qquad (4.1)$$

The error of using the classical solution (Eq. 1) produces about 1.69% error while Eq. 2 is about -0.003%.

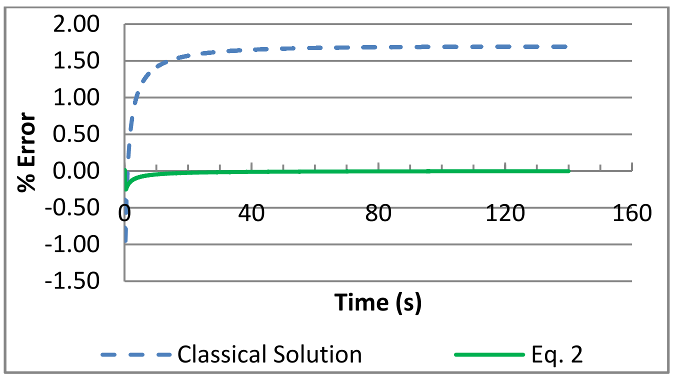

Figure 4.4. Comparison between the differences of using the classical solution and Eq. 2 with respect to FEHT.

Fig. 4.5 shows different diameter ratios (DR = r_e/r_s) of different probe sizes. The r_{sen} = 120 μm is used in this part of the study in order to have $r_{sen} < r_e$ for all cases, especially for the case of r_s = 275 μm with DR = 0.5. The reason for the chosen r_{sen} location is for better comparisons among different probe sizes. Changing the location of r_{sen} for different probe sizes does not have a fixed point to compare the temperature responses produced by Eq. 1, Eq. 2, and FEHT.

The results of Fig. 4.5 indicate that the bigger the probe size (r_s) becomes, the higher the errors appear for the classical solution (Fig. 4.5 a, c, and e). However, the errors can be reduced as much as 2.4 times if the DR increases from 0.5 to 0.9 for the same probe size. Eq. 2 also shows that smaller probe size gives much lower errors (at least 15 times lower) than those of using the classical solution, but the error levels off as the time increases (Fig. 4.5 b, d, and f).

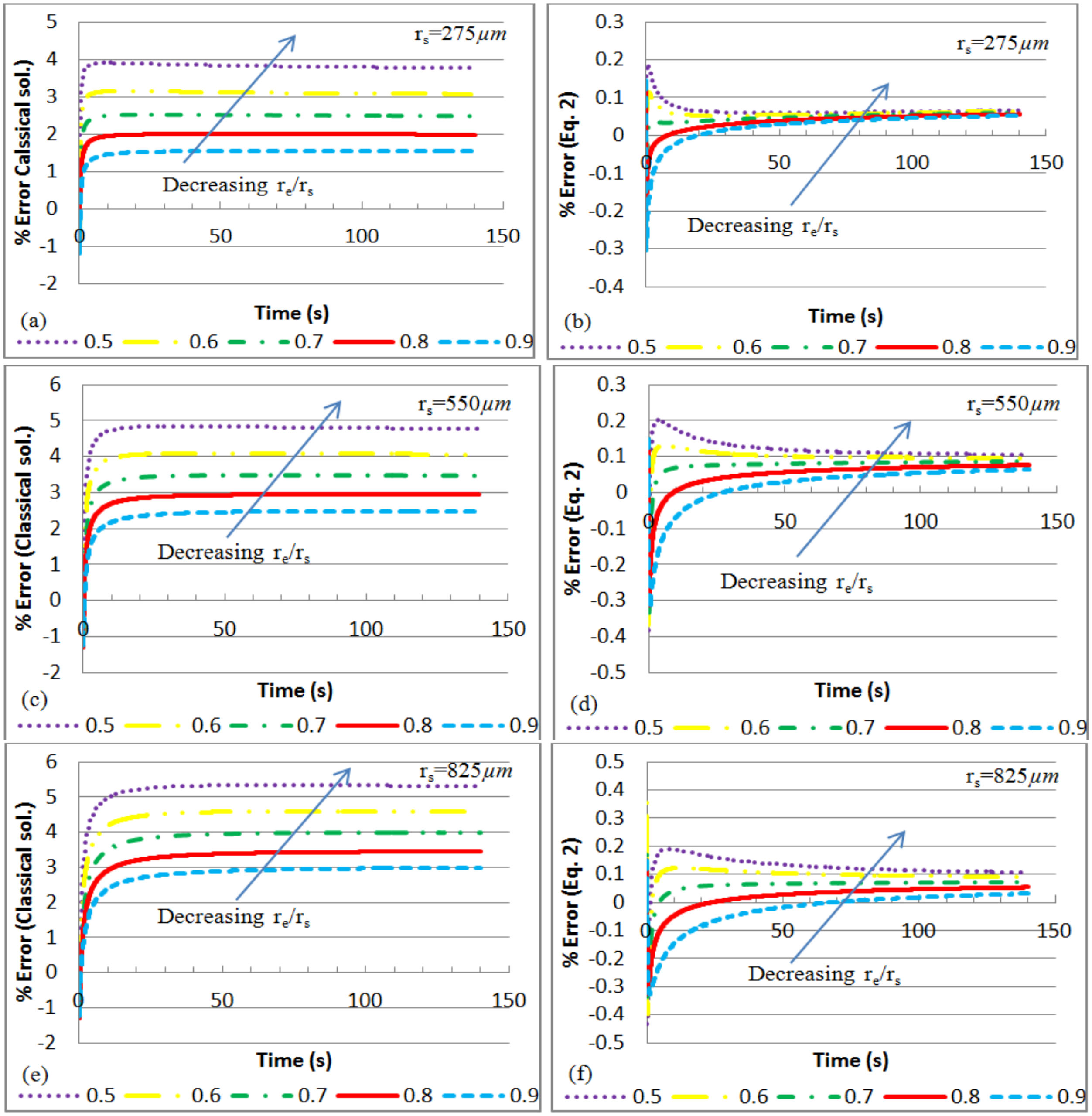

Figure 4.5. Comparisons of the classical solution and Eq. 2 with FEHT when different diameter ratios (DR = r_e/r_s) ($0.5 \le DR \le 0.9$) and different probe sizes (r_s) are used. (a) and (b): r_s = 275 μm. (c) and (d): r_s = 550 μm. (e) and (f): r_s = 825 μm

For all studied probe sizes in Fig. 4.5, the DRs produce almost the same errors (less than 0.1%) at large time (after 100 *s*) using Eq. 2. Unlike the classical solution, the spread of errors of Eq. 2 due to different DRs, depending on the probe size. The larger the probe size, the larger spread of errors among the DRs before they all level-off at large time. But they are still very small compared to the spread of errors of the classical solution. The case of DR = 0.9 appears to produce the lowest errors for all of the studied probe sizes. The finding about the increase in errors for a larger probe size agrees with Bristow *et al.* [19] and Murakami *et al.* [23]. The reason stays in the values of k_e and α_e. The values of k_e and α_e are closer to the values of k_m and α_m more than the values of k_s and α_s are. As a result, the heat propagation phenomenon are more similar to that of the sampling medium if the layer of epoxy is larger and the layer of steel is smaller; thus, making the assumption of line heat source in the classical solution becomes more accurate, leading to smaller error when larger DR is considered. Therefore, the classical solution and Eq. 2 can better estimate the temperature response of the TCP with higher DRs of the TCP. In addition, due to the thermal capacitance of the probe, Eq. 2 can predict the temperature response much more accurately than the classical solution.

Further analyzing the errors resulted from the classical solution (Eq. 1) and Eq. 2 leads to the results in Fig. 4.6, which shows their errors as compared to the results by FEHT for different heating powers. Except for the heating power, the values of other parameters remain the same as those tabulated in Table 4.1. The figure indicates that as the heating power increases, the less accurate both Eqs. 1 and 2 can predict the temperatures rise simulated by FEHT. For higher heating power, the classical solution gives higher errors, which are about 4.65%, 3.04%, 1.69%, and 0.94% for 12 W/m, 6.0W/m, 3.0W/m, and 1.5W/m respectively. However, the errors of using Eq. 2 for different heating powers are almost the same (about 0.06%) and much lower than those of the classical solution (from 0.48% to 4.65%).

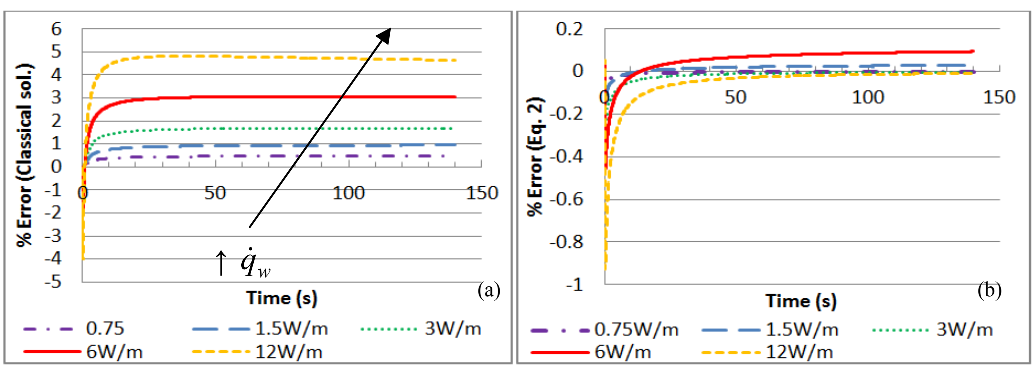

Figure 4.6. Comparison of different heating powers.

Fig. 4.7 illustrates the errors associated with the use of classical solutions and Eq. 2 for different values of k_m while α_m remains constant. The figure indicates that as the medium being measured is less heat conductive (or behaves more like a thermal insulator), the error increases. The error can range from 21% to less than 0.05% depending on which equation is used and how heat conductive the sampling medium is. When k_m and k_e are similar, both equations have small errors. Also, the results from Fig. 4.7 further confirm the findings of Elustondo *et al.* [34] that when the differences in thermal conductivities between the TCP and the sampling medium are large, the error increases. However, the error for k_m being smaller than k_e is much more prominent than that for k_m being larger than k_e.

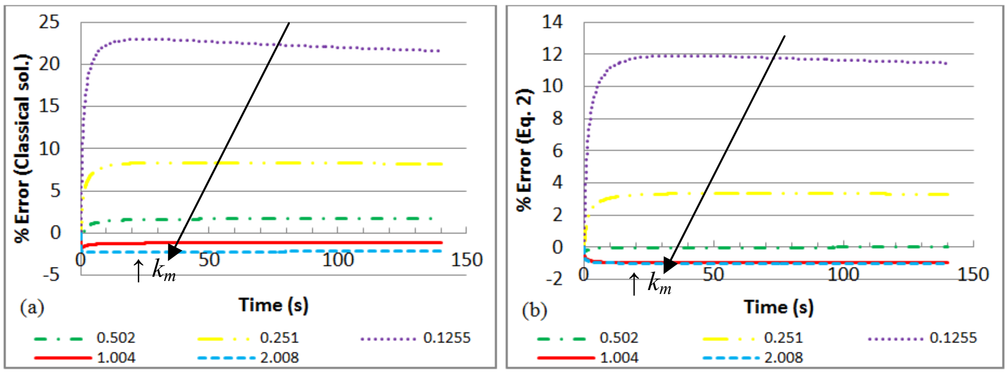

Figure 4.7. Comparisons of different k_m while α_m is kept constant. Legend shows the thermal conductivity of the sampling medium (k_m) (W/m·K).

Fig. 4.8 displays the errors of using Eq. 1 and Eq. 2 in comparison with FEHT's temperature output. The parameters in Table 4.1 are kept constant except for α_m, thermal diffusivity of the sampling medium. Also, as time increases, the errors of having different α_m converge at large time (> 120 *s*) for both Eqs. 1 and 2. In other words, the thermal diffusivity of the sampling medium theoretically does not have strong effects in the temperature output as compared to k_m in Fig. 4.7. Also, using Eq. 2, the errors from different α_m are almost zero and much less than those using Eq. 1.

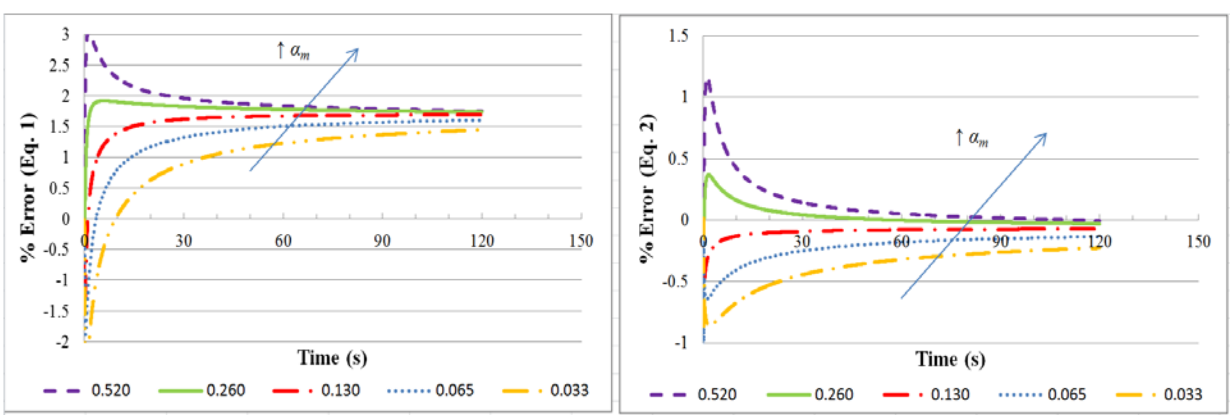

Figure 4.8. Percentage error vs time with different α_m values shown in the legend (mm^2/s).

Fig. 4.9 illustrates the errors of Eqs. 1 and 2 in comparison with FEHT when only k_e and k_s change. The legend shows the thermal conductivity ratios *(k_e/k_s)*. As k_s increases within each equation, the error becomes bigger. This effect further strengthens the conclusions of Elustondo *et al.* [34] and Fig. 4.5 that errors grow when the k and α of TCP's construction materials are very different from those of the sampling medium. Once again, the results of Eq. 2 are closer to the results of FEHT than those of Eq. 1.

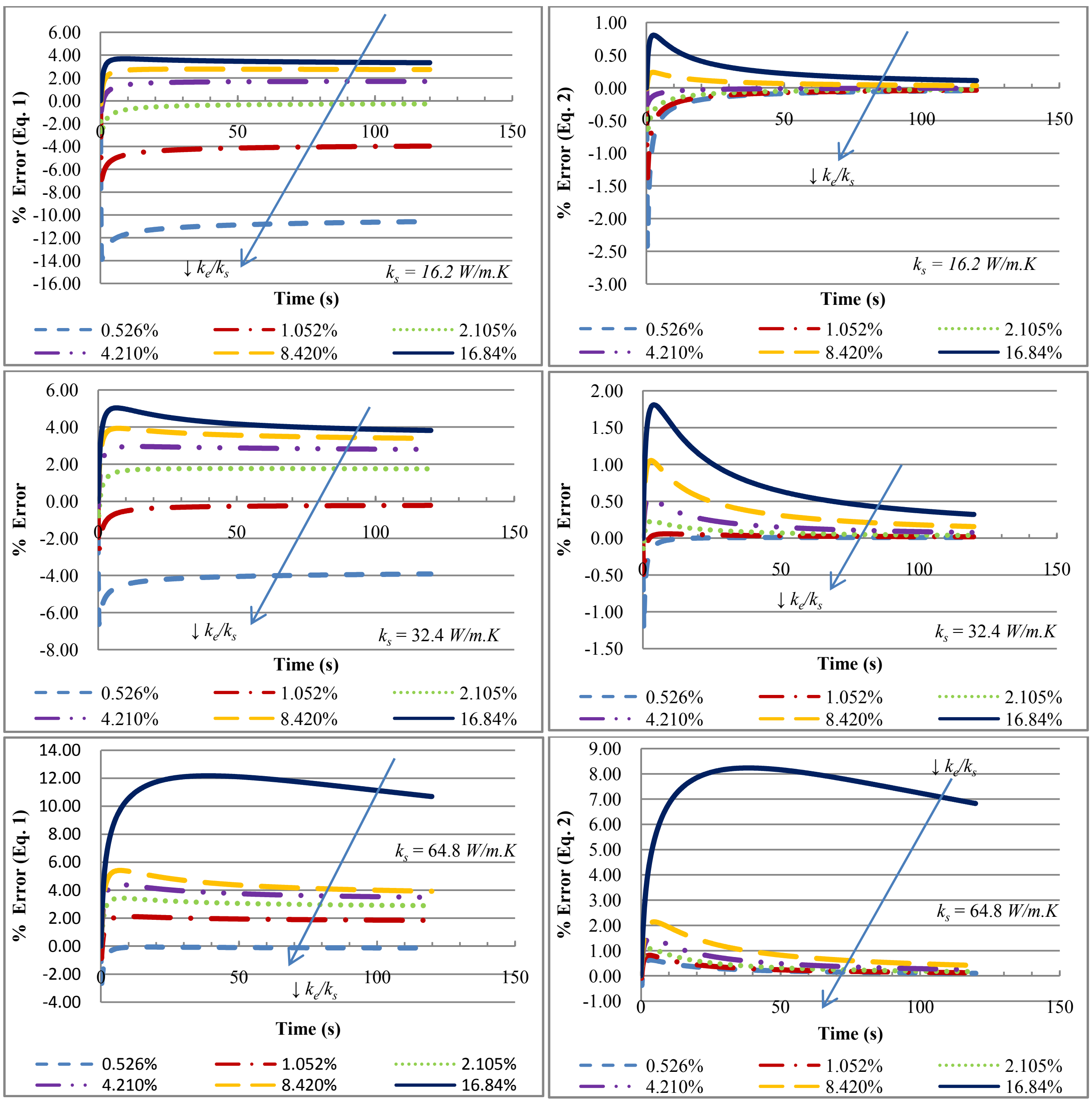

Figure 4.9. Errors between the equations and FEHT for different thermal conductivity ratios (k_e/k_s) when the thermal conductivities of the probe's materials are changed. The thermal diffusivities of the probe's materials remain constant.

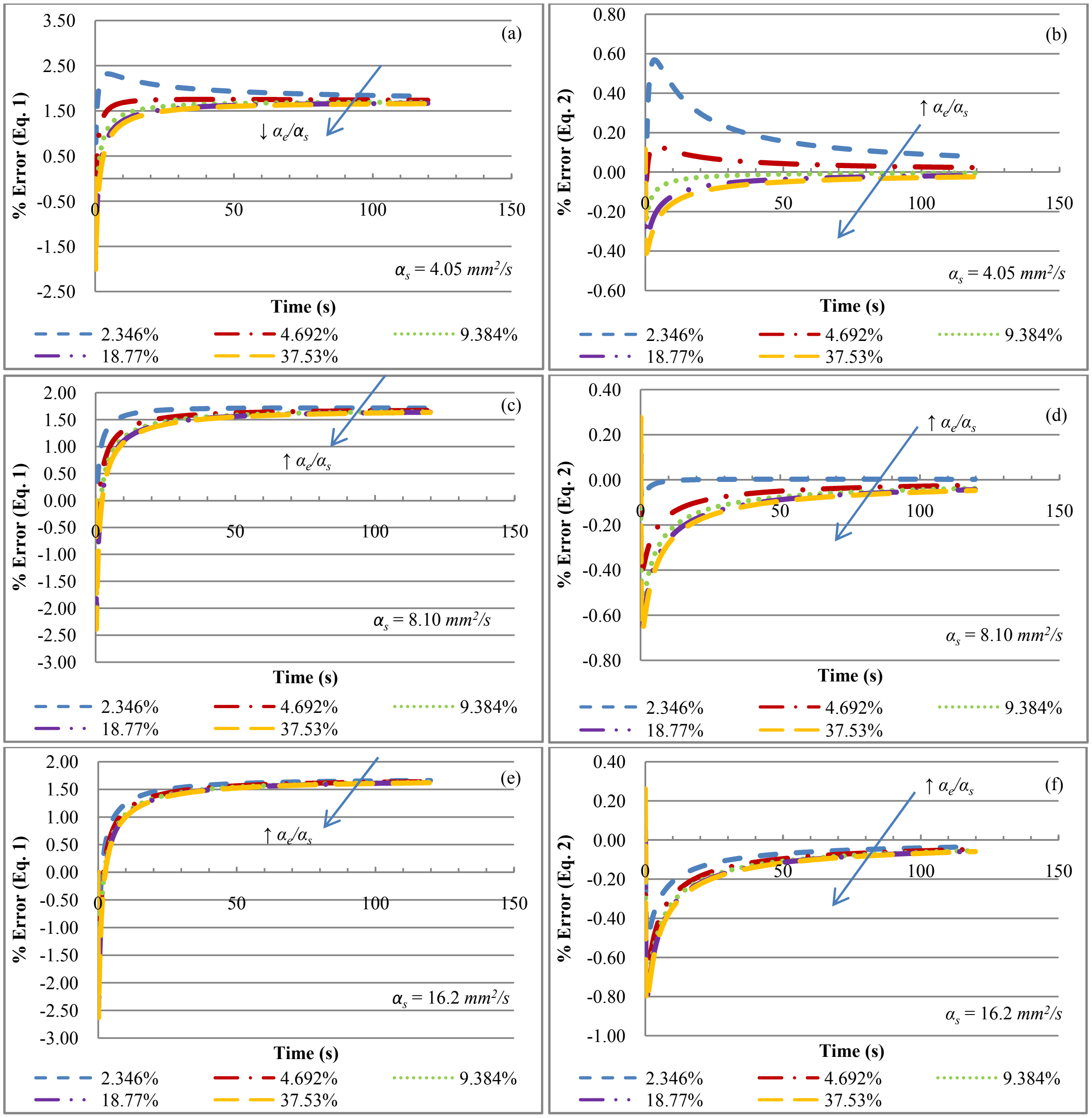

Figure 4.10. Errors between the equations and FEHT for different thermal diffusivity ratios (α_e/α_s) when the thermal diffusivities of the probe's construction materials are changed. (a) and (b): α_s = 4.05 mm^2/s. (c) and (d): α_s = 8.10 mm^2/s. (e) and (f): α_s = 16.2 mm^2/s.

Figure 4.10 shows the errors of Eqs. 1 and 2 in comparison with FEHT when the thermal diffusivities of the TCP's construction materials are changed but the thermal conductivities of the materials remain constant. Other properties of the sampling medium and TCP are in Table 4.1. As one can see from Fig. 4.10, the thermal diffusivity of the construction materials have small effects to the temperature prediction of Eq. 1 when the temperature predictions are compared to those from FEHT, *i.e.*, when the time is sufficiently long enough, the errors from both equations remain almost constant regardless how α_e and α_s change.

Fig. 4.11 shows the errors of using Eqs. 1 and 2 when different r_{sen} is positioned within the epoxy layer. The legend shows the thermocouple location (r_{sen}) while the height level of r_{sen} remains constant. Fig. 4.11a shows that as the location of the thermocouple r_{sen} is further away from the central axis of the TCP, Eq. 1 becomes more accurate. Combining this result with Fig. 4.6a shows that when seeing more intense heat from the heating wire (due to either higher heating power or closer to the heating wire), the thermocouple will theoretically measureless accurately according to Eq. 1. However, according to Eq. 2, the location of the thermocouple has theoretically slight dependences on the heating power of the heating wire or the location of the thermocouple as shown in Figs. 4.6b and 4.11b. Also, Eq. 1 over estimates the temperature rise while Eq. 2 slightly underestimates the thermal response.

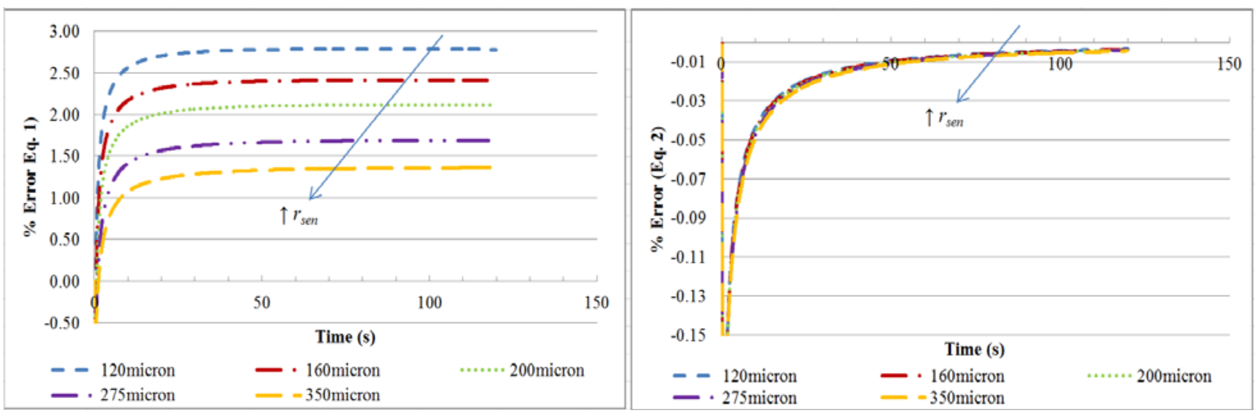

Figure 4.11. Errors of using Eqs. 1 and 2 when r_{sen} is varied. Height level of r_{sen} is constant.

4.4 - COMSOL Analysis

A TCP inserted into a cylindrical sampling medium is modeled using COMSOL, as shown in Figs. 4.12 and 4.17 for adiabatic and isothermal boundary conditions respectively. The glowing part in the axial center is the TCP heated by a very fine heating wire. The material properties and dimensions used for the COMSOL model are from Table 4.1. Also, the cylindrical sampling medium is Ø60 *mm* × 80 *mm* to ensure that the radial infinite medium condition is achieved during the heating period of the TCP whose theoretical dimensions are Ø1.10 *mm* × 50.0 *mm*. In this Section, two cases are investigated: adiabatic boundaries and isothermal boundaries. The axial heat conduction will be investigated and compared with the results of Blackwell [39].

4.4.1 - Adiabatic boundaries

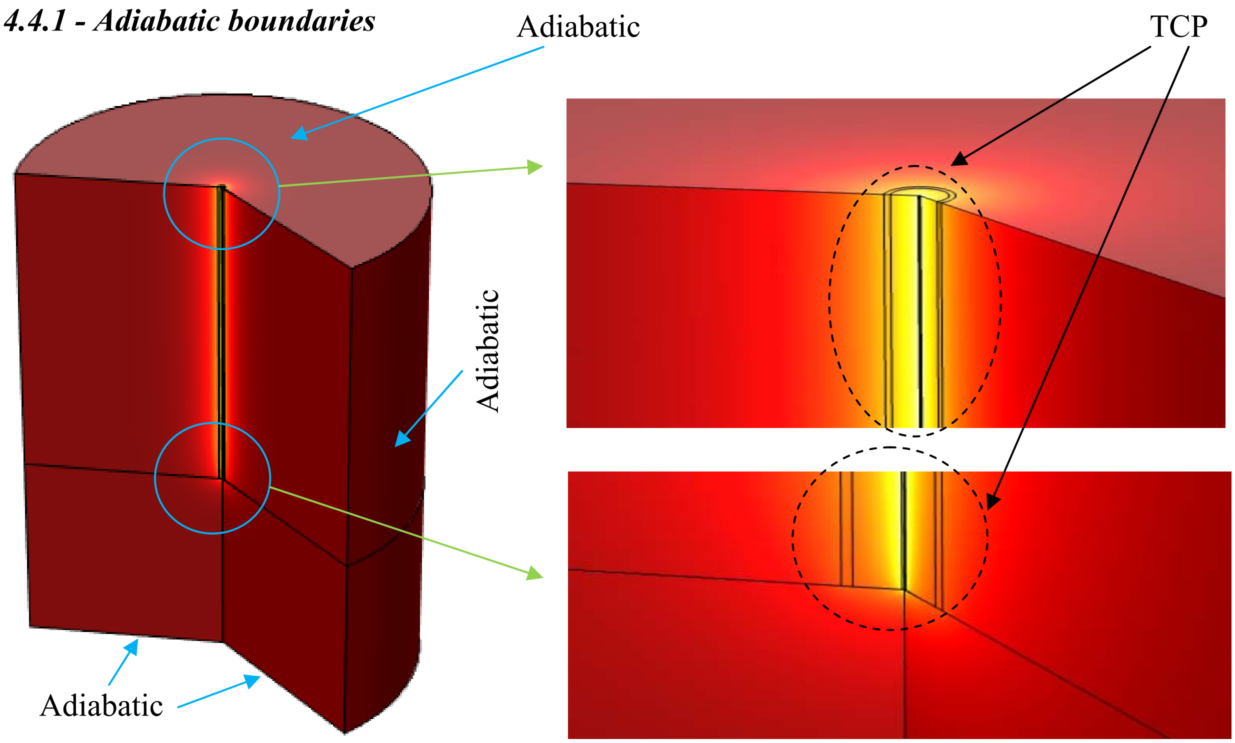

Figure 4.12. COMSOL model of how TCP is inserted into sampling medium (80mm high). Clockwise from left: overall model, closer look at TCP top, and closer look at TCP bottom.

Because of the drawing limitations in COMSOL, the infinite medium is broken into two cylindrical parts bordering the TCP, as shown in Fig. 4.12. Moreover, in order to run simulations with the COMSOL model, the following conditions are used:

1. Mesh: "Extremely fine Predefined" and "Free Triangular" as in Fig. 4.13
2. Study: time dependent (or transient)
3. Simulation time: 120 *s* with 0.01 *s* time step which is shown to be justifiable by Fig. 4.14
4. Pure conduction and perfect contact at the TCP-medium interface
5. Boundary conditions: adiabatic

The COMSOL study in this Section is "qualitative", *i.e.*, the mesh size and shape are reasonably chosen. The reason is that the size of the sampling medium is so much larger than the TCP's, so finer and more sophisticated meshes can take a long time to run simulations.

The heating powers used are 3 *W/m* and 10 *W/m* (or heat sources are 2.387×10^9 W/m^3 and 7.958×10^9 W/m^3 respectively) to study the temperature rise of r_{sen} when r_{sen} is varied along the axial and radial directions of the TCP. The bottom of the TCP is defined as $h = 0$ *mm*. The results of the temperatures at different heights with the same radial location are shown in Fig. 4.14 ($h >$ 0 *mm*). The equation used for the Temperature Difference (TD) axis of Fig. 4.14 is:

$$TD = T(r_{sen}, h_i) - T(r_{sen}, h = 25mm) \tag{4.2}$$

where h_i is the height of the thermocouple at the same radius of 275 μm.

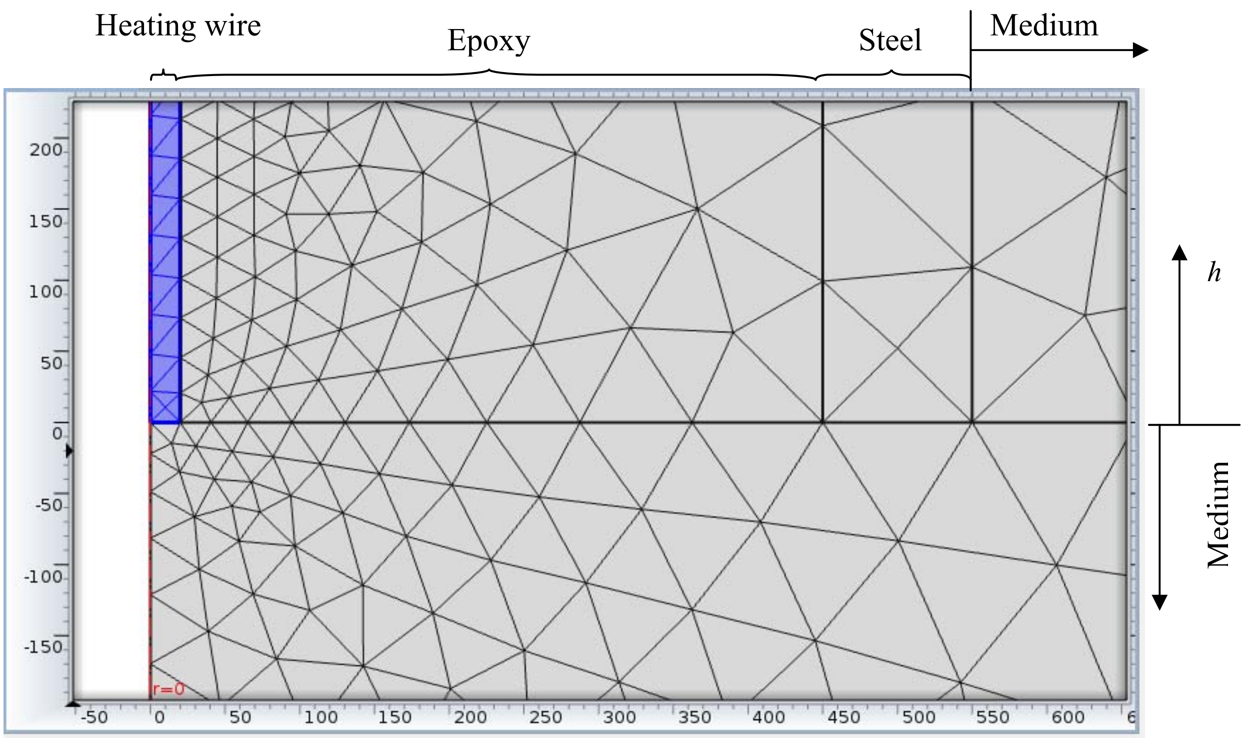

Figure 4.13. Mesh used in COMSOL model. Numerical values are in µm.

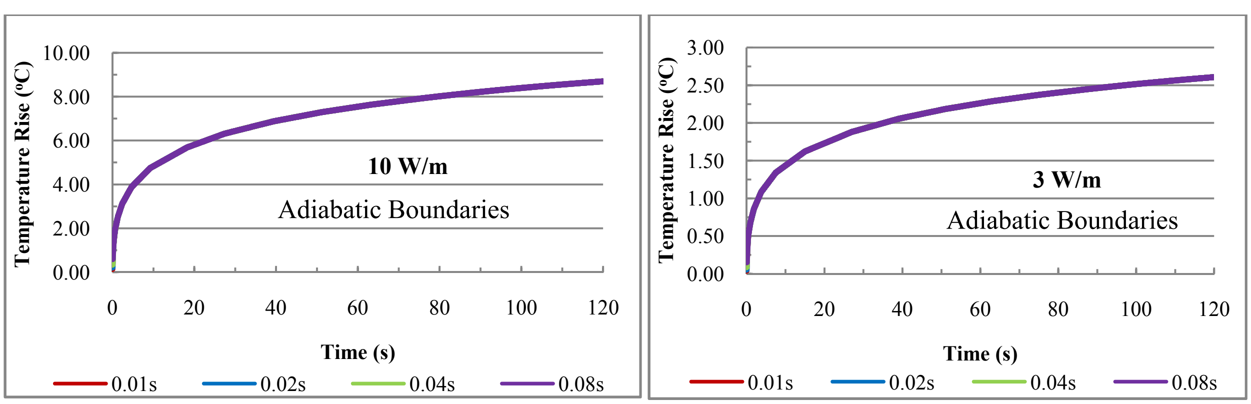

Figure 4.14. Temperature rise vs. time at r_{sen} = 275 µm with different time steps.

Figs. 4.12 and 4.14 indicate that axial heat conduction does exist. The more the TCP is heated (*i.e.*, higher heating power), the more different the axial temperatures along the TCP become. Figs. 4.14b and 4.14d show very slight variations of temperature differences (up to 0.00065°C) at various height levels along the TCP. The variations might have resulted from the "qualitative" mesh used. However, it is not until less than 12 *mm* above the bottom of the TCP that the temperature differences become about 0.1°C or greater (Figs. 4.14a, and 4.14c). Consequently, the axial position of the thermocouple can be placed within ±5 *mm* of the TCP's centroid (at h = 25 *mm*) so that the temperature difference is practically negligible, *i.e.*, TD < 0.001°C.

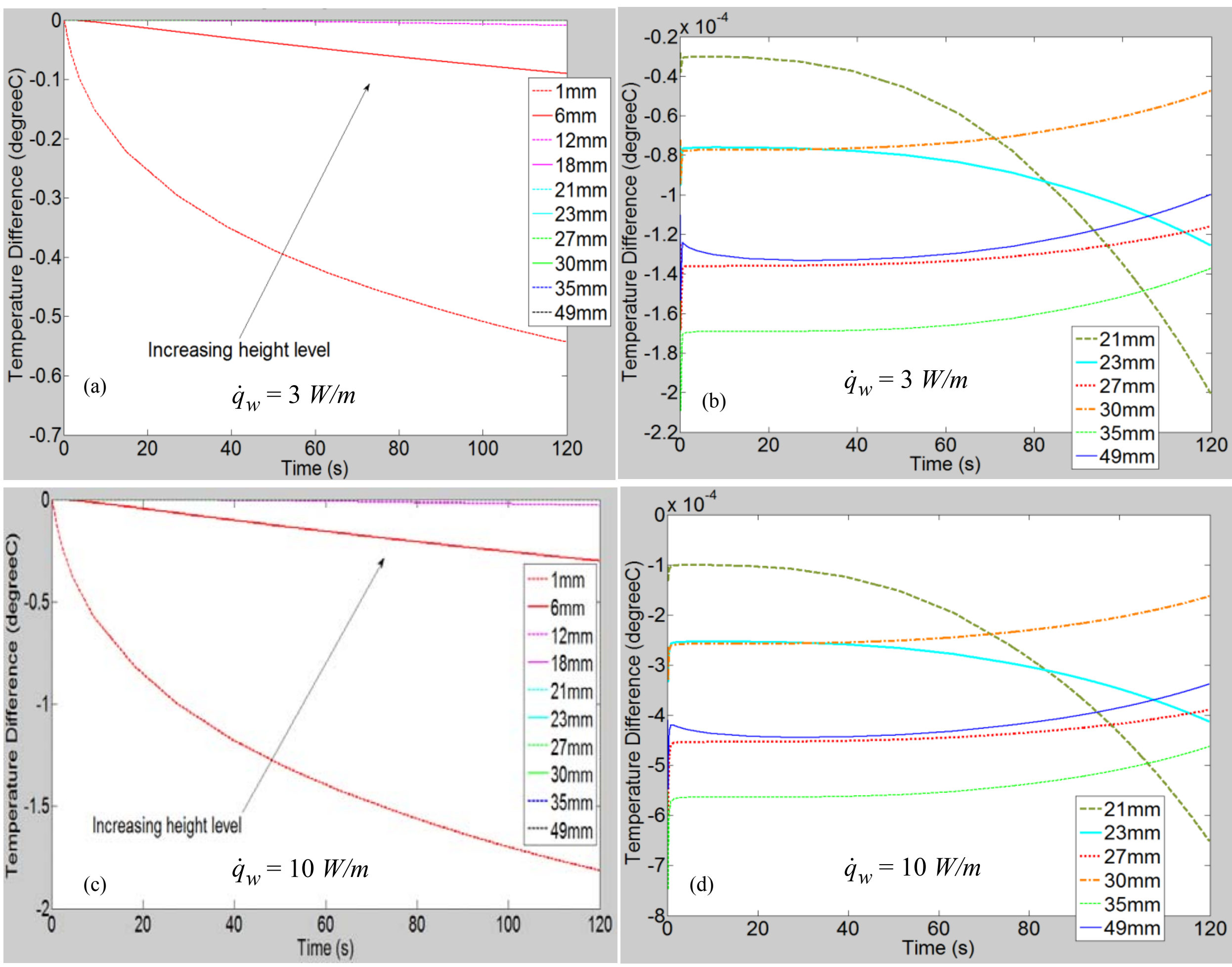

Figure 4.15. Adiabatic boundaries: temperature difference between r_{sen} at different heights and r_{sen} at the height of 25 mm. Probe length is 50 mm. (a) and (c): for heights of 1 mm - 49 mm with $\dot{q}_w$ of 3 W/m and 10 W/m respectively. (b) and (d): for heights of 21 mm - 49 mm with $\dot{q}_w$ of 3 W/m and 10 W/m respectively.

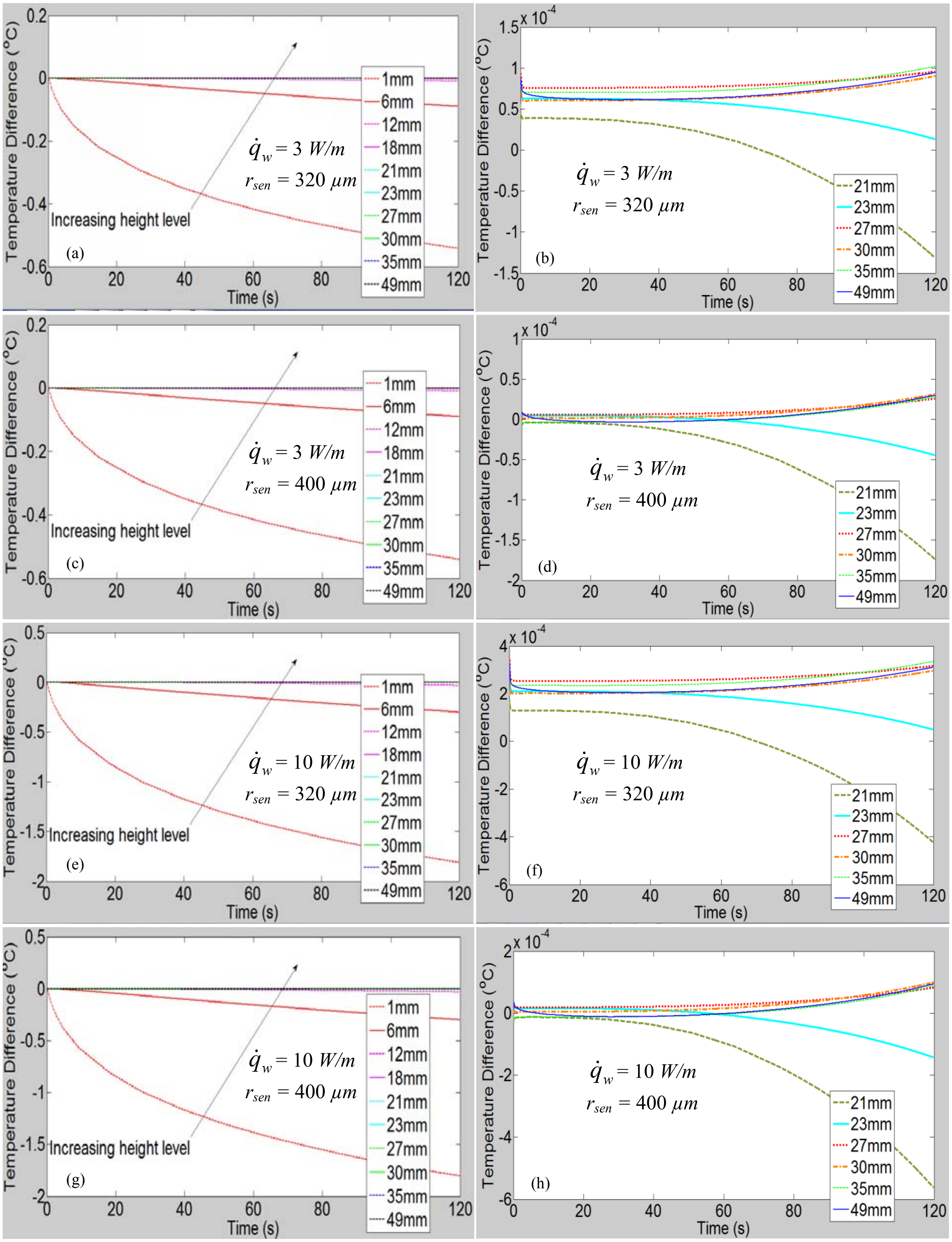

Figure. 4.16. Temperature Difference vs. time of various heating powers and r_{sen}. (a), (c), (e), and (f): for heights from 1 mm - 49 mm. (b), (d), (f), and (h): for heights from 21 mm - 49 mm.

In order to better learn how the location of the thermocouple can affect the temperature output, Fig. 4.16 is made with various heating powers, and radial and axial distances. The temperature rises at various heights and heating powers are compared with the corresponding temperature rise at h = 25 mm. For example, Fig. 4.16a shows the same $\dot{q}_w$ of 3 W/m and r_{sen} = 320 μm but the height of the thermocouple is changed from 1 mm to 49 mm. The vertical axis of Fig. 4.16a is the temperature difference (TD) using Eq. 4.2.

As shown in Fig. 4.16, if the thermocouple is radially further away from the heating wire, TD is less. When Figs. 4.15b, 4.16b, and 4.16d are combined together, one can observe that TD is reducing. When r_{sen} (or the position of the thermocouple) is radially further away from the heating wire, the TDs are lower. The same trends can be seen from Figs. 4.15d, 4.16f, and 4.16h. Moreover, from Figs. 4.15 and 4.16, it can be seen that for heights more than 25 mm, their TDs are slightly different. This suggests that when a TCP is about to be manufactured, the thermocouple should be placed (preferably within 5 mm) above the TCP centroid in the axial direction, *i.e.*, further away from the bottom of the TCP if the top of TCP is adiabatic.

4.4.2 - Isothermal boundaries

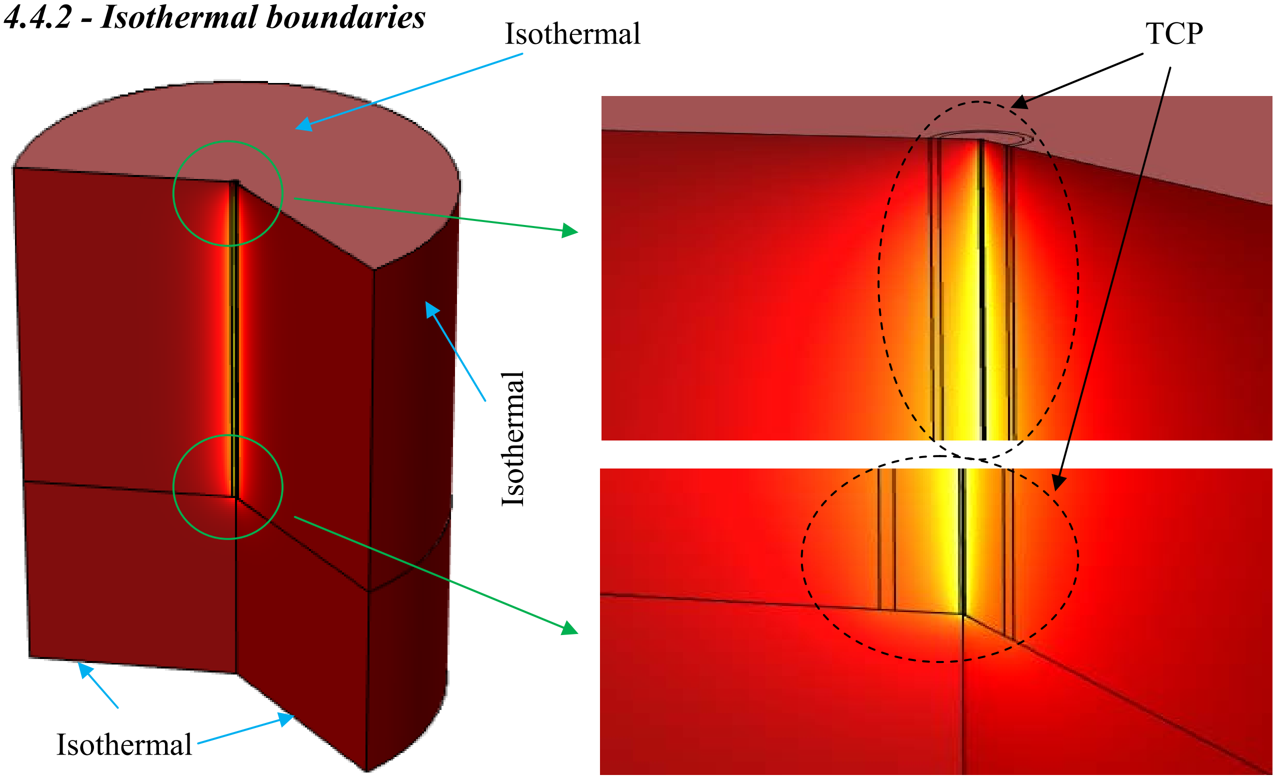

Figure 4.17. COMSOL model (isothermal boundaries at 20°C) of how TCP is inserted into sampling medium. Clockwise from left: overall model, closer look at TCP top and bottom.

In this Subsection, the simulation setups, inputs and steps are the same as those in Subsection 4.4.1 except for the boundary conditions. The outermost surfaces of the cylinder shown in Fig. 4.17 are set at the constant temperature of 20°C during the heating duration. Temperature rise convergence is shown in Fig. 4.19.

Fig. 4.18 shows the TD vs. time in the case of isothermal boundaries. At the height of 49 *mm*, the TD is highest for all of the heating powers applied. Also, the higher the heating power is, the larger the TD becomes, which is similar to the influence of $\dot{q}_w$ in Fig. 4.15. However, the TDs at the heights of 23 *mm* and 27 *mm* are very small and significantly less than those at heights further away from the TCP centroid. Also, the temperature at the height of 23 *mm* is closest to that at the centroid. Comparing Figs. 4.15 and 4.18, one can note that the TD is least (<0.001°C) within ±2 *mm* height from the TCP centroid (at h = 25 *mm*) for the case of isothermal boundaries. Therefore, to be conservative, the thermocouple should be placed axially within ±2 *mm* of the TCP centroid and radially further away from the heating wire.

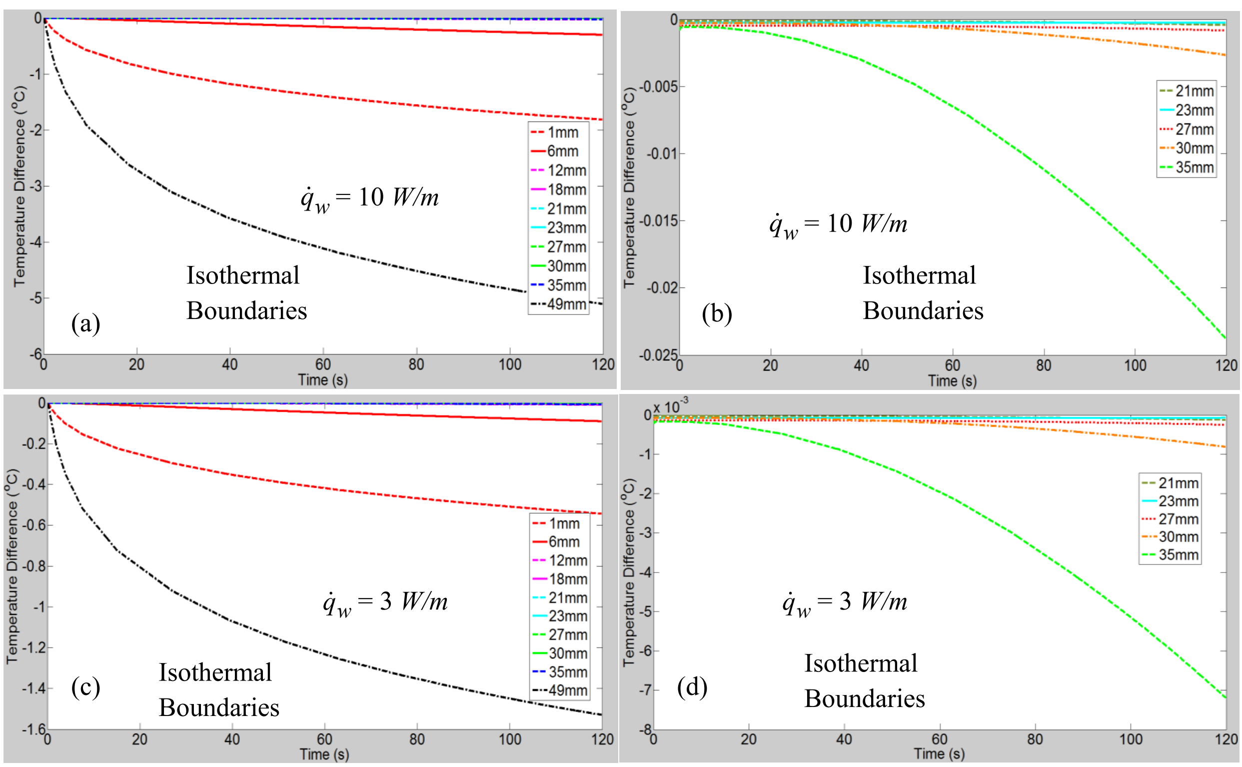

Figure 4.18. Isothermal boundaries: temperature difference between r_{sen} at different heights and r_{sen} at the height of 25 mm. Probe length is 50 mm. (a) and (c): for heights of 1 mm - 49 mm with $\dot{q}_w$ of 10 W/m and 3 W/m respectively. (b) and (d): for heights of 21 mm - 49 mm with $\dot{q}_w$ of 10 W/m and 3 W/m respectively.

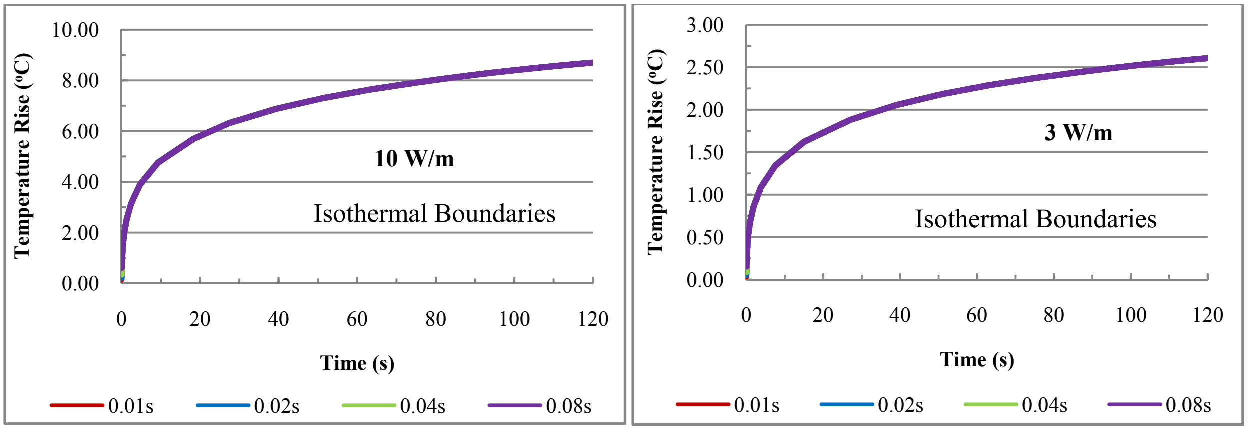

Figure 4.19. Temperature rise vs. time at r_{sen} = 275 μm with different time steps.

In order to explore the effects of varying the radial location of the thermocouple, Fig. 4.20 is plotted against time with heating powers of 3 *W/m* and 10 *W/m*. The legend shows the thermocouple axial locations. From Fig. 4.20, the temperature variations at the same axial height are not much when the thermocouple are radially moved further away from the heating wire. However, the temperature differences are much more significant along the TCP axis at the same radial position. In other words, being different from the case of adiabatic conditions, the temperature response does not vary much when the thermocouple is moved further away from the TCP axis. Meanwhile, the temperature difference is almost constant when the thermocouple is radially moved further away from the TCP axis. As a result, in the case of isothermal boundaries, the thermocouple can be put at any radial location and the temperature differences among various radiuses are almost the same. When this result is combined with Fig. 4.11, the location of the thermocouple does not cause significant errors to the temperature response in the radial direction. On the other hand, in the case of adiabatic boundaries, the further the thermal sensor radially goes away from the TCP axis, the less the temperature difference turns various. In order to investigate whether the axial heat conduction can cause significant errors, the next Subsection is discussed.

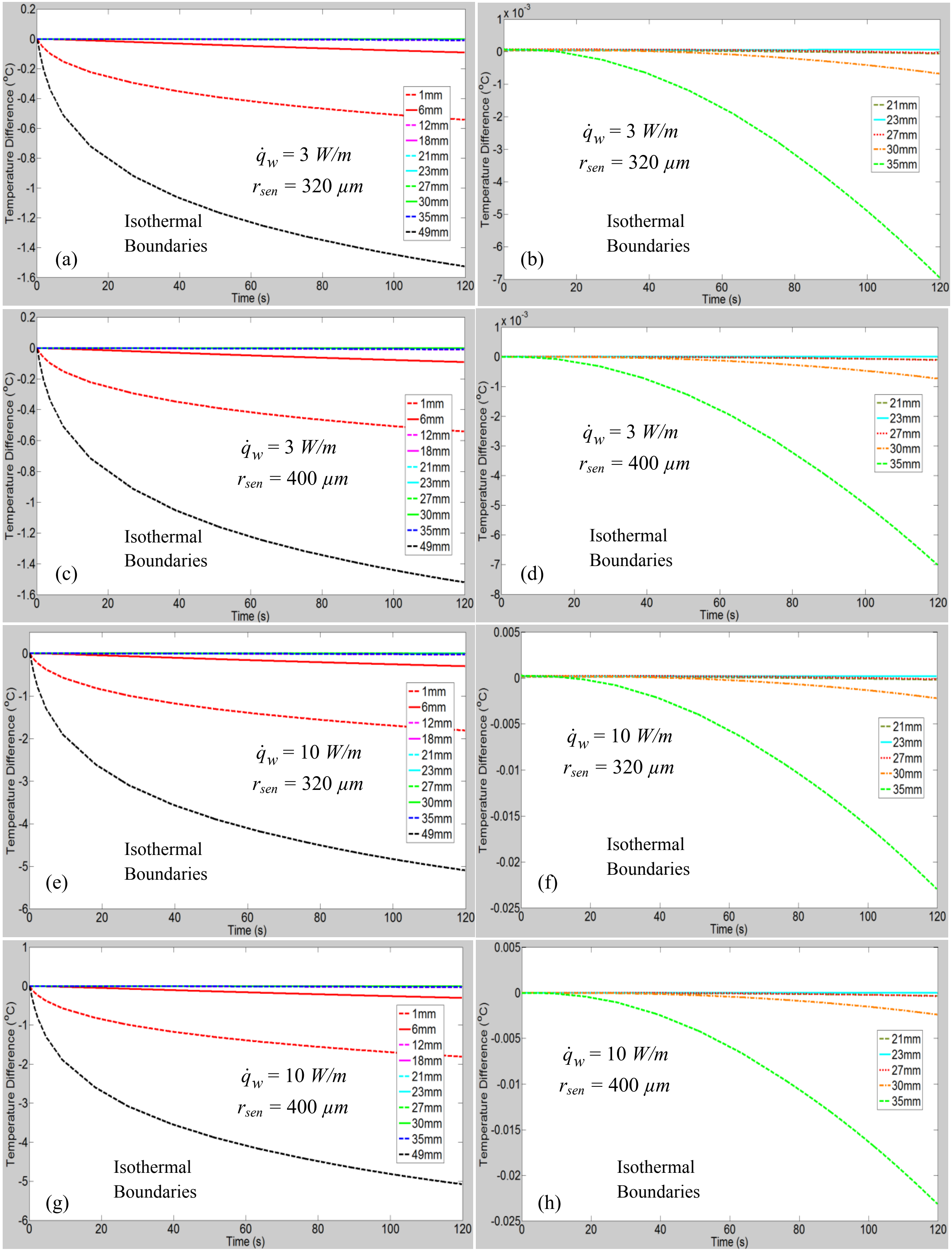

Figure. 4.20. Temperature Difference vs. time of various of heating powers and r_{sen}. (a), (c), (e), and (f): for heights from 1 mm - 49 mm. (b), (d), (f), and (h): for heights from 21 mm - 49 mm.

4.4.3 - The effects of axial heat conduction

In the derivation of Eq. 1, Carslaw and Jaeger [16] ignored the heat conduction in the axial direction. However, in reality, the TCP is of cylindrical shape and may exhibit axial heat conduction. Blackwell [39] estimated that the axial heat flow error would be less than 0.05% for probes with length-to-diameter ratio more than 30, which is in good agreement with the results of Fig. 4.21.

Fig. 4.21 displays the heat flux ratio vs. time with different heating powers in the two cases (adiabatic boundaries and isothermal boundaries) at the TCP center (h = 25 mm). The heat flux ratio is defined as:

$$ratio_{HF} = \frac{q_{axial}}{q_{radial}} \approx \frac{\Delta T_{axial}}{\Delta h} \cdot \frac{\Delta r}{\Delta T_{radial}} \tag{4.3}$$

where HF means heat flux, q is the heat flux in a direction, ΔT_{axial} and ΔT_{raial} are the temperature differences (from COMSOL) between two points in the axial and radial directions respectively, Δh is the difference of the heights of the two points, and Δr is the difference of the radial locations of the two points.

When $\Delta h = \Delta r = 0.1$ μm, Eq. 4.3 becomes

$$ratio_{HF} \approx \frac{\Delta T_{axial}}{\Delta T_{radial}} \tag{4.4}$$

As the time is large (greater than 20 s) the heat flux ratio is constant at about 1.63×10^{-3}, which means that the axial heat conduction is about 0.163% of the radial one. Also, Fig. 4.21 indicates that the heating power and the boundary conditions examined have insignificant influences on the heat flux ratio. The ratio in the case of adiabatic boundaries levels off as time becomes larger whereas the ratio in the isothermal case gradually decreases as time passes. The reason for the difference of the curves is that the TCP is exposed to bi-directional thermal gradients in the axial direction for the isothermal boundary case. Meanwhile, for the case of adiabatic boundaries, the axial heat conduction has a unidirectional thermal gradient towards the bottom of the TCP. Consequently, the axial conduction decreases more in the isothermal case than in the adiabatic case. So the heat flux ratio gradually decreases with isothermal boundaries but levels off with adiabatic boundaries.

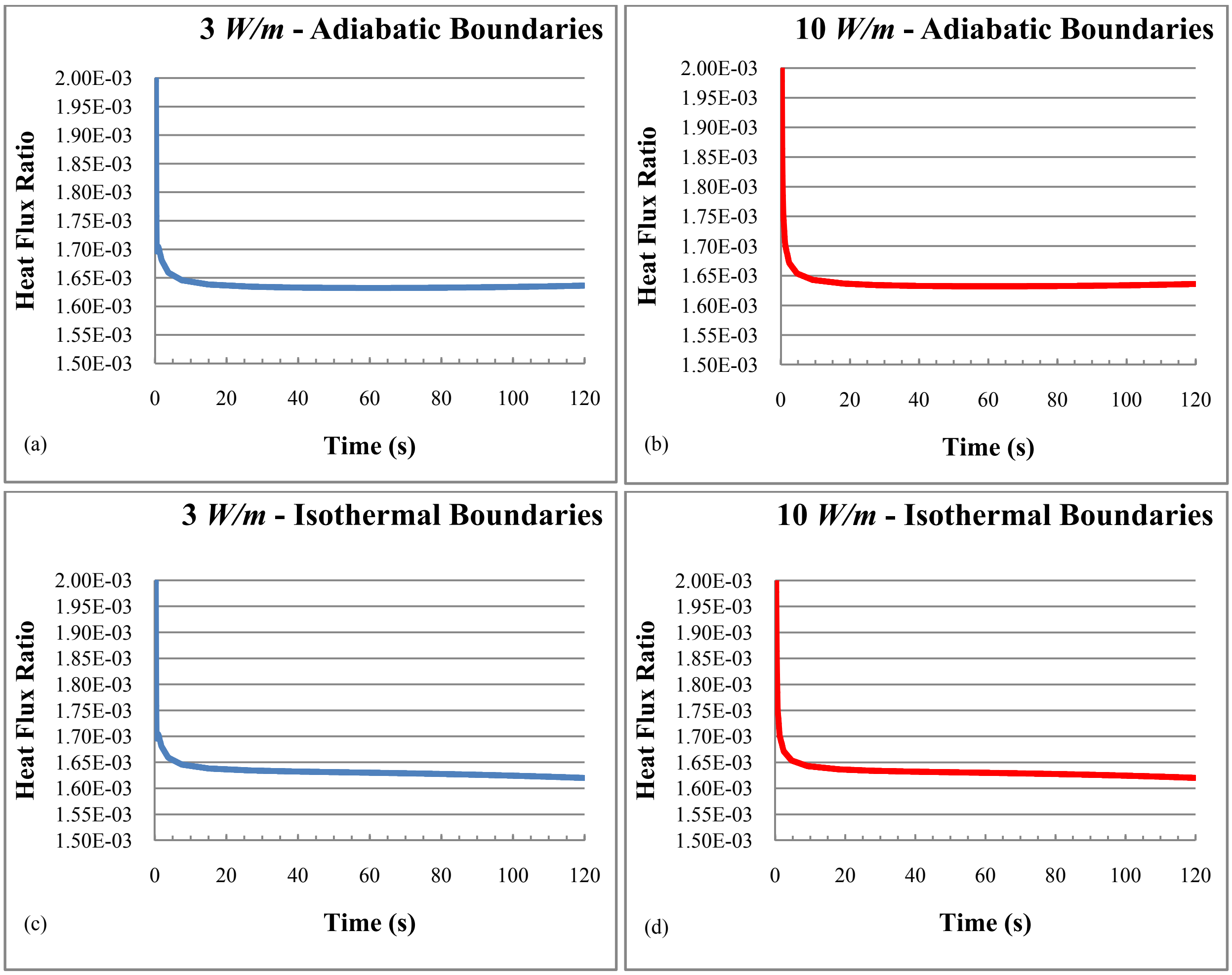

Figure 4.21. Heat flux ratio vs. time with different heating powers in the two case studies. (a) and (b): adiabatic boundaries. (c) and (d): isothermal boundaries.

Moreover, a look at the early time of 0.01 *s* (a time that most actual TCPs do not sense) shows that the heat flux ratio at that time is about 0.95% for all cases (adiabatic and isothermal) and heating powers. However, in most TCP experiments, the temperature response in the first 20 *s* is usually ignored. Therefore, with the length-to-diameter ratio of 45, the axial heat conduction can be ignored with an uncertainty of about 0.163%.

4.5 - Summary

This chapter theoretically and numerically compares Eq. 1 and Eq. 2 with numerical software packages FEHT and COMSOL using input parameters shown in Table 4.1. The comparisons demonstrate that Eq. 2 always agrees more with the numerical results than Eq. 1 does. In particular:

1. Larger TCP diameters produce higher errors. The reason is due to the difference in the materials and construction of the TCP. The more different the thermal properties of the TCP materials are, the less accurate the TCP can be. For example, when r_s = 275 μm, diameter ratio (DR = r_e/ r_s) of 0.5 produces about 3.8% error, but DR of 0.9 produces about 1.6% error using Eq. 1. With r_s = 825 μm and DR of 0.9, the error of using Eq. 1 is about 3%. However, the error of using Eq. 2 is significantly less than that of using Eq. 1. Although bigger TCP results in higher errors in Eq. 2, the errors converge to about 0.1% after long time (>160 *s*).
2. Heating power does affect the temperature prediction of Eq. 1. Higher $\dot{q}_w$ makes Eq. 1 less accurate theoretically. When the heating power is 0.75 *W/m*, Eq. 1 gives 0.5% error. Meanwhile, $\dot{q}_w$ = 12 *W/m* gives 4.8% error. On the other hand, by using Eq. 2, the error with different heating powers can be reduced to within ±0.1%.
3. When the sampling material is more heat resistant (lower k_m and α_m), the errors for predicting the temperature rise using Eqs. 1 and 2 grow. To be more precise, the thermal conductivity of the sampling medium plays an important role in the temperature prediction of Eqs. 1 and 2 while the thermal diffusivity of the sampling medium does not influence as much.
4. Changing k_e and k_s also affects the errors. As pointed out by Elustondo *et al.* [34], when the in-homogeneity among the materials of the TCP and the sampling medium becomes bigger, the measuring accuracy decreases. In other words, ignoring the construction of the TCP in Eq. 1 can be a big mistake, depending on what materials are used to make the TCP. Although Eq. 2 can lower the error by half of Eq. 1, the homogeneity of the TCP materials and sampling medium still plays an important role in the accuracy of the temperature predictions of both equations. To be more precise, the thermal conductivity of the materials are more important than the thermal diffusivity of the materials because

the errors are much more sensitive to the values of the thermal conductivity than to the values of the thermal diffusivity of the TCP materials, as shown in Figs. 4.9 and 4.10.

5. The location of the thermocouple can create errors in the temperature response by using Eq. 1. The closer to the heating wire the thermocouple is, the higher the error becomes. However, by using Eq. 2, the location of the thermocouple has small influences on the error as shown in Fig. 4.11.
6. The location of the thermocouple can affect the temperature readings. Depending on where the thermal sensor is placed inside the epoxy layer, the difference in the temperatures can vary significantly or slightly. The further away from the heating wire the thermocouple is placed, the less the temperature variation is in the axial direction as shown in Figs. 4.14 and 4.16. Moreover, by ignoring the axial heat conduction, one would get an error ranging from 0.16% to 1.0% with the length-to-diameter ratio of 45, which is in good agreement with Blackwell [39]. The researcher estimated that with the ratio of 30 or more, the axial heat flow error would be less than 0.05%. Moreover, it should be noted that the numerical results from COMSOL were obtained by using the parameters shown in Table 4.1. Other parameters may produce different results of the axial flow error.

CHAPTER 5 - TCP EXPERIMENTAL SETUPS AND PROCEDURES

In this chapter, the following experimental procedures and apparatus are discussed:

1. **TCP:**
   a) *Apparatus:* What were used during the TCP experiments are listed.
   b) *Sand sample preparations:* How C109 sand samples of different water contents were prepared before the samples were heated. Different moisture contents were 0.1, 0.2, 0.3, 0.5, 0.7, and 1.0 in terms of saturation ratio $\left(= \forall_{water} / \forall_{pore}\right)$.
   c) *Manufacturing of TCP:* How a TCP was made is described.
   d) *Experimental procedures:* How the sand samples and TCPs were put together is mentioned.
2. **Epoxy:**
   a) *Apparatus:* What were used during the epoxy experiment are listed.
   b) *Epoxy sample preparation:* How solid epoxy was made from liquid ingredients is described.
   c) *Experimental procedures:* How epoxy was tested is shown.

5.1 - TCP Measurement

Dr. Vlodek Tarnawski and his research staff at Saint Mary's University in Halifax, Nova Scotia, Canada spent a tremendous amount of their time and efforts producing careful experiments and useful experimental data which were sent to the author of this thesis to be analyzed. The results of the analysis is shown in Chapter 6. Section 5.1 is heavily based on the papers by Tarnawski *et al*. [11], [21], and [43].

5.1.1 - Apparatus for TCP measurements

The following equipment was used:

1. A forced air-convection oven (Memmert UE-500-AQ).
2. Manually manufactured TCPs (which are described in Subsection 5.1.5).
3. Two acrylic soil samplers.
4. A constant DC power supply (HP E3611A, Hewlett-Packard Development Co.).
5. Two data acquisition systems: DT-9802 (12 bit) and DT-9822 (24 bit).
6. DT Foundry 5.0 software package (Data Transition Inc.).
7. A 1.0 Ω (±0.001 Ω) precision resistor.

The DC power supply (HP E3611A, Hewlett-Packard Development Co.) provided a constant current (I) to the probe heater. Measuring time intervals for data records were set by the DT Foundry 5.0 software package (Data Transition Inc.). A 1.0 Ω (±0.001 Ω) precision resistor (R_{pr}) was used to serve as an electricity regulator and measuring tool across which the voltage change was usually set at 70±0.3 mV. The heater current (I) was calculated (by using $I = V_{pr}/ R_{pr}$) with an uncertainty of 0.4 mA. The data acquisition systems were used to record thermocouple electromotive force E (in μV) and to control the heating time.

5.1.2 - Dry Soil Sample Preparation [11]

Sand samples (C109 Ottawa sand) were packed into samplers made of an acrylic tube (Ø64 *mm* × 80 *mm*). The sampler size was chosen from the following relationship by de Vries and Peck [51] such that the heat flux through the sample boundaries is negligible when compared with the heat flux released by the TCP:

$$\exp\left(\frac{-r^2}{4\alpha_m \tau}\right) << 1 \tag{5.1}$$

where r is the radius of a cylindrical soil sample (0.032 m), α_m is the thermal diffusivity of dry C109 sand (~2.66×10^{-7} m^2/s for dry C109), and τ is the heating period (120 s).

Sand was compacted by repeatedly tapping the sampler's cylindrical surface. The total mass of the sand, for a specified volume, was measured. An acrylic plate with a concentric hole to insert the TCP handle was used to seal the sampler. During insertion, the TCP could wander off the intended position, so a TCP guide was placed on the top of the acrylic plate to ensure proper insertion and alignment between the TCP and the soil sampler's central axis (Fig. 5.1).

5.1.3 - Fully Saturated Soil Sample Preparation [43]

Woodside *et al*. [52] stated that preparation of fully saturated sand samples could be very hard because water could form layers on top of the specimen and prevent further penetration of water into the deeper content of the specimen. Consequently, highly scattered thermal conductivity data points were obtained [53]. Therefore, fully saturated sand samples were prepared carefully.

Compacting and saturating sand were carried out in a primary cylindrical cell with a closed-bottom acrylic tube (Ø64 *mm* × 70 *mm*) and a shorter cylinder of 20 *mm* length placed on the top. The tube and cylinder were joined and sealed along the contact edge using electrical pressure sensitive tapes. After that, for a certain volume of the primary cylinder, an estimated mass of sand (assumably dry bulk density), was added. Fully saturated sand was also compacted in the same way dry sand was. Because not all water was able to percolate down due to the presence of trapped air, the combined sample cell, with tested sand and water, was put in a laboratory exicator. The air in the exicator was depressurized down to between 1 *mmHg* to 10 *mmHg*. Consequently, trapped air was quickly removed and the water completely infiltrated the soil, which, as Baker [54] mentioned, provides an excellent uniformity of water distribution. Because water could boil while trapped air was removed from the sand, special care was made to prevent boiling by keeping air pressure in the exciator to be above the saturation pressure of water. Water was added and monitored after each air-removing process until the inter-particle volume (which initially contained air) was very close to the required water volume added. After that, the top cylinder was taken away and an acrylic lid was used to cover and seal the sample cell with a rubber splicing tape. Then, for proper vertical insertion of the TCP and alignment with the central axis of the sample cell, a TCP handle slide-way guide was attached to the sample cell cover plate (Fig. 5.1).

5.1.4 - Partially Saturated Soil Sample Preparation

Dry sand was thoroughly mixed with water. The required mass of water was:

$$m_{water} = \rho_{water} \phi \forall_{cylinder} Sr \tag{5.2}$$

where *Sr* is the desired saturation that water must be in the sampling sand and m_{water} is the mass of water required to achieve the *Sr*.

The sand-water mixture was left to stand for 24 h for more uniform moisture distribution in the mixture. Some water was lost during the waiting time, so an additional 0.1 *g* to 0.2 g of water was added. The total mass required for a sand sample was:

$$m_{total} = \rho_{quartz} \theta_{quartz} (1-\phi) \forall_{cylinder} + \rho_{water} \phi \forall_{cylinder} Sr \tag{5.3}$$

After the required total mass was confirmed, the mixture was compacted into a sampling cylinder (Fig. 5.1) by tapping or pushing a rod until the mixture completely fits inside the cylinder.

5.1.5 - Thermal Conductivity Probe

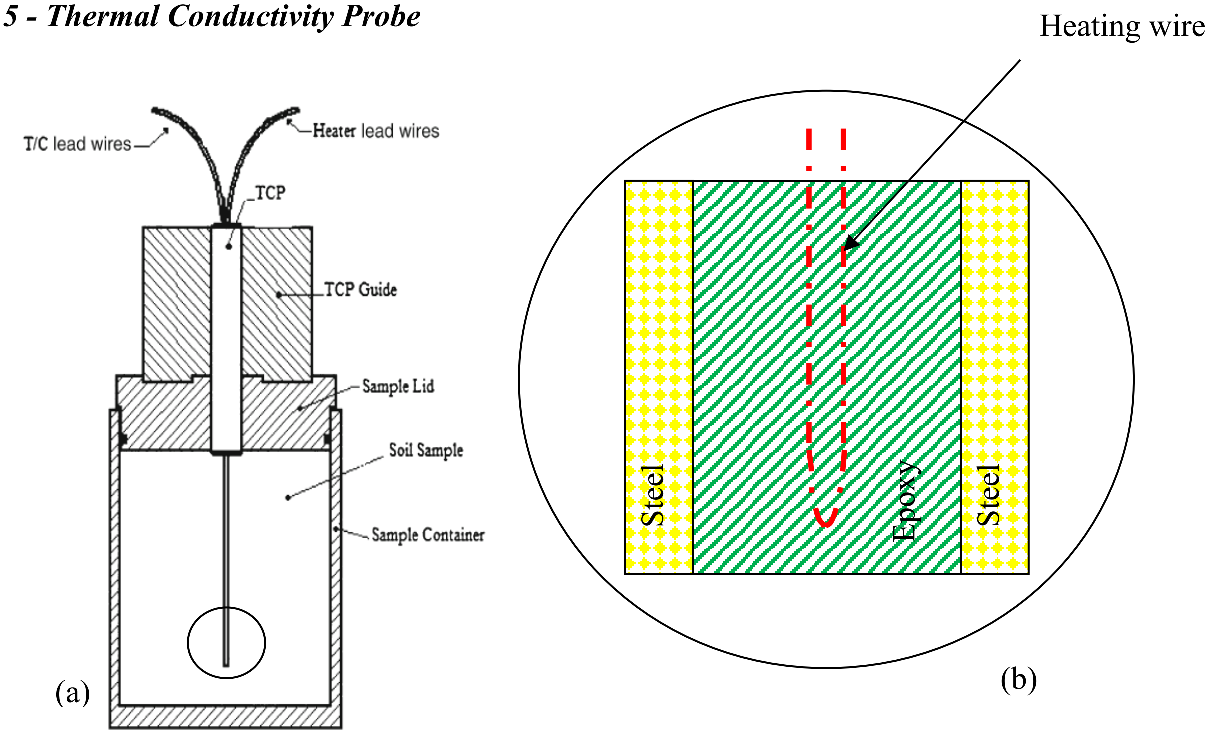

Figure 5.1. (a): Soil sampler assembly (adopted from [11]*) and (b): end cross section of TCP.*

Fig. 5.1 illustrates what the TCP had inside (Fig. 5.1b) and how the TCP was used to measure samples (Fig. 5.1a). The TCP outer cover was made of a stainless steel hypodermic tube (d_{TCP} = 1.06 *mm* and 88.9 *µm* wall thickness) of 55 *mm* effective length (*L*). The inner space of the steel tube contained a thermocouple and heating wire. The thermocouple was T-type and was made of 0.1 *mm* copper/constantan wires coated with formvar (vinyl acetal). The heating wire (HW) was made of 0.1 *mm* constantan wire coated with a single polyurethane nylon (MSW Wires Industries). The thermocouple junction was electrically insulated from the heater and the hypodermic sheath and was positioned approximately at the point corresponding to the middle of the effective probe length (*i.e., L*/2). The inner space of the steel tube was filled with ultra-low viscosity epoxy resin which was later cured and secured the thermocouple and HW in place.

The tube was then fixed on a printed circuit board (PCB) having the thermocouples and heater terminals (as shown in Fig. 5.2). The wire terminals were coated with a high performance polyimide electrical insulation film (Corona) to prevent short circuits. The TCP handle was made of an acrylic tube (9 *mm* outer diameter and 50 *mm* length) and located in the center of the PCB. The remaining space was filled with a five-minute-to-cure epoxy resin. The tip of the stainless steel tube was covered and smoothed to enhance insertion into granular or soft media. A cold junction of the thermocouple was put into a reference sample at the same ambient environment as the tested sand. The thermocouple and the TCP heater could make measuring errors due to induced voltages, so their extension wires were twisted to minimize measuring errors.

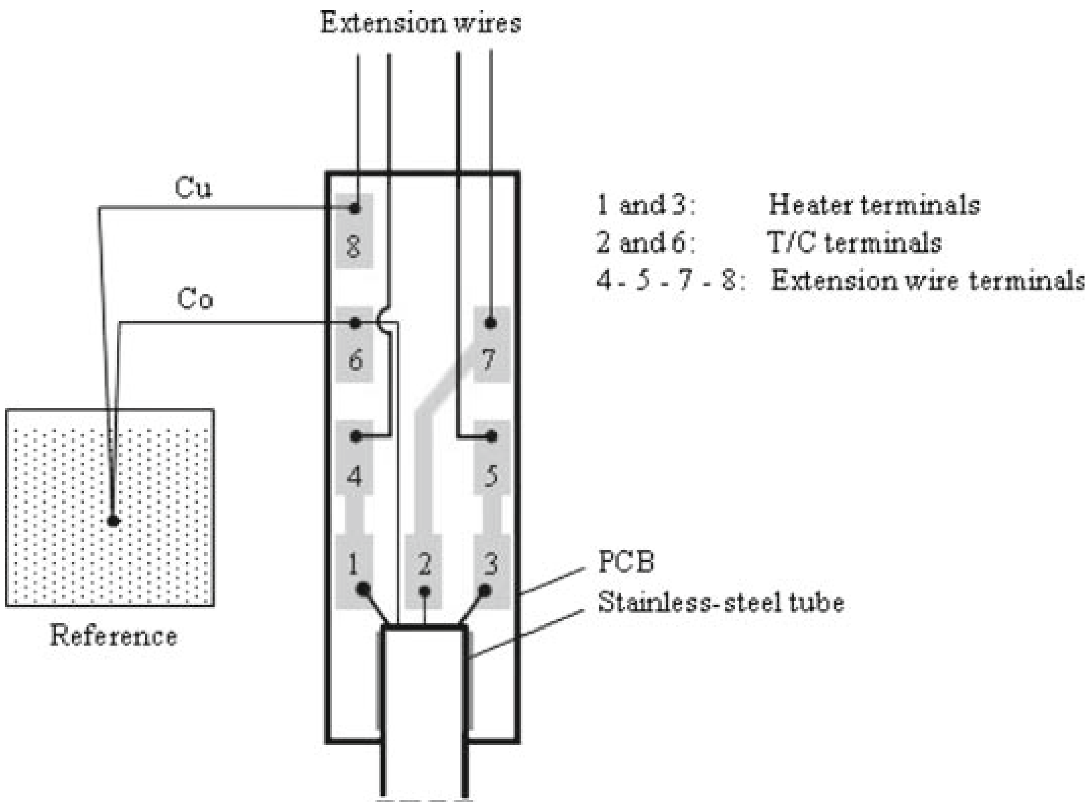

Figure 5.2. Printed circuit board assembly. (adopted from [11]*)*

The TCP was then calibrated against 1% agar-gelled distilled water of (25, 40, 50, 60, and 70)^{o}C. The thermal conductivity obtained from the TCP (k_{TCP}) was compared with the publication of Sengers and Watson [55] (k_{ref}). The procedure was repeated three times for each of the calibrating temperatures and averaged. After the calibration, it was found that the relative error of the calibrated probe ranged from 0.3% to 2.7%.

5.1.6 - TCP Experimental Procedures

Sand samplers of different compactions (*i.e.,* porosity of 0.32 and 0.38) were put in a force-air oven (Memmert UE-500-AQ) at 20-25^{o}C. The sampling sand was left in the oven for approximately four hours in order to have uniform initial temperature everywhere inside the sampling sand. Electricity was passed through the heating wire (HW) of the TCP such that the heating power of the HW ranged from 5 *W/m* to 1 *W/m*. The length-to-diameter ratio of the probe (L/d_{TCP}) was about 50 because Blackwell [39] and Xie *et al*. [13] suggested the length-to-diameter ratio to be larger than 25 in order to minimize the heat flux along the probe's axis. With the $L/d_{TCP} > 50$, the TCP acts as a perfect line heat source [56]. The time heating the TCP was 120 *s* so that the heat from the TCP could not reach the lateral walls of the sampler containing the sand sample at the end of the experiment (240 *s*), *i.e.*, the infinite medium size was still maintained. After each experiment (*i.e.,* one cycle of heating and cooling the TCP for 240 *s*), the TCP was left in the sampler for about 6 *h* so that the sand had sufficient time to come back to the oven temperature. Then many more trials were repeated. Since three samples were tested for each trial, there would be a total of nine measurements for each set of conditions.

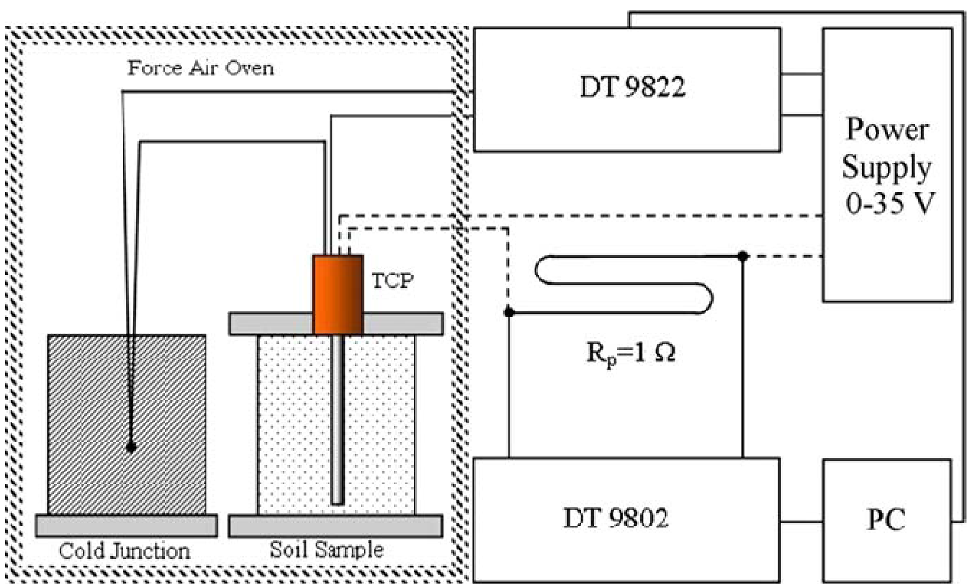

Figure 5.3. Schematic diagram of experimental setup. (adopted from [11]*)*

Moreover, the epoxy thermal conductivity (k_e) was found to play a significant role in the temperature response of the TCP based on the studies in Chapter 4 (for Eq. 2 and Eq. 3). Dr. Tarnawski was contacted for the k_e value in his TCPs but he reported that k_e was unknown as the manufacturer did not provide the k_e value to him. The manufacturer was also consulted for the k_e but did not find the answer as they were only interested in the viscosity of the Ultra Low Viscosity Kit that Dr. Tarnawski purchased. In addition, there are many reported k_e values of epoxies, depending on the grades and the constituents. However, there is no value for ultra-low viscosity epoxies.

As a result, one Ultra Low Viscosity Kit from SPI Supplies [57] was purchased to find out the k_e value used in Dr. Tarnawski's TCPs.

5.2 - Testing Epoxy

5.2.1 - Epoxy Apparatus

The experiment was set up with the following components:

1. Ultra Low Viscosity Kit from SPI Supplies with the following mixing portions: 66*mL* n-OSA, 33*mL* ERL 4221, 8.25*mL* BDE, and 9.9*mL* DMAE.
2. One 5*cm*-long and 76.2*μm*-round constantan wire (covered in single polyurethane nylon) from MSW Wire with the Lot number: 75334-02. The wire's resistance is 0.10004 *Ω/m*.
3. Insulated constantan wire: five 15*cm*-long and two 8*cm* long wires, 76.2*μm* -round, Omega Engineering Inc. (PN: TFCC-003-50-FT).
4. Insulated copper wire: five 15*cm*-long and two 8*cm* long wires, 0.003"-round, Omega Engineering Inc. (PN: TFCP-003-50-FT).
5. Magnetic spice jar [58] as shown in Fig 5.5.
6. Daytronic System 10 data acquisition system from Daytronic.
7. Z-Up 10-20 power supply from Lambda Inc.: 10*V* and 20*A* max.
8. Resistor: 1*Ω*, 1% tolerance, liquid metal through hole.
9. A computer system for automating the experiment.
10. Insulation taken from the lab room.
11. Two 0.03"-thick and 2.3"-round plastic sheets.

6 holes were drilled into The spice jar (#5) as in Fig. 5.4. The plastic sheets (#11) were glued using carpenter glue to the bottom of the spice jar and the inside of the lid of the spice jar. Ten 15*cm*-long #3 and #4 wires were soldered to make thermocouples. Four 8*cm*-long copper wires (#4) were soldered to the two ends of the wire (#2) to make an effective 38.1*mm* heating wire. The pairs and the heating wire (#2) were then inserted into the holes of the spice jar as in Fig. 5.5.

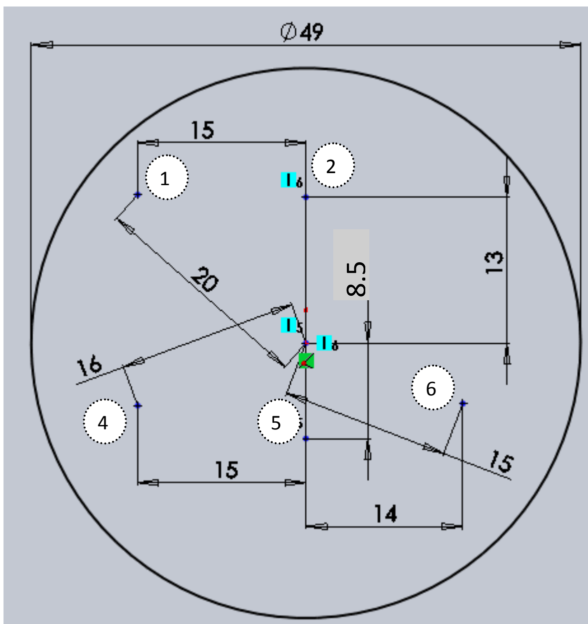

Figure 5.4. Punched hole locations on plastic sheets with thermocouples' numbers (in dotted circles). Dimensions in mm.

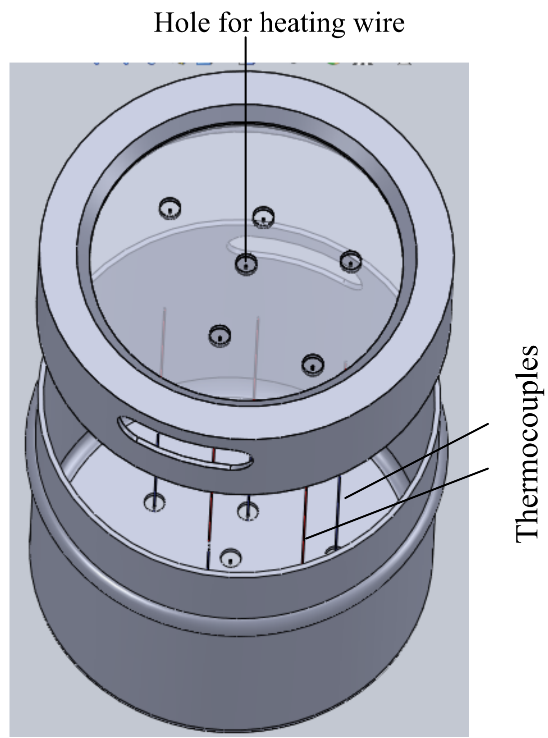

Figure 5.5. Jar and thermocouples.

The thermocouple and the heating wire were later connected to the Daytronic data acquisition system (#6) to measure the temperatures of the thermocouples and the voltage drop across the heating wire. One copper wire soldered to one end of the heating wire was then soldered to the resistor (#8) which was connected to the Z-Up power supply (#7).

After that, liquid epoxy (#1) was mixed and poured into the spice jar and air-solidified for two weeks. While the liquid epoxy was solidifying, a Microsoft Visual Basic 6.0 program was written so that the data acquisition system could import the temperature readings to Microsoft Excel to make further analysis.

After the liquid epoxy solidified, the temperature readings from the data acquisition system were calibrated with a thermometer that measured the room's temperature when no power was passed through the heating wire. Then temperature readings were started and recorded.

5.2.2 - Experimental Procedures for Testing Epoxies

The spice jar was covered with insulation to reduce thermal disturbances from the surrounding environment. It was noted that the thermocouple numbered 5 in Fig. 5.4 was best to deal with because it was closest to the center (or the heating wire) and had enough data to do further analysis in the coming parts of this research. However, thermocouples at locations 1 and 6 were also used to obtain the final k_e and α_e.

With the Visual Basic 6 program, many trials were done to obtain more accurate results under different heating powers (from 1 *W/m* to 17 *W/m*) and heating times (from 4 *minutes* to 1 *hour*). There were five thermocouples capable of taking measurements. The heating power was constant for each trial, but different trials had different heating powers and heating durations.

CHAPTER 6 - RESULTS AND DISCUSSION

In this chapter, the TCP data obtained from experiments are applied to Eqs. 1, 2, and 3 (from Chapter 3) for both the heating and cooling periods. Comparisons and differences among the three equations will be heavily focused on. This chapter includes:

1. the expressions for k_m, α_m, thermal contact resistance (TCR),
2. k_e and α_e measured from the epoxy experiment, and
3. the graphs and results in conjunction with the TCP data.

For point #3, the graphs of the thermal contact resistance (TCR) will be shown and discussed first. Secondly, from the TCR, plots of k_m values are illustrated and analyzed. Values of k_{agar} in the heating and cooling periods are investigated. Then, k_{soil} in both periods are studied. Lastly, the uncertainty from the epoxy experiment is explored to find out the relationship between its uncertainties and the calculated k_m values.

Moreover, experimental limitations are described and analyzed. The content of this chapter can help researchers refine and further improve TCPs by comparing and/or verifying the results.

6.1 - Calculating Methods

6.1.1 - Thermal Conductivity of the Sampling Medium

For more thorough comprehension of the slope of a $Term_{Mx}$, Fig. 6.1 is plotted.

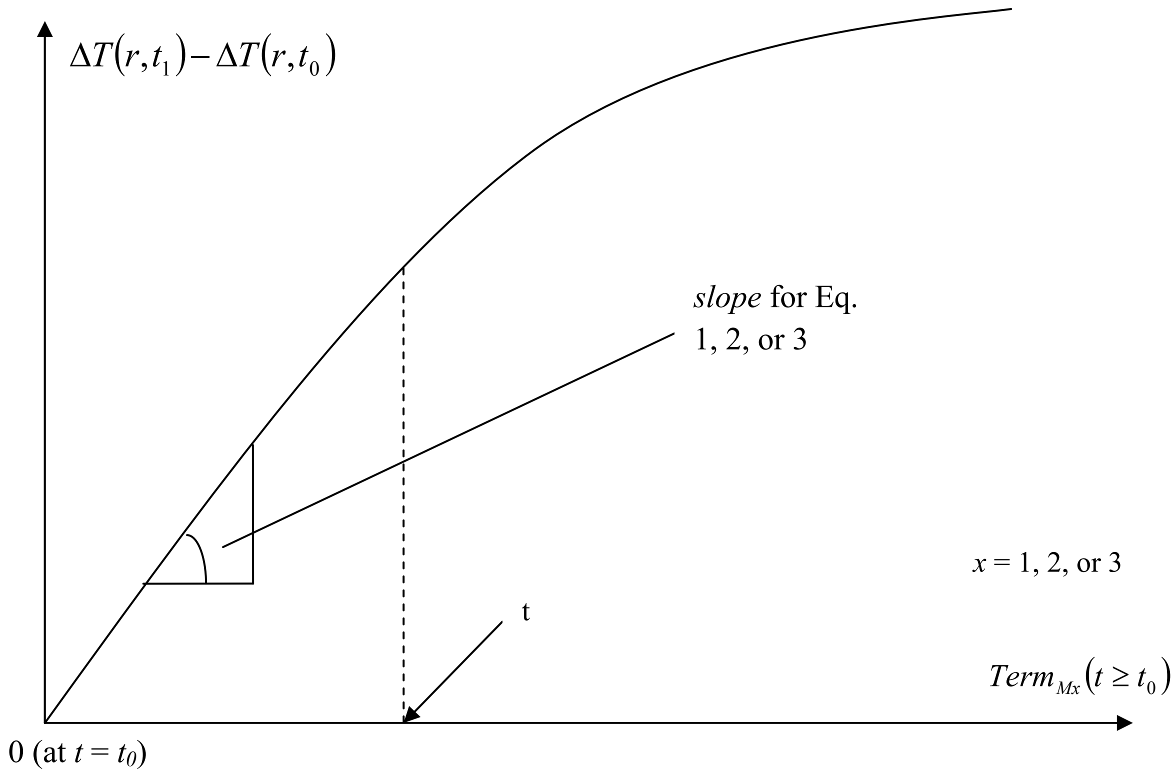

Figure 6.1. Illustration of slopes for Eqs. 1, 2 and 3.

Classically, the exponential integral function $-Ei\left(\frac{-r_{sen}^2}{4\alpha_m t}\right)$ in Eq. 3.1 (*i.e.*, the line heat source model) has been approximated as $-\gamma + \ln\left(\frac{4\alpha_m t}{r_{sen}^2}\right)$ for $\frac{4\alpha_m t}{r_{sen}^2} >> 1$ and an arbitrary fixed time (t_0) is chosen such that $\Delta T(r,t_1) - \Delta T(r,t_0) \approx \frac{\dot{q}_w}{4\pi k_m} \ln\left(\frac{t}{t_0}\right)$ for $\frac{4\alpha_m t_0}{r_{sen}^2} >> 1$ and $t \geq t_0$. Hence the thermal conductivity can be calculated as:

$$k_{m\_heat\_classical} \approx \frac{\dot{q}_w}{4\pi} \frac{1}{slope_{heat\_Eq1}} \tag{6.1}$$

where $slope_{heat\_Eq1}$ is the slope of $\Delta T(r,t) - \Delta T(r,t_0)$ vs. $Term_{M1}$ as shown in Fig. 6.1, $Term_{M1} = \ln\left(\dfrac{t}{t_0}\right)$ and $\Delta T(r,t)$ and $\Delta T(r,t_0)$ are from experiments.

Applying similar concepts to Eq. 3.2, we have: $$k_{m\_heat\_Eq2} = \frac{\dot{q}_w}{4\pi}\frac{1}{slope_{heat\_Eq2}} \tag{6.2}$$

where $slope_{heat\_Eq2}$ is the slope of $\Delta T(r,t) - \Delta T(r,t_0)$ vs.$Term_{M2}$ as shown in Fig. 6.1,

$\Delta T(r,t_1)$ and $\Delta T(r,t_0)$ are from experimental data, and

$$Term_{M2} = -Ei\left(\frac{-r_s^2}{4\alpha_m t}\right)[Term_1(t)] + \frac{k_m \cdot Term_2(t)}{\dot{q}_w/(4\pi)} + Ei\left(\frac{-r_s^2}{4\alpha_m t_0}\right)[Term_1(t_0)] - \frac{k_m \cdot Term_2(t_0)}{\dot{q}_w/(4\pi)}.$$

Term₁(t) and *Term₂*(t) are defined in Eq. 3.2; and $Term_1(t_0)$ and $Term_2(t_0)$ are $Term_1$ and $Term_2$ in terms of t_0 (at a fixed time).

Also, applying similar concepts to Eq. 3.4:

$$k_{m\_heat\_Eq3} = \frac{\dot{q}_w}{4\pi}\frac{1}{slope_{heat\_Eq3}} \tag{6.3}$$

where $slope_{heat\_Eq3}$ is the slope of $\Delta T(r,t) - \Delta T(r,t_0) Term_{M3}$ as shown in Fig. 6.1, $\Delta T(r,t_1)$ and $\Delta T(r,t_0)$ are from experimental data, and

$$\begin{aligned} Term_{M3} = {} & -Ei\left(\frac{-r_s^2}{4\alpha_m t}\right)[Term_1(t)] + \frac{k_m \cdot Term_2(t)}{\dot{q}_w/(4\pi)} + \frac{k_m \cdot TCR(t)}{\dot{q}_w/(4\pi)} \\ & + Ei\left(\frac{-r_s^2}{4\alpha_m t_0}\right)[Term_1(t_0)] - \frac{k_m \cdot Term_2(t_0)}{\dot{q}_w/(4\pi)} - \frac{k_m \cdot TCR(t_0)}{\dot{q}_w/(4\pi)} \end{aligned}$$

$Term_1(t)$ and $Term_2(t)$ are defined in Eq. 3.2; $TCR(t)$ is defined in Eq. 3.4; $Term_1(t_0)$, $Term_2(t_0)$, and $TCR(t_0)$ are $Term_1$, $Term_2$, and TCR in terms of t_0 (at a fixed time).

For the cooling period ($t > t_c$), the thermal conductivity of the sampling medium can also be calculated following the same procedures for the second expression of Eq. 3.1, and Eq. 3.3 and

Eq. 3.5. Also, re-arranging the three equations yields $k_{m\_cool\_Eq1}$, $k_{m\_cool\_Eq2}$, and $k_{m\_cool\_Eq3}$ in Eq. 6.4, Eq. 6.5, and Eq. 6.6 respectively as follow:

$$k_{m\_cool\_Eq1} = \frac{\dot{q}_w}{4\pi} \frac{1}{slope_{cool\_Eq1}} \tag{6.4}$$

$$k_{m\_cool\_Eq2} = \frac{\dot{q}_w}{4\pi} \frac{1}{slope_{cool\_Eq2}} \tag{6.5}$$

$$k_{m\_cool\_Eq3} = \frac{\dot{q}_w}{4\pi} \frac{1}{slope_{cool\_Eq3}} \tag{6.6}$$

where $slope_{cool\_Eq1}$, $slope_{cool\_Eq2}$, and $slope_{cool\_Eq3}$ are the slopes of $\Delta T(r,t)_{cool} - \Delta T(r,t_0)_{cool}$ vs. $Term_{M1}(t) - Term_{M1}(t-t_c)$, $Term_{M2}(t) - Term_{M2}(t-t_c)$, and $Term_{M3}(t) - Term_{M3}(t-t_c)$ respectively, and $\Delta T(r,t)_{cool}$ and $\Delta T(r,t_0)_{cool}$ are from experimental data.

The initiating time t_0 is the time after the start of each period. Some examples of t_0 and the corresponding temperature responses are shown in Table 6.1. t_c = 120 s. $Term_{Mx}(t)$ and $Term_{Mx}(t-t_c)$ follow the same trend.

Table 6.1. Examples of t_0 values and the corresponding temperature responses.

PERIOD	***Heating***				***Cooling***			
t_0	10 s	20 s	....	60 s	10s	20s	....	60s
$T(r,t_0)$	$T(r, 10\ s)$	$T(r, 20\ s)$	....	$T(r, 60\ s)$	$T(r, 130\ s)$	$T(r, 140\ s)$	....	$T(r, 180\ s)$

Since k_m is unknown, an iterative method is applied to obtain the value of k_m for Eqs. 6.2 and 6.3. First of all, k_m is assigned a value within a reasonable range (which could be k_m obtained by Eq. 6.1) and α_m is then calculated as $k_m/(\rho c_p)$ where ρc_p is defined in Eq. 6.7 in order to determine the $slope_{heat\_Eq2}$ in Eqs. 6.2 and 6.3. Later, a new value of k_m is from Eqs. 6.2 and 6.3. The new value of k_m is used to calculate a new value of α_m as before. With the new values of k_m and α_m, the cycle repeats until the new value of k_m converges to within 0.1% of the previous value. The same iterative method is used for Eqs. 6.5 and 6.6 to obtain $k_{m\_cool\_PC}$, and $k_{m\_cool\_TCR}$.

The iteration procedures for calculating Eq. 6.3 can only work if α_m and R_c are known. As a result, in calculating k_m using Eqs. 6.3 and 6.6 in this thesis, the following steps were applied:

a. Obtain k_m and am with Eqs. 6.2 and 6.5 by the iteration procedure already described.
b. Obtain R_c using the method described in Subsection 6.1.3.
c. Obtain k_m and α_m with Eqs. 6.3 and 6.6 by the iteration procedure already described.

6.1.2 - Thermal Diffusivity of the Sampling Medium

Ottawa sand C109 was used as the sampling medium by Tarnawski *et al.* [11], [43], and [21]. The sand consists of air, water, and quartz, whose densities and specific heat capacities are known and listed in Table 6.2.

Table 6.2. Thermal properties at 25°C of air, water, and quartz (Appendix 1 of Cengel [10])

	Air	*Water*	*Quartz*
ρ (kg/m^3)	1.20	997.5	2650
c_p ($J/kg{\cdot}K$)	1000	4181	745.0

The porosity of C109 is defined as $\phi = \dfrac{volume\ of\ space}{total\ volume}$. Volume of space is the non-solid volume, which can contain air or water or both, inside the sand sample.

The saturation ratio of C109 is defined as $Sr = \dfrac{volume\ of\ water}{volume\ of\ space}$.

There are seven experimental saturation ratios for C109 sand samples: 0.0, 0.1, 0.2, 0.3, 0.5, 0.7, and 1.0. Sr = 0.0 is for completely dry sand and Sr = 1.0 is for fully saturated sand. Other *Sr's* are for unsaturated (or partially saturated) sands.

The overall volumetric heat capacity (VHC) of a C109 sample using the weighted average method is defined as (Bristow *et al.* [19]):

$$\rho \cdot c_p = \left(\rho \cdot c_p \cdot \theta\right)_{air} + \left(\rho \cdot c_p \cdot \theta\right)_{water} + \left(\rho \cdot c_p \cdot \theta\right)_{quartz} \tag{6.7}$$

where $\theta_{air} = \frac{volume\ of\ air}{total\ volume} = (1 - Sr) \cdot \phi$, $\theta_{water} = \frac{volume\ of\ water}{total\ volume} = Sr \cdot \phi$, and $\theta_{quartz} = \frac{volume\ of\ quartz}{total\ volume} = 1 - \phi$

Applying Eq. 6.7, the thermal diffusivity of a C109 sand sample can be calculated as:

$$\alpha_m = \frac{k_m}{(\rho \cdot c_p)_{soil}} \tag{6.8}$$

where k_m is the thermal conductivity of C109.

6.1.3 - Thermal Contact Resistance - R_c value

The method to obtain R_c suggested by Blackwell [59] and shown in Appendix A.4 does not produce unique solutions for the TCP data from Dr. Tarnawski. As a result, in order to obtain R_c, k_m from Eq. 6.2 and volumetric heat capacity of the sampling medium from Eq. 6.7 are used for Eq. 3. The root mean square error (RMSE) for each period (heating or cooling) is defined as:

$$RMSE_i = \left\{ \sqrt{\sum_{t=TI}^{120s} \frac{\left(T_{Eq3} - T_{\exp eriment}\right)^2}{n}} \right\}_i \tag{6.9}$$

where TI stands for time increment (= 0.0667 *s*) as used in the experiment, *i* is the i^{th} experiment of TCP, and *n* is the number of time increments within 120 *s*.

The value of R_c is systematically varied over a reasonable range ($10^{-6} \leq R_c \leq 3\times10^{-3}$ $m^2 \cdot K/W$) until the RMSE during a period (heating or cooling) of a TCP experiment in Eq. 6.9 is smallest. When RMSE is smallest, the corresponding R_c is reported as the R_c value for that particular period of TCP measurement.

6.2 - Epoxy Data

Typical samples of the temperature response from the thermocouples of an epoxy test are shown in Fig. 6.2. Because the temperature was measured during the heating period, the first part of Eq. 1 can be calculated as follows:

$$k_e = \frac{\dot{q}_w}{4\pi} \frac{1}{slope_{heat\_Eq.1}} \quad \text{for } t > t_0 \tag{6.10}$$

where $slope_{heat\_Eq1}$ is the slope of $\Delta T(r,t) - \Delta T(r,t_0)$ vs. $\ln(t/t_0)$ as shown in Fig. 6.1.

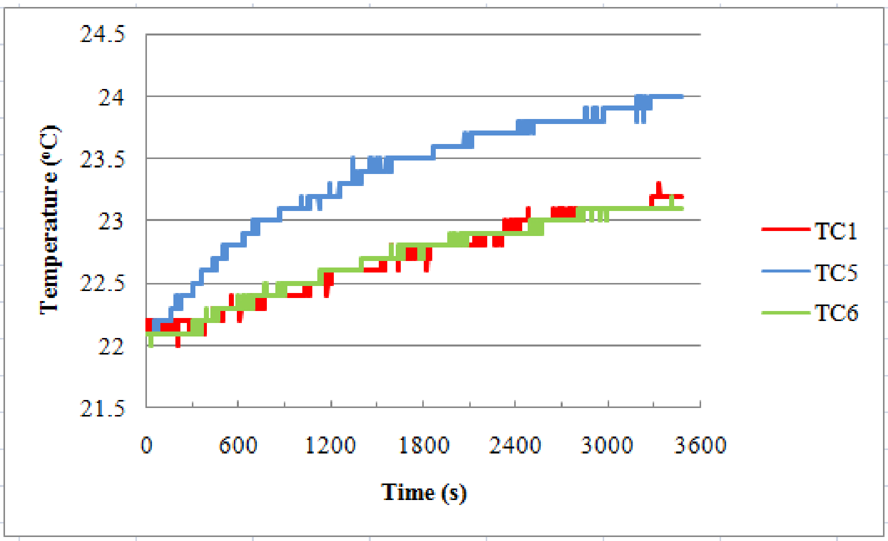

Figure 6.2. Sample T-t plot from thermocouples of an epoxy test.

Eq. 6.10 can only be applied when $r_{thermocouple} << \sqrt{4\alpha_e \tau}$ where $r_{thermocouple}$ is the radial location of the thermocouple away from the heating wire and τ is the heating period. Because α_e is unknown and can cause large errors if the t_0 is not properly selected (which will be explained in Section 6.3), the first expression of Eq. 1 is used to fit the experimental temperature responses at thermocouple locations 1, 5 and 6. The least square (or minimum root mean square error) method is used to obtain the best fit with the following steps:

1. Assume $k_e = 0.68$ $W/m{\cdot}K$ and $\alpha_e = 3.8\times10^{-7}$ m^2/s (from Table 4.1).

2. Calculate $RMSE_i = \sqrt{\sum_{t=TI}^{HD_i} \frac{\left(T_{Eq1} - T_{experiment\_i}\right)^2}{n}}$ where TI is the time increment of temperature readings (1 s), HD is the heating duration, i is a particular experiment, n is the number of seconds within a HD, and T is the temperature.
3. Calculate average $RMSE_i$ as: $RMSE_{avg} = \sum_{i=1}^{120} \frac{RMSE_i}{120}$ where i is the experiment number. In total, there were 120 experiments in the epoxy test.
4. Re-assume the values of k_e and α_e and re-calculate $RMSE_{avg}$ until $RMSE_{avg}$ is smallest.

The smallest $RMSE_{avg}$ ($\overline{X}$) was found to be 0.058ºC with k_e = 0.205 $W/m{\cdot}K$ and $\alpha_e = 1.14\times10^{-7}$ m^2/s. The $RMSE$ values for the 120 experiments are plotted in Fig. 6.3. The legend shows the thermocouple numbers. Other statistics of the $RMSE$ are $S_{\overline{X}} = 0.0035^oC$, $t_{student} - distribution \approx 1.980$, and $P_{\overline{X}} = 0.007^oC$ (refer to Appendix A7 for more information). Since k_e and α_e are obtained by curve-fitting the experimental data with Eq. 1, the random error of the epoxy experiment is from $P_{\overline{X}}$.

Applying Eq. A.7.2 for Eq. A.7.1 (in Appendix A.7) with V_{hw}, V_{SR}, k_e, $Shunt\_R$, and LHW as the variables with errors, the relative random error of the experiment is 12.07% by Eq. 6.11a.

$$\left(\frac{S_{k_e}}{k_e}\right)^2 = \left(\frac{S_{\overline{V}_w}}{\overline{V}_w}\right)^2 + \left(\frac{S_{\overline{V}_{SR}}}{\overline{V}_{SR}}\right)^2 + \left(\frac{S_{\overline{T}}}{\overline{T}}\right)^2 + \left(\frac{S_{Shunt\_R}}{Shunt\_R}\right)^2 + \left(\frac{S_{LHW}}{LHW}\right)^2 + \left(\frac{P_{\overline{X}}}{\overline{X}}\right)^2 \tag{6.11a}$$

$$\left(\frac{B_{k_e}}{k_e}\right)^2 = \left(\frac{B_{V_w}}{V_w}\right)^2 + \left(\frac{B_{V_{SR}}}{V_{SR}}\right)^2 + \left(\frac{B_T}{T}\right)^2 + \left(\frac{B_{Shunt\_R}}{Shunt\_R}\right)^2 + \left(\frac{B_{LHW}}{LHW}\right)^2 \tag{6.11b}$$

where $\frac{S_{\overline{V}_w}}{\overline{V}_w} = \frac{S_{\overline{V}_{SR}}}{\overline{V}_{SR}} = \frac{S_{\overline{T}}}{\overline{T}} = \frac{S_{LHW}}{LHW} \approx 0$, $\frac{B_{V_w}}{V_w} = \frac{B_{V_{SR}}}{V_{SR}} = 0.05\%$, $\frac{B_T}{T} = 0.5\%$, $\frac{B_{Shunt\_R}}{Shunt\_R} = 1\%$, and $\frac{B_{LHW}}{LHW} = 0.67\%$, $\frac{B_x}{x}$ is the relative systematic error of parameter x, and $\frac{S_{\overline{x}}}{\overline{x}}$ is the relative random error of parameter x.

The systematic relative error (B_{k_e}) is 1.31% by using Eq. 6.11b.

Therefore, the relative overall uncertainty of k_e at the 95% confidence level is

$\left(U_{k_e}\right)_{0.95} = \sqrt{12.07^2 + 1.31^2} = 12.14\%$.

Applying similar procedures, the relative random and systematic errors of α_e are 17.07% and 3.59% respectively by using Eq. 6.12.

$$\left(\frac{S_{\alpha_e}}{\alpha_e}\right)^2 = \left(\frac{S_{\bar{V}_w}}{\bar{V}_w}\right)^2 + \left(\frac{S_{\bar{V}_{SR}}}{\bar{V}_{SR}}\right)^2 + \left(\frac{S_{\bar{T}}}{\bar{T}}\right)^2 + \left(\frac{S_{Shunt\_R}}{Shunt\_R}\right)^2 + \left(\frac{S_{LHW}}{LHW}\right)^2 + \left(\frac{P_{\bar{X}}}{\bar{X}}\right)^2 + \left(\frac{S_{\bar{r}}}{\bar{r}}\right)^2 + \left(\frac{S_{k_e}}{k_e}\right)^2 \quad (6.12a)$$

$$\left(\frac{B_{\alpha_e}}{\alpha_e}\right)^2 = \left(\frac{B_{V_w}}{V_w}\right)^2 + \left(\frac{B_{V_{SR}}}{V_{SR}}\right)^2 + \left(\frac{B_T}{T}\right)^2 + \left(\frac{B_{Shunt\_R}}{Shunt\_R}\right)^2 + \left(\frac{B_{LHW}}{LHW}\right)^2 + \left(\frac{B_r}{r}\right)^2 + \left(\frac{B_{k_e}}{k_e}\right)^2 \quad (6.12b)$$

where $\frac{B_r}{r} = 3\%$: the relative systematic error of a thermocouple's location, and $\frac{S_{\bar{r}}}{\bar{r}} \approx 0$: the relative random error of a thermocouple's location.

Therefore, the relative overall uncertainty of α_e is $\sqrt{17.07^2 + 3.59^2} = 17.44\%$.

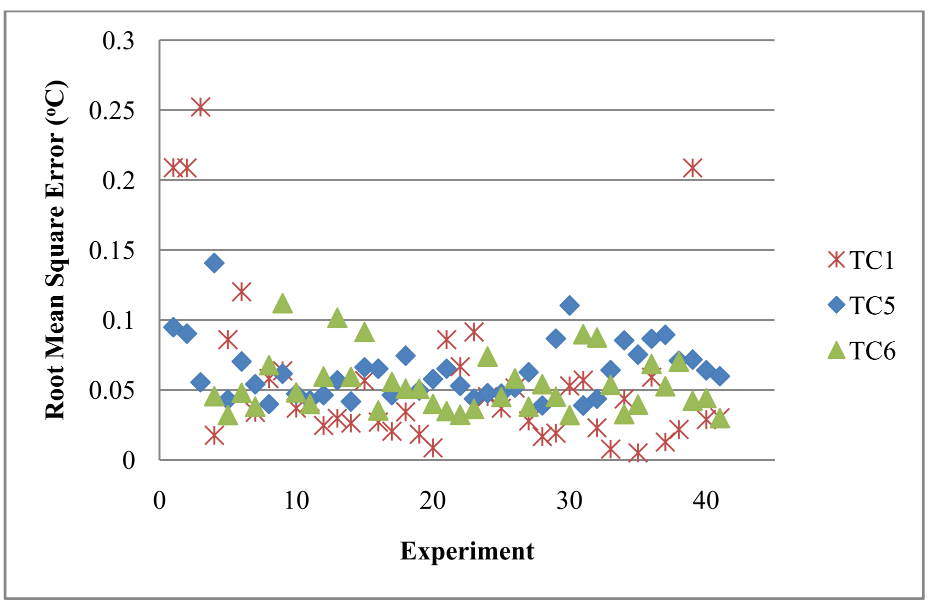

Figure 6.3. Calculated $RMSE_i$ at minimum $RMSE_{avg}$ of 0.058ºC.

The uncertainties came from many sources. The first source was the built-in accuracies of the experimental equipment that came from the tolerances during their manufacturing processes. The second source was from the thermal disturbances of the surrounding environment of the experiment such as the temperature fluctuations inside the lab room when another student was working on another experiment generating a lot heat, the HVAC setup of the lab room, and so on. Last but not least was from the mathematical manipulation of the experimental data such as the round-off errors of the mathematical functions and numbers used.

6.3 - TCP Data

6.3.1 - Approximation of r_{sen}

Table 6.3 lists the properties of the TCP used for Section 6.3.

Table 6.3. List of TCP properties from experiment at 25ºC.

Parameter	k_e $(W/m{\cdot}K)$	α_e (m^2/s)	k_s $(W/m{\cdot}K)$	α_s (m^2/s)	k_{water} $(W/m{\cdot}K)$
Value	0.205	1.14×10^{-7}	14.90	3.95×10^{-6}	0.607
Parameter	r_e (μm)	r_s (μm)	r_w (μm)	ρ_{agar} (kg/m^3)	$c_{p\ water}$ $(J/kg.K)$
Value	444.5	533.0	38.10	997.5	4181

The actual TCP construction has a U-shaped heating wire and a thermocouple within the epoxy layer as shown in Fig. 5.1b. The exact locations of the heating wire and thermocouple are unknown. So, in order to use Eqs. 1, 2, and 3, the TCP experimental data of agar are used to approximate (or calibrate) the location of the thermocouple with the assumption of a line heating wire at the center of the epoxy layer.

First of all, the root mean square error (RMSE) of the heating period, defined in Eq. 6.13, was applied as:

$$\left(RMSE_i\right)_{calibration} = \left\{ \sqrt{\sum_{t=TI}^{120s} \frac{\left(T_{Eq(1\,or\,2)} - T_{\exp eriment}\right)^2}{n}} \right\}_i \qquad (6.13)$$

where TI stands for time increment (= 0.0667 s) as used in the experiment, i is the i^{th} experiment of TCP, n is the number of time increments during the heating or cooling period (120 s)and agar is used to calibrate the location of the thermocouple of each TCP because the thermal properties of agar (*i.e.,* water) are known.

Secondly, r_{sen} in Eq. 2 was varied such that $\left(RMSE_i\right)_{calibration}$ was minimum.

Lastly, different values of r_{sen} in different measurements with the same TCP were averaged to represent the r_{sen} of the TCP in future studies. The averaged r_{sen} values for the TCPs examined are shown in Table 6.4.

Table 6.4. Averaged values of calculated r_{sen} for different TCPs using Eq. 2.

TCP #	02	16	17	29	32
r_{sen} (μm)	308.2	325.4	305.0	324.0	367.1

6.3.2 - Thermal Contact Resistance

The R_c for measurements of the same probe and same sampling medium were averaged as shown in Figs. 6.4 and 6.5. The legends in Figs. 6.4b and 6.5b display the TCP number and saturation ratio, *e.g.*, 16-0.1 means TCP16 and $Sr = 0.1$.

The general trend in Figs. 6.4 and 6.5 is that increasing water content (*i.e.*, higher saturation ratio) will decrease the thermal contact resistance. There are values that do not follow the general trend because during the actual experiments, the water could have migrated to another site away from the TCP's outermost surface due to the TCP's heat. Also, different probes produced different contact resistances due to the manual manufacturing and experimenting processes of each probe.

Because R_c is calculated (using Eq. 6.9) based on the k_m obtained by Eq. 2 with subjectively chosen initiating time t_0, the time is varied from 10 to 60 s to explore the influence of the time on the TCR. As shown in Figs. 6.4 and 6.5, the value of R_c levels off as higher initiating times are chosen. The reason is from the transient nature of the TCP. When the TCP was first heated up, it took some "warm-up" time for the TCP due to the thermal capacitance of the TCP.

In addition, R_c in the cooling period is usually higher than that in the heating period, indicating that even after electricity was turned off, the residual heat transfer from the TCP was still probably causing water movement away from the TCP-medium interface due to the temperature gradient. Also, some water, after having migrated to another site, did not move back immediately because of many factors such a temperature gradients and water's high viscosity, and capillary forces in the porous medium. In the case of agar, air bubbles could have formed on the surfaces of the TCPs during heating or inserting of the TCPs. For saturated sand, there may have been some dissolved air being released from the water when being heated by the TCP due to relatively high heating power (about 10 *W/m*) of the TCP and water migration in the sand. As a result, the R_c obtained from the cooling period is almost always twice the value of that from the heating period.

Further examination of the graphs in Appendix A.6 shows that after each experiment, water could have moved back to the TCP-sand interface, hence lower R_c values for partially saturated C109 sand. In contrast, there are cases where water did not move back to the interface because of many factors such as geometry and distribution of pores and temperature gradients, thus higher R_c values.

Moreover, comparing the R_c values from Figs. 6.4 and 6.5 with those from Liu *et al.* [42], the R_c value of dry sand was one order of magnitude (or about 10 times) higher than that of agar. Liu *et al.* calculated H_c values ($H_c = 1/R_c$) with their Ø1.27 *mm* TCP to be 113 $W/m^2 \cdot K$ (or $R_c = 8.85\times10^{-3}$ $m^2 \cdot K/W$) for air-dried Great Sand Hill sand and 1056±60 $W/m^2 \cdot K$ (or $R_c = 9.47\times10^{-4}$ $m^2 \cdot K/W$) for agar. The R_c values in this thesis are obtained to be 1.71×10^{-3} $m^2 \cdot K/W$ for dry C109 sand and 1.74×10^{-4} $m^2 \cdot K/W$ for 1% agar from TCPs of Ø1.06 *mm* which are about 5 time smaller than the values of Liu *et al* [42]. Liu *et al* [42] did not specify the amount of agar-to-water ratio they used. Also, the TCP construction of Liu *et al.* was not clearly described.

After R_c was obtained, k_m from Eq. 3 can be calculated with the steps shown in Subsection 6.1.1. The calculated k_m values using Eqs. 1, 2 and 3 will be compared in Subsection 6.3.3. The calculating methods to obtain k_m values with different equations for Subsection 6.3.3 were described in Subsection 6.1.1.

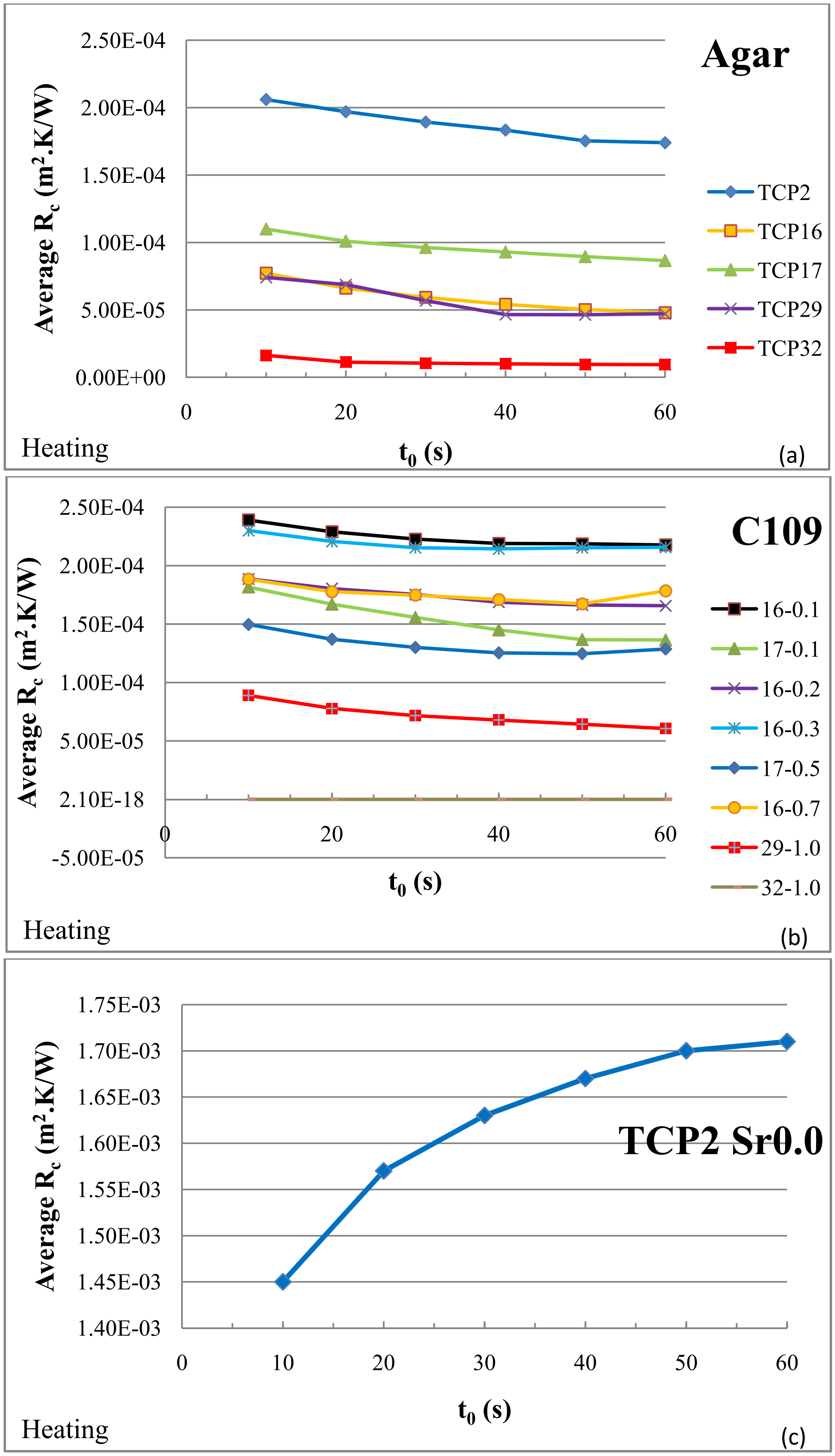

Figure 6.4. Average R_c values vs. t_0 for different TCPs and sampling media based on heating period.

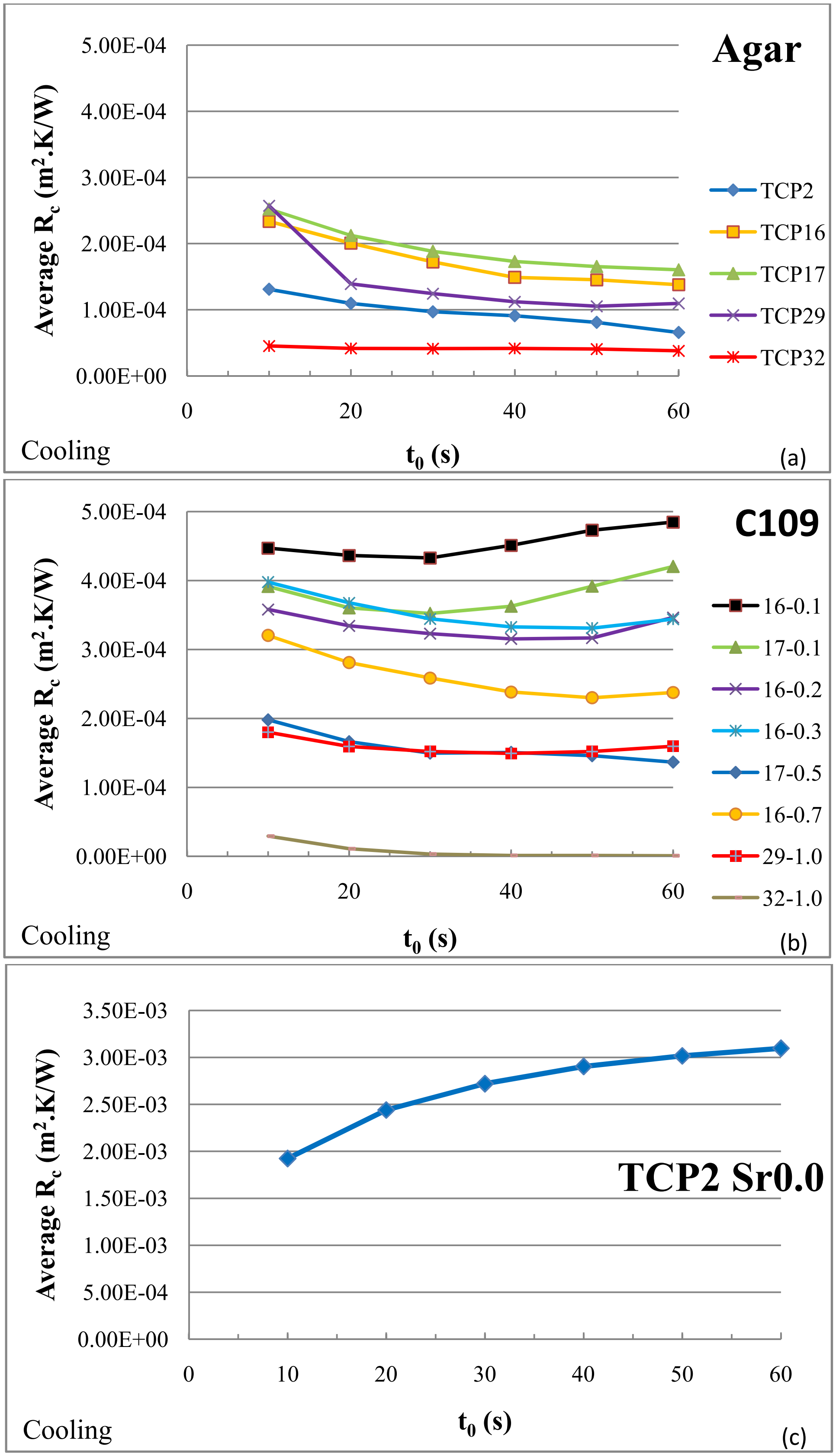

Figure 6.5. Average R_c values vs. t_0 for different TCPs and sampling media based on cooling period.

6.3.3 - k_m in Heating and Cooling Periods

Fig. 6.6 shows the calculated k_{agar} using Eqs. 6.1, 6.2 and 6.3 vs. the initiating time t_0 during the heating period, *i.e.*, all the temperature data ($t_0 \leq t \leq 120\ s$) in the heating zone from the experiment are used to obtain the graphs. As one can note that when t_0 is higher, k_{agar} appears to level off. The reason is from the transient nature of the TCP and is similar to the R_c values discussed in Subsection 6.3.2. In addition, except for TCP2, the k_{agar} obtained from Eq. 6.3 is not much different than that from Eq. 6.2. Consequently, R_c has slight influences on the thermal conductivity of the sampling medium.

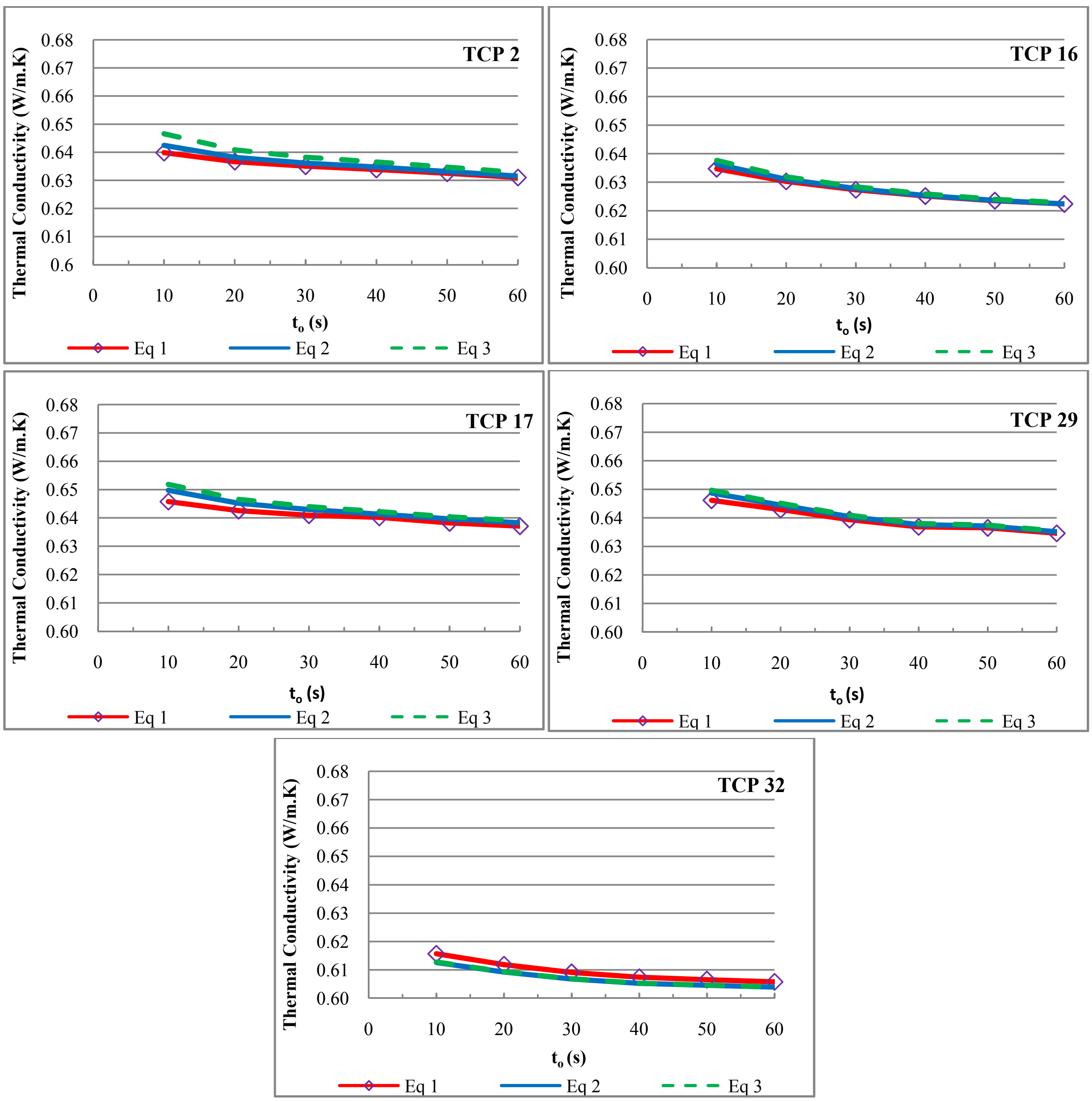

Figure 6.6. k_{agar} estimated by Eqs. 6.1, 6.2, and 6.3 during the heating period.

This R_c result agrees well with those of Murakami *et al.* [23] and Elustondo *et al.* [34]. The researchers explained that R_c only shifted the *T-t* plot (the plot of temperature T vs. time t) but did not change the slope of the *T-t* plot. With using Eq. 6.1, the calculation of k_m is influenced by how much the slope changes but not how much the *T-t* plot is shifted. Also, the k_{agar} values calculated are not the same for all but vary among the probes because each probe was made manually and has slight variations with each other.

In order to better study how accurately Eqs. 6.1, 6.2 and 6.3 are, the reference k-value (k_{ref}) of agar was assumed that of water at 25°*C*, *i.e.*, 0.607 $W/m \cdot K$ (p.854 Cengel [10]). The experiments of Tarnawski *et al.* [11], [21], [43] were at around 25°*C*. The reference k-value was then used to calculate the errors of k_{agar} obtained by Eqs. 6.1, 6.2 and 6.3 by the following equation:

$$\%Error = \frac{k_{Eq.} - k_{ref}}{k_{ref}} \times 100\% \tag{6.14}$$

where $k_{Eq.}$ is the k_{agar} obtained from a particular equation and k_{ref} is the reference thermal conductivity of water at 25°C from Cengel [10].

The values of %Error are plotted in Fig. 6.7. As shown in Fig. 6.7, Eq. 6.1 seems more accurate than Eqs. 6.2 and 6.3 in estimating the thermal conductivity of agar. However, thermal conductivity measurements on other materials may prove differently. As shown in Fig. 4.6 in Chapter 4, making measurements on different materials theoretically produces different errors in temperature responses. Meanwhile, in the literature, the k_m values from TCP measurements have been mostly calculated by using Eq. 6.1 and the asymptotic approximation. Therefore, in order to make more accurate comparisons, a GHPA or equivalent should be used to obtain the k_m values which are then compared with those calculated using Eqs. 6.1, 6.2 and 6.3.

So far, the heating period has been extensively studied but the cooling period is rarely reported. As a result, Fig. 6.8 is plotted to show the k_{agar} obtained using the experimental temperature data from the cooling period.

From Fig. 6.8, one can see that the thermal contact resistance (TCR) does make a difference in the calculation of k_{agar}. However, by comparing the results from Eq. 6.2 with those from Eq. 6.3, the difference is relatively small. The difference is further studied in comparison with k_{ref} as shown in Fig. 6.9. The calculation steps in Fig. 6.9 are the same as those in Fig. 6.7.

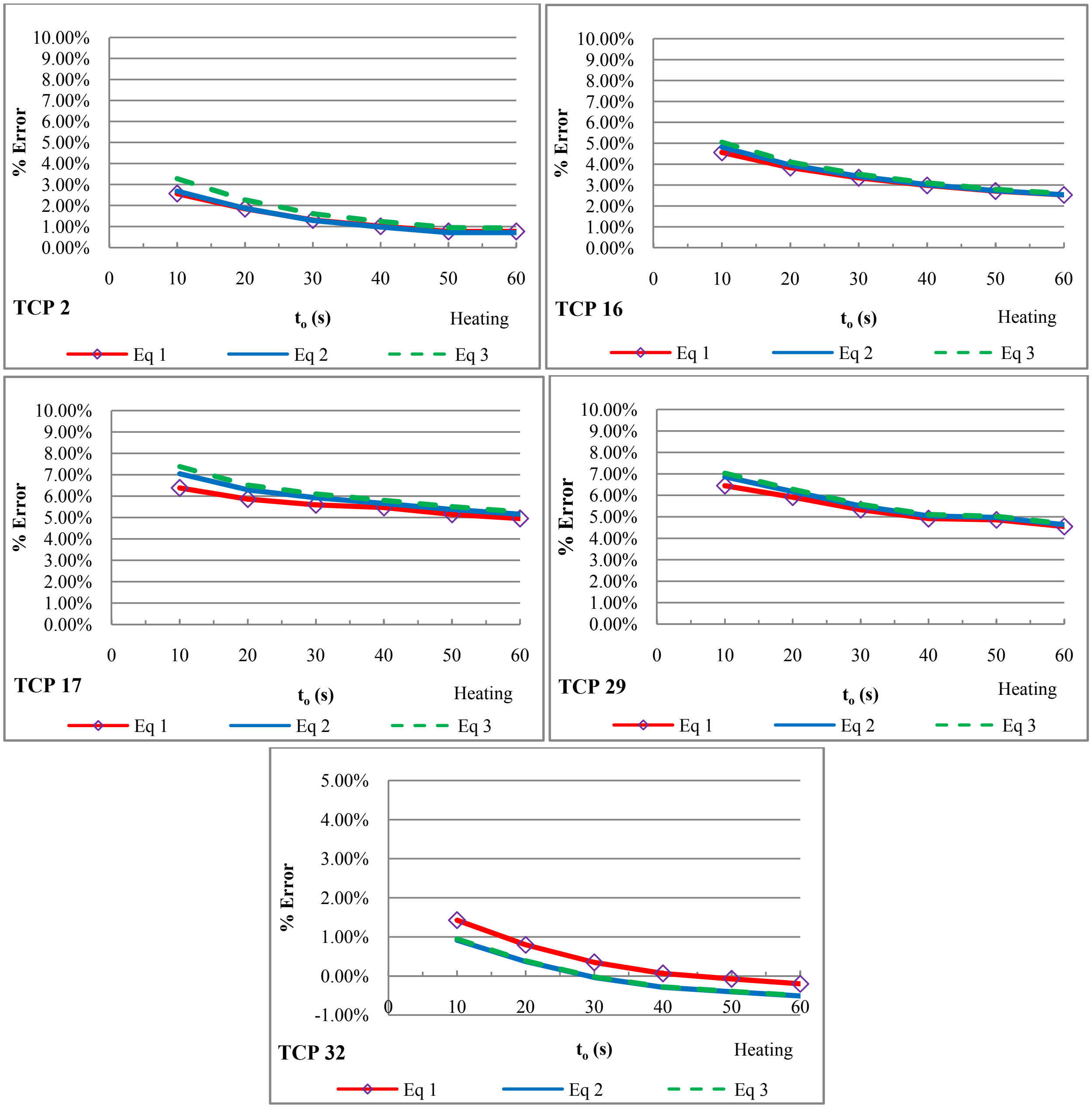

Figure 6.7. Percent error of calculated k_{agar} during the heating period.

In Fig. 6.8, the k_{agar}-value obtained by Eq. 6.5 is quite different from that obtained by Eq. 6.6. The reason for the difference in the periods stays in the heat sink model (HSM) for the cooling period. Basically, the model considers the temperature response in the cooling period as the difference between the heat rise at 0 *s* and at the time the electricity of the heating wire is cut off (Liu *et al.* [42] and de Vries [47]), *i.e.*, $\Delta T(r,t)-\Delta T(r,t-t_c)$.

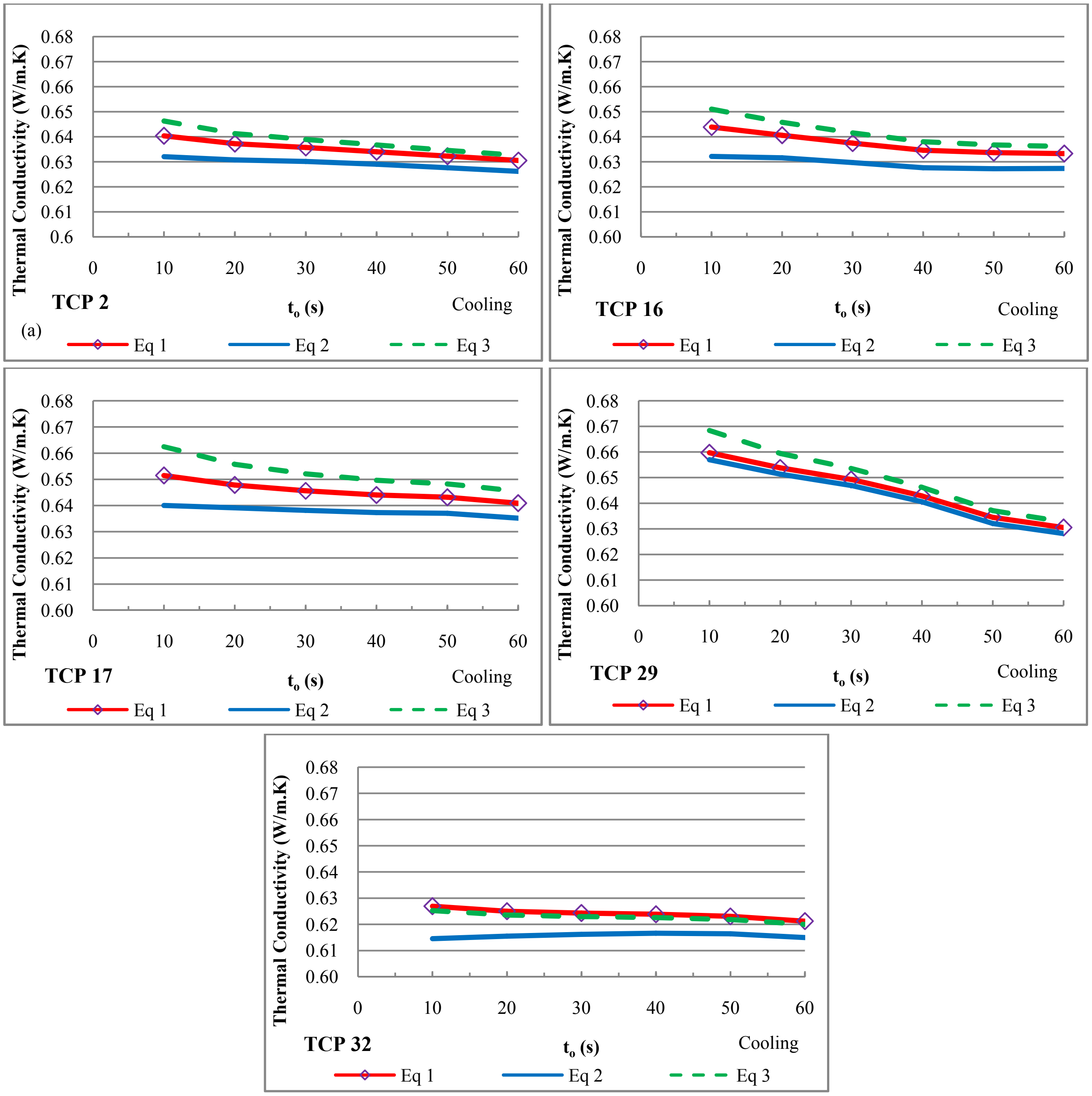

Figure 6.8. k_{agar} estimated by Eqs. 6.4, 6.5, and 6.6 based the cooling period.

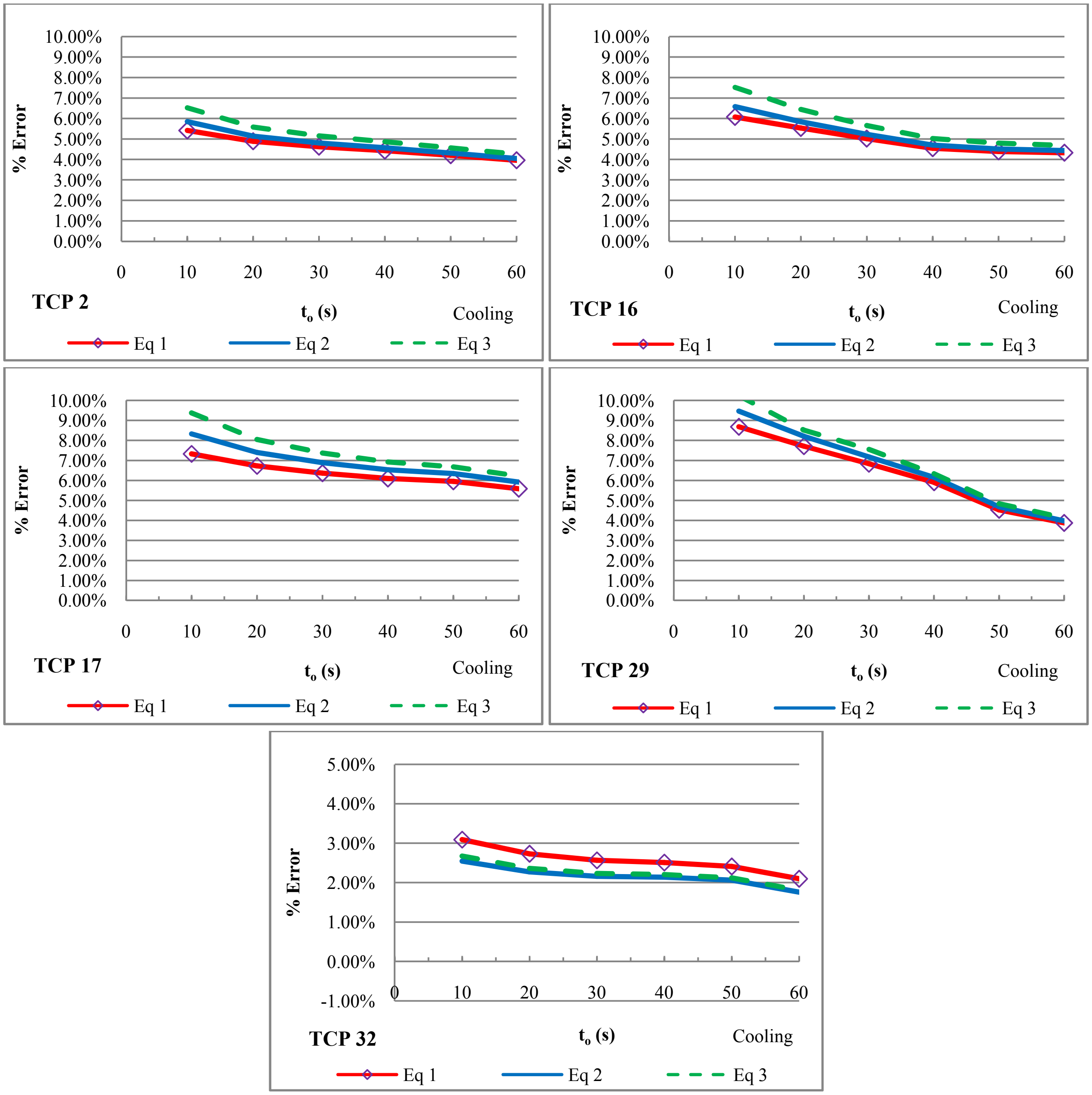

Figure 6.9. Percent error of calculated k_{agar} based on the cooling period.

Comparing Fig. 6.7 with Fig. 6.9, the k_m obtained from the cooling period is of lower accuracy than that of the heating period. The errors in Fig. 6.9 are always higher than those in Fig. 6.7. The reason might be due to the enlargement of the TCP hole during the experiment. From the TCP heat, the hole where the TCP was immersed in agar-water gel solution might have reacted to the thermal rise and grown. Although agar can prevent the convection of water during TCP experiments, no study has been found in terms of the thermal expansion of the agar-water gel solution. Also, the hole may not have had enough time to shrink back to the condition when the

TCP was first inserted during the heating period of the TCP. As a result, the TCR and R_c value could not be held constant while Eq. 3 assumes R_c is a fixed and constant value. Consequently, the errors associated with k_m values obtained using Eq. 6.6 in the cooling period are higher than those in the heating period.

To better compare the heating and cooling periods, Fig. 6.10 is plotted. The figure shows the average values of k_{agar} from different measurements. With the same probe and t_0, the k_{agar} values are averaged. Then, with the same probe, the average k_{agar} values are averaged among different t_0 values (overall average). The horizontal axis of Fig. 6.10 shows the equation number while the vertical axis displays the overall averages of TCPs. The legend indicates the TCP number. As one can notice, the k_{agar} values obtained from the heating period using Eqs. 1, 2 and 3 are more accurate than those from the cooling period. Also, using Eq. 1 produces slightly lower errors than those of Eqs. 2 and 3, depending on the particular TCP. However, whether Eq. 1 is always more accurate than Eqs. 2 and 3 is still too early to conclude since more media should be tested from and compared with other measuring techniques such as a GHPA.

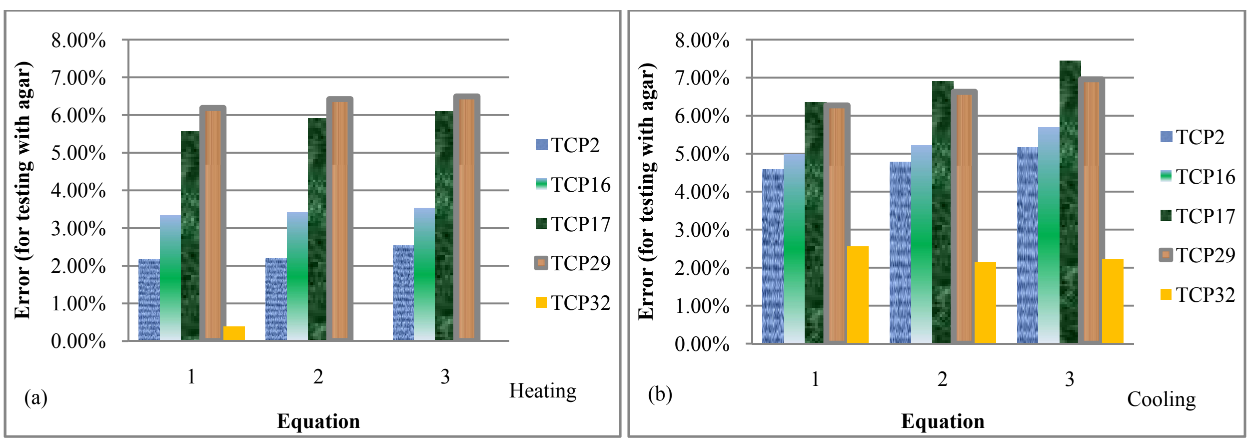

Figure 6.10. Average error of k_{agar} values for different TCPs using Eqs. 1, 2 and 3.

Fig. 6.11 illustrates the calculated k_{dry_C109} (Sr = 0.0) of C109 Ottawa sand as a function of t_0. The left of the figure shows the k_{dry_C109} values using the data from the heating period while the right part shows those from the cooling period. Similar to R_c and k_{agar} values, k_{dry_C109} also levels off when t_0 is large enough. If the experimenter is about to use a randomly picked t_0, mild to severe errors can happen. Also, the curves of Eq. 3 on both parts (left and right) are similar, indicating that the TCR layer remained unchanged, so the R_c value stayed constant. In addition, there are some differences in the curves calculated using Eq. 1 from the heating and cooling periods. The reason comes from the neglected TCP construction and the TCR. Moreover, by comparing Fig. 6.11a and Fig. 6.7, the particular construction of the TCP2 creates the difference in the k_m value predicted by Eq. 2 and by Eq. 3.

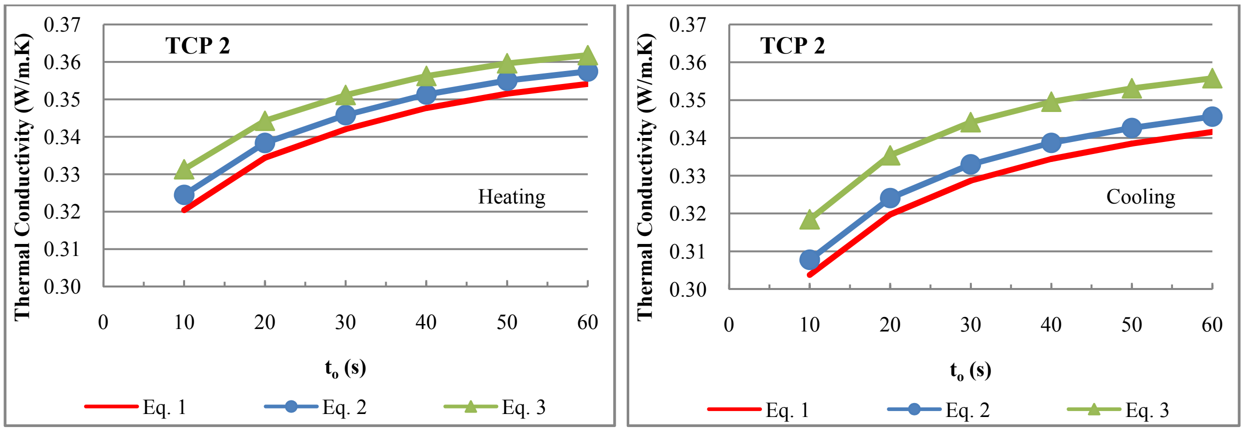

Figure 6.11. k-value of dry C109 Ottawa sand vs. t_0.

Fig. 6.12 illustrates the thermal conductivity values of partially saturated C109 sands vs. initiating time t_0 by using Eqs. 1, 2 and 3 in both heating and cooling periods. The legend shows the saturation ratios. Within a period (heating or cooling), the k_m-values from Eq. 2 are higher than those from Eq. 1 but lower than those from Eq. 3. Also, similar to the trend of R_c and k_{agar}, k_{PS_C109} values also level off as t_0 is sufficiently large enough. In addition, by using Eq. 1 for both periods, the k-values obtained are more similar to each other for higher Sr. However, with the application of Eq. 2, the k_m values for the partially saturated C109 sands are higher than those calculated by Eq. 1 in both periods. The reason can be explained by the neglected TCP construction of Eq. 1 (Nusieh and Abu-Hamdeh [60] and Abu-Hamdeh [61]). By looking at Table 6.3, the k_e is smaller than the k_{soil} of partially saturated conditions. With the same temperature values and less conduction through the epoxy layer, Eq. 1 underestimates the k_m values. In other words, when the line heat source theory is applied to the TCP, the thermal properties of the TCP materials are ignored. However, because the thermal properties of the epoxy layer are less than those of the soils, the thermocouple in the TCP reads higher temperature values; hence the calculated k_{soil} values are less.

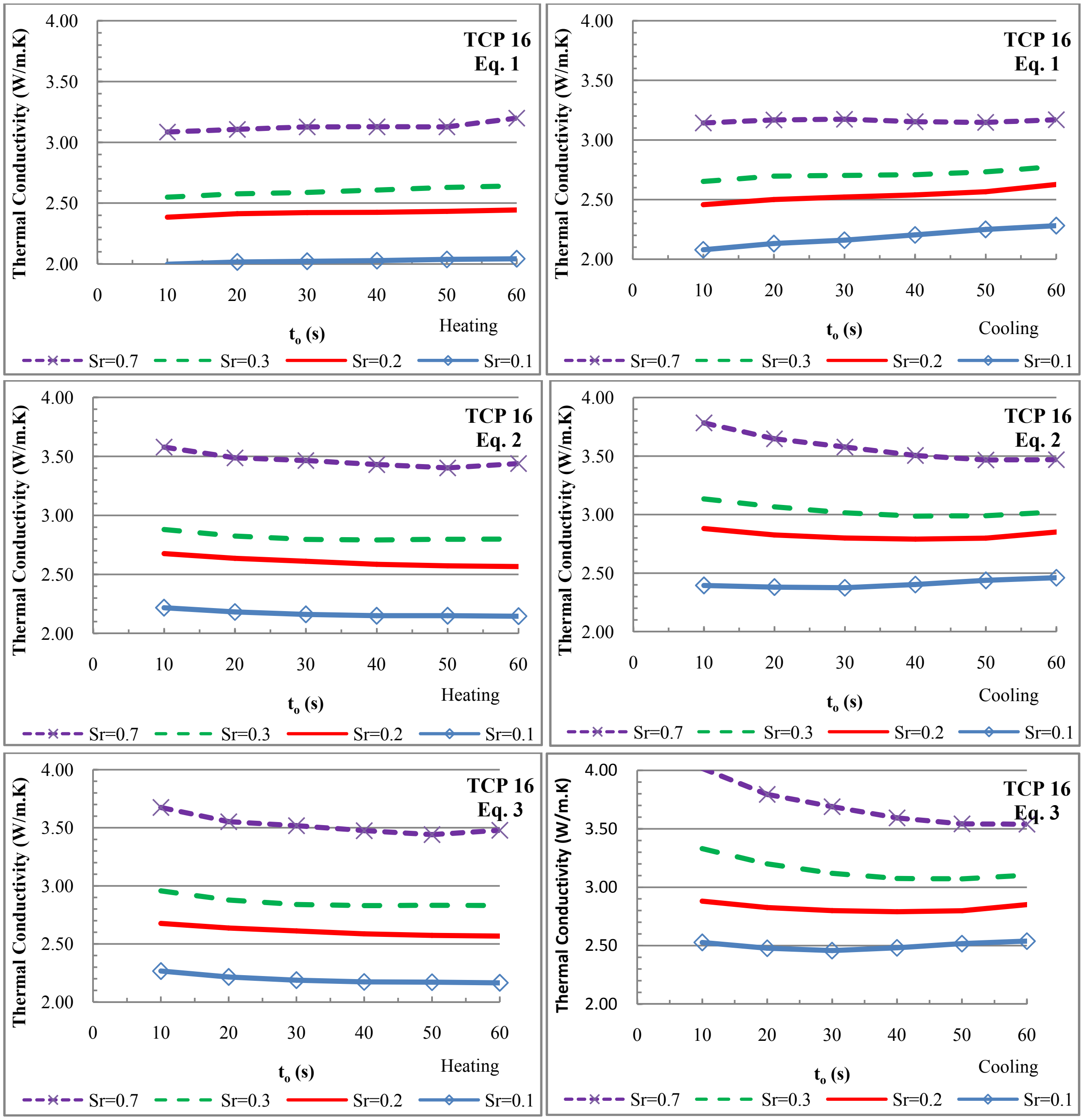

Figure 6.12. k_{PS_C109} vs. time for TCP 16 using Eqs. 1, 2 and 3 in heating and cooling periods.

Moreover, since the value of k_s is much higher than those of epoxy and soils and the steel layer is relatively small in thickness, the layer acts as a "perfect" conductor that do not prevent heat (which is determined by the heating power) easily moving from the TCP to the soil. Therefore, Fig. 6.12 agrees well with Fig. 4.9 that the thermal conductivity of the steel layer has little effects on the error.

Furthermore, the k_m values obtained by Eq. 3 are similar to those by Eq. 2 in both periods if the initiating time t_0 is large enough. This result agrees with those of Murakami *et al.* [23], Goto and Matsubayashi [41], and Cull [62] that the TCR has small effects on determining k_m.

Similarly, the k_m values from TCPs numbered 17, 29 and 32 are plotted in Figs. 6.13-6.15. The trends in the plots and those in Fig. 6.13 are very alike. The only odd exception in Figs. 6.13-614 is the case of the cooling period for TCP 29 in Fig. 6.14. The reason could be from the particular construction of the TCP 29 and/or the setup of the experiments. Also, by comparing Figs. 6.7, 6.9, 6.11, 6.12, 6.13, 6.14, and 6.15 with Fig. 6.10, the cooling period may or may not produce worse k_m values than the heating period does. In other words, one should consider the particular construction of each TCP and the measurement setup to judge whether the heating or cooling period can produce more accurate k_m values. With the construction methods from Tarnawski *et al.* [11], the heating period mostly gives more accurate k_m results than the cooling period does. Other construction methods of TCPs may have different results.

The reason for the difference in the periods lies in the heat sink model (HSM) for the cooling period. Basically, the model considers the temperature response in the cooling period as the difference between the heat rise at 0 *s* and at the time the electricity of the heating wire is cut off (de Vries [47] and Liu *et al.* [42]), *i.e.*, $\Delta T(r,t)-\Delta T(r,t-t_c)$. During the derivation of Eq. 3.1a, Carslaw and Jaeger [16] assume that the initial temperature at every point of the sampling medium is the same. However, the initial temperature T_i at the beginning of the cooling period is not same for every point in the sampling medium as in the heating period.

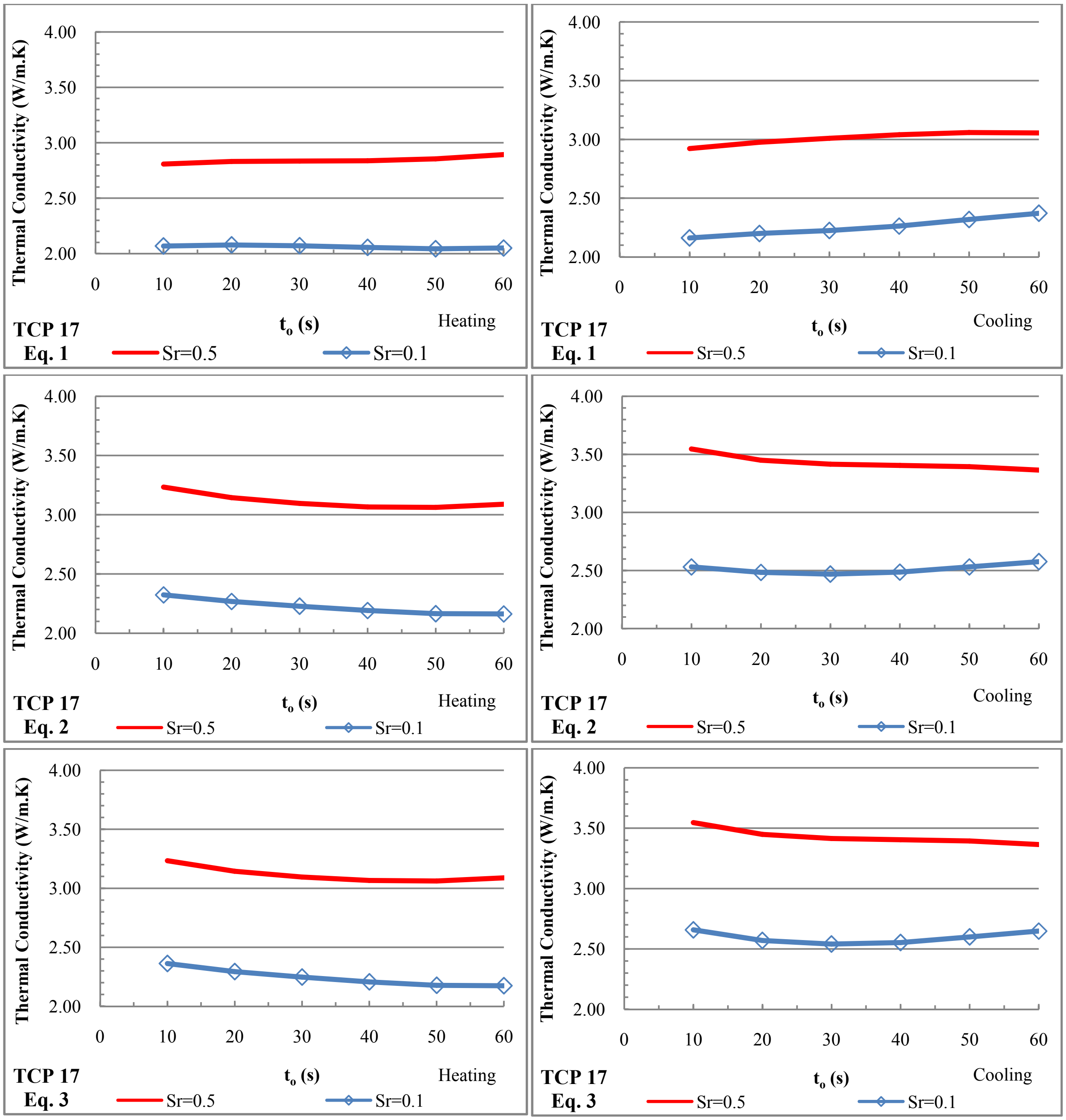

Figure 6.13. k_{PS_C109} vs. time for TCP 17 using Eqs. 1, 2 and 3 in heating and cooling periods.

By looking at the k_m values shown in Fig. 6.7, 6.10 and 6.12-6.15, the R_c value has small effects on the values of k_m. This result agrees well with Murakami *et al.* [23], Goto and Matsubayashi [41], Cull [62], and Liang *et al.* [27].

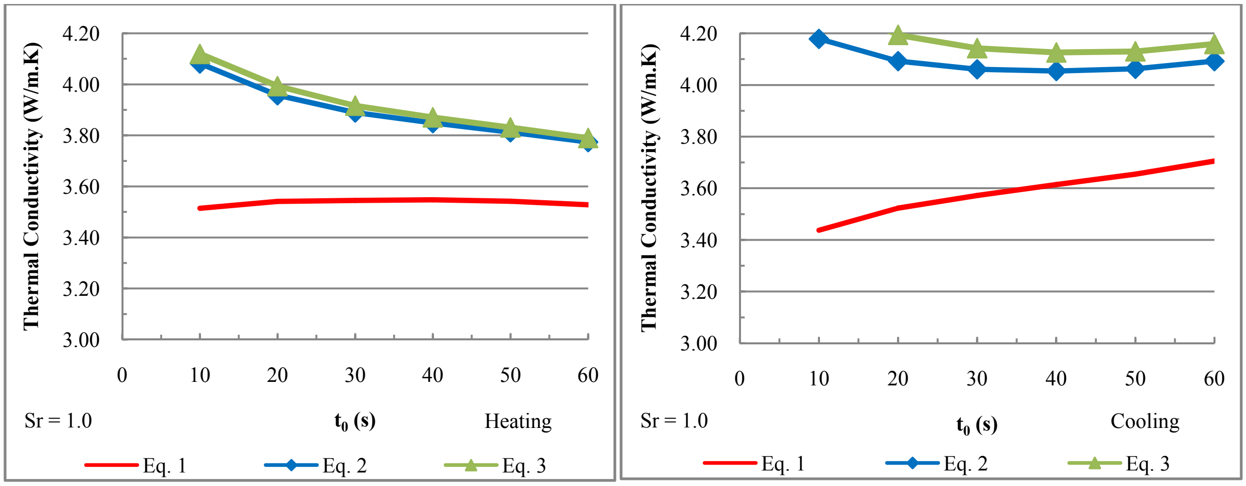

Figure 6.14. k_{FS_C109} vs. time for TCP 29 using Eqs. 1, 2 and 3 in heating and cooling periods.

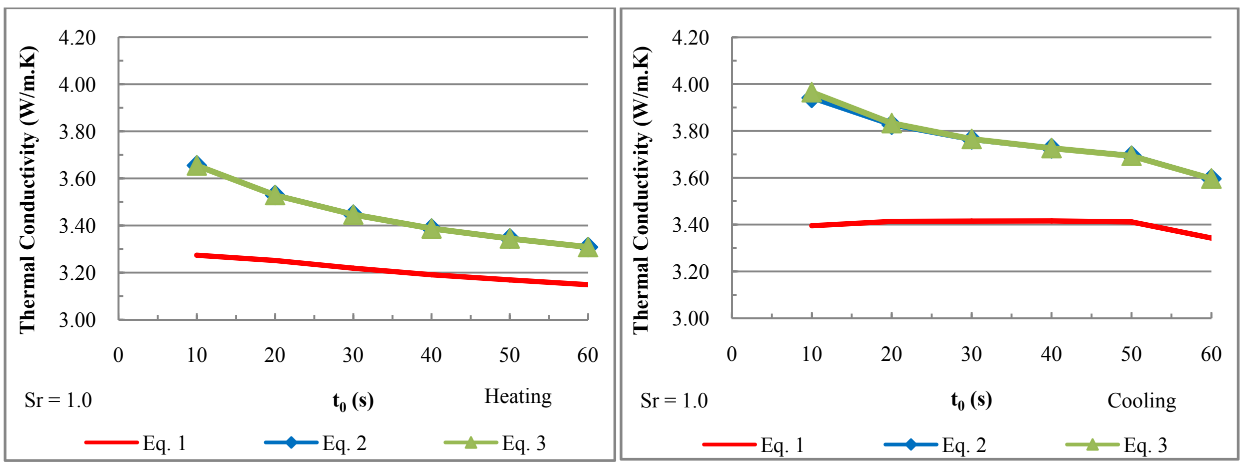

Figure 6.15. k_{FS_C109} vs. time for TCP 32 using Eqs. 1, 2 and 3 in heating and cooling periods.

Kersten [63] published k_m data of C109 sands obtained by a GHPA. Farouki [64] tested sands of similar grain size distribution and compaction with the TCP method and reported disagreement with the data from Kersten. In addition to the moisture migration problems from the GHPA, choosing an inappropriate t_0 may also cause additional errors since the values of k_m level off as t_0 increases.

Because the uncertainties of k_e and α_e are relatively high (±12.14% and ±17.44% respectively), one may question how k_m is affected by the changing values of k_e and α_e. As a result, Figs. 6.16-6.19 are plotted to investigate the sensitivity of k_m to k_e and α_e. The changing values of k_e and α_e used are shown in Table 6.5, which shows the ±20% of the values of k_e and α_e that are shown in Table 6.3.

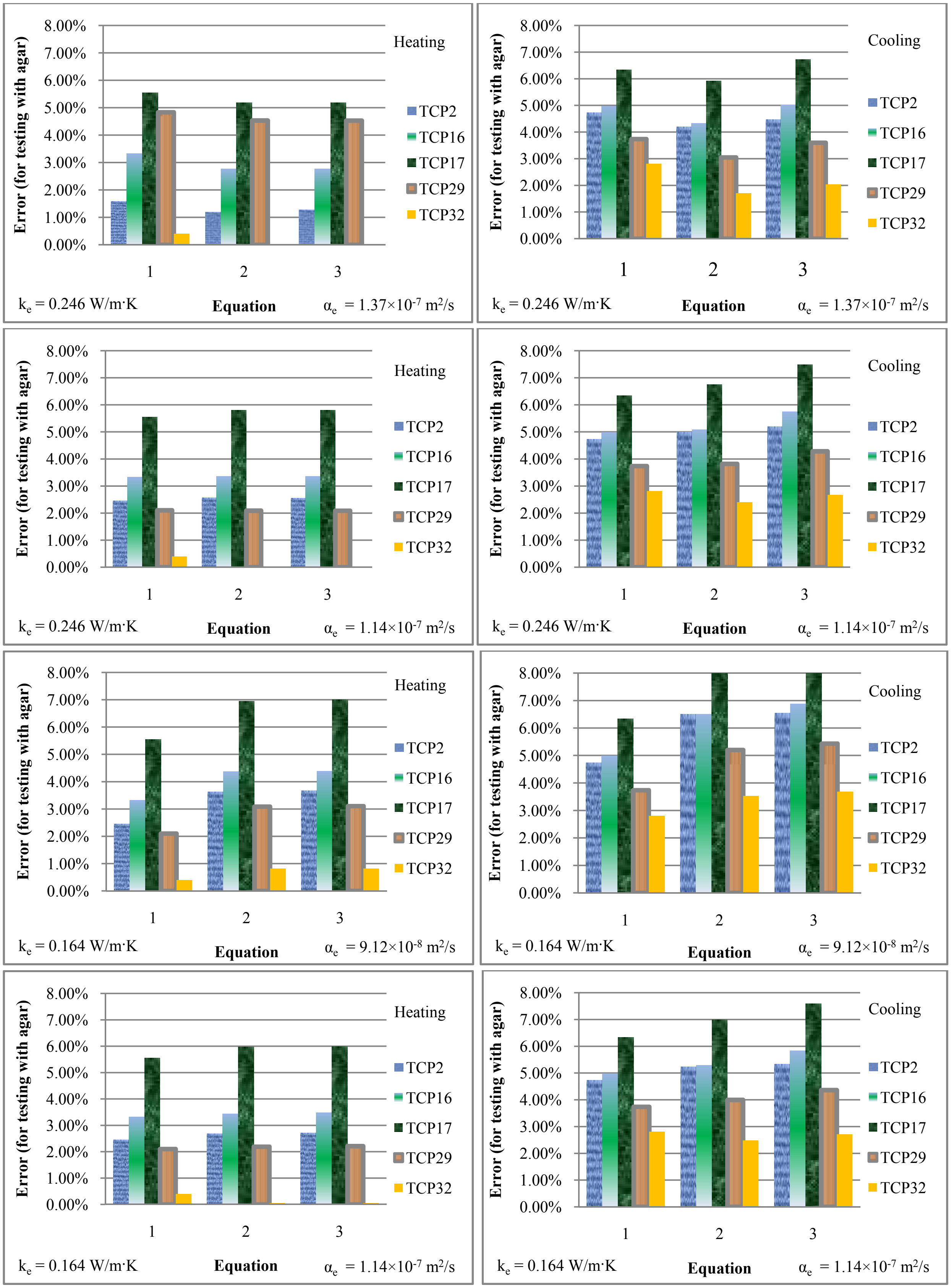

Figure 6.16. Error of average k_{agar} for using Eqs. 1, 2 and 3 with different values of k_e and α_e.

Table 6.5. List of investigated sets of values for k_e and α_e.

Parameter	**Case 1**	**Case 2**	**Case 3**	**Case 4**	**Unit**
k_e	0.246	0.246	0.164	0.164	$W/m \cdot K$
α_e	1.37×10^{-7}	1.14×10^{-7}	9.12×10^{-8}	1.14×10^{-7}	m^2/s

Fig. 6.16 shows the errors of k_{agar} obtained by using Eqs. 1, 2 and 3 in both heating and cooling periods. Basically, the difference between Fig. 6.16 and Fig. 6.10 is the set of values of k_e and α_e. From Fig. 6.16, the error of k_{agar} is sensitive to the values of k_e and α_e. Also, the error is more sensitive to α_e than to k_e. For example, for TCP17 with Eq. 2 and Eq. 3, increasing k_e by 20% will decrease the error by 0.2% whereas raising α_e by the same percentage only reduces the error by 1.0%. Therefore, the more accurately α_e is known, the more confidently the experimenter can report the measured k_{agar}. This result for confidence does not contradict the results of Figs. 4.8 and 4.9. In fact, they enhance each other. From Figs. 4.8 and 4.9, the experimenter can decide which materials to use for the TCP construction to have low errors. After the right materials are selected from a manufacturer's catalogue, the experimenter can ask the manufacturer to provide the materials with properties of higher accuracies. If the manufacturer does not have good enough materials, the experimenter can look for other manufacturers who produce the desired materials. Also, the more accurate the properties are, the more expensive the materials become. So knowing which property requires a higher accuracy from the manufacture can save the cost of the finished TCP. However, the experimenter needs to balance between the cost and the error.

Fig. 6.17 shows the k_m values of dry C109 sands as a function of t_0. Various sets of values of k_e and α_e are included. By comparing Fig. 6.16 with Fig. 6.11, k_m of dry C109 sand is more sensitive to α_e than to k_e. Therefore, if the value of α_e is more accurately known, k_m of dry C109 reported may be closer to each other.

Figs. 6.18-6.21 show the thermal conductivities of partially saturated C109 sands vs. t_0 by using Eq. 1, 2 and 3. The difference between the group of Figs. 6.18-6.21 and Fig. 6.12 is the sets of values of k_e and α_e.

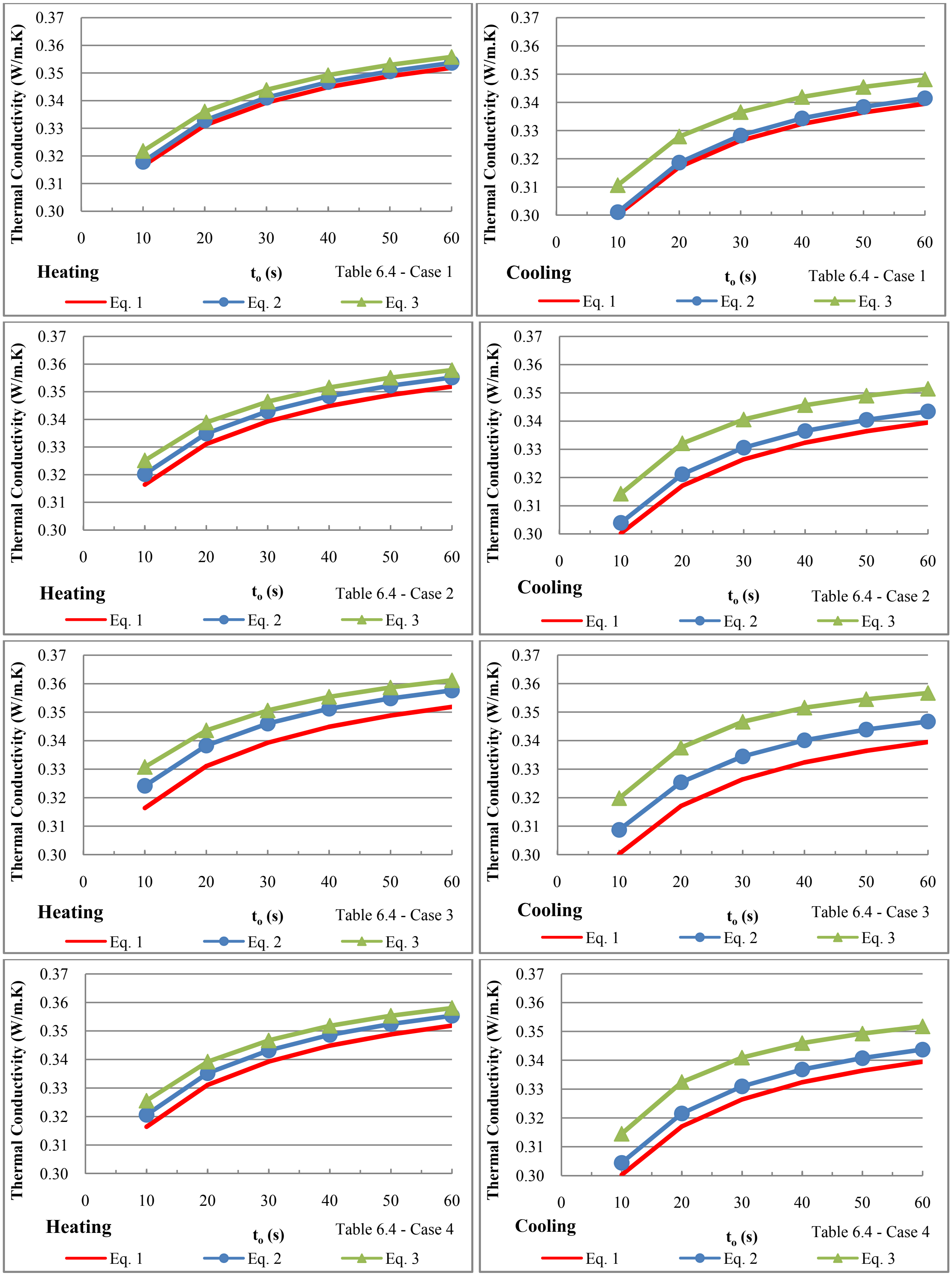

Figure 6.17. Error of k_{dry_C109} for using Eqs. 1, 2 and 3 with different values of k_e and α_e.

To better understand how the uncertainties of k_e and α_e affect the calculated k_m, Fig. 6.21 is plotted to display the differences of k_m for the cases shown in Table 6.5. The equation to calculate % difference of k_m is:

$$\%\ Difference = \frac{(k_m)_{Case\ i} - (k_m)_{Table\ 6.2}}{(k_m)_{Table\ 6.2}} \times 100\% \tag{6.15}$$

where $(k_m)_{Table\ 6.2}$ is the thermal conductivity value that is calculated using the experimental data and the parameters shown in Table 6.3, and

$(k_m)_{Case\ i}$ is the k_m value that is obtained using the experimental data and the parameters in Table 6.3 whose values of k_e and α_e are replaced by those of Case i shown in Table 6.5.

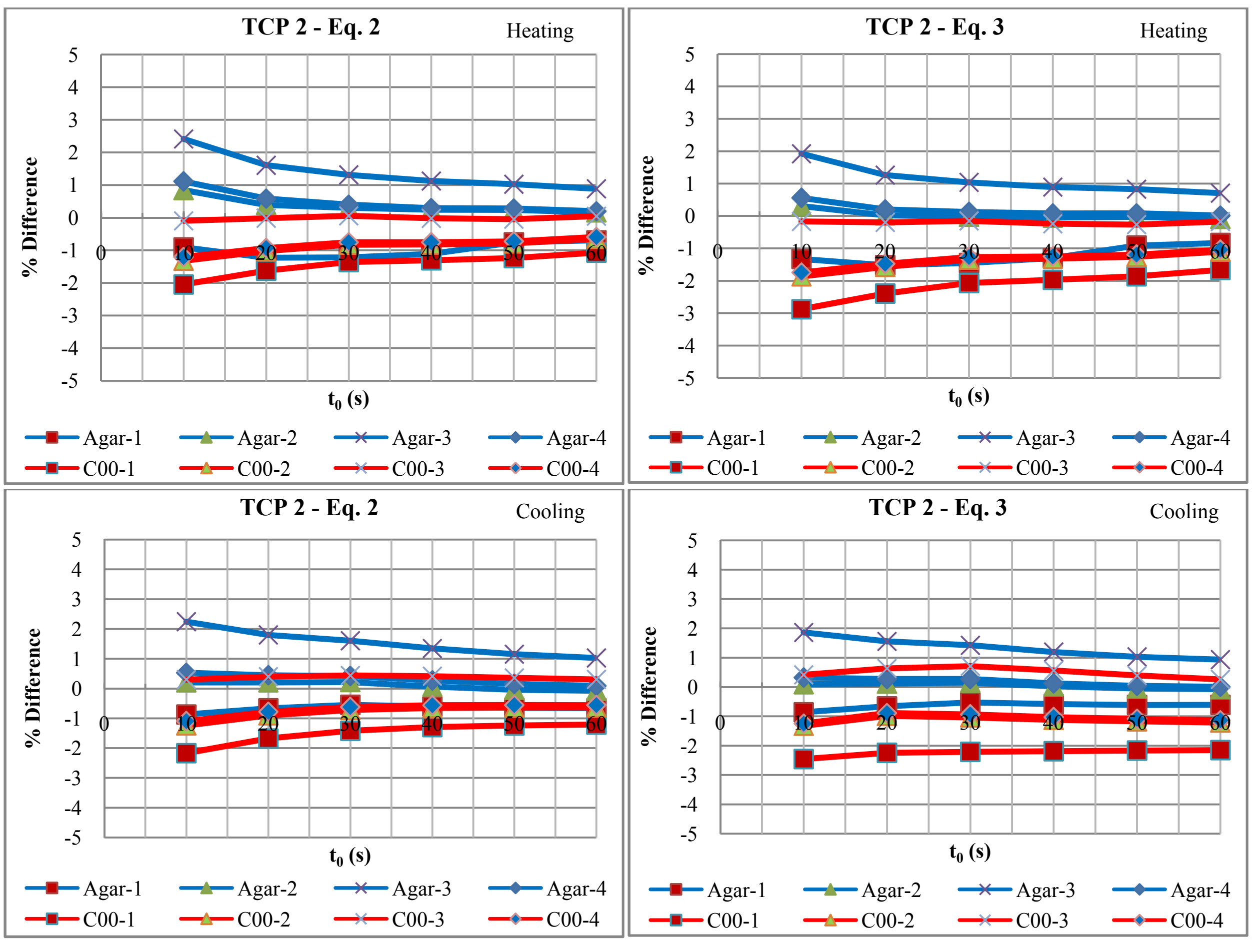

Figure 6.18. Percent Difference of thermal conductivities values vs. initiating time t_0 for the four cases shown in Table 6.5. TCP2 is applied.

One horizontal increment of the Fig. 6.18 represents 5 *s*. The legend indicates the sampling medium from which the % Difference is calculated and the case number tabulated in Table 6.5. For example, Agar-1 refers to the curve for the % difference that is from agar and the values of k_e and α_e of Case 1 in Table 6.5. Also, C00-3 means dry C109 sand (Sr = 0.0) and the Case 3 in Table 6.5.

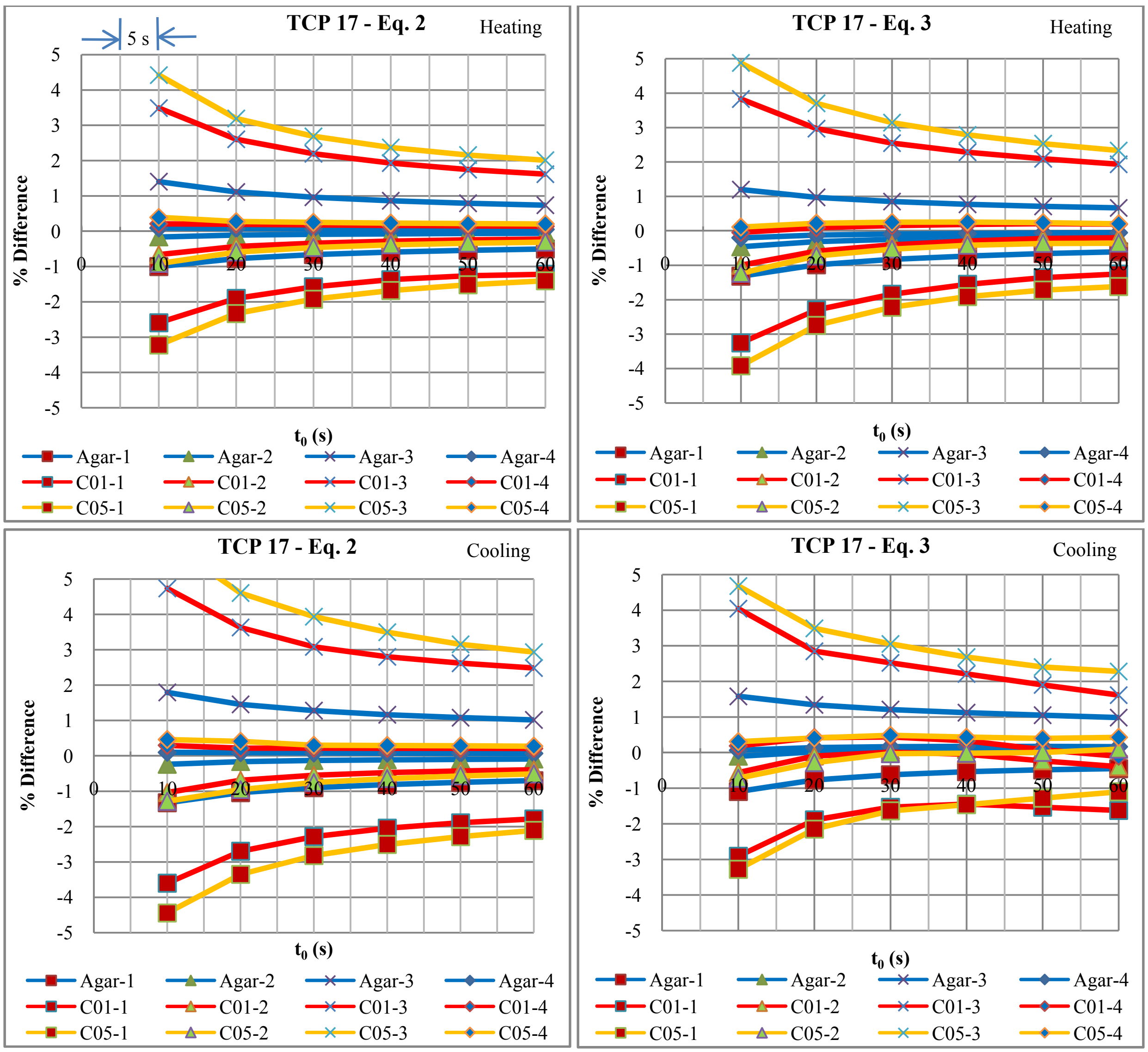

Figure 6.19. Percent Difference of thermal conductivities values vs. initiating time t_0 for the four cases shown in Table 6.5. TCP17 is applied.

Similar to the results of Fig. 6.18, the thermal conductivities of the sampling medium does vary as shown in Fig. 6.19. Depending on how accurate the values of k_e and α_e are, the reported k_m values may have small to large differences. For example, when TCP17 is used to measure the k_m

of C109 sand (Sr = 0.5), the k_m can have ±5% with short initiating time t_0 due to a ±20% change in α_e. However, the changing percentages of k_e and α_e can be from the dependencies on temperature of the two parameters. In other words, the material properties of the two parameters can vary with temperature during the measurement, so the reported k_m of the sampling medium has errors that the experimenter may not be aware of. Fortunately, the differences from varying k_e and α_e are relatively low and decreasing with higher initiating time t_0.

Nevertheless, the relatively low percentage difference of k_m values reported in this Section only applies to the particular TCP construction from Tarnawski *et al.* [11]. Other TCP construction methods may not produce the same percentage difference. The experimenter is recommended to verify his/her results by varying the thermal properties of the TCP materials.

6.4 - Design Parameters for TCP

In this Section, the errors of the k_m values are obtained by using the temperature responses from FEHT under different simulation conditions which are various t_0, heating powers, TCP materials, diameter ratios, TCP sizes, and thermocouple locations. The materials, of TCP and of sampling medium, with their thermal properties are listed in Tables 6.6 and 6.7. In addition, due to simulation and time restraints, Eqs. 1 and 2 are used to calculate, from FEHT temperature responses, the k_m values which are then compared with the k_m values that are input into the FEHT models. However, the effects of t_0 will be studied using both experimental and simulation data.

Table 6.6. Possible TCP materials with their corresponding thermal conductivities and thermal diffusivities ([65], [66], [34], [48], [50]).

TCP Material	*Silicon Rubber*	*Epoxy*	*Macor*	*Steel*	*Aluminum*	*Copper*
Shortened name	SR	E	M	S	A	C
***k* (W/m·K)**	0.170	0.682	1.470	16.20	204.0	385.9
α (m²/s)	2.00×10^{-7}	3.80×10^{-7}	7.23×10^{-7}	4.05×10^{-6}	8.41×10^{-5}	1.12×10^{-4}

Table 6.7. Sampling media with their corresponding thermal conductivities and thermal diffusivities ([65], [66], [17], [67], [10]).

TCP Material	*Stoneware Clay*	*Soil*	*Water*
Shortened name	SC	SL	WR
***k* (W/m·K)**	0.388	0.502	0.607
α (m²/s)	2.00×10^{-7}	3.80×10^{-7}	1.45×10^{-7}

The values for the parameters shown in Tables 6.6 and 6.7 are for present analysis only. The manufacturing processes of the TCP using such materials may or may not be possible or practical in reality. The errors of k_m values in Subsections 6.4.2 - 6.4.5 are defined as follows:

$$\%\ Error = 100 \times \frac{(k_m)_{Eq.} - (k_m)_{FEHT}}{(k_m)_{FEHT}} \tag{6.16}$$

6.4.1. Varying t_0

To better study the effect of t_0 on the calculate k_m, Fig. 6.20 is plotted and shows the percentage error of k_{agar} versus t_0 for different probes using TCP experimental data. As it can be seen, the lowest errors happen for t_0 in the range of 70 - 100 *s*. In addition, to better investigate the t_0 range in sand samples, Fig. 6.21 is plotted to illustrate the k_m values of dry and fully saturated C109 sand samples using TCP2 and TCP29. The calculated k_m values reach an extreme and then fluctuate. The extreme for all the calculated k_m values is generally in the range of 70 - 100 *s* of t_0. Before the reason for the unusual behaviors of the calculated k_m values is mentioned, it is important to first have a look at the FEHT numerical simulations to examine other parameters described at the beginning of Section 6.4 in Subsections 6.4.2 - 6.4.5. The errors in Subsection 6.4.1 are defined as follows:

$$\%\ Error = 100 \times \frac{(k_{agar})_{Eq.} - (k_{agar})_{ref}}{(k_{agar})_{ref}} \tag{6.17}$$

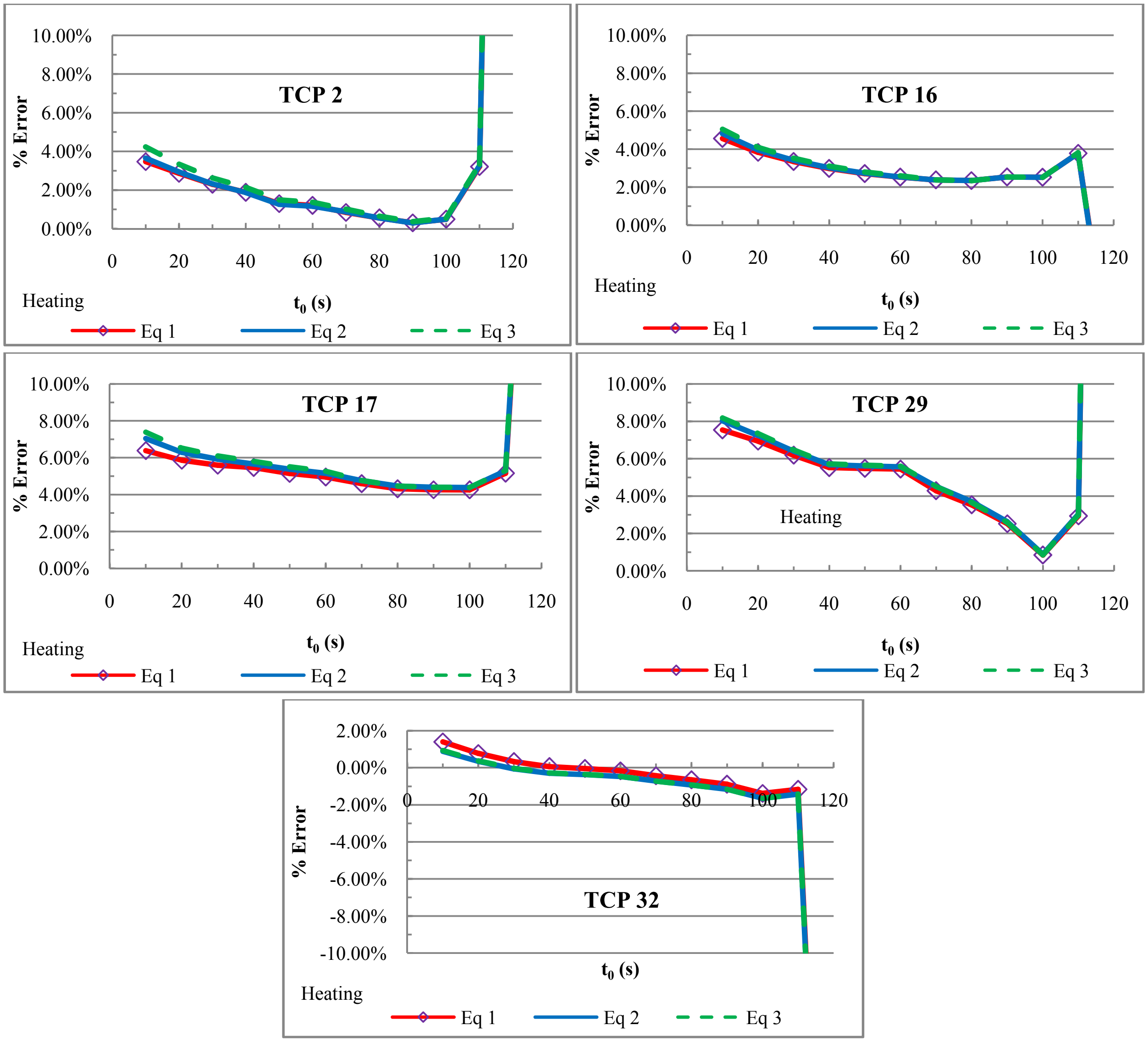

Figure 6.20. Percent error of calculated k_{agar} during the heating period from 0 - 120 s.

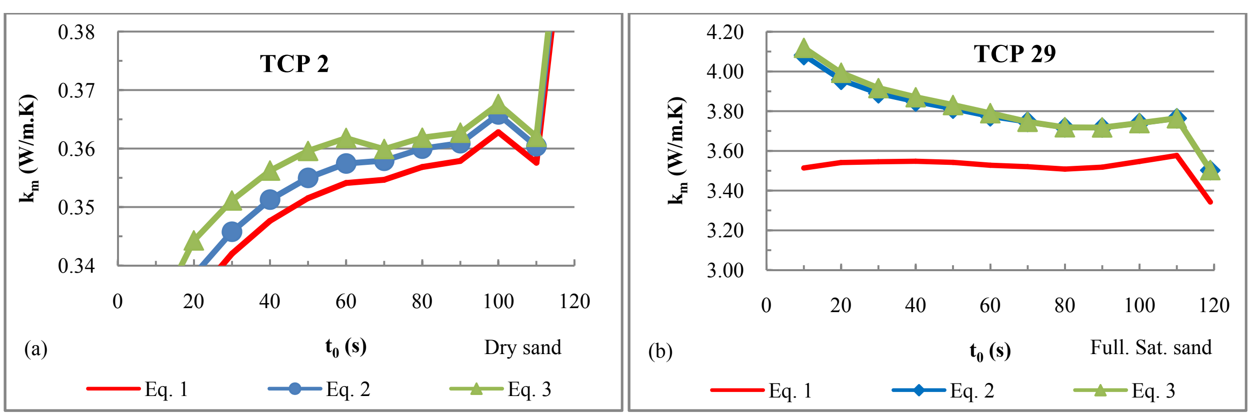

Figure 6.21. Percent error of calculated k_m during the heating period from 0 - 120 s for various TCPs and C109 sand samples. (a): TCP2 and dry sand. (b): TCP29 and fully saturated sand.

6.4.2 - Various Heating Powers

In Table 6.8, with different heating powers (HP), the errors of the k_m calculated by Eqs. 1 and 2 are shown. The initiating time t_0 is also included in the table. The first column of Table 6.8 displays the percentage error with different HPs shown in the last row using Eq. 1. The second column displays the t_0. The last column displays the percentage error with different HPs shown in the last row using Eq. 2. From Table 6.8, the errors of k_m by using Eq. 1 are higher than those by using Eq. 2. In addition, the errors decrease with increasing t_0 in both equations. However, varying HPs does not much affect the errors of the calculated k_m. Nevertheless, one should be careful of too high heating power as it can cause convection and moisture migration in porous media such as soils. On average, the error of using Eq. 1 with different HPs is 2.953% while that of using Eq. 2 is 0.273%. The high percentage error at small t_0 from applying Eq. 1 is due to the neglected thermal capacitance of the TCP at the beginning of the heating period. As time increases further, the TCP is closer to the steady state and the thermal capacitance of the TCP is less important.

Table 6.8. Percent error of calculated k_m with different heating powers (HP) using Eqs. 1 and 2. TCP materials and sizes are from Table 4.1.

Eq1					t_0 (s)	Eq2				
5.150	5.150	5.150	5.150	5.150	*10*	0.508	0.508	0.508	0.508	0.508
4.074	4.074	4.074	4.074	4.074	*20*	0.394	0.394	0.394	0.394	0.394
3.518	3.517	3.517	3.517	3.517	*30*	0.334	0.334	0.334	0.334	0.334
3.518	3.517	3.517	3.517	3.517	*40*	0.334	0.334	0.334	0.334	0.334
2.898	2.897	2.897	2.897	2.897	*50*	0.267	0.266	0.266	0.266	0.266
2.698	2.697	2.697	2.697	2.697	*60*	0.245	0.245	0.245	0.245	0.245
2.538	2.537	2.537	2.537	2.537	*70*	0.228	0.228	0.228	0.228	0.228
2.406	2.404	2.404	2.404	2.404	*80*	0.215	0.213	0.214	0.214	0.214
2.294	2.292	2.292	2.292	2.292	*90*	0.204	0.201	0.202	0.202	0.202
2.200	2.194	2.195	2.195	2.195	*100*	0.196	0.191	0.191	0.191	0.192
2.120	2.108	2.110	2.110	2.110	*110*	0.193	0.181	0.183	0.182	0.183
2.106	1.948	2.053	2.051	2.046	*119*	0.238	0.083	0.186	0.184	0.179
0.75	*1.5*	*3*	*6*	*12*	**HP (W/m)**	*0.75*	*1.5*	*3*	*6*	*12*

6.4.3 - Various Sampling Media and TCP Materials

Table 6.9 illustrates the percent errors by measuring different sampling media with different TCP material combinations. For example, the second row of the table shows the percent error of measuring different sampling media with a TCP constructed from epoxy and steel (E-S). In general, it seems to illustrate that measuring a sampling medium with low k_m using a TCP tends to have a higher error. The third row of the table shows the percent error of measuring different sampling media with a TCP constructed from epoxy and aluminum (E-A). From Table 6.9, it can be seen that having a less conductive buffering material (*i.e.*, the "epoxy" layer of TCP), the k_m value calculated can have higher errors. Also, having steel at the outermost layer produces lowest errors among the three tested metals. The overall average error for using Eq. 1 in the sampling media examined is 4.107% while that for using Eq. 2 is 1.291%.

Table 6.9. Percent error of calculated k_m with different sampling media, whose shortened names are from Table 6.7, using Eqs. 1 and 2. TCP materials and sizes are from Tables 4.1 and 6.6.

Eq1			TCP Materials	Eq2		
5.730	2.698	2.631	***E-S***	1.308	0.245	0.468
6.400	3.319	3.164	***E-A***	1.927	0.825	0.963
5.978	2.927	2.829	***E-C***	1.522	0.442	0.634
6.294	3.204	3.030	***SR-S***	2.687	1.743	1.983
6.965	3.824	3.562	***SR-A***	3.315	2.330	2.483
6.539	3.431	3.226	***SR-C***	2.902	1.940	2.147
5.651	2.632	2.593	***M-S***	0.958	-0.139	0.091
6.322	3.254	3.126	***M-A***	1.576	0.441	0.585
5.899	2.863	2.791	***M-C***	1.172	0.059	0.258
SC	***SL***	***WR***	**Medium**	***SC***	***SL***	***WR***

6.4.4 - Various TCP Sizes and Materials

Tables 6.10 - 6.12 shows the percent error of using Eqs. 1 and 2 with a TCP of various sizes, diameter ratios (DR), and materials. The sampling medium used to produce Tables 6.10 - 6.12 is Soil shown in Table 6.7. For example, the sixth row of Table 6.10 displays the errors of using Eqs. 1 and 2 with a TCP made from silicon rubber and aluminum (SR-A) and of Ø0.55 *mm* with various diameter ratios. Similar to Table 6.9, Tables 6.10 - 6.12 indicate that having a less conductive material in the buffering layer of the TCP produces higher errors of the calculated k_m. In addition, it is observed that having a larger buffering layer for the TCP makes the TCP less accurate in general. Furthermore, having steel at the outermost layer of the TCP produces lower errors. The overall average errors for using Eq. 1 with TCPs of Ø0.55 *mm*, Ø1.10 *mm*, and Ø1.65 *mm* are 1.594%, 3.510% and 6.156% respectively. The overall average errors for using Eq. 2 with TCPs of Ø0.55 *mm*, Ø1.10 *mm*, and Ø1.65 *mm* are 0.802%, 1.125% and 1.713% respectively.

Table 6.10. Percent error of calculated k_m with different diameter ratios (DR) using Eqs. 1 and 2 when various TCP materials are used. t_0 = 60 s, TCP diameter is 0.55 mm, and Soil as medium.

Eq1					TCP Materials	Eq2				
1.190	1.280	1.387	1.510	1.649	***E-S***	0.283	0.406	0.551	0.718	0.907
1.694	1.710	1.729	1.751	1.776	***E-A***	0.763	0.815	0.876	0.947	1.028
1.376	1.439	1.513	1.599	1.696	***E-C***	0.448	0.546	0.662	0.796	0.948
1.266	1.388	1.531	1.697	1.885	***SR-S***	0.440	0.654	0.908	1.200	1.532
1.769	1.816	1.872	1.937	2.011	***SR-A***	0.919	1.062	1.233	1.429	1.653
1.451	1.545	1.656	1.785	1.931	***SR-C***	0.604	0.793	1.017	1.277	1.573
1.174	1.260	1.361	1.477	1.609	***M-S***	0.232	0.331	0.449	0.584	0.737
1.678	1.690	1.703	1.719	1.736	***M-A***	0.712	0.740	0.774	0.814	0.858
1.361	1.419	1.487	1.566	1.656	***M-C***	0.397	0.472	0.560	0.663	0.778
0.5	***0.6***	***0.7***	***0.8***	***0.9***	**DR**	***0.5***	***0.6***	***0.7***	***0.8***	***0.9***

Table 6.11. Percent error of calculated k_m with different diameter ratios (DR) using Eqs. 1 and 2 when various TCP materials are used. t_0 = 60 s, TCP diameter is 1.10 mm, and Soil as medium.

Eq1					TCP Materials	Eq2				
2.422	2.660	2.940	3.263	3.628	***E-S***	-0.375	-0.042	0.351	0.805	1.319
3.835	3.865	3.900	3.940	3.986	***E-A***	0.940	1.080	1.246	1.437	1.653
2.948	3.107	3.296	3.513	3.760	***E-C***	0.077	0.342	0.657	1.020	1.433
2.595	2.908	3.277	3.702	4.184	***SR-S***	0.218	0.840	1.578	2.435	3.413
4.007	4.111	4.235	4.378	4.541	***SR-A***	1.536	1.961	2.466	3.049	3.711
3.118	3.352	3.630	3.950	4.315	***SR-C***	0.669	1.224	1.883	2.650	3.528
2.403	2.635	2.908	3.223	3.579	***M-S***	-0.520	-0.251	0.067	0.433	0.848
3.817	3.841	3.869	3.901	3.937	***M-A***	0.795	0.871	0.961	1.064	1.182
2.930	3.083	3.265	3.474	3.712	***M-C***	-0.067	0.135	0.373	0.649	0.962
0.5	***0.6***	***0.7***	***0.8***	***0.9***	**DR**	***0.5***	***0.6***	***0.7***	***0.8***	***0.9***

Table 6.12. Percent error of calculated k_m with different diameter ratios (DR) using Eqs. 1 and 2 when various TCP materials are used. t_0 = 60 s, TCP diameter is 1.65 mm, and Soil as medium.

Eq1					TCP Materials	Eq2				
4.394	4.766	5.205	5.713	6.290	***E-S***	-0.900	-0.353	0.294	1.043	1.897
6.798	6.819	6.844	6.872	6.903	***E-A***	1.274	1.506	1.781	2.098	2.457
5.292	5.532	5.815	6.144	6.518	***E-C***	-0.155	0.282	0.800	1.401	2.087
4.624	5.098	5.659	6.309	7.050	***SR-S***	0.273	1.376	2.697	4.239	6.022
7.030	7.155	7.303	7.473	7.667	***SR-A***	2.482	3.281	4.234	5.346	6.617
5.518	5.860	6.266	6.738	7.276	***SR-C***	1.023	2.019	3.211	4.609	6.220
4.397	4.773	5.217	5.730	6.313	***M-S***	-1.145	-0.707	-0.190	0.409	1.090
6.801	6.826	6.855	6.889	6.926	***M-A***	1.026	1.148	1.292	1.458	1.646
5.297	5.540	5.828	6.162	6.541	***M-C***	-0.398	-0.071	0.318	0.767	1.279
0.5	***0.6***	***0.7***	***0.8***	***0.9***	**DR**	***0.5***	***0.6***	***0.7***	***0.8***	***0.9***

6.4.5 - Various Thermocouple Locations

Table 6.13 displays the percent error using Eqs. 1 and 2 with different thermocouple locations inside the epoxy layer. The TCP materials are shown in Table 4.1. By increasing the distance from the axis of the TCP, the calculated k_m becomes slightly less accurate. The overall average of using Eq. 1 for various thermocouple locations is 3.560% while that of using Eq. 2 is 0.335%. The reason for the high percentage error at small t_0 was explained in Subsection 6.4.2.

Table 6.13. Percent error of calculated k_m with different thermocouple (TC) locations using Eqs. 1 and 2 when various heating powers are used. TCP diameter is 1.10 mm, and Soil as medium.

Eq1					t_0 (s)	Eq2				
5.041	5.061	5.087	5.150	5.234	***10***	0.487	0.491	0.495	0.507	0.522
3.993	4.008	4.027	4.074	4.135	***20***	0.376	0.379	0.383	0.393	0.406
3.451	3.463	3.479	3.517	3.568	***30***	0.318	0.321	0.324	0.333	0.344
3.099	3.110	3.123	3.157	3.201	***40***	0.281	0.283	0.286	0.294	0.304
2.845	2.855	2.867	2.897	2.937	***50***	0.254	0.256	0.259	0.266	0.275
2.649	2.658	2.670	2.697	2.734	***60***	0.233	0.235	0.238	0.244	0.253
2.493	2.501	2.511	2.537	2.571	***70***	0.217	0.219	0.221	0.227	0.235
2.363	2.370	2.380	2.404	2.436	***80***	0.203	0.205	0.207	0.213	0.221
2.253	2.260	2.269	2.292	2.322	***90***	0.192	0.194	0.196	0.201	0.208
2.158	2.165	2.173	2.195	2.224	***100***	0.183	0.184	0.186	0.191	0.198
2.076	2.082	2.089	2.110	2.137	***110***	0.175	0.176	0.177	0.182	0.189
2.015	2.033	2.042	2.053	2.077	***119***	0.174	0.186	0.190	0.186	0.190
120	***160***	***200***	***275***	***350***	**TC Location (μm)**	***120***	***160***	***200***	***275***	***350***

Furthermore, combining Figs. 6.20 and 6.21 and Tables 6.8 and 6.13 show that for a t_0 value too close to the end of the heating period (t_c = 120 s), the calculated k_m will become strange. The reason is from the number of data points of the temperature response available to calculate k_m using the methods in Section 6.1 described earlier. The sampling rate of the experimental TCPs was 15 readings per second. As a result, there were less than 300 temperature data points for the calculations of k_m in Figs. 6.20 and 6.21 with 100 $s < t_0 \leq 119$ s. Similar situations also happened to the simulations shown in Tables 6.8 and 6.13. Since the time step was 0.01 s, there were only 100 temperature data points to calculate k_m for t_0 = 119 s. Consequently, the errors for t_0 = 119 s in Tables 6.8 and 6.13 sometimes do not follow the norm of higher t_0 producing more accurate k_m. The same behaviors of the k_m calculated in Figs. 6.20 and 6.21 also do not follow the norm with too high t_0. Therefore, it is recommended that a TCP with higher sampling rates should be used so that there are more temperature data points at larger t_0 to produce more accurate k_m.

6.5 - Summary

In this chapter, the following parameters were investigated:

1. Thermal contact resistance (TCR). By using the temperature responses in the heating period, the R_c values were found to be from 5×10^{-5} to 2.5×10^{-4} $m^2\cdot K/W$ for agar-water, from 2×10^{-3} to 3.1×10^{-4} $m^2\cdot K/W$ for dry C109 sands, and from 2×10^{-4} to 4.9×10^{-4} $m^2\cdot K/W$ for partially saturated C109 sands. The R_c values for the fully saturated C109 sands were very similar to those of agar-water. However, the cooling period was found to produce higher R_c values because of the reactions to heat of the sampling media. For example, the TCP hole in the agar-water gel solution could have enlarged during the measurements. In addition, moisture migration of partially saturated C109 Ottawa sands occurred in the TCP experiments. Depending on the factors such as geometry of the sampling media and the thermal gradients, the moisture migrated away from the TCP and may or may not return in the cooling period. In fully saturated C109 sands, the TCP could have attracted air bubbles (a possible error from the sample preparation procedures) by the high heating power of approximately 10 *W/m*. The water content of the fully saturated sands may or may not return in the cooling period due to the geometry of the sampling media and the low thermal gradients. Furthermore, the R_c values show a decreasing trend with increasing water content as illustrated in Fig. 6.4. Nevertheless, this parameter has a little influence on the calculated k_m values of the sampling media. Also, Murakami *et al.* [23], Elustondo *et al.* [34] and Liang *et al.* [27] reported that the TCR does not greatly affect the calculated k_m values. The reason is the TCR only shifts the *T-t* plot (*e.g.*, Fig. 6.1) up or down but does not change the slope of the plot, on which the k_m value heavily depends.
2. Initiating time t_0. The parameter t_0 is the time where researchers initiate the calculation of the thermal conductivity of the sampling medium from the temperature response. As shown in Figs. 6.4 - 6.19, the higher the value of the time is, the higher accuracies can be reported with R_c and k_m. This time parameter t_0 has been highly subjective and unexplained. ASTM [22] recommends ignoring the temperature data of the first 10 to 30 *s* with probes of diameter 2.5 *mm* or less without providing any reasons. Searches in the literature also provided no clarification to which value of t_0 to use to obtain more accurate k_m. In this thesis, the t_0 was found to play an important factor in the levelling off of the

calculated k_m. At small values, the time parameter can lead to highly erroneous k_m as shown in Figs. 6.11, 6.14, 6.15, 6.17, 6.18, and 6.19. As t_0 gets larger, the calculated k_m converges. If the experimenter is about to report the k_m value calculated from insufficient (or small) t_0, the convergent error could occur. Kersten [63] reported k_m data of C109 sands from GHPA measurements. Farouki [64] re-touched the sands with the TCP method and observed disagreed data with those of Kersten. Other than the moisture migration problems with the GHPA, choosing inappropriate t_0 in TCP measurements can lead to additional errors that the experimenter may not be aware of. Also, searches in the literatures provides no previous work on how t_0 affects the calculated k_m. Furthermore, in Section 6.4, by combining experimental results with FEHT simulations, it was found that an insufficient number of temperature data points at larger t_0 produces unreliable calculated k_m values. It is recommended that there should be at least 300 temperature data points to obtain reliable and more accurate k_m values (at large t_0) from TCP experiments.

3. The thermal conductivity (k_e) and thermal diffusivity (α_e) of the epoxy. One Ultra Low Viscosity Kit from SPI Supplies was bought and tested for the k_e and α_e. The values of the two parameters were found to be 0.205 $W/m{\cdot}K$ ±12.04% and 1.14×10^{-7} m^2/s ±17.44%. Although the parameters have high uncertainties, the k_m values of the sampling media were found to be mostly within ±5.0% with ±20% changes in k_e and α_e as shown in Figs. 6.18 and 6.19. Also, the uncertainty of α_e affects the changes in k_m more than k_e does. The changes in k_m by varying k_e and α_e can help the experimenter become more confident in the reported k_m because k_e and α_e may be sensitive to the temperature. Moreover, the experimenter can save manufacturing costs of the TCP by understanding which material property is more important to have higher accuracy from the manufacturer. Together with the results of Figs. 4.8 and 4.9, the experimenter can better select the desirable materials for more accurate and less expensive TCPs.
4. The comparisons between the heating and cooling periods. In this chapter, the cooling period was found to produce less accurate k_m values. The reason is from the heat sink model (HSM), as follows:

$$\Delta T_{cool}(r,t) = \Delta T_{heat}(r,t) - \Delta T_{heat}(r,t-t_c) \text{ for } t > t_c \tag{6.18}$$

where t_c is the heating time of the TCP.

The right hand side (RHS) of Eq. 6.18 means the difference between the temperature rise starting from the heating period and the temperature rise starting from the cooling period using Eq. 3.1a. The second term on the RHS of Eq. 6.16 means the heat sink for the cooling period. In deriving Eq. 3.1a, Carslaw and Jaeger [16] assumed uniform initial temperature for all points in the TCP and the sampling medium. However, the assumption is not true in the cooling period. Therefore, applying the HSM to the cooling period produces less accurate values of the calculated k_m. In other words, the cooling period produces less accurate results of k_m values.

5. In reality, the thermal properties of the TCP materials and sampling media mostly cannot be varied individually. In other words, the thermal conductivity and thermal diffusivity are related to each other. Also, due to the funding and time restraints of this thesis, errors of calculated k_m by varying the following parameters were investigated numerically:
   - Probe sizes, sampling media, and TCP materials: Different TCP diameters, TCP materials, and diameter ratios were studied. It was found that bigger TCPs produces less accurate k_m. Also, more conductive buffering layer (*i.e.*, the "epoxy" layer of TCP) should be used to improve the accuracy of k_m. With the tested theoretical values shown in Tables 4.1 and 6.6, the overall average errors of TCPs with diameters of 0.55 *mm*, 1.10 *mm* and 1.65 *mm* were respectively 1.594%, 3.510% and 6.156% for Eq. 1 while those for Eq. 2 are 0.802%, 1.125% and 1.713%.
   - Heating powers: Different heating powers (HPs) were used. It was found that the HPs have slight to no effects on the k_m calculated. The overall average errors of various HPs were 3.642% for Eq. 1 and 0.347% for Eq. 2. However, high heating powers in TCP experiments can create moisture migration in porous media which was not considered in the simulations using FEHT.
   - Thermocouple location: By varying the thermocouple location (r_{sen}), it was found that the further away from the central axis the TCP is, the less accurate the calculated k_m becomes. However, increasing r_{sen} insignificantly decreases the accuracy of the calculated k_m.

CHAPTER 7 - CONCLUSION AND RECOMMENDATIONS

7.1 - Concluding Remarks

TCPs (*e.g.*, as shown in Fig. 5.1) are very attractive being an excellent technique to obtain the thermal conductivities of a variety of materials with relatively better accuracies than other measuring methods such as GHPAs. The TCPs are versatile for making inline measurements, *i.e.* the sampling medium is not required to be taken apart to make measurements. The TCPs are also very portable and easily carried to the test site. In addition, they are relatively inexpensive. Due to its high versatility, simplicity and relatively inexpensiveness, TCPs have been extensively applied with various designs. The application fields for TCPs include biomedical engineering, food and ground source heat pump systems for buildings. With a better knowledge of the thermal conductivities of materials, human lives can be enhanced. For example, Yi *et al.* [26] found that radiofrequency ablation (RFA) causes the thermal conductivities of the biomaterials to increase. And Liang *et al.* [27] realized that the moisture content in biomaterials greatly affect the thermal conductivities. Combining the results of Yi *et al.* and Liang *et al.*, RFA can be better used on the individual basis.

A thermal conductivity probe is usually made of a stainless steel hypodermic tube with epoxy filling the inner space. Within the epoxy layer of the TCP, there lie an electrical heating wire and a thermocouple. The steel tube is for providing insertion strength into a sampling medium (a liquid or a soft or granular solid) while the epoxy acts as a buffer to protect the heating wire and the thermocouple. The heating wire is electrically heated and the thermocouple senses the temperature rise at a point inside the epoxy layer. The temperature rise is then used to calculate the thermal conductivity of the sampling medium. Most thermal conductivities obtained from TCP measurements have been calculated by Eq. 1.3 using asymptotic approximation as follows (Carslaw and Jaeger [16]):

$$T(r,t) = \frac{-\dot{q}_w}{4\pi k_m} Ei\left(\frac{-r^2}{4\alpha_m t}\right) + T_i \tag{1.3a}$$

or $$T(r,t) \approx \frac{\dot{q}_w}{4\pi k_m}\left[\ln\left(\frac{4\alpha_m t}{r^2}\right)-\gamma\right]+T_i \qquad \text{for } \frac{4\alpha_m t}{r^2} >> 1 \tag{1.3b}$$

For a chosen temperature $T(r,t)$ at time t_0, the thermal conductivity of the sampling medium can be calculated from:

$$k_m = \frac{\dot{q}_w}{4\pi}\frac{1}{slope} \qquad \text{for } \frac{4\alpha_m t_0}{r^2} >> 1 \text{ and } t_1 \geq t_0 \tag{1.4}$$

where *slope* is the slope of linear portion that is typically as shown in Fig. 1.4.

However, in deriving Eq. 1.3, Carslaw and Jaeger [16] made several assumptions and simplifications that have been studied and reported as errors. The errors are listed as follow.

7.1.1 - Errors from Probe Sizes

By looking at Eq. 1.3, regardless of how big the TCP is, the same equation is applied. In other words, Carslaw and Jaeger [16] assumed that the probe size is insignificant. As indicated by Bristow *et al.* [23] and Cheng *et al.* [24], bigger probes produce higher errors. Murakami *et al.* [23] even suggested making a customized probe for a particular measurement, which poses high manufacturing costs.

Nevertheless, the researchers only reported the outermost diameter of the TCPs as one source of errors but did not mentioned the wall thickness of the probes as another possible source of errors. And due to the high costs and time required to manufacture TCPs with various wall thicknesses of the steel tubes, the errors from the wall thickness were theoretically and analytically studied. The theoretical and analytical errors in comparisons with FEHT are defined as:

$$\%Error = \left(\frac{T_{Eq}-T_{FEHT}}{T_{FEHT}}\right)\times 100 \tag{4.1}$$

From Fig. 4.4, it was found that not only does bigger probe produce higher errors but also does the wall thickness of the TCP. With the probe sizes examined, the error range could be from 1.5% (DR = 0.9) to 3.8% (DR = 0.5) for the smallest probe (Ø0.55 *mm*) and from 3.0% (DR =

0.9) to 5.5% (DR = 0.5) for the biggest probe (Ø1.65 *mm*) using Eq. 1. On the other hand, by using Eq. 2, the error ranged from 0.6% (DR = 0.9) to 0.1% (DR = 0.5) for the smallest probe (Ø0.55 *mm*) and from 0.2% (DR = 0.9) to 0.1% (DR = 0.5) for the biggest probe (Ø1.65 *mm*). The reason is from the inhomogeneous properties of the materials. The values of k_e and α_e were chosen to be closer to those of k_m and α_m than the values of k_s and α_s are. As a result, with a larger steel section, the homogeneous assumption was more violated and higher errors appeared.

However, the error defined in Eq. 4.1 is for the error of the temperature responses. The error of the calculated k_m is defined as

$$\%Error = 100 \times \frac{(k_m)_{Eq.} - (k_m)_{ref}}{(k_m)_{ref.}} \tag{6.17}$$

By looking at Tables 6.10 - 6.12, it was shown that bigger DRs and TCP diameters give less accurate k_m values for using both equations. The changes in the error of the calculated k_m by increasing DR and using Eq. 1 are slight while those by increasing DR and using Eq. 2 are more. Nevertheless, using Eq. 2 produces more accurate k_m. In general, with the parameters whose values are shown in Tables 4.1 and 6.6, the errors of using Eq. 1 range from 1.174 - 2.011% while those of using Eq. 2 are from 0.283 - 1.653%.

7.1.2 - Errors from Heating Powers (HP)

Searches in the literatures provided no prior study on the effect of how changing the heating power can produce errors in the temperature response. Consequently, it is worth to theoretically and analytically explore the situation. As indicated by Fig. 4.6, by using Eq. 1in comparison with FEHT in the heating period, the errors ranged from 0.5% to 4.9% for heating powers from 0.75 *W/m* to 1.5 *W/m* respectively. However, by using Eq. 2 in comparison with FEHT, the errors were in the interval of 0.0% and 0.1% for heating powers from 0.75 *W/m* to 1.5 *W/m*.

Nevertheless, by using Eq. 6.17 to understand how k_m is affected by changing HPs, Table 6.8 shows that HP slightly influences the error of the calculated k_m with both Eqs. 1 and 2. The values of the errors can range from 2.046 - 5.150% with Eq. 1 and 0.083 - 0.508% with Eq. 2, depending on the value of t_0.

7.1.3 - Errors from Sampling Different Media

The assumption of homogeneous material may be violated with measuring various sampling media. As theoretically and analytically shown in Figs. 4.6 and 4.7, when the thermal properties of the materials were more different, the absolute values of errors increased. Also, the errors were more sensitive to the k_m value than the α_m value. However, the errors preferred more heat resistant sampling media, *i.e.*, media with lower k_m values produced higher errors. By applying Eq. 1, the error ranged from 22% (for k_m = 0.126 *W/m·K*) to -2.5% (for k_m = 2.008 *W/m·K*). Meanwhile, by using Eq. 2, the error ranged from 12% (for k_m = 0.126 *W/m·K*) to -1.0% (for k_m = 2.008 *W/m·K*). Also, the errors tended to converge at large time at 1.7% for Eq. 1 and 0.0% for α_m from 0.033 mm^2/s to 0.520 mm^2/s.

However, in reality, the thermal conductivity is related to the thermal diffusivity in all materials. In other words, the two parameters cannot be studied individually. As a result, different sampling media with different thermal properties were chosen to be analyzed numerically. With Tables 4.1 and 6.9 and Eq. 6.17, it was shown that with different sampling media, the errors of the calculated k_m can vary.

7.1.4 - Errors from Thermal Properties of TCP Materials

In the literatures, the thermal properties of the materials used to build TCPs have been extensively grouped together as one homogeneous material (*e.g.*, Blackwell [39] and Murakami *et al.* [23]). However, the definition of the grouping has been unclear. And there is a tremendous amount of materials that can be used to construct TCPs. Therefore, the thermal properties of the TCP materials were theoretically and analytically studied. From Figs. 4.8 and 4.9, the more inhomogeneous the TCP materials are to the sampling medium, the more the errors become. By using Eq. 1, the error ranged from -10% (for k_e = 0.085 *W/m·K* and k_s = 16.20 *W/m·K*) to +4.0% (for k_e = 2.728 *W/m·K* and k_s = 16.20 *W/m·K*) and from 0.0% (for k_e = 0.341 *W/m·K* and k_s = 64.8 *W/m·K*) to +10% (for k_e = 10.91 *W/m·K* and k_s = 64.8 *W/m·K*). On the other hand, by using Eq. 2, the error ranged from 0.0% (for k_e = 0.085 $W/m{\cdot}K$ and k_s = 16.20 $W/m{\cdot}K$) to +0.2% (for k_e = 2.728 $W/m{\cdot}K$ and k_s = 16.20 $W/m{\cdot}K$) and from 0.0% (for k_e = 0.341 $W/m{\cdot}K$ and k_s = 64.8 $W/m{\cdot}K$) to +7.0% (for k_e = 10.91 $W/m{\cdot}K$ and k_s = 64.8 $W/m{\cdot}K$). Moreover, changing the thermal diffusivities of the TCP construction materials did not much affect the theoretical error defined in Eq. 4.1 for both Eqs. 1 and 2 as shown in Fig. 4.9.

However, with Tables 4.1 and 6.9 and Eq. 6.17, it was found that the buffering layer (or the epoxy layer shown in Fig. 41) should be more heat conductive in order to obtain more accurate k_m values. In general, with the tested sampling media, the errors of using low thermal conductive "epoxy" range from 2.59% to 6.965% for Eq. 1 and -0.139% to 3.315% for Eq. 2.

7.1.5 - Errors from Thermocouple Locations

In Eqs. 1 and 2, there exists a parameter for the location of the thermocouple. This parameter can create errors. However, in reality, it is hard to position the thermocouple to the desired location with a position tolerance of 1 μm or less. Consequently, theoretical and analytical studies were made to explore the possible errors from the locations of the thermocouple. As shown in Fig. 4.10, by using Eq. 1, the radially further away from the central axis the thermocouple was, the more accurate the temperature response was. With the examined thermocouple locations, the error ranged from +2.6% for r_{sen} = 120 μm to +1.4% for r_{sen} = 350 μm. On the contrary, by using Eq. 2, the error stayed almost constant at about -0.05% at large time.

Furthermore, to study how k_m varies with changing r_{sen}, Eq. 6.17 should be used. By varying r_{sen} with the parameters shown in Table 4.1, Table 6.13 illustrated that higher r_{sen} slightly decreases the accuracy of the obtained k_m with both Eqs. 1 and 2, depending on the t_0 value. In general, the errors of calculated k_m range from 2.015% to 5.234% for using Eq. 1 and from 0.174% to 0.522% for using Eq. 2.

7.1.6 - Errors from Boundary Conditions of the Sampling-Medium Container

Two cases of boundary conditions were investigated: adiabatic and isothermal. For both cases, when the thermocouple was axially varied within ±2 mm of the centroid (h = 25 mm) of the TCP, the differences in the temperature response of the thermal sensor were almost zero with various heating powers. The equation used for the temperature difference (TD) was defined as:

$$TD = T(r_{sen}, h_i) - T(r_{sen}, h = 25mm) \tag{4.2}$$

where h_i is the height level of the thermocouple of the same radius.

Moreover, the TD for the isothermal case was found to be analytically constant among various radial locations of the thermocouple. On the contrary, the TD for the adiabatic case analytically exhibited a reducing trend as the thermocouple moved radially further away from the central axis of the TCP.

7.1.7 - Errors from Axial Heat Conduction of the Length-to-Diameter Ratio (LDR) of 50

As theoretically studied by Blackwell [39], the axial flow error of TCPs with LDR of 30 was 0.051%. With a higher LDR, the error would be less. However, the researcher applied assumed and arbitrary values to calculate the error caused by the axial flow. As a result, COMSOL simulations were run to verify the result of Blackwell. The input parameters for COMSOL were shown in Table 4.1. And two cases of boundary conditions were studied: adiabatic and isothermal. The heat flux ratio was defined as

$$ratio_{HF} = \frac{q_{axial}}{q_{radial}} \approx \frac{\Delta T_{axial}}{\Delta h} \cdot \frac{\Delta r}{\Delta T_{radial}} \tag{4.3}$$

where *HF* means heat flux, q is the heat flux in a direction, ΔT_{axial} and ΔT_{raial} are the temperature differences (from COMSOL) between two points in the axial and radial directions respectively, Δh is the difference of the heights of the two points, and Δr is the difference of the radial locations of the two points.

When $\Delta h = \Delta r = 0.1\ \mu m$, Eq. 4.3 becomes

$$ratio_{HF} \approx \frac{\Delta T_{axial}}{\Delta T_{radial}} \tag{4.4}$$

In both cases of the boundary conditions studied, the $ratio_{HF}$ was found to be about 0.163% for $t > 20\ s$. Because the temperature response in the first 20 s is mostly ignored in TCP measurements, the error caused by the axial flow is expected to be 0.163%. However, the error of 0.163% may not be true when the parameters in Table 4.1 have other values.

7.1.8 - Errors from Thermal Contact Resistance (TCR)

In deriving Eq. 1, Carslaw and Jaeger [16] ignored the TCR, which may be a significant source of errors. Researchers such as Elustondo *et al.* [34] and Murakami *et al.*[23] questioned the validity of the neglected TCR and investigated the parameter. The results from the investigations revealed that the TCR has few to no effects on the calculated k_m, which is in good agreement with the TCR studies in this thesis. By looking the curves produced by Eq. 2 and Eq. 3 in figures such as Fig. 6.6, one can observe that the differences from the two equations were small to very small at large time. The reason is at large time, the TCR term in Eq. 3 is almost constant, so the difference between two temperature responses cancels the term.

7.1.9 - Errors from the Initiating Time t_0

Although not being in Eqs. 1, 2 and 3, this parameter is important in the calculation of k_m. Searches through the literatures gave subjective choices of t_0, the time where the calculation of k_m is initiated. ASTM [22] recommends t_0 from 10 to 30 *s* with TCPs of diameters of 2.5 *mm* or less without any justification. Tarnawski *et al.* [21] also applied t_0 at 20 *s* with no clarification. As a result, most of the figures in Chapter 6 was calculated based on various t_0 values to investigate the influence of the parameter on k_m. As shown in most of the figures in Chapter 6, k_m converges to a certain value when t_0 becomes large enough. In other words, arbitrary selection of t_0 can be a significant source of errors.

However, choosing t_0 of too high values can produce low to high errors. As shown in Figs. 6.20 and 6.21 and Tables 6.8 and 6.13, the k_m values calculated from high t_0 can be bad to report. In the TCP experiments, the sampling rate was 15 readings per second. For 100 $s < t_0 < 120$ s, there are at max 300 temperature data points to calculate k_m and Figs. 6.20 and 6.21 showed that the calculated k_m becomes out of norm, *i.e.*, higher t_0 makes the k_m levels off. In FEHT simulations, the time step was 0.01 *s*. The calculated k_m also becomes out of norm with $t_0 \geq 119$ s. Therefore, it is recommended to have at least 300 temperature data points in TCP experiments.

7.1.10 - Errors from the Decision to Use Heating or Cooling Period for k_m

Theoretically, both the heating and cooling periods can be used to obtain k_m. How to calculate k_m from the heating period is by Eqs. 1.3 and 1.4. The heat sink model (HSM) can be used to obtain k_m from the cooling period as follows (de Vries [47] and Liu *et al.*[42]):

$$\Delta T_{cool}(r,t) = \Delta T_{heat}(r,t) - \Delta T_{heat}(r,t_c) \quad \text{for } t > t_c \tag{3.1b}$$

Basically, the right hand side (RHS) of Eq. 3b means the temperature difference of the temperature rises starting at 0 *s* and at the end of the heating period. The second term on the RHS is the heat sink. The definition for each term on the RHS of Eq. 3.1b is defined in Eq. 1.3a. However, there are problems with the HSM. First of all, the initial temperature at the beginning of the heating period is not the same as that of the cooling period at every point in the TCP and the sampling medium. But the HSM assumes the initial temperatures in both periods are the same. Secondly, in practical situations, the residual heat of the TCP after the electricity has been cut off may or may not last through the measuring time of the cooling period. But the HSM assumes the residual heat lasts forever. With the two assumptions, the cooling period is suspected to produce less accurate k_m values.

7.1.11 - Errors from the Tolerance in the Thermal Properties of the TCP Materials

From the epoxy measurement, the values of k_e and α_e were found to be 0.205 $W/m{\cdot}K$ ±12.04% and 1.14×10^{-7} m^2/s ±17.44% respectively. The relatively high uncertainties could produce inconsistent k_m values. As a result, the nominal values of k_e and α_e were extended by ±20.0% to explore the relationship between the extension and the changes in k_m values. It was found that by using Eq. 2 and 3, the extension caused the k_m values to range in the interval of ±5.0% as shown in Figs. 6.18 and 6.19. Also, the changes in k_m was more sensitive to α_e than to k_e. Moreover, the ±20.0% could be from the dependencies of the thermal values on temperature. Furthermore, knowing which uncertainty is required to have a better accuracy can save the manufacturing costs and improve the TCP quality.

7.2 - Recommendations for Future Works

The following suggestions are recommended for further development of TCPs:

1. Simulate the cooling period in FEHT and COMSOL and compare the temperature responses from Eqs. 1 and 2.
2. Apply different values for the parameters in Table 4.1 and re-investigate the situations studied in Chapter 4.
3. Theoretically and analytically explore more on the combinational effects of the parameters in Eq. 2. In this thesis, the parameters in Chapter 4 were investigated based on the individual basis. The combination of the parameters may produce different results since the parameters can join and/or interfere with each other as shown in Section 6.4.
4. Construct a new TCP whose k_e and α_e values are known with high precision (*i.e.* the values have tolerances of ±5.0% or less). Re-measure the tested sampling media in Chapter 6 and study how the tolerances of k_s and α_s can influence k_m.
5. Investigate the heat capacity of the sampling medium $(\rho c_p)_m$ in the heating period with the following procedures:
    a. Obtain k_m using Eq. 1.
    b. Obtain α_m using Eq.2 with k_m from step (a).
    c. Obtain k_m using m_{Eq2} with α_m from step (b). m_{Eq2} is the *slope* shown in Eq. 6.2.
    d. Obtain R_c using Eq. 3 with k_m from step (c) and α_m from step (b).
    e. Obtain $(\rho c_p)_m = k_m / \alpha_m$ and compare with the $(\rho c_p)_m$ defined in Eq. 6.7.
6. Examine the heat capacity of the sampling medium in the cooling period with the steps shown in Recommendation # 5 and compare the results.

7.3 - Practical Implication

Fig. 7.1 is a schematic presentation of a vertical GSHP system. The total heat transfer is of biggest interest and is defined as shown in Eq. 7.1.

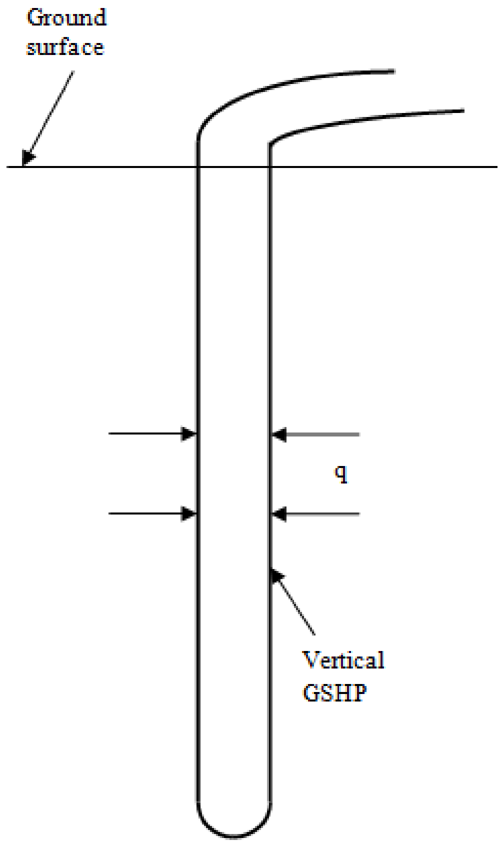

Fig. 7.1. Schematic drawing of a GSHP system

$$Q = qA = -k_m \frac{\partial T}{\partial r_{VG}} \pi D_{VG} L_{VG} \quad (7.1)$$

where *VG* means vertical GSHP, *D*: diameter, *L*: length, *r*: the distance from the central axis of GSHP.

By looking at Figs. 6.7, 6.9, 6.10, 6.20, and 6.21 and Tables 6.8 - 6.13, it can be seen that the calculated k_m values from TCP experiments are mostly over predicted, *i.e.*, the actual k_m in Eq. 7.1 is smaller then what it is. As a result the L_{VG} or D_{VG} must be increased correspondingly. For example, if k_m is found to be 3% bigger than the actual value TCP experiments, L_{VG} or D_{VG} must be increased by 3% to compensate for the over predicted k_m.

APPENDIX

Assumptions:

- Homogeneous and isotropic materials, so the material properties are the same in all directions.
- The size of the probe is much smaller than that of the medium, so the medium can be treated as an infinite medium.
- No bulk flow in the medium and no radiation effects.
- The TCP does not have any deflection in its length.
- The length-to-diameter ratio of the TCP is much greater than 50, so the axial flow error is less than 1% as reported by Blackwell [39] and Bilskie [40].
- Thermal contact resistances are ignored in the Infinite Line Heat Source (ILHS) model and are treated in subsequent sections.

A.1 - Derivation of Line Heat Source Model

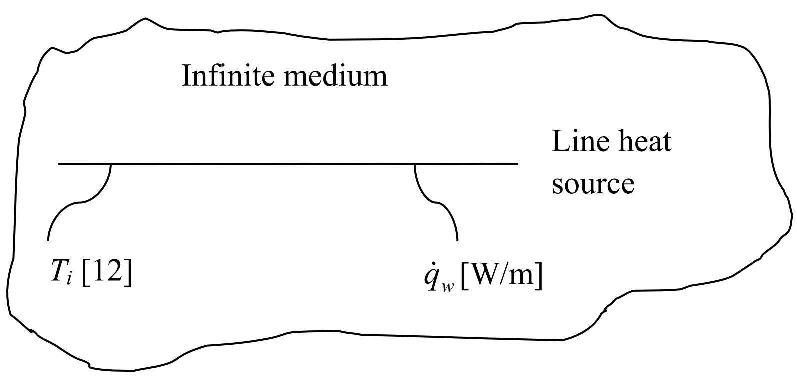

Figure A.1.1. Infinite medium and a line heat source.

Fig. A.1.1 describes a heating wire with constant $\dot{q}$ power generating capacity (*W/m*). The temperature variation in the medium is *T(x,y,t)*. Assume that there is no thermal contact resistance between the wire and the infinite medium.

Heat conduction equation: $\frac{1}{\alpha}\frac{\partial T}{\partial t} = \frac{1}{r}\frac{\partial}{\partial r}\left(r\frac{\partial T}{\partial r}\right) = \frac{\partial^2 T}{\partial r^2} + \frac{1}{r}\frac{\partial T}{\partial r}$ (A.1.1)

Let $\theta(r,t) = T(r,t) - T_i$ and $\theta(r,0) = 0 \Rightarrow \frac{1}{\alpha}\frac{\partial \theta}{\partial t} = \frac{\partial^2 \theta}{\partial r^2} + \frac{1}{r}\frac{\partial \theta}{\partial r}$ (A.1.2)

Boundary conditions:

- $\lim_{r\to 0} - kA\frac{\partial T}{\partial r} = \lim_{r\to 0} - k2\pi rL\frac{\partial T}{\partial r} = \dot{Q}_w$ (A.1.3)
- $\lim_{r\to\infty} T(r,t) = T_i$ or $\lim_{r\to\infty} \theta(r,t) = 0$ (A.1.4)

Taking Laplace transformation of:

- Heat conduction equation:
  - $\frac{1}{\alpha}\left(p\overline{\theta} - \theta(r,0)\right) = \frac{\partial^2 \overline{\theta}}{\partial r^2} + \frac{1}{r}\frac{\partial \overline{\theta}}{\partial r}$
  - $\theta(r,0) = 0 \Rightarrow \frac{\partial^2 \overline{\theta}}{\partial r^2} + \frac{1}{r}\frac{\partial \overline{\theta}}{\partial r} - \frac{p}{\alpha}\overline{\theta} = 0$ or $r^2\frac{\partial^2 \overline{\theta}}{\partial r^2} + r\frac{\partial \overline{\theta}}{\partial r} - \frac{p}{\alpha}r^2\overline{\theta} = 0$ (A.1.5)
- Boundary conditions:
  - $\lim_{r\to 0}\left(-k2\pi rL\frac{\partial \overline{\theta}}{\partial r}\right) = \frac{\dot{Q}_w}{p}$ (A.1.6)
  - $\lim_{r\to\infty} \overline{\theta}(r,t) = 0$ (A.1.7)

The solution to Eq. A.1.5 is $\overline{\theta}(r,p) = AI_o(\lambda r) + BK_o(\lambda r)$ (A.1.8)

where $\lambda = \sqrt{p/\alpha}$ and A and B are two arbitrary constants independent of r

From Fig. 12 on p. 42 of [68], $\lim_{x\to\infty} I_o(x) = \infty$ and $\lim_{x\to\infty} K_o(x) = 0$ and $\overline{\theta}(r\to\infty, p) = 0 \Rightarrow A = 0$ so that Eq. A.1.8 has a solution.

Using Eq. A.1.6, $\lim_{r\to 0}\left(k2\pi rLB\frac{\partial K_o(\lambda r)}{\partial r}\right)=\lim_{r\to 0}\left(k2\pi rL\lambda B\frac{\partial K_o(\lambda r)}{\partial(\lambda r)}\right)=-\frac{\dot{Q}_w}{p}$ (A.1.9)

Also, $\frac{\partial K_o(x)}{\partial x}=-K_1(x)\quad\Rightarrow\lim_{r\to 0}\{2k\pi L\lambda B[rK_1(\lambda r)]\}=\frac{\dot{Q}_w}{p}$ (A.1.10)

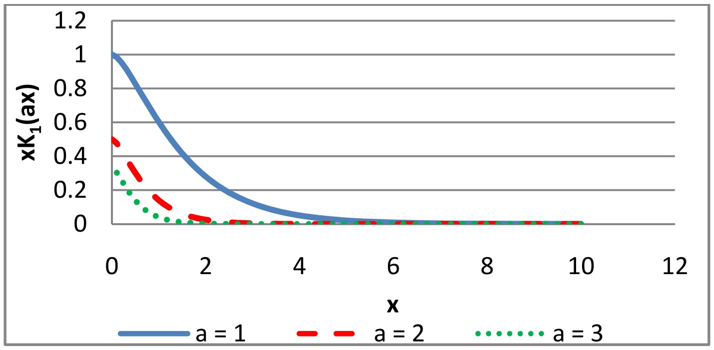

Figure A.1.2. Plot of xK₁(ax) vs. x. As $x\to 0$, $xK_1(ax)\to 1/a$.

With Excel testing as shown in Fig. A.1.2, Eq. A.1.10 becomes: $\lim_{r\to 0}\left\{2k\pi L\lambda B\frac{1}{\lambda}\right\}=\frac{\dot{Q}_w}{p}=2\pi kLB$

$\Rightarrow B=\frac{\dot{q}_w}{2\pi kp}$. So, Eq. A.1.5's solution is $\bar{\theta}(r,p)=\frac{\dot{q}_w}{2\pi kp}K_o(\lambda r)=\frac{\dot{q}_w}{2\pi kp}K_o\left(\sqrt{\frac{r^2}{\alpha}}p^{0.5}\right)$ (A.1.11)

From p. 17 of [69], $L^{-1}\left\{K_o\left(2\sqrt{\frac{r^2}{4\alpha}}p^{0.5}\right)\right\}=\frac{1}{2t}e^{\frac{-r^2}{4\alpha t}}$ and p. 45 of [11], $L^{-1}\left\{\frac{F(p)}{p}\right\}=\int_0^t f(u)du$

$$\Rightarrow L^{-1}\left[\frac{1}{p}K_o\left(\sqrt{\frac{r^2}{4\alpha}}p^{0.5}\right)\right]=\frac{1}{2}\int_0^t\frac{1}{t}e^{\frac{-r^2}{4\alpha t}}dt \quad (A.1.12)$$

Let $u=\frac{r^2}{4\alpha t}\Rightarrow\frac{\partial u}{\partial t}=\frac{-r^2}{4\alpha t^2}\Rightarrow dt=\frac{4\alpha t^2}{-r^2}du$, so Eq. A.1.12 becomes:

$$\frac{1}{2}\int_0^t\frac{1}{t}e^{\frac{-r^2}{4\alpha t}}dt=\frac{1}{2}\int_\infty^u\frac{1}{t}e^{-u}\frac{4\alpha t^2}{r^2}du=\frac{1}{2}\int_\infty^u e^{-u}\frac{4\alpha t}{r^2}du=\frac{1}{2}\int_\infty^u-\frac{e^{-u}}{u}du=\frac{1}{2}\int_u^\infty\frac{e^{-u}}{u}du=\frac{1}{2}E_1(u) \quad (A.1.13)$$

In addition, $E_1(u) = -Ei(-u) = \int_x^{\infty} \frac{e^{-t}dt}{t}$

$$\Rightarrow \theta(r,t) = L^{-1}\left[\overline{\theta}(r,p)\right] = L^{-1}\left[\frac{\dot{q}_w}{2\pi k}\frac{1}{p}K_o(\lambda r)\right] = \frac{-\dot{q}_w}{4\pi k}Ei\left(-\frac{r^2}{4\alpha t}\right) \quad \text{(A.1.14)}$$

Therefore, the solution to the transient heat conduction of Eq. A.1.1 is

$$T(r,t) = \frac{-\dot{q}_w}{4\pi k}Ei\left(-\frac{r^2}{4\alpha t}\right) + T_i \quad \text{(A.1.15)}$$

For $\frac{4\alpha t}{r^2} >> 1$, $\Rightarrow -Ei\left(\frac{-r^2}{4\alpha t}\right) \approx -\gamma + \ln\left(\frac{4\alpha t}{r^2}\right) \Rightarrow T(r,t_2) - T(r,t_1) \approx \frac{\dot{q}_w}{4\pi k}\ln\left(\frac{t_2}{t_1}\right)$ for $\frac{4\alpha t}{r^2} >> 1$

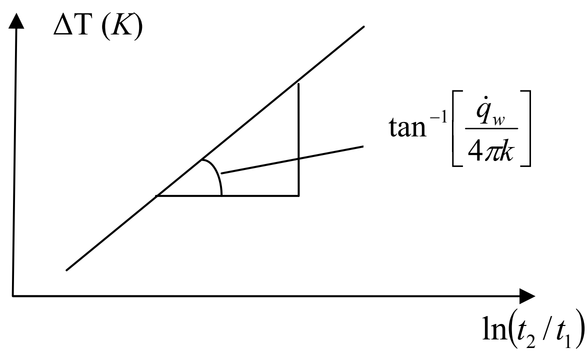

Figure A.1.3. Typical graph of temperature vs. logarithmic time ratio for line heat source.

A.2 - Derivation of Perfect Contact TCP Model

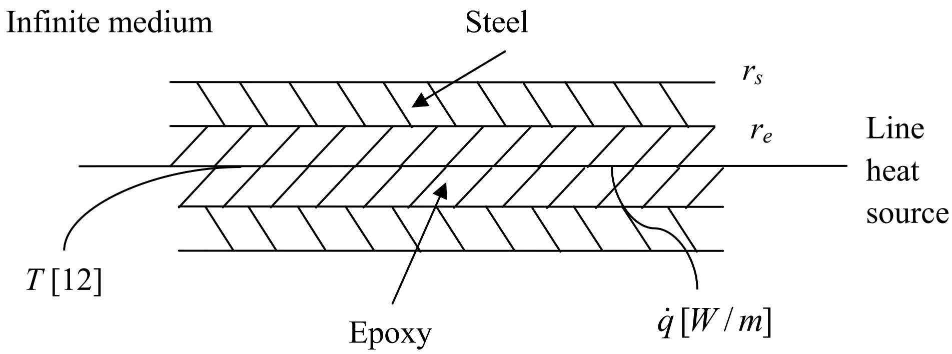

Figure A.2.1. Probe with finite thickness containing line heat source.

Introduce dimensionless parameter $\eta = \sqrt{u} = \dfrac{r}{2\sqrt{\alpha t}} \Rightarrow d\eta = \dfrac{1}{2}u^{-0.5}du \Rightarrow du = 2u^{0.5}d\eta = 2\eta d\eta$

From Eq. A.1.13, $\dfrac{1}{2}\int_u^\infty \dfrac{e^{-u}}{u}du = \int_{\eta^2}^\infty \dfrac{e^{-\eta^2}}{2\eta^2}2\eta d\eta = \int_{\eta^2}^\infty \dfrac{e^{-\eta^2}}{\eta}d\eta$ (A.2.1)

From Eq. A.1.15 and Eq. A.2.1, it can be deduced that $T(r,t) = C\int_{\eta^2}^\infty \dfrac{e^{-\eta^2}}{\eta}d\eta + D$ (A.2.2)

where C and D are two arbitrary constants independent of η.

Since the temperature function of the line heat source does not change form when r expands or shrinks, let's consider the medium in Fig. A.1.1 is surrounded by additional two layers. In other words, the line heat source is embedded in three layers: the epoxy, the steel, and the medium to be measured by the probe. The situation now becomes the problem as shown in Fig P5 where the temperature function in each layer has the form of Eq. A.2.2. The inner layer is considered as the line heat source of the outer layer.

So the temperature functions in the epoxy, steel and medium are:

- $T_e(r,p) = C_e\int_{\eta^2}^\infty \dfrac{e^{-\eta^2}}{\eta}d\eta + D_e = \dfrac{C_e}{2}Ei(-\eta^2) + D_e$ (for $r_{hw} < r < r_e$) (A.2.3)

- $T_s(r,p) = C_s \int_{\eta^2}^{\infty} \frac{e^{-\eta^2}}{\eta} d\eta + D_s = \frac{C_s}{2} Ei\left(-\eta^2\right) + D_s$ (for $r_e < r < r_s$) (A.2.4)
- $T(r,p) = C \int_{\eta^2}^{\infty} \frac{e^{-\eta^2}}{\eta} d\eta + D = \frac{C}{2} Ei\left(-\eta^2\right) + D$ (for $r_2 < r$) (A.2.5)

where C's and D's are arbitrary constants independent of η

New boundary conditions:

- For epoxy: $\dot{Q} = \lim_{r \to 0} \left[-2\pi r L k_e \frac{\partial T_e}{\partial r} \right]$ and $T_e(r,0) = T_{e_i}$ (A.2.6)

- For steel: $k_e \left. \frac{\partial T_e}{\partial r} \right|_{r_e} = k_s \left. \frac{\partial T_s}{\partial r} \right|_{r_e}$ and $T_s(r,0) = T_{s_i}$ (A.2.7)

- For medium: $k_s \left. \frac{\partial T_s}{\partial r} \right|_{r_s} = k \left. \frac{\partial T}{\partial r} \right|_{r_s}$ and $T(r,0) = T_i$ (A.2.8)

Also, $\frac{\partial T}{\partial r} = \frac{\partial T}{\partial \eta} \frac{\partial \eta}{\partial r} = \frac{\partial T}{\partial \eta} \frac{1}{2\sqrt{\alpha t}} = \frac{C}{\eta} e^{-\eta^2} \frac{1}{2\sqrt{\alpha t}} = \frac{C}{\eta} e^{-\frac{r^2}{4\alpha t}} \frac{1}{2\sqrt{\alpha t}}$ (A.2.9)

For epoxy:

- From Eqs. 3.2.3, 3.2.6, and 3.2.9: $\dot{Q} = \lim_{r \to 0} \left[-2\pi r L k_e \frac{\partial T_e}{\partial r} \right] = \lim_{r \to 0} \left[\frac{-2\pi r L k_e}{2\sqrt{\alpha_e t}} \frac{C_{e2}}{\eta_e} e^{-\frac{r^2}{4\alpha_e t}} \right]$

$$\Rightarrow \dot{Q} = \lim_{r \to 0} \left[-2\pi L k_e \frac{C_{e_2}}{\eta_e} e^{-\frac{r^2}{4\alpha_e t}} \frac{r}{2\sqrt{\alpha_e t}} \right] = \lim_{r \to 0} \left[-2\pi L k_e \frac{C_{e_2}}{\eta_e} e^{-\frac{r^2}{4\alpha_e t}} \eta_e \right] = \lim_{r \to 0} \left[-2\pi L k_e C_{e_2} e^{-\frac{r^2}{4\alpha_e t}} \right]$$

$$\Rightarrow \dot{Q} = -2\pi L k_e C_e \Rightarrow C_e = -\frac{\dot{q}}{2\pi k_e}$$

- $T_e(r,0) = T_{e_i} = 0 + D_e \Rightarrow D_e = T_{e_i}$

- $\Rightarrow T_e(r,t) = -\frac{\dot{q}_w}{4\pi k_e} Ei\left(-\frac{r^2}{4\alpha_e t} \right) + T_{e_i}$ (A.2.10)

For steel:

- From Eqs. 3.2.4, 3.2.7, and 3.2.9: $k_e \left.\frac{\partial T_e}{\partial r}\right|_{r_e} = k_s \left.\frac{\partial T_s}{\partial r}\right|_{r_e}$

$$\Rightarrow k_e \frac{C_e}{\eta_e} e^{-\frac{r^2}{4\alpha_e t}} \left.\frac{1}{2\sqrt{\alpha_e t}}\right|_{r_e} = k_s \frac{C_s}{\eta_s} e^{-\frac{r^2}{4\alpha_s t}} \left.\frac{1}{2\sqrt{\alpha_s t}}\right|_{r_e}$$

$$\Rightarrow k_e C_e \frac{\sqrt{\alpha_e t}}{r} e^{-\frac{r^2}{4\alpha_e t}} \left.\frac{1}{\sqrt{\alpha_e t}}\right|_{r_e} = k_s C_s \frac{\sqrt{\alpha_s t}}{r} e^{-\frac{r^2}{4\alpha_s t}} \left.\frac{1}{\sqrt{\alpha_s t}}\right|_{r_e} \Rightarrow k_e C_e e^{-\frac{r_e^2}{4\alpha_e t}} = k_s C_s e^{-\frac{r_e^2}{4\alpha_s t}}$$

$$\Rightarrow C_s = \frac{k_e}{k_s} C_e e^{\frac{r_e^2}{4\alpha_s t} - \frac{r_e^2}{4\alpha_e t}} = -\frac{\dot{q}}{2\pi k_s} e^{\frac{r_e^2}{4\alpha_s t} - \frac{r_e^2}{4\alpha_e t}}$$

- $T_s(r,0) = T_{s_i} = 0 + D_s \Rightarrow D_s = T_{s_i}$

- $\Rightarrow T_s(r,t) = -\frac{\dot{q}_w}{4\pi k_s} e^{\frac{r_e^2}{4\alpha_s t} - \frac{r_e^2}{4\alpha_e t}} Ei\left(-\frac{r^2}{4\alpha_s t}\right) + T_{s_i}$

  (A.2.11)

For medium:

- From Eq. A.2.5, A.2.8, and A.2.9: $k_s \left.\frac{\partial T_s}{\partial r}\right|_{r_s} = k \left.\frac{\partial T}{\partial r}\right|_{r_s}$

$$\Rightarrow k_s \frac{C_s}{\eta_s} e^{-\frac{r^2}{4\alpha_s t}} \left.\frac{1}{2\sqrt{\alpha_s t}}\right|_{r_s} = k \frac{C}{\eta} e^{-\frac{r^2}{4\alpha t}} \left.\frac{1}{2\sqrt{\alpha t}}\right|_{r_s}$$

$$\Rightarrow k_s C_s \frac{\sqrt{\alpha_s t}}{r} e^{-\frac{r^2}{4\alpha_s t}} \left.\frac{1}{\sqrt{\alpha_s t}}\right|_{r_s} = kC \frac{\sqrt{\alpha t}}{r} e^{-\frac{r^2}{4\alpha t}} \left.\frac{1}{\sqrt{\alpha t}}\right|_{r_s} \Rightarrow k_s C_s e^{-\frac{r_s^2}{4\alpha_s t}} = kCe^{-\frac{r_s^2}{4\alpha t}}$$

$$\Rightarrow C = \frac{k_s}{k} C_s e^{\frac{r_s^2}{4\alpha t} - \frac{r_s^2}{4\alpha_s t}} = -\frac{\dot{q}_w}{2\pi k} e^{\frac{r_e^2}{4\alpha_s t} - \frac{r_e^2}{4\alpha_e t} + \frac{r_s^2}{4\alpha t} - \frac{r_s^2}{4\alpha_s t}}$$

- $T(r,0) = T_i = 0 + D \Rightarrow D = T_i$

- $\Rightarrow T(r,t) = -\frac{\dot{q}_w}{4\pi k} e^{\frac{r_e^2}{4\alpha_s t} - \frac{r_e^2}{4\alpha_e t} + \frac{r_s^2}{4\alpha t} - \frac{r_s^2}{4\alpha_s t}} Ei\left(-\frac{r^2}{4\alpha t}\right) + T_i$ (A.2.12)

If the epoxy and steel are replaced by the medium, we have $\alpha_e = \alpha_s = \alpha$

$\Rightarrow e^{\frac{r_e^2}{4\alpha_s t} - \frac{r_e^2}{4\alpha_e t} + \frac{r_s^2}{4\alpha t} - \frac{r_s^2}{4\alpha_s t}} = e^{\frac{r_e^2}{4\alpha t} - \frac{r_e^2}{4\alpha t} + \frac{r_s^2}{4\alpha t} - \frac{r_s^2}{4\alpha t}} = 1 \Rightarrow$ Eq. A.2.12 becomes Eq. A.1.15 as shown previously.

However, because the steel's surface temperature cannot be measured when the probe is contacting the medium, the thermocouples must be placed somewhere in the epoxy layer. So the probe cannot produce the temperature values in Eq. A.2.12. The probe can only give the temperature values where the thermocouples are placed.

From Eq. A.2.11 at r_s and Eq. A.2.12 at r_s:

$$T_s(r_s,t) = -\frac{\dot{q}_W}{4\pi k_s} e^{\frac{r_e^2}{4\alpha_s t} - \frac{r_e^2}{4\alpha_e t}} Ei\left(-\frac{r_s^2}{4\alpha_s t}\right) + T_{s_i} \quad \text{and} \quad T_s(r_e,t) = -\frac{\dot{q}_W}{4\pi k_s} e^{\frac{r_e^2}{4\alpha_s t} - \frac{r_e^2}{4\alpha_e t}} Ei\left(-\frac{r_e^2}{4\alpha_s t}\right) + T_{s_i}$$

$$\Rightarrow T_s(r_e,t) - T_s(r_s,t) = -\frac{\dot{q}_W}{4\pi k_s} e^{\frac{r_e^2}{4\alpha_s t} - \frac{r_e^2}{4\alpha_e t}} \left[Ei\left(-\frac{r_e^2}{4\alpha_s t}\right) - Ei\left(-\frac{r_s^2}{4\alpha_s t}\right) \right] \tag{A.2.13}$$

Using boundary condition $T_e(r_e,t) = T_s(r_e,t)$, we have:

$$T_s(r_e,t) - T_s(r_s,t) = T_e(r_e,t) - T_s(r_s,t) = -\frac{\dot{q}_W}{4\pi k_s} e^{\frac{r_e^2}{4\alpha_s t} - \frac{r_e^2}{4\alpha_e t}} \left[Ei\left(-\frac{r_e^2}{4\alpha_s t}\right) - Ei\left(-\frac{r_s^2}{4\alpha_s t}\right) \right]$$

$$\Rightarrow T_s(r_s,t) = T_e(r_e,t) + \frac{\dot{q}_W}{4\pi k_s} e^{\frac{r_e^2}{4\alpha_s t} - \frac{r_e^2}{4\alpha_e t}} \left[Ei\left(-\frac{r_e^2}{4\alpha_s t}\right) - Ei\left(-\frac{r_s^2}{4\alpha_s t}\right) \right] \tag{A.2.14}$$

From Eq. A.2.12 at r_s: $T(r_s,t) = -\frac{\dot{q}_W}{4\pi k} e^{\frac{r_e^2}{4\alpha_s t} - \frac{r_e^2}{4\alpha_e t} + \frac{r_s^2}{4\alpha t} - \frac{r_s^2}{4\alpha_s t}} Ei\left(-\frac{r_s^2}{4\alpha t}\right) + T_i$

Using boundary condition $T_s(r_s,t) = T(r_s,t)$, we have:

$$T_e(r_e,t) + \frac{\dot{q}_W}{4\pi k_s} e^{\frac{r_e^2}{4\alpha_s t} - \frac{r_e^2}{4\alpha_e t}} \left[Ei\left(-\frac{r_e^2}{4\alpha_s t}\right) - Ei\left(-\frac{r_s^2}{4\alpha_s t}\right) \right] = -\frac{\dot{q}_W}{4\pi k} e^{\frac{r_e^2}{4\alpha_s t} - \frac{r_e^2}{4\alpha_e t} + \frac{r_s^2}{4\alpha t} - \frac{r_s^2}{4\alpha_s t}} Ei\left(-\frac{r_s^2}{4\alpha t}\right) + T_i$$

$$\Rightarrow T_e(r_e,t) = -\frac{\dot{q}_w}{4\pi k} e^{\frac{r_e^2}{4\alpha_s t}-\frac{r_e^2}{4\alpha_e t}+\frac{r_s^2}{4\alpha t}-\frac{r_s^2}{4\alpha_s t}} Ei\left(-\frac{r_s^2}{4\alpha t}\right) - \frac{\dot{q}_w}{4\pi k_s} e^{\frac{r_e^2}{4\alpha_s t}-\frac{r_e^2}{4\alpha_e t}}\left[Ei\left(-\frac{r_e^2}{4\alpha_s t}\right) - Ei\left(-\frac{r_s^2}{4\alpha_s t}\right)\right] + T_i \tag{A.2.15}$$

Using Eq. A.2.10 at r_1 and Eq. A.2.15, we have:

$$T_e(r_e,t) = -\frac{\dot{q}_w}{4\pi k_e} Ei\left(-\frac{r_e^2}{4\alpha_e t}\right) + T_{e_i}$$

$$= -\frac{\dot{q}_w}{4\pi k} e^{\frac{r_e^2}{4\alpha_s t}-\frac{r_e^2}{4\alpha_e t}+\frac{r_s^2}{4\alpha t}-\frac{r_s^2}{4\alpha_s t}} Ei\left(-\frac{r_s^2}{4\alpha t}\right) - \frac{\dot{q}_w}{4\pi k_s} e^{\frac{r_e^2}{4\alpha_s t}-\frac{r_e^2}{4\alpha_e t}}\left[Ei\left(-\frac{r_e^2}{4\alpha_s t}\right) - Ei\left(-\frac{r_s^2}{4\alpha_s t}\right)\right] + T_i$$

$$\Rightarrow T_{e_i} = \frac{\dot{q}_w}{4\pi k_e} Ei\left(-\frac{r_e^2}{4\alpha_e t}\right) - \frac{\dot{q}_w}{4\pi k} e^{\frac{r_e^2}{4\alpha_s t}-\frac{r_e^2}{4\alpha_e t}+\frac{r_s^2}{4\alpha t}-\frac{r_s^2}{4\alpha_s t}} Ei\left(-\frac{r_s^2}{4\alpha t}\right) - \frac{\dot{q}_w}{4\pi k_s} e^{\frac{r_e^2}{4\alpha_s t}-\frac{r_e^2}{4\alpha_e t}}\left[Ei\left(-\frac{r_e^2}{4\alpha_s t}\right) - Ei\left(-\frac{r_s^2}{4\alpha_s t}\right)\right] + T_i$$

Now substituting T_{e_i} from above to Eq. A.2.10 yields the temperature for epoxy at $r < r_e$:

$$T_e(r,t) = -\frac{\dot{q}_w}{4\pi k} e^{\frac{r_e^2}{4\alpha_s t}-\frac{r_e^2}{4\alpha_e t}+\frac{r_s^2}{4\alpha t}-\frac{r_s^2}{4\alpha_s t}} Ei\left(-\frac{r_s^2}{4\alpha t}\right) - \frac{\dot{q}_w}{4\pi k_e}\left[Ei\left(-\frac{r^2}{4\alpha_e t}\right) - Ei\left(-\frac{r_e^2}{4\alpha_e t}\right)\right] - \frac{\dot{q}_w}{4\pi k_s} e^{\frac{r_e^2}{4\alpha_s t}-\frac{r_e^2}{4\alpha_e t}}\left[Ei\left(-\frac{r_e^2}{4\alpha_s t}\right) - Ei\left(-\frac{r_s^2}{4\alpha_s t}\right)\right] + T_i$$

Comparing Eq. A.1.15 and Eq. A.2.16, we have the following results:

$$T(r,t) = -\frac{\dot{q}_w}{4\pi k} Ei\left(-\frac{r^2}{4\alpha t}\right)(Term_1) + T_i + Term_2 \tag{A.2.17}$$

where $Term_1 = e^{\frac{r_e^2}{4\alpha_s t}-\frac{r_e^2}{4\alpha_e t}+\frac{r_s^2}{4\alpha t}-\frac{r_s^2}{4\alpha_s t}}$

$$Term_2 = -\frac{\dot{q}_w}{4\pi k_e}\left[Ei\left(-\frac{r^2}{4\alpha_e t}\right) - Ei\left(-\frac{r_e^2}{4\alpha_e t}\right)\right] - \frac{\dot{q}_w}{4\pi k_s} e^{\frac{r_e^2}{4\alpha_s t}-\frac{r_e^2}{4\alpha_e t}}\left[Ei\left(-\frac{r_e^2}{4\alpha_s t}\right) - Ei\left(-\frac{r_s^2}{4\alpha_s t}\right)\right]$$

Note that Eq. A2.17 is only valid when $r_w < r_{sen} < r_e$.

A.3 - Derivation of TCP Model with TCR

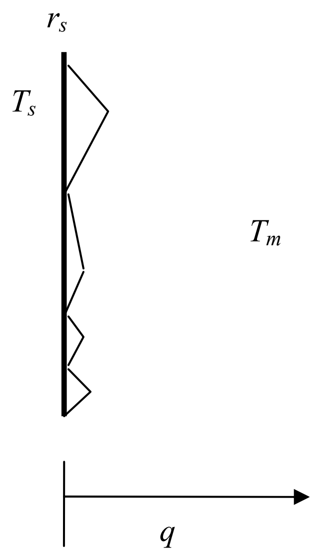

Figure A.3.1. Schematic drawing for Eq. 3.4.

From Fig. A.3.1, $R_c = \dfrac{T_s - T_m}{q}$ where $q = -k_s \left.\dfrac{\partial T_s}{\partial r}\right|_{r=r_s}$ (A.3.1)

$$\Rightarrow T_{soil}(r = r_m, t) = T_s(r = r_s, t) + k_s R_c \left.\frac{\partial T_s}{\partial r}\right|_{r=r_s} \qquad \text{(A.3.2)}$$

where R_c is the thermal contact resistance.

$$\begin{aligned}\Rightarrow T_m(r = r_m, t) &= T_s(r = r_s, t) + k_s R_c \frac{C_s}{r_s} \exp\left(\frac{-r_s^2}{4\alpha_s t}\right) \\ &= T_s(r = r_s, t) - R_c \frac{\dot{q}_w}{2\pi r_s} \exp\left(\frac{-r_s^2}{4\alpha_s t}\right)\end{aligned} \qquad \text{(A.3.3)}$$

(See Eq. A.2.11 for more information of C_s)

Combing Eqs. A.3.3 and A.2.14, and let $A_t = R_c \dfrac{\dot{q}_w}{2\pi r_s} \exp\left(\dfrac{-r_s^2}{4\alpha_s t}\right)$, we have:

$$T_m(r_m, t) = T_e(r_e, t) + \frac{\dot{q}_w}{4\pi k_s} \exp\left(\frac{r_1^2}{4\alpha_s t} - \frac{r_1^2}{4\alpha_e t}\right)\left[Ei\left(\frac{-r_e^2}{4\alpha_s t}\right) - Ei\left(\frac{-r_s^2}{4\alpha_s t}\right)\right] - A_t \qquad \text{(A.3.4)}$$

$$\Rightarrow T_e(r_e, t) = T_m(r_m, t) + A_t - \frac{\dot{q}_w}{4\pi k_s} \exp\left(\frac{r_1^2}{4\alpha_s t} - \frac{r_1^2}{4\alpha_e t}\right)\left[Ei\left(\frac{-r_e^2}{4\alpha_s t}\right) - Ei\left(\frac{-r_s^2}{4\alpha_s t}\right)\right] \qquad \text{(A.3.5)}$$

Joining Eqs. A.2.12 and A.3.5, and let $B_t = \dfrac{\dot{q}_w}{4\pi k_s} \exp\left(\dfrac{r_1^2}{4\alpha_s t} - \dfrac{r_1^2}{4\alpha_e t}\right)\left[Ei\left(\dfrac{-r_e^2}{4\alpha_s t}\right) - Ei\left(\dfrac{-r_s^2}{4\alpha_s t}\right)\right]$:

$$T_e(r_e, t) = -\frac{\dot{q}_w}{4\pi k_m} \exp\left(\frac{r_1^2}{4\alpha_s t} - \frac{r_1^2}{4\alpha_e t} + \frac{r_2^2}{4\alpha_m t} - \frac{r_2^2}{4\alpha_s t}\right) Ei\left(\frac{-r^2}{4\alpha_m t}\right) + T_{m_i} + A_t - B_t \qquad \text{(A.3.6)}$$

Combining Eqs. A.2.10 and A.3.6, we have (for $r_e < r < r_s$):

$$T_{e_i} = \frac{\dot{q}_w}{4\pi k_e} Ei\left(\frac{-r^2}{4\alpha_e t}\right) - \frac{\dot{q}_w}{4\pi k_m} \exp\left(\frac{r_1^2}{4\alpha_s t} - \frac{r_1^2}{4\alpha_e t} + \frac{r_2^2}{4\alpha_m t} - \frac{r_2^2}{4\alpha_s t}\right) Ei\left(\frac{-r^2}{4\alpha_m t}\right) + A_t - B_t + T_{m_i} \qquad \text{(A.3.7)}$$

Plugging Eq. A.3.7 back to Eq. A.2.10, we have (for $r_e < r < r_s$):

$$T_e(r,t) = -\frac{\dot{q}_w}{4\pi k} Ei\left(\frac{-r_s^2}{4\alpha_m t}\right)(Term_1) + Term_2 + TCR(t) + T_{m_i} \tag{A.3.8}$$

where $Term_1(t) = \exp\left(\frac{r_e^2}{4\alpha_s t} - \frac{r_e^2}{4\alpha_e t} + \frac{r_s^2}{4\alpha_m t} - \frac{r_s^2}{4\alpha_s t}\right)$, $A_t = TCR(t)$, and

$$Term_2(t) = \frac{-\dot{q}_w}{4\pi k_e}\left[Ei\left(\frac{-r_{sen}^2}{4\alpha_e t}\right) - Ei\left(\frac{-r_e^2}{4\alpha_e t}\right)\right] - \frac{\dot{q}_w}{4\pi k_s} e^{\frac{r_e^2}{4\alpha_s t} - \frac{r_e^2}{4\alpha_e t}}\left[Ei\left(\frac{-r_e^2}{4\alpha_s t}\right) - Ei\left(\frac{-r_s^2}{4\alpha_s t}\right)\right]$$

A.4 - Calculating Method for R_c

As mentioned by Liu *et al.* [42], Blackwell [59] and Waite *et al.* [70], the small time estimated temperature solution of the TCP can be expressed as:

$$T(r,t) \approx Z_1 t - Z_1 Z_2 t^2 + Z_1 Z_2 Z_3 t^{2.5} \quad \text{for } t \leq \frac{r_s^2}{\alpha_m} \tag{A.4.1}$$

where Z_1, Z_2, and Z_3 are fitting parameters.

H_c is (Liu *et al.*, Blackwell, and Waite *et al.*):

$$H_c = \frac{1}{R_c} = \dot{q}_w \frac{Z_2}{Z_1} \tag{A.4.2}$$

Eq. A.4.1 is then compared with the experimental values up to $t \leq \frac{r_s^2}{\alpha_m}$ such that $\sum_{i=1}^{N} \left(T_{Eq} - T_{Exp}\right)_i^2 = \min$ where N is the total number of measuring increments of the reading from the TCP until time t, which called the sum squared method.

A.5 - Estimation of Medium's Minimum Radius for FEHT

When the TCP is inserted into a sampling medium, the ideal condition is the dimensions of the medium are infinite. However, that ideal condition is impossible to achieve when the infinity is used in finite element softwares such as FEHT (Finite Element Heat Transfer). As a result, there is a limit to the "infinite" condition from the assumptions of the classical solution and Eq 32.

Tarnawski *et al.* [11] comes up with the following equation to estimate the minimum radius of the medium to simulate the infinite medium condition for the TCP:

$$\exp\left(\frac{r^2}{4\alpha\tau}\right) >> 1 \qquad \text{(A.5.1)}$$

where τ is the heating period, which is set to 120*s* in this paper.

As a result, if $\exp\left(\frac{r^2}{4\alpha\tau}\right) = 1.836 \times 10^6$, Eq. A1 is satisfied.

Hence, with $\alpha = 1.3 \times 10^{-7}$ m^2/s, $\tau = 120$ s, min r is calculated to be 0.03 m which is 30,000 μm.

$r > 30{,}000$ μm can be used for FEHT but the time to manually make the grid using FEHT is longer while the infinite condition (Eq. 5.1) is already reached.

A.6 - Graphs of Thermal Contact Resistance

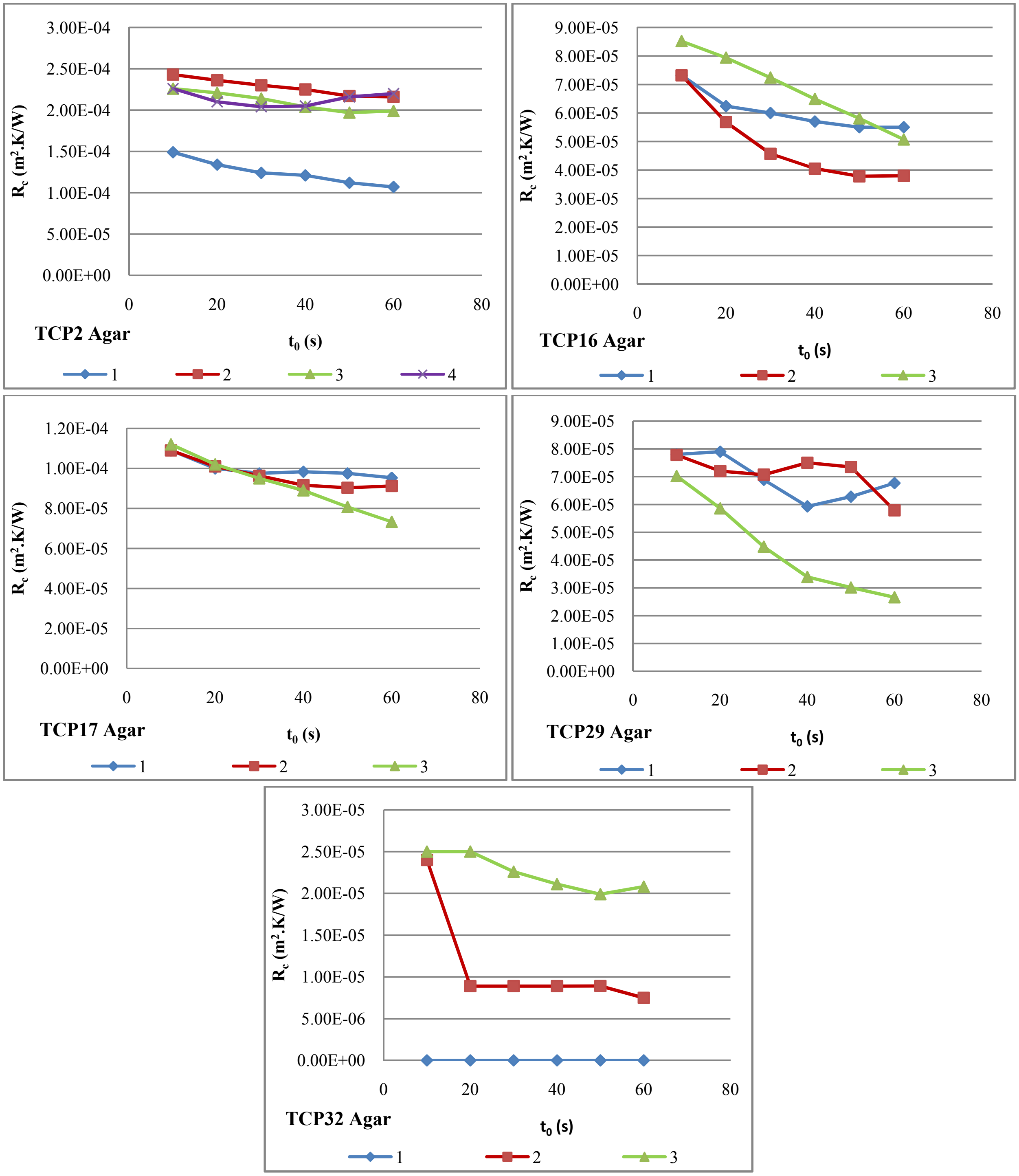

Figure A.6.1. Thermal contact resistance value R_c for testing agar during heating.

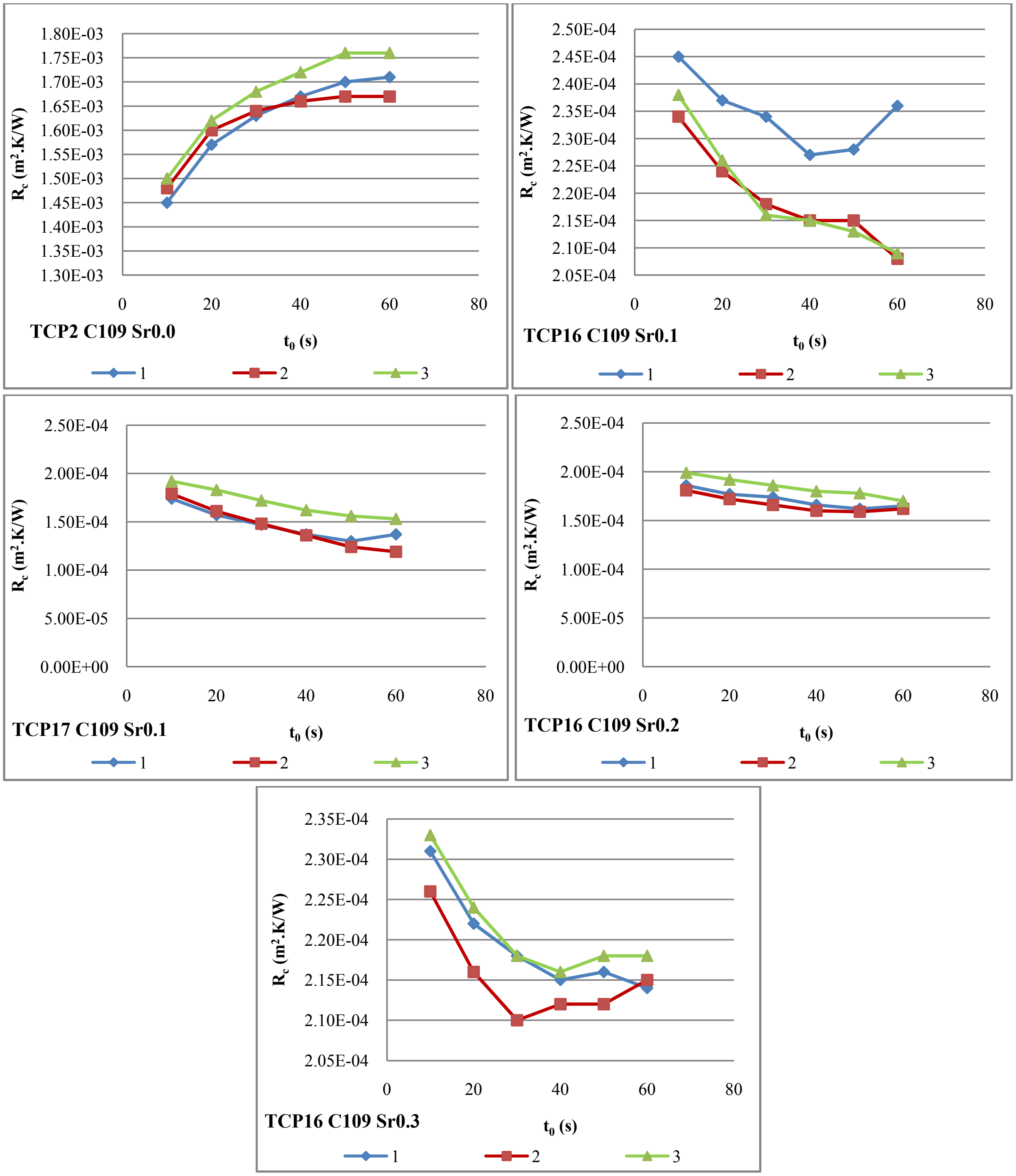

Figure A.6.2. Thermal contact resistance value R_c for testing C109 sand during heating.

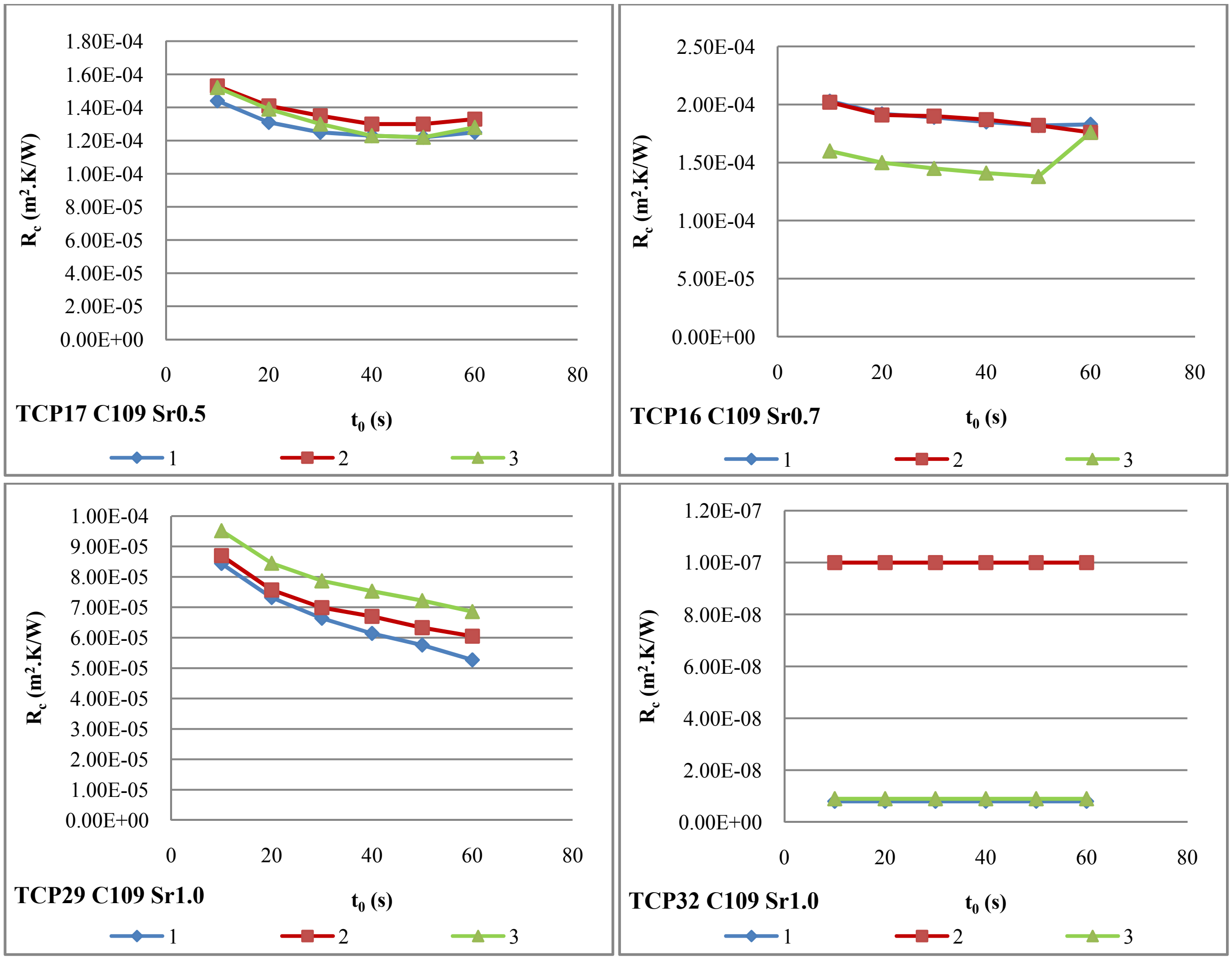

Figure A.6.2. (Cont.) Thermal contact resistance value R_c for testing C109 sand during heating.

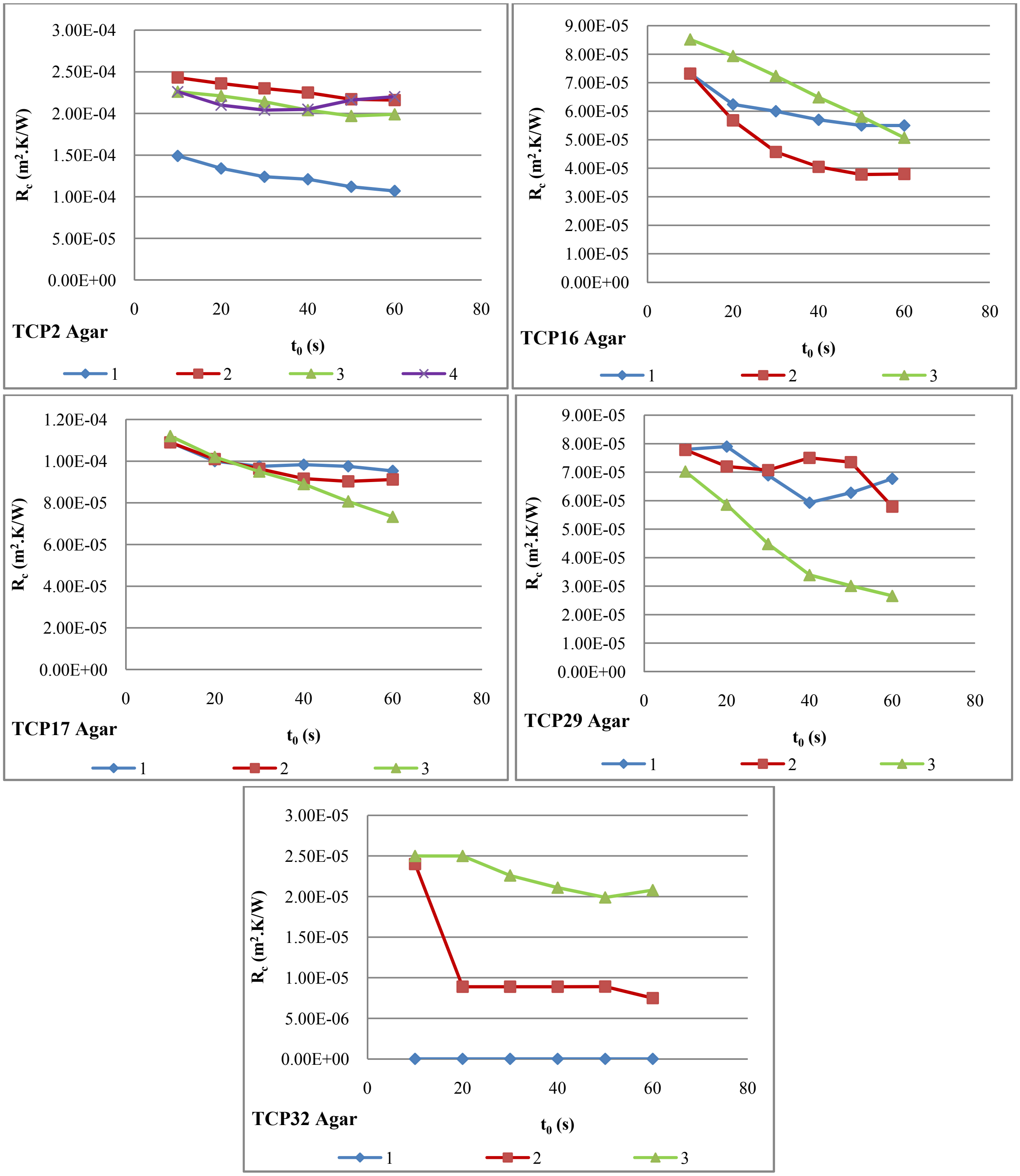

Figure A.6.3. Thermal contact resistance value R_c for testing agar during cooling using r_{sen} from the heating period during calibration.

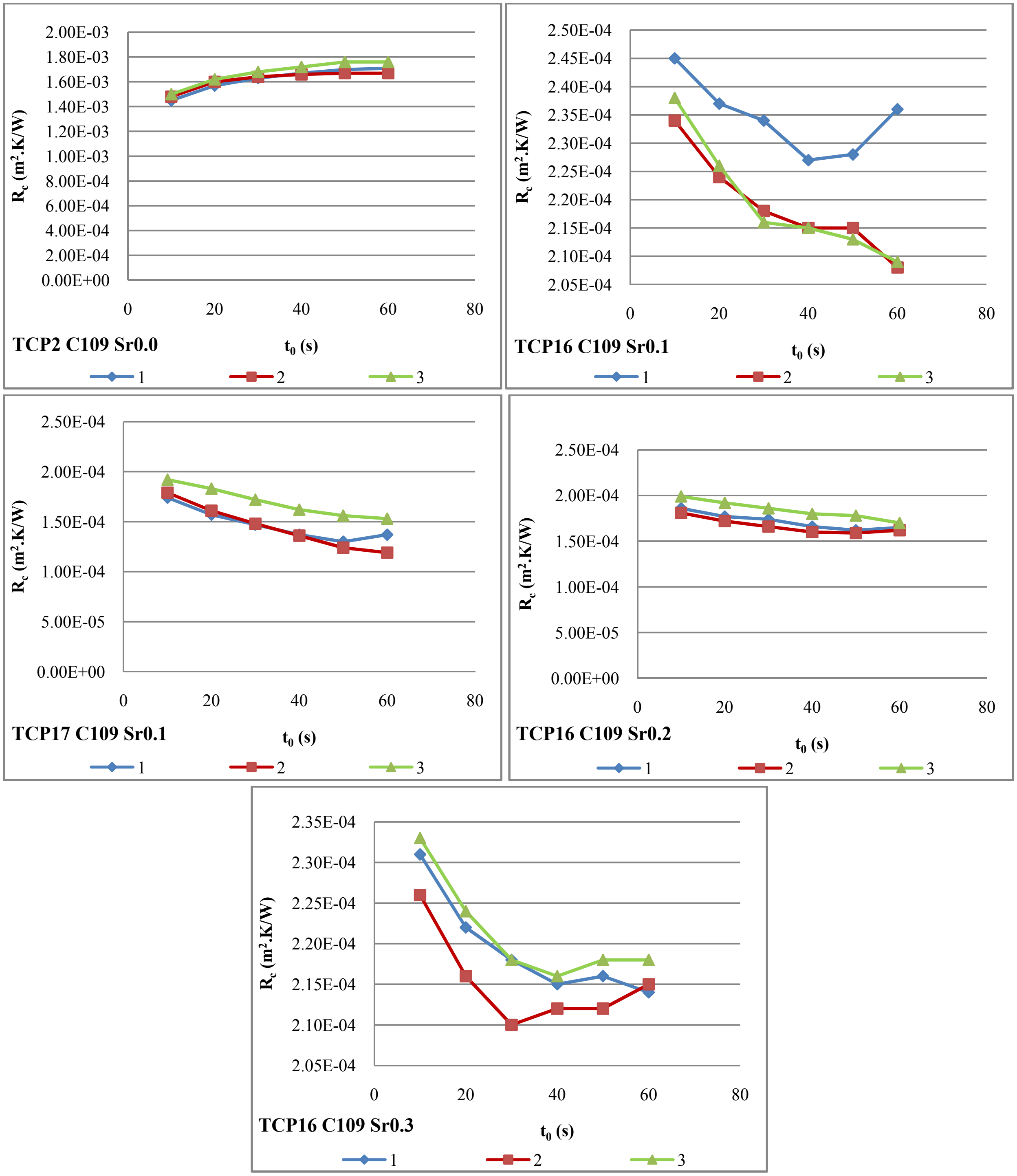

Figure A.6.4. Thermal contact resistance value R_c for testing C109 sand during cooling using r_{sen} from the heating period during calibration.

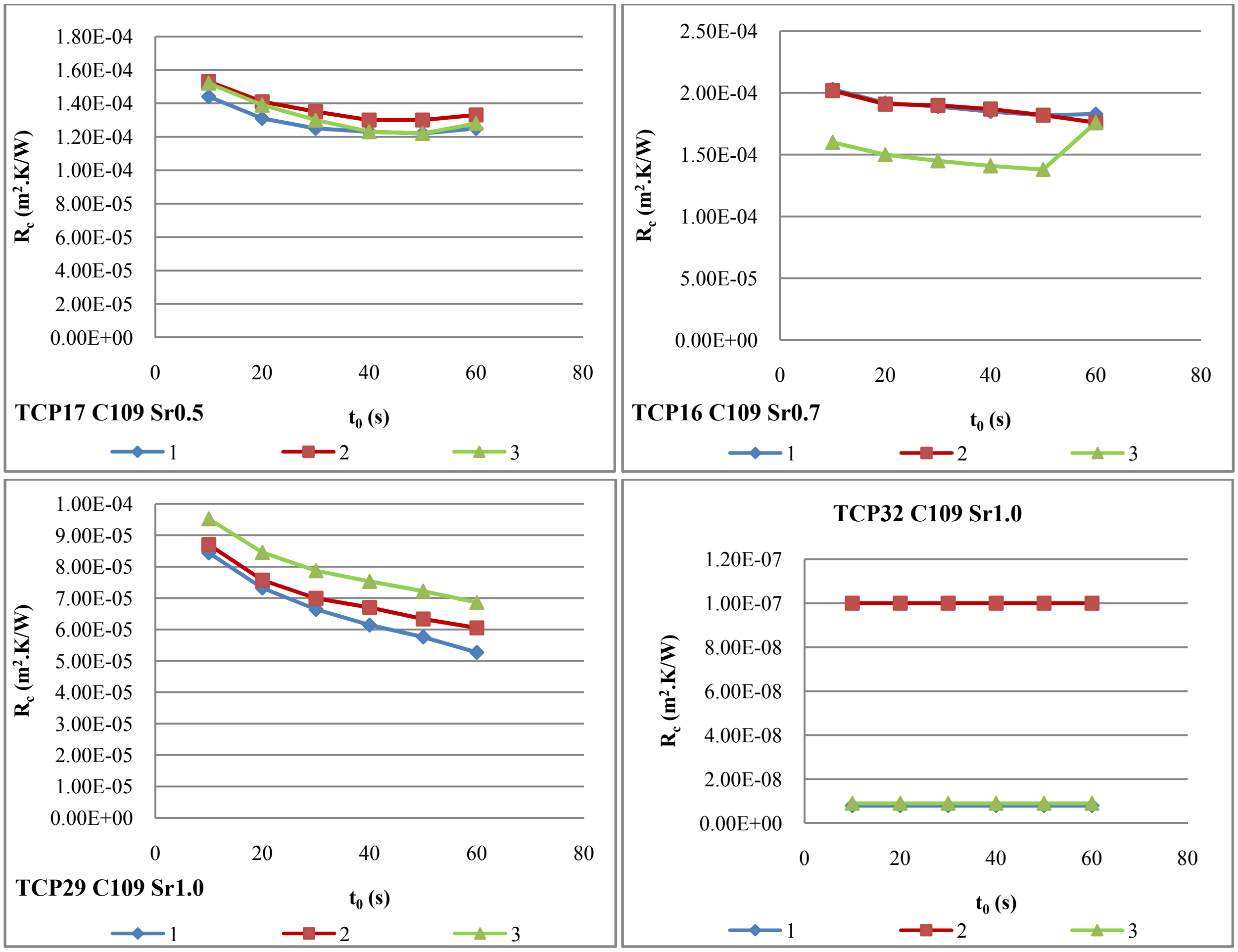

Figure A.6.4. (Cont.) Thermal contact resistance value R_c for testing C109 sand during cooling using r_{sen} from the heating period during calibration.

A.7 - Uncertainty Analysis from Epoxy Experiment

Calculations of random errors for k_e (pages 24, 25, and 27 of [71])

$\overline{X} = \frac{1}{N}\sum_{i=1}^{N} X_i$ where $\overline{X}$ is the average value of N number of X's

$S_{\overline{X}} = \sqrt{\frac{1}{N(N-1)}\sum_{i=1}^{N}\left(X_i - \overline{X}\right)^2}$ where $S_{\overline{X}}$ is the standard deviation of a sample with finite amount of N measurements

$P_{\overline{X}} = tS_{\overline{X}}$ where t is the t-distribution of the sample and $P_{\overline{X}}$ is the random uncertainty of $\overline{X}$.

The actual equation that was used to obtain k_e was:

$$k_e = \frac{V_{hw} \times V_{SR}}{4\pi \times \left[T_1(r,t_1) - T_0(r,t_0)\right] \times Shunt\_R \times LHW} \ln\left(\frac{t_1}{t_0}\right) \qquad \text{(A.7.1)}$$

Calculations of systematic errors for k_e (pages 49 and 51 of [71])

The following equation (Eq. 3.6 of [71]) was used to derive the equations for the relative errors:

$$f = f\left(X_1, X_2, X_3, ...X_j\right) \qquad \text{(A.7.2a)}$$

$$\left(\frac{U_f}{f}\right)^2 = \sum_{i=1}^{j}\left(\frac{X_i}{f}\frac{\partial f}{\partial X_i}\right)^2 \cdot \left(\frac{U_{X_i}}{X_i}\right)^2 \qquad \text{(A.7.2b)}$$

where $\frac{U_f}{f}$ is the relative error for dependent parameter f, X is an independent parameter in the expression of f, j is the number of independent parameters in the expression of f, and i is the i^{th} component.

Applying Eq. A.7.2 for Eq. A.7.1 with V_{hw} (voltage across heating wire), V_{SR} (voltage across shunt resistor), k_e (thermal conductivity of epoxy), *Shunt_R* (resistance of shunt resistor), and *LHW* (length of heating wire) as the variables with errors, we have:

$$\left(B_{k_e}\right)^2 = \left(\frac{V_{hw}}{k_e}\frac{\partial k_e}{\partial V_{hw}}\right)^2\left(\frac{U_{V_{hw}}}{V_{hw}}\right)^2 + \left(\frac{V_{SR}}{k_e}\frac{\partial k_e}{\partial V_{SR}}\right)^2\left(\frac{U_{V_{SR}}}{V_{SR}}\right)^2 + \left(\frac{T}{k_e}\frac{\partial k_e}{\partial T}\right)^2\left(\frac{U_T}{T}\right)^2 + \left(\frac{Shunt\_R}{k_e}\frac{\partial k_e}{\partial Shunt\_R}\right)^2\left(\frac{U_{Shunt\_R}}{Shunt\_R}\right)^2 + \left(\frac{LHW}{k_e}\frac{\partial k_e}{\partial LHW}\right)^2\left(\frac{U_{LHW}}{LHW}\right)^2 \tag{A.7.3}$$

<u>*Calculations of systematic errors for $\alpha_{e:}$*</u> (pages 49 and 51 of [71])

The thermal diffusivity of epoxy can be obtained from:

$$\alpha_e = \frac{r^2}{4t}\exp\left(\gamma + \frac{4\pi k_e \times Shunt\_R}{V_{hw} \times V_{SR} \times \left[T(r,t) - T_i\right]}\right) \tag{A.7.4}$$

Applying equation 3.6 on page 49 of [71] for Eq A.7.4 with V_w, V_{SR}, k_e, *Shunt_R*, *LHW, k_e, and r* as the variables with errors, we have:

$$\left(\frac{U_{\alpha_e}}{\alpha_e}\right)^2 = \left(\frac{V_{hw}}{\alpha_e}\frac{\partial \alpha_e}{\partial V_{hw}}\right)^2\left(\frac{U_{V_{hw}}}{V_{hw}}\right)^2 + \left(\frac{V_{SR}}{\alpha_e}\frac{\partial \alpha_e}{\partial V_{SR}}\right)^2\left(\frac{U_{V_{SR}}}{V_{SR}}\right)^2 + \left(\frac{T}{\alpha_e}\frac{\partial \alpha_e}{\partial T}\right)^2\left(\frac{U_T}{T}\right)^2 + \left(\frac{Shunt\_R}{\alpha_e}\frac{\partial \alpha_e}{\partial Shunt\_R}\right)^2\left(\frac{U_{Shunt\_R}}{Shunt\_R}\right)^2 + \left(\frac{LHW}{\alpha_e}\frac{\partial \alpha_e}{\partial LHW}\right)^2\left(\frac{U_{LHW}}{LHW}\right)^2 + \left(\frac{k_e}{\alpha_e}\frac{\partial \alpha_e}{\partial k_e}\right)^2\left(\frac{U_{k_e}}{k_e}\right)^2 + \left(\frac{r_5}{\alpha_e}\frac{\partial \alpha_e}{\partial r_5}\right)^2\left(\frac{U_r}{r}\right)^2$$

(A.7.5)

Where $\frac{U_{k_e}}{k_e} = 1.31\%$ and $\frac{U_r}{r} = 3.00\%$

A.8 - k_{FS_C109} values for different value sets of k_e and α_e

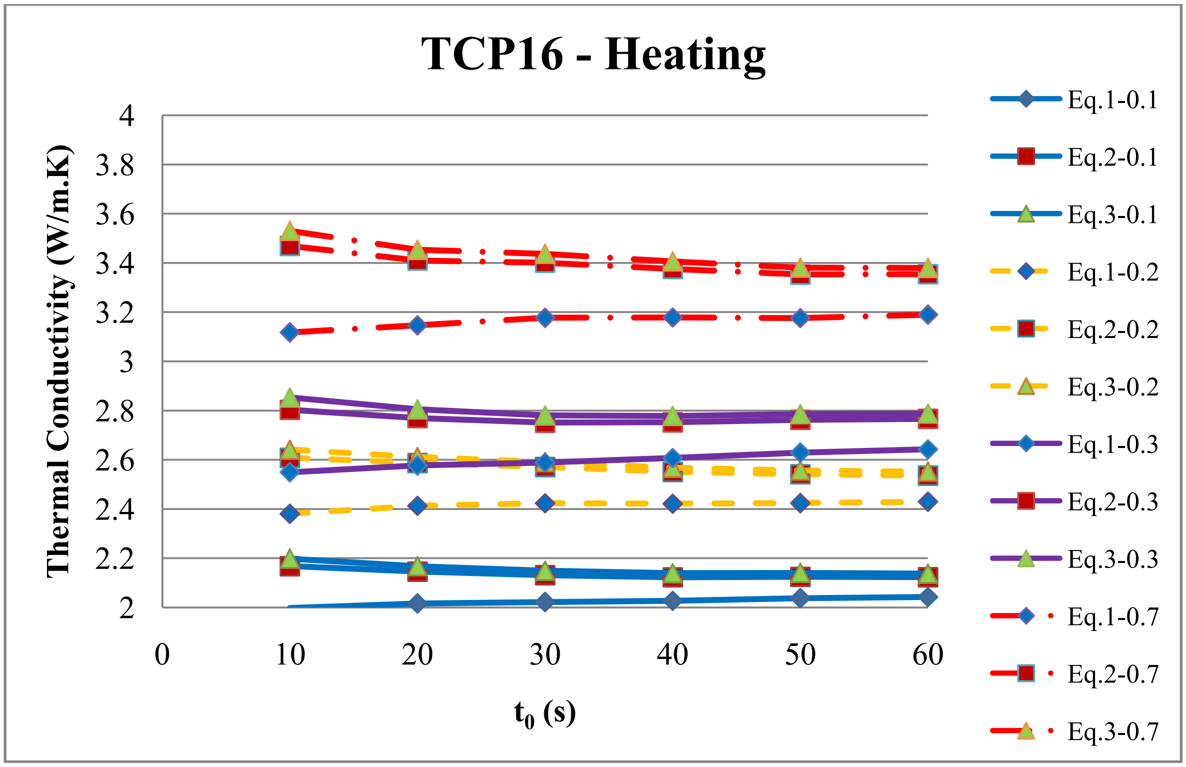

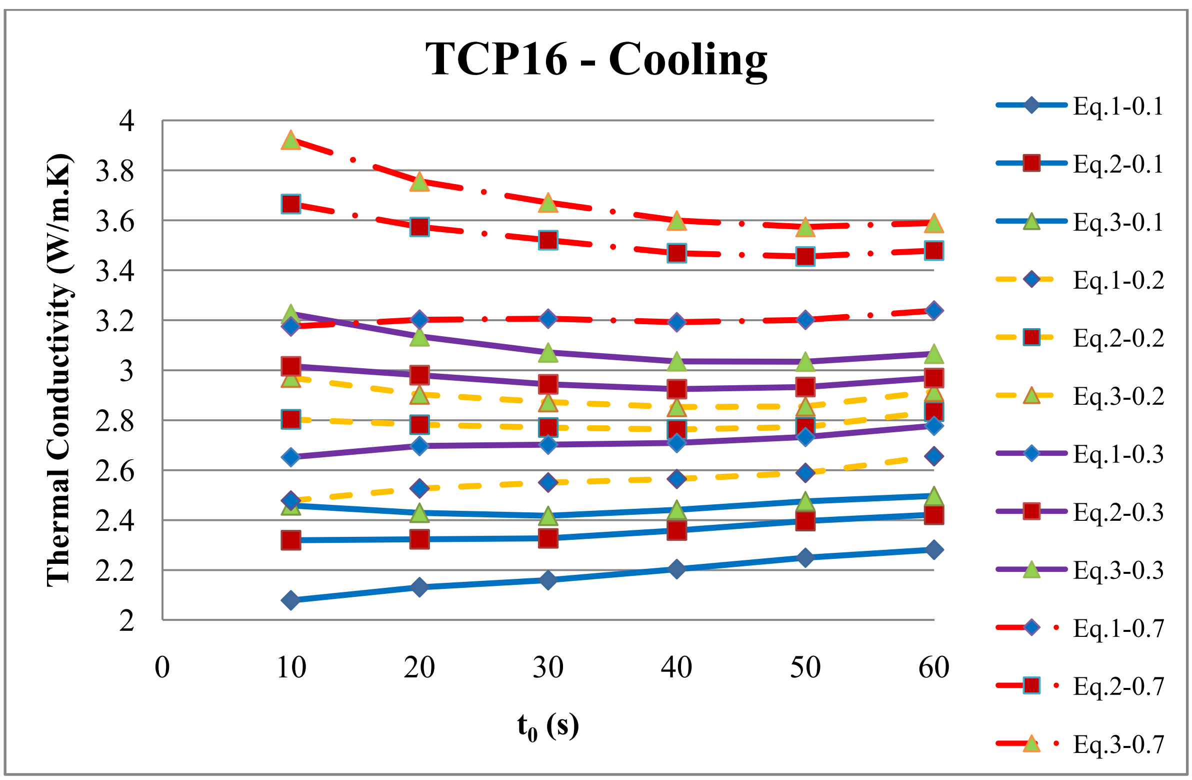

Figure 6.8.1. Error of k_{PS_C109} for using Eqs. 1, 2 and 3 with values of k_e and α_e as shown in Case 1 of Table 6.4.

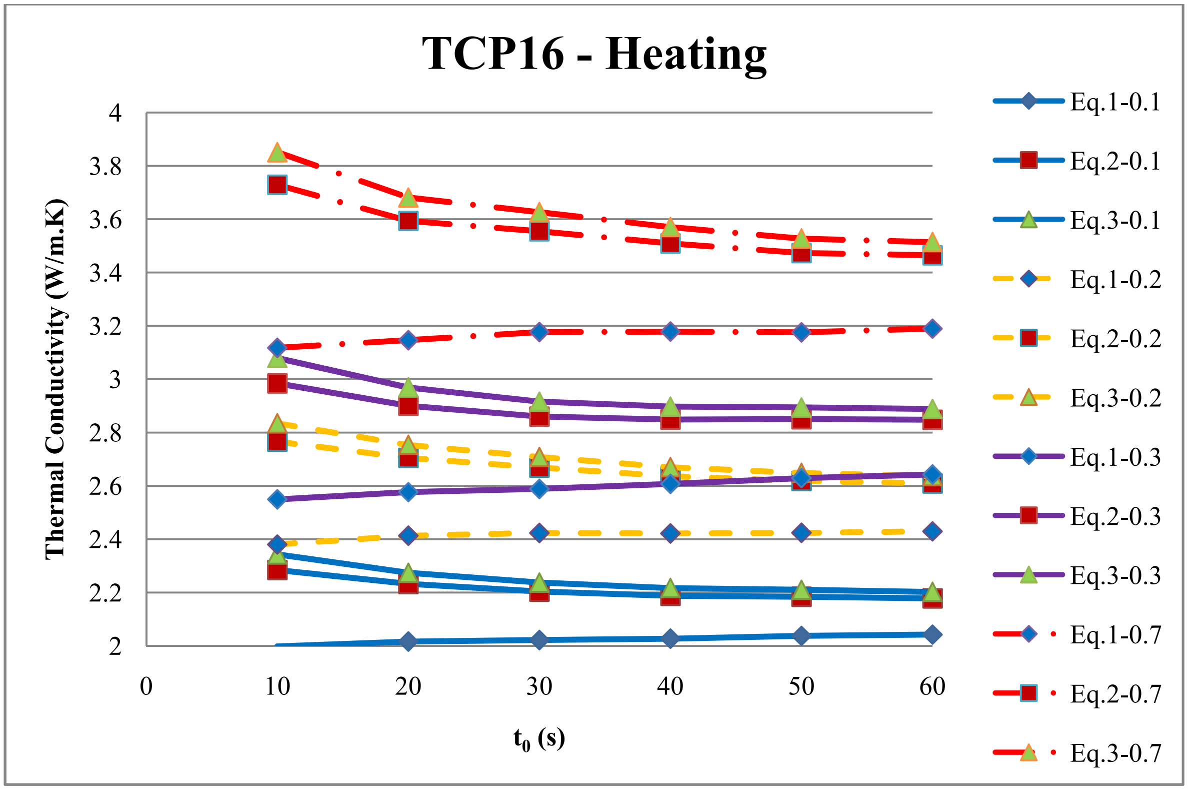

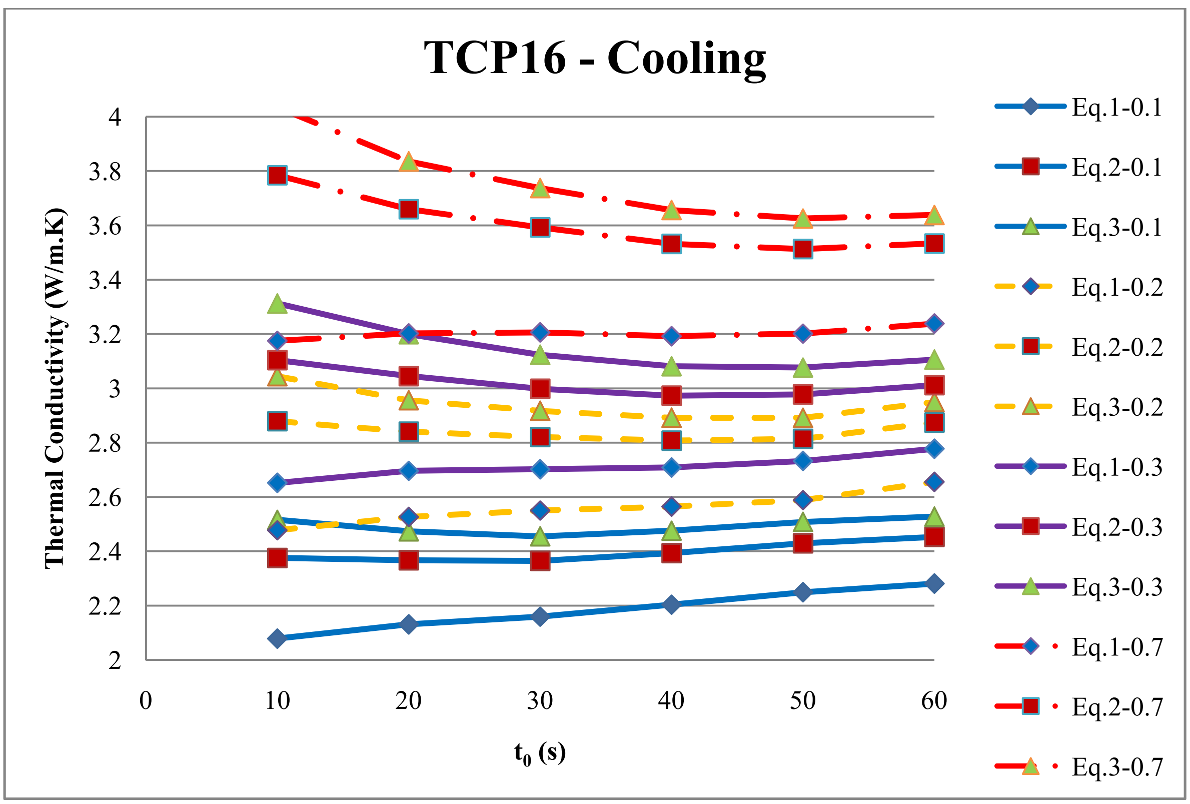

Figure 6.8.2. Error of k_{PS_C109} for using Eqs. 1, 2 and 3 with values of k_e and α_e as shown in Case 2 of Table 6.4.

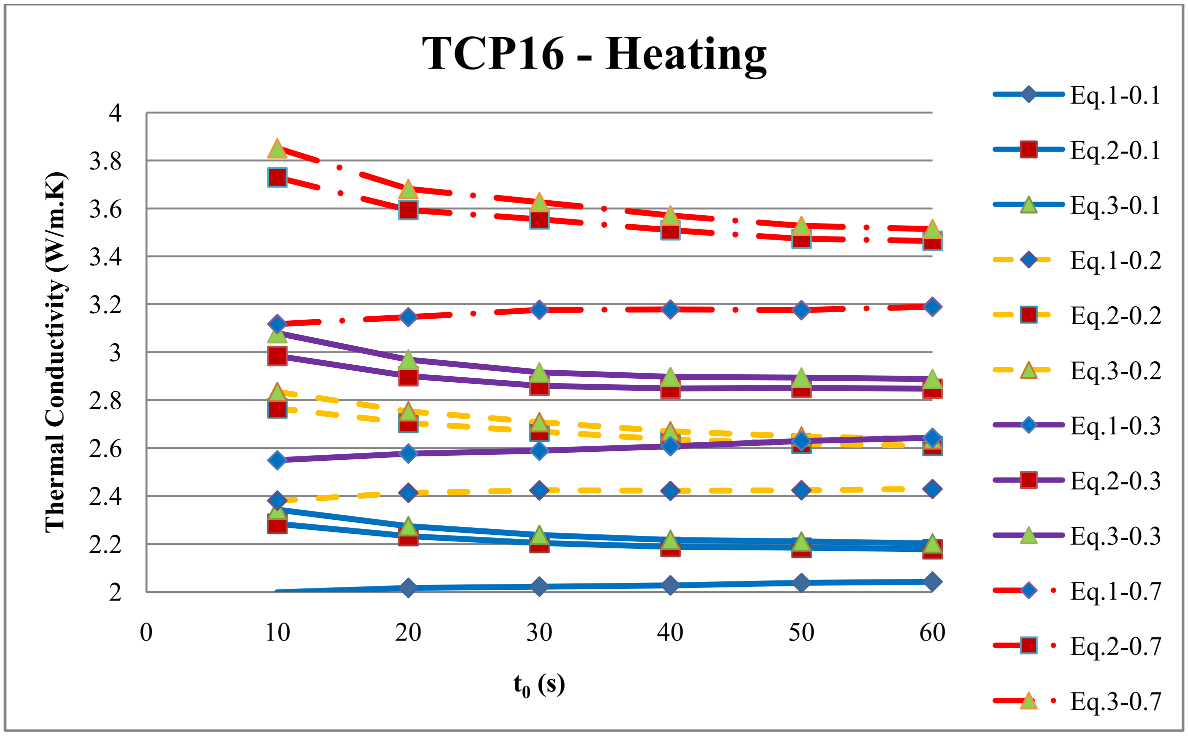

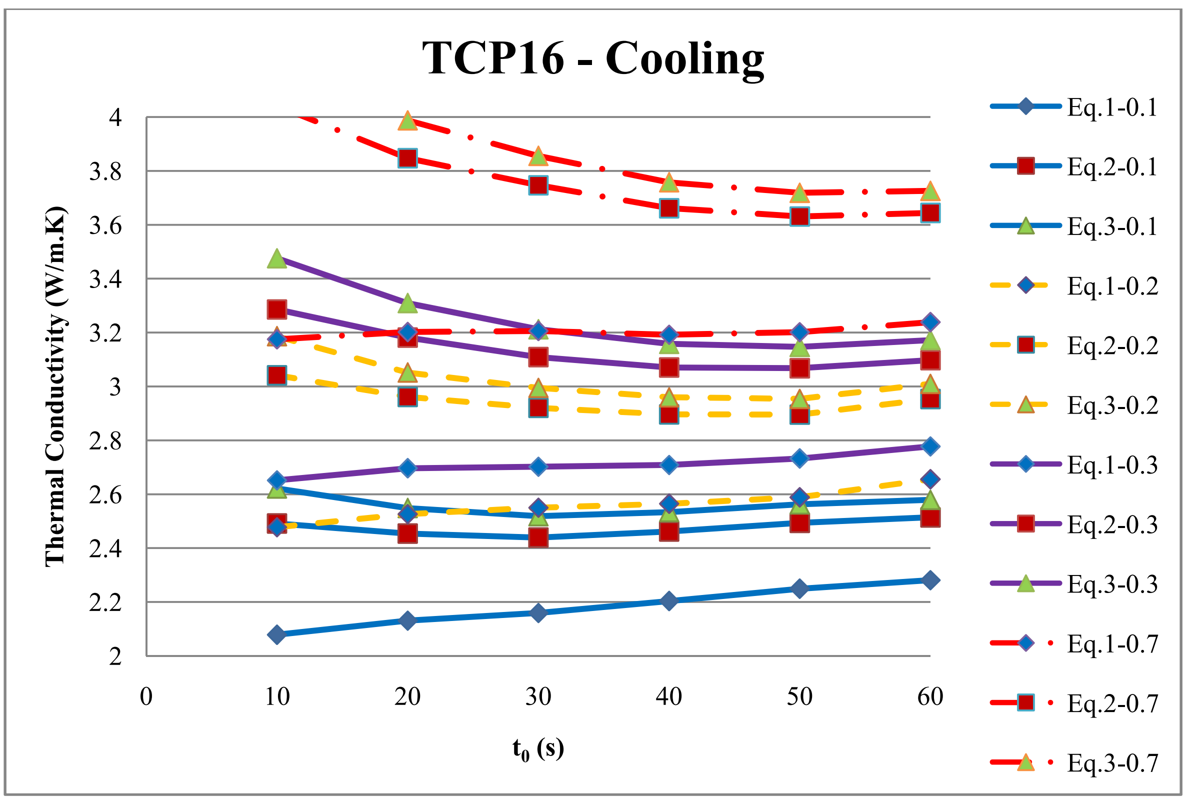

Figure 6.8.3. Error of k_{PS_C109} for using Eqs. 1, 2 and 3 with values of k_e and α_e as shown in Case 3 of Table 6.4.

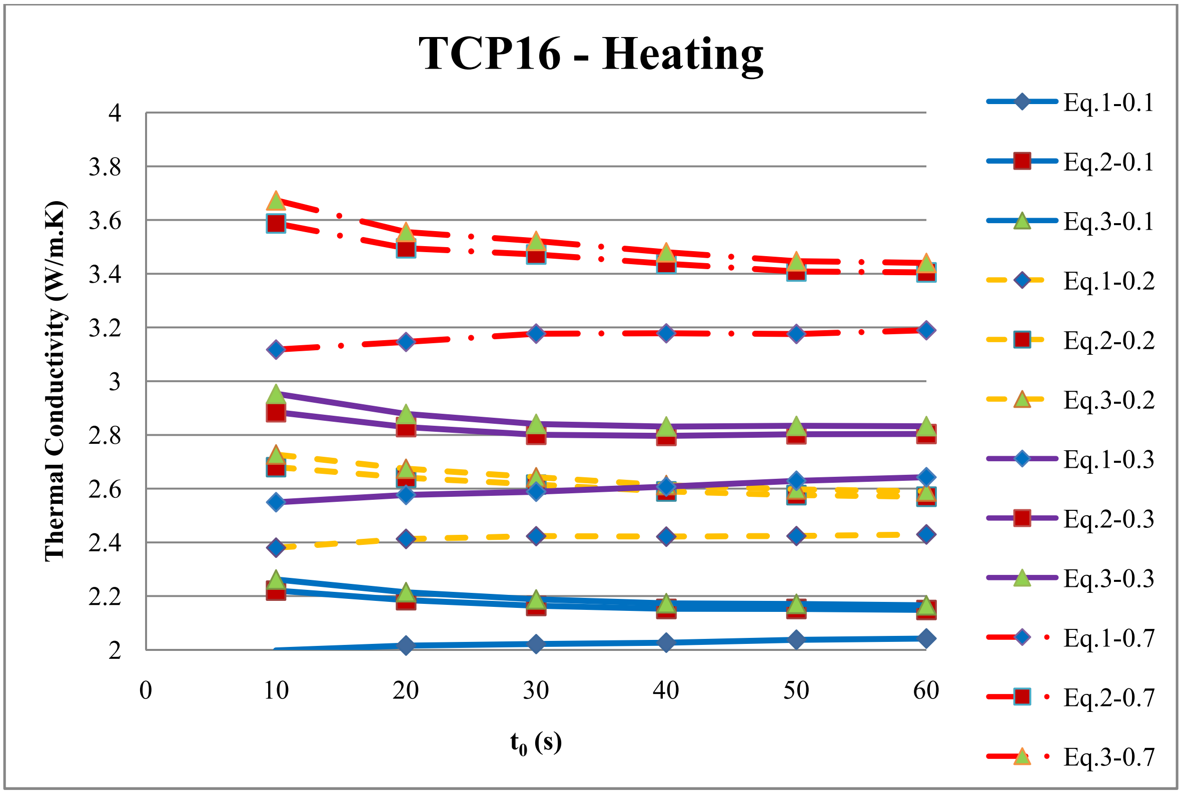

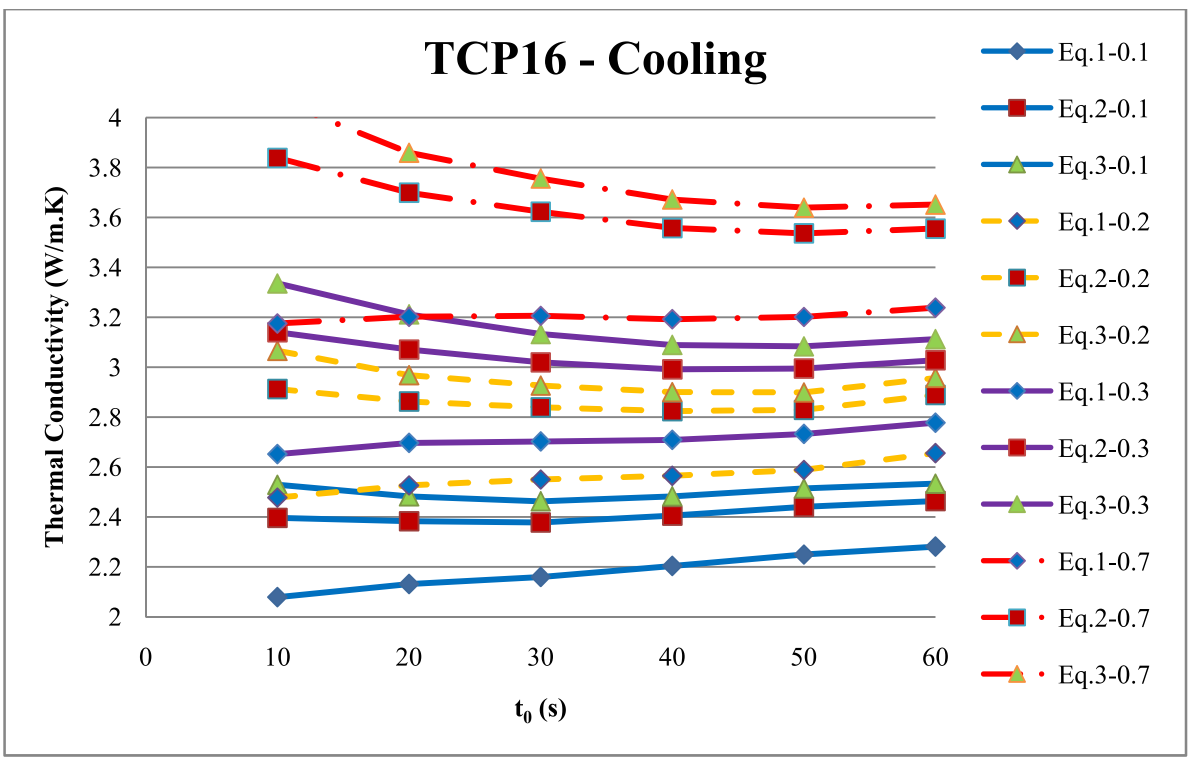

Figure 6.8.4. Error of k_{PS_C109} for using Eqs. 1, 2 and 3 with values of k_e and α_e as shown in Case 4 of Table 6.4.

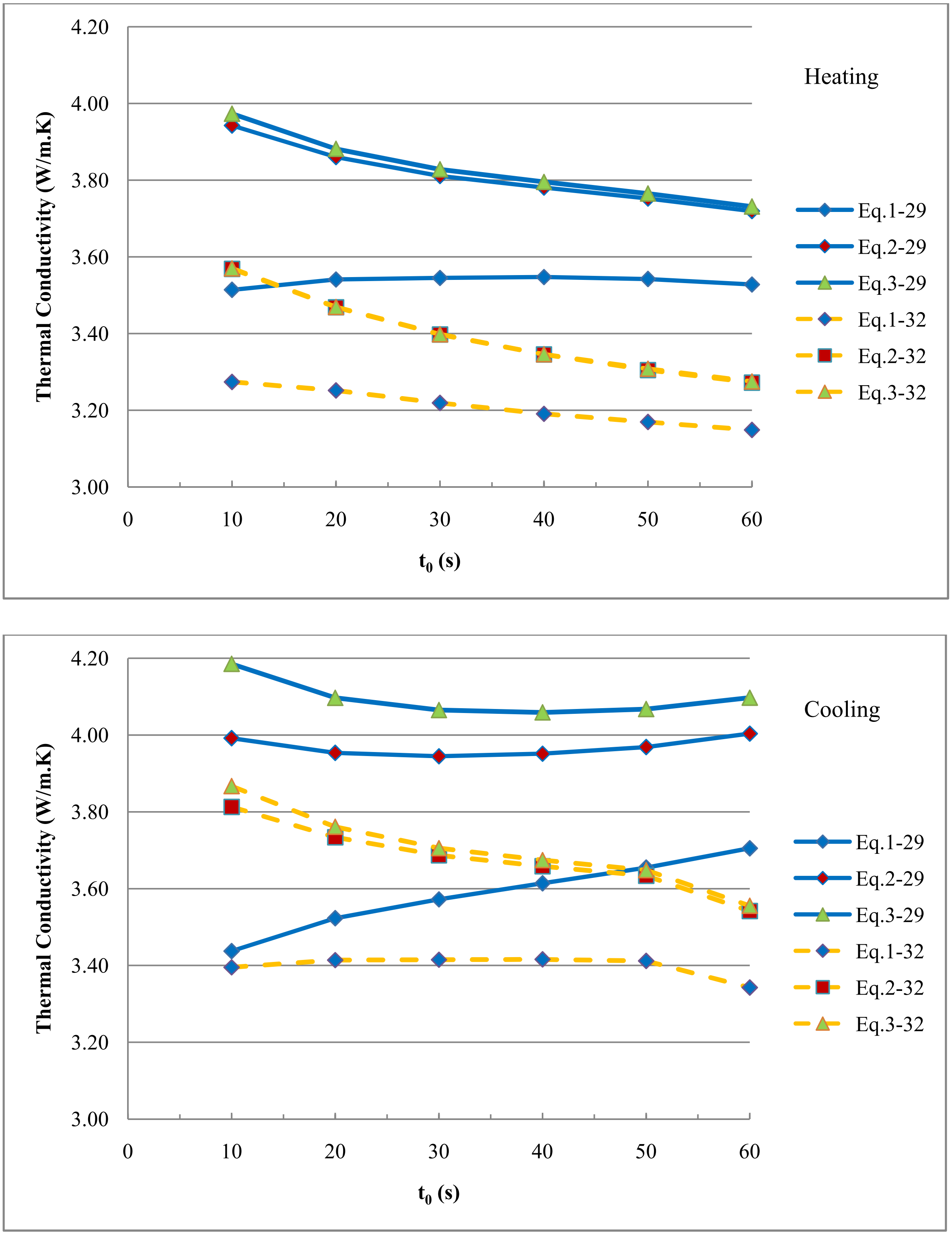

Figure 6.8.5. Thermal conductivities of k_{FS_C109} for using Eqs. 1, 2 and 3 with values of k_e and α_e as shown in Case 1 of Table 6.4.

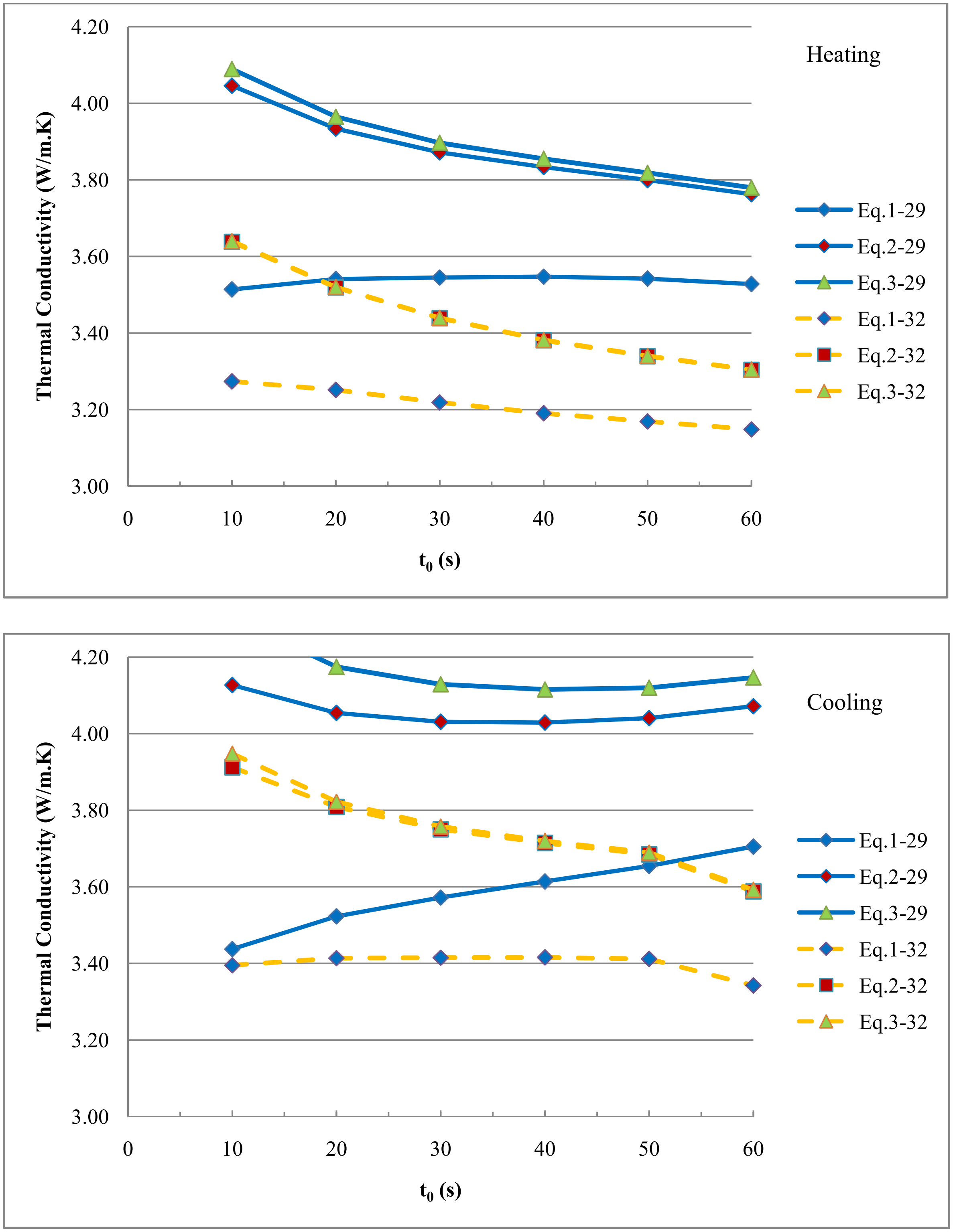

Figure 6.8.6. Thermal conductivities of k_{FS_C109} for using Eqs. 1, 2 and 3 with values of k_e and α_e as shown in Case 2 of Table 6.4.

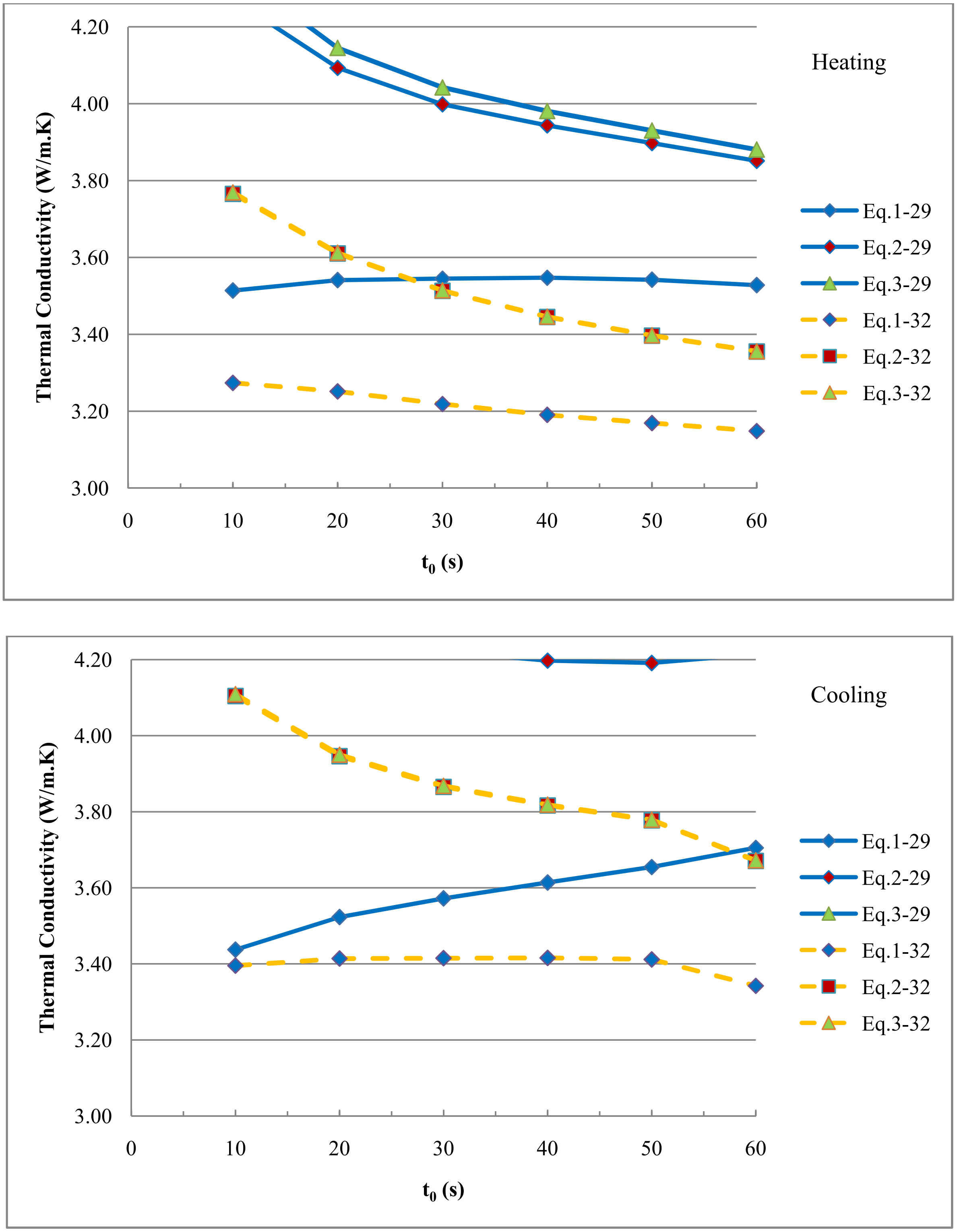

Figure 6.8.7. Thermal conductivities of k_{FS_C109} for using Eqs. 1, 2 and 3 with values of k_e and α_e as shown in Case 3 of Table 6.4.

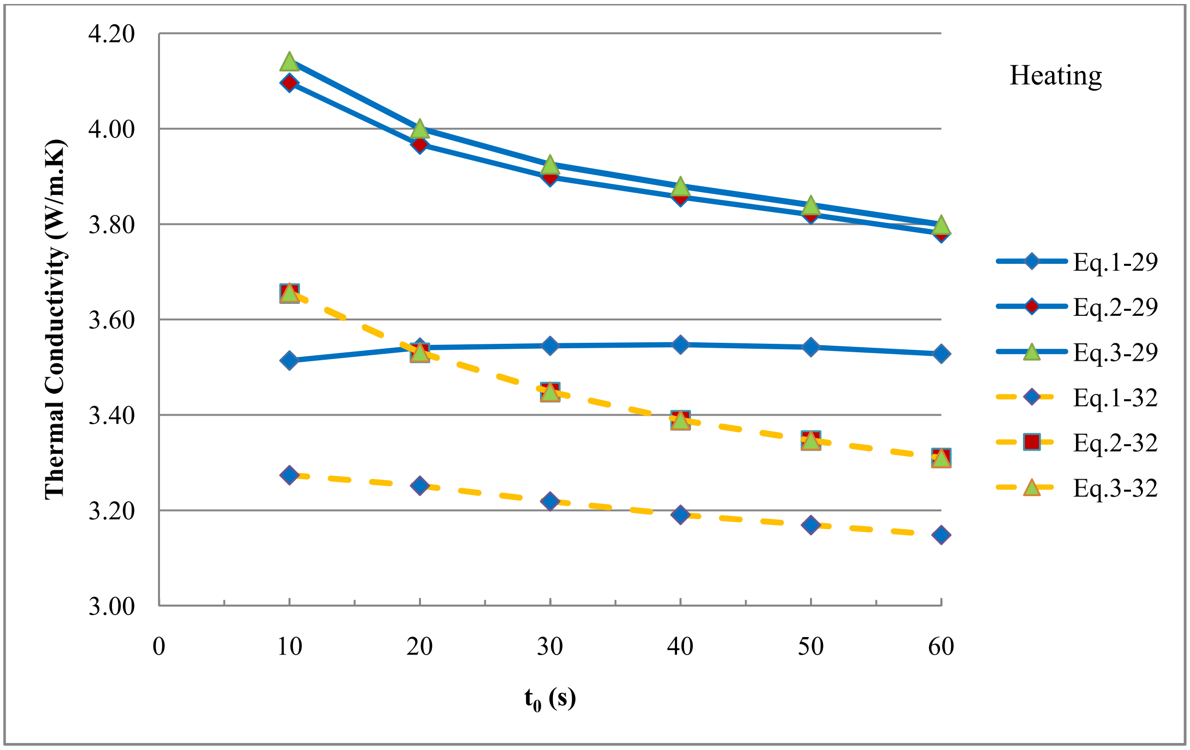

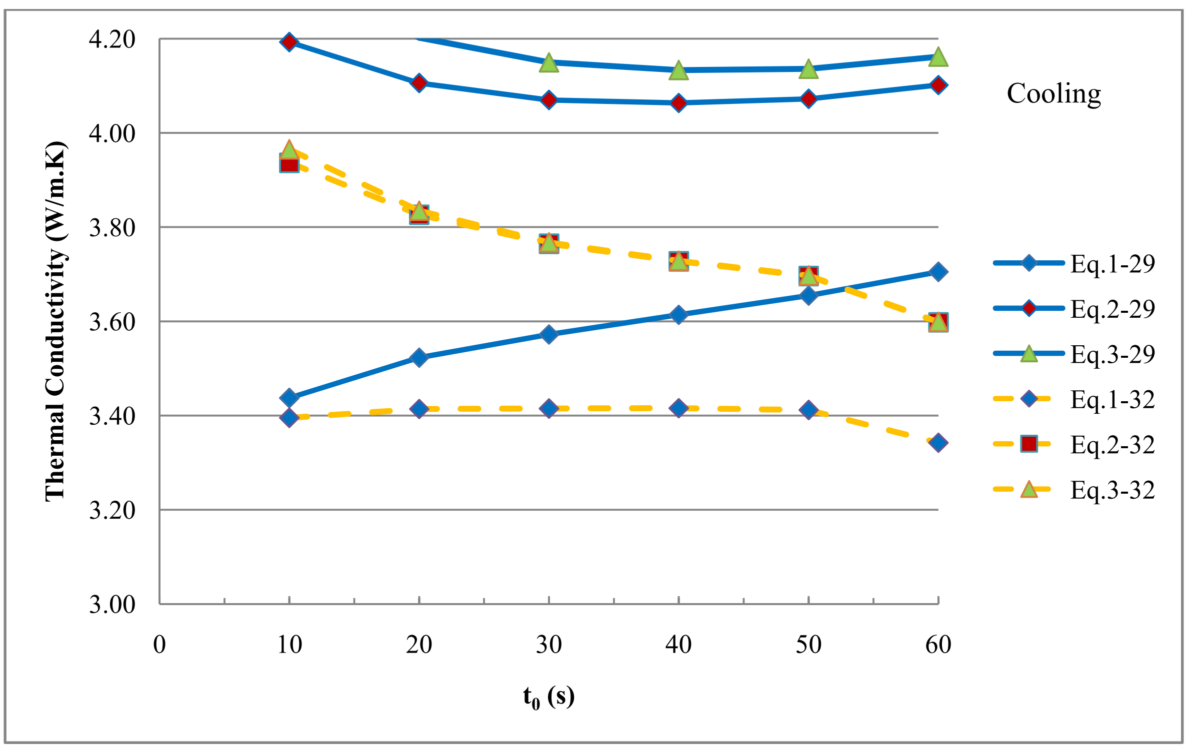

Figure 6.8.8. Thermal conductivities of k_{FS_C109} for using Eqs. 1, 2 and 3 with values of k_e and α_e as shown in Case 4 of Table 6.4.

A.9 - TCP Experimental Graphs

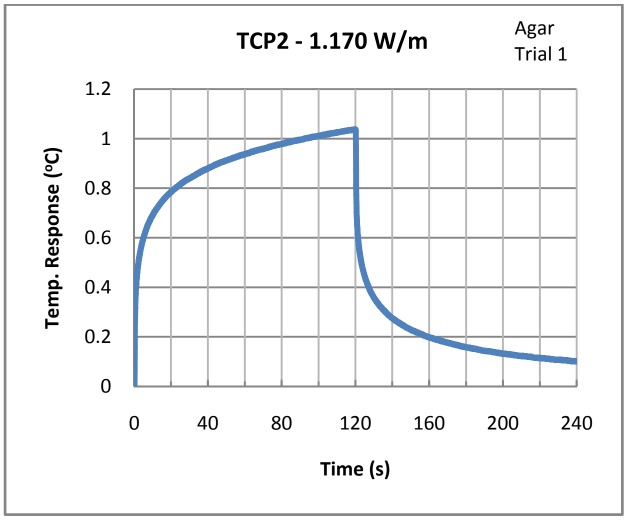

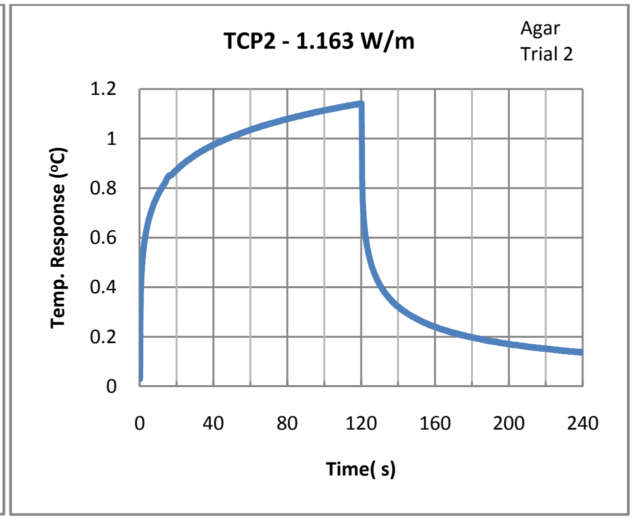

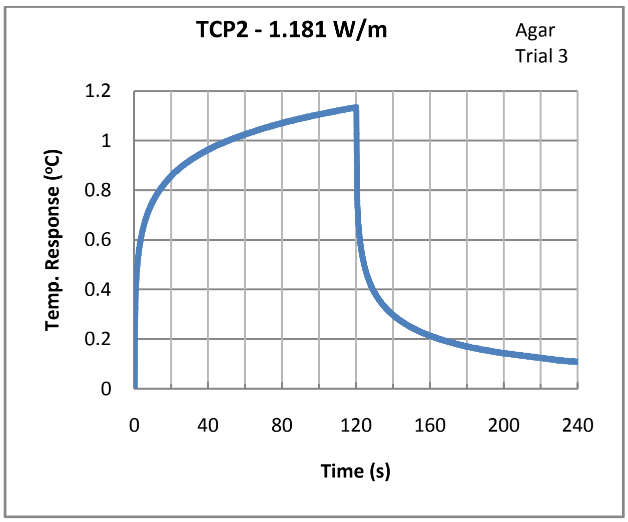

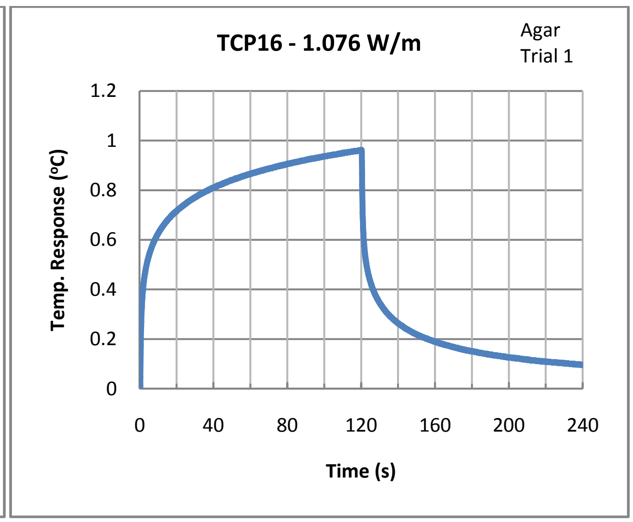

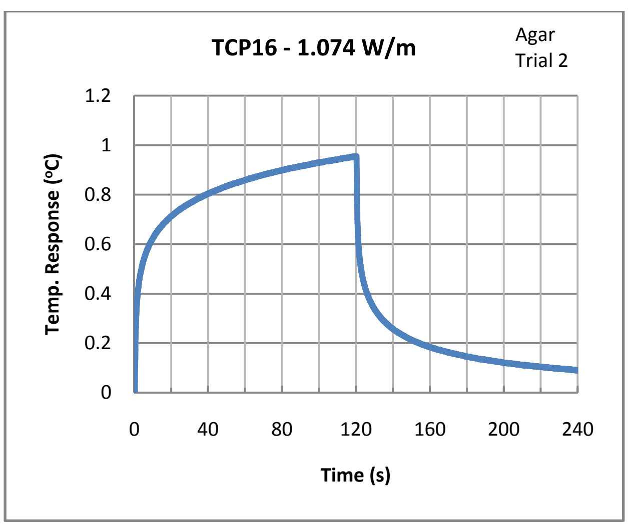

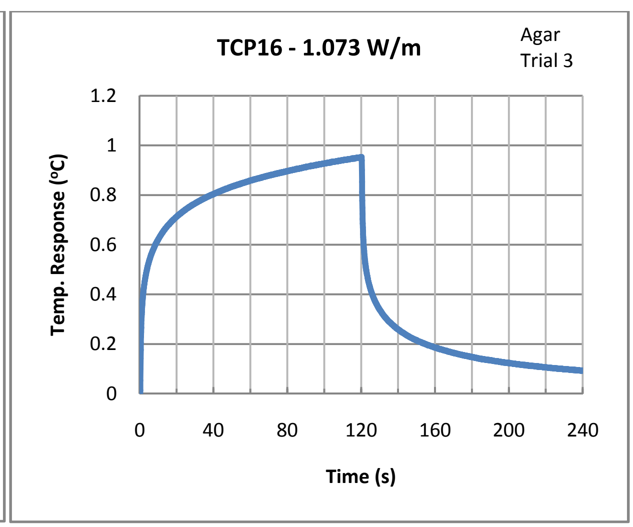

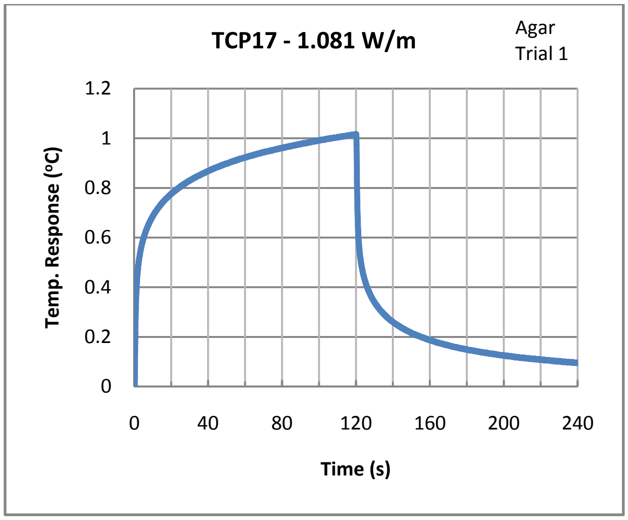
TCP17 - 1.081 W/m
Agar
Trial 1
Temp. Response (ºC)
1.2
1
0.8
0.6
0.4
0.2
0
0
40
80
120
160
200
240
Time (s)

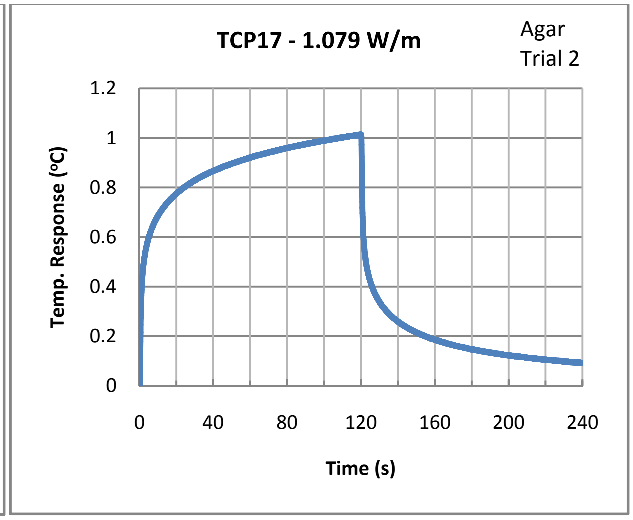
TCP17 - 1.079 W/m
Agar
Trial 2
Temp. Response (ºC)
1.2
1
0.8
0.6
0.4
0.2
0
0
40
80
120
160
200
240
Time (s)

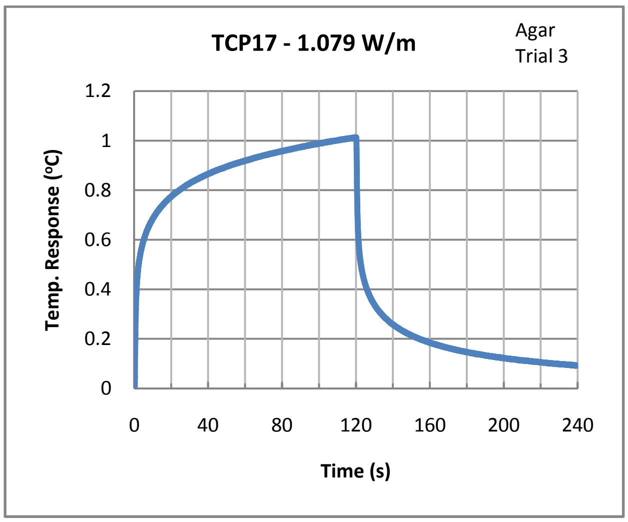
TCP17 - 1.079 W/m
Agar
Trial 3
Temp. Response (ºC)
1.2
1
0.8
0.6
0.4
0.2
0
0
40
80
120
160
200
240
Time (s)

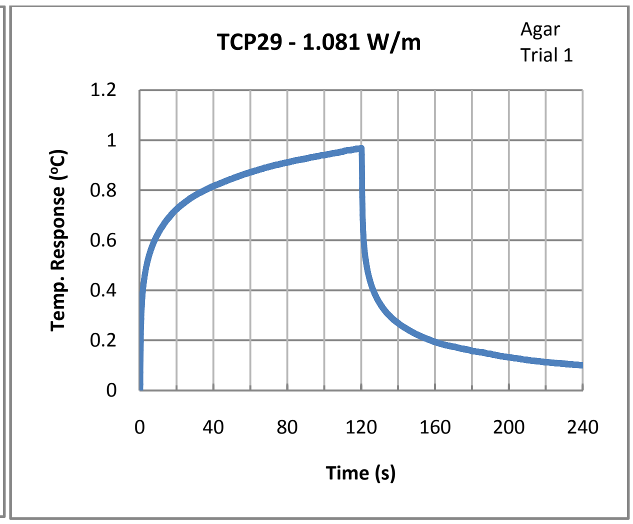
TCP29 - 1.081 W/m
Agar
Trial 1
Temp. Response (ºC)
1.2
1
0.8
0.6
0.4
0.2
0
0
40
80
120
160
200
240
Time (s)

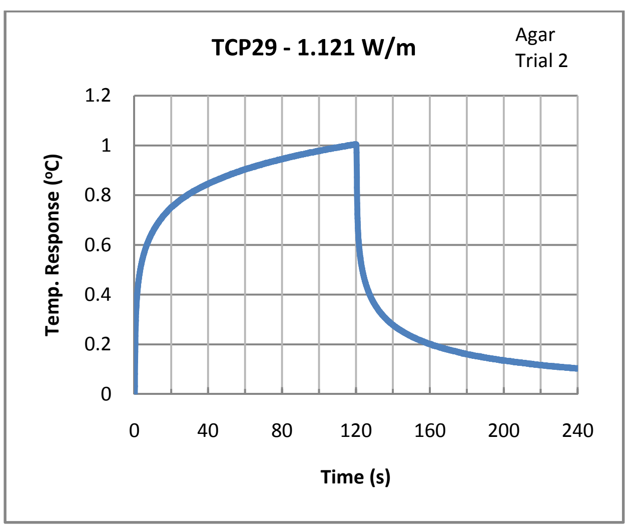
TCP29 - 1.121 W/m
Agar
Trial 2
Temp. Response (ºC)
1.2
1
0.8
0.6
0.4
0.2
0
0
40
80
120
160
200
240
Time (s)

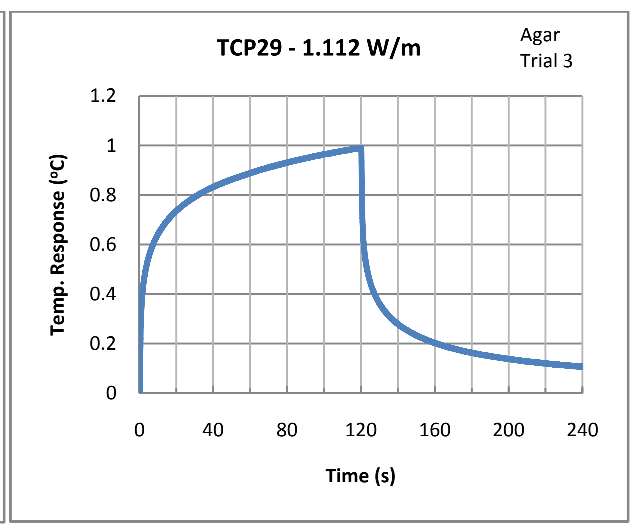
TCP29 - 1.112 W/m
Agar
Trial 3
Temp. Response (ºC)
1.2
1
0.8
0.6
0.4
0.2
0
0
40
80
120
160
200
240
Time (s)

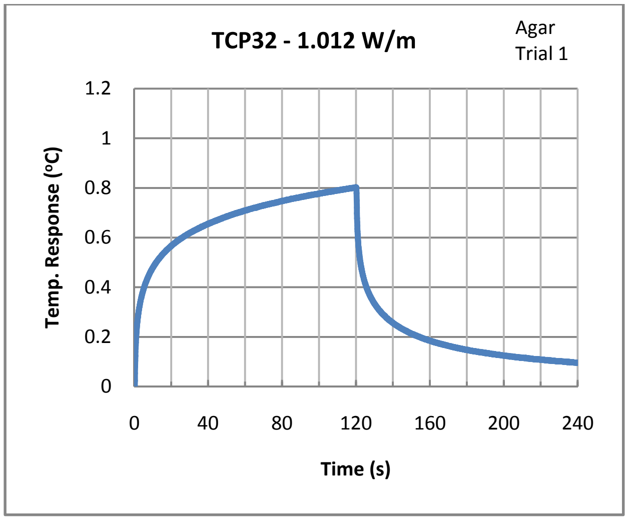
TCP32 - 1.012 W/m
Agar
Trial 1
Temp. Response (ºC)
Time (s)

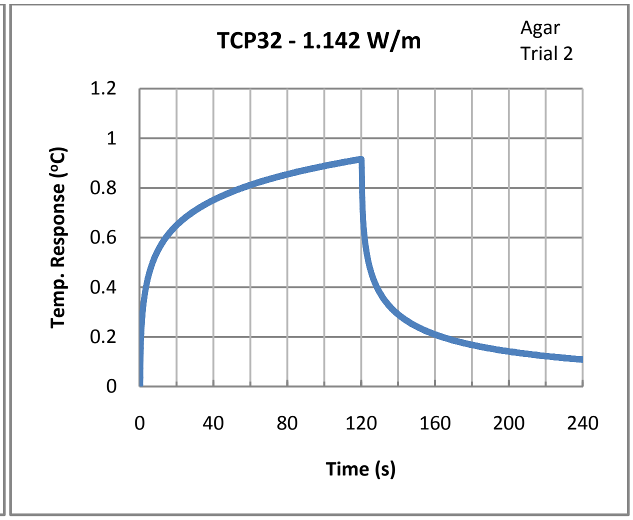
TCP32 - 1.142 W/m
Agar
Trial 2
Temp. Response (ºC)
Time (s)

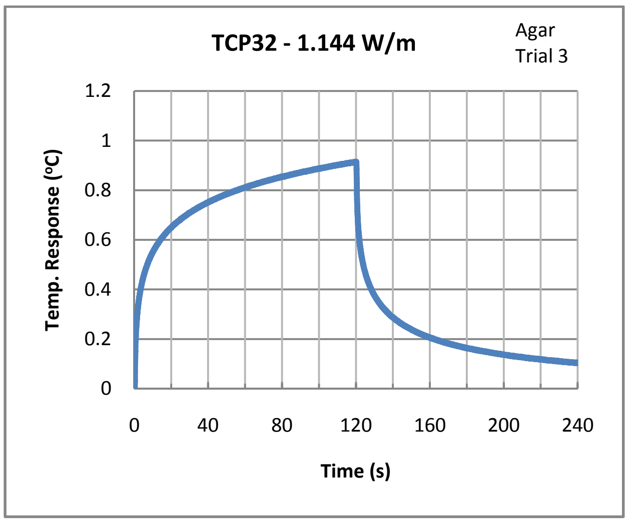
TCP32 - 1.144 W/m
Agar
Trial 3
Temp. Response (ºC)
Time (s)

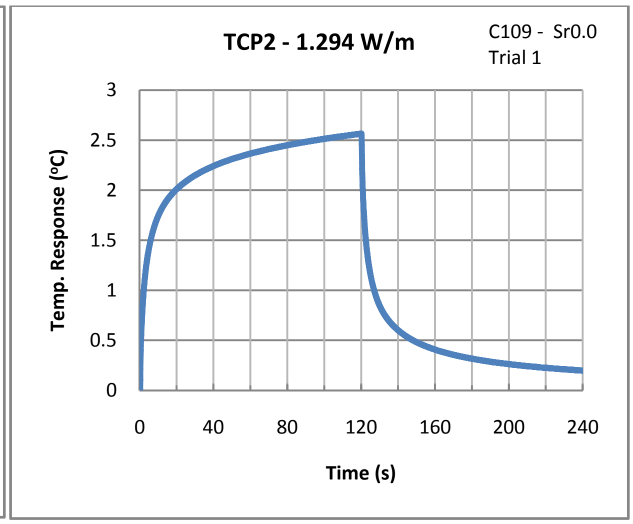
TCP2 - 1.294 W/m
C109 - Sr0.0
Trial 1
Temp. Response (ºC)
Time (s)

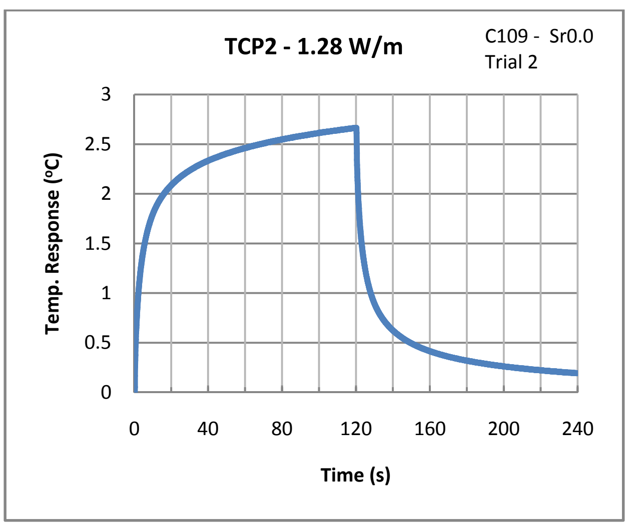
TCP2 - 1.28 W/m
C109 - Sr0.0
Trial 2
Temp. Response (ºC)
Time (s)

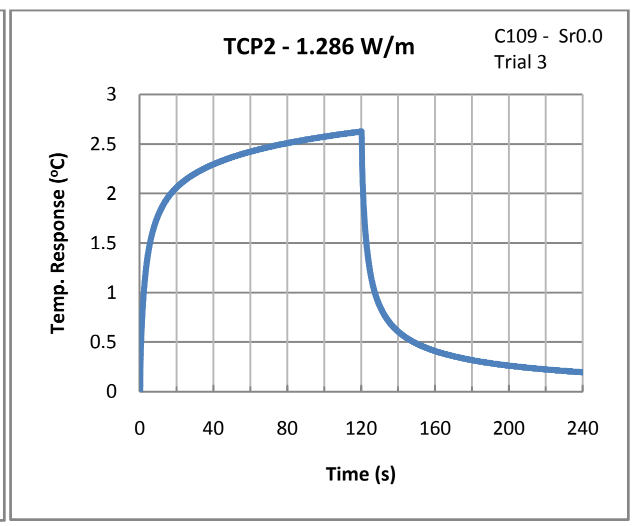
TCP2 - 1.286 W/m
C109 - Sr0.0
Trial 3
Temp. Response (ºC)
Time (s)

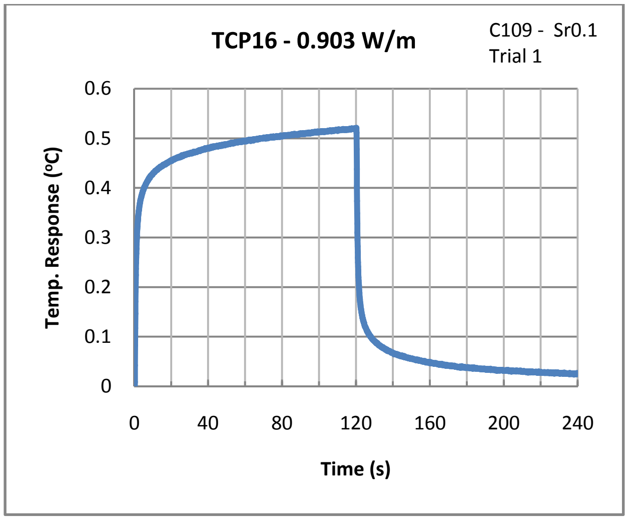
TCP16 - 0.903 W/m
C109 - Sr0.1
Trial 1
Temp. Response (ºC)
0.6
0.5
0.4
0.3
0.2
0.1
0
0
40
80
120
160
200
240
Time (s)

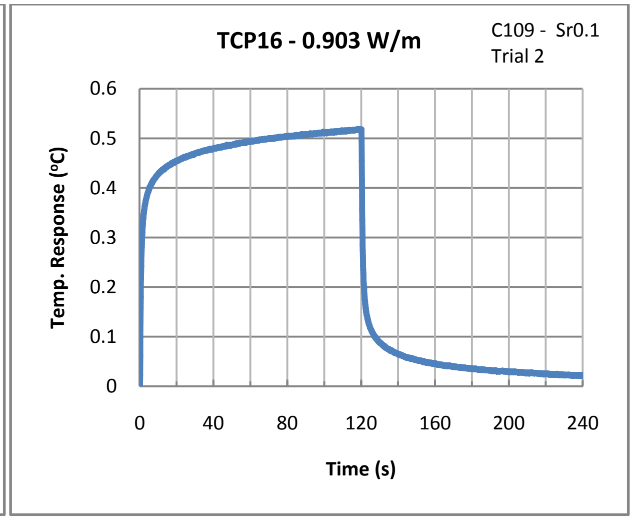
TCP16 - 0.903 W/m
C109 - Sr0.1
Trial 2
Temp. Response (ºC)
0.6
0.5
0.4
0.3
0.2
0.1
0
0
40
80
120
160
200
240
Time (s)

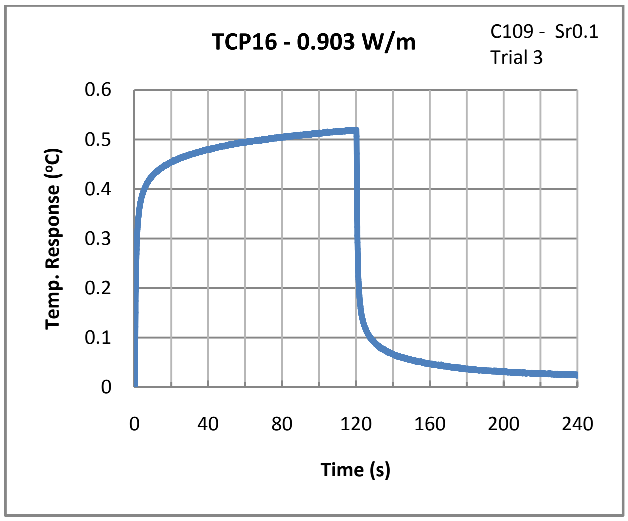
TCP16 - 0.903 W/m
C109 - Sr0.1
Trial 3
Temp. Response (ºC)
0.6
0.5
0.4
0.3
0.2
0.1
0
0
40
80
120
160
200
240
Time (s)

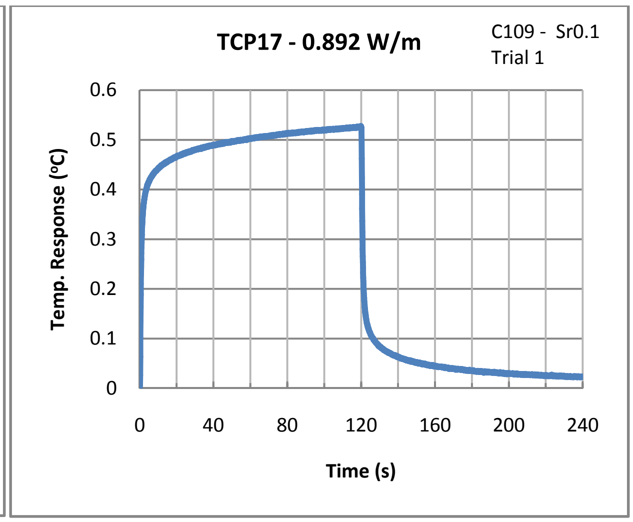
TCP17 - 0.892 W/m
C109 - Sr0.1
Trial 1
Temp. Response (ºC)
0.6
0.5
0.4
0.3
0.2
0.1
0
0
40
80
120
160
200
240
Time (s)

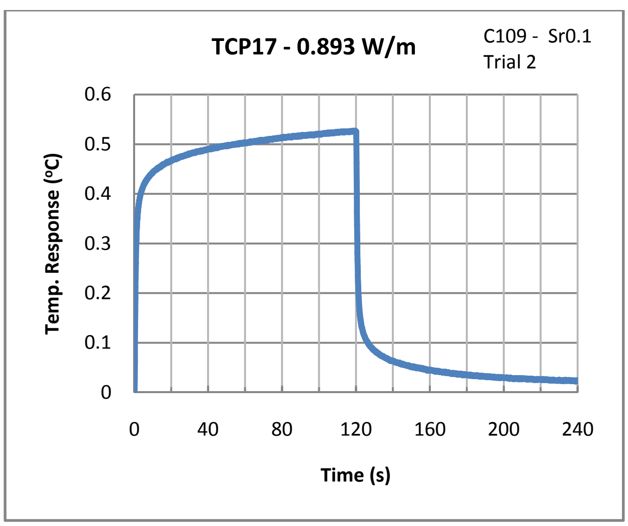
TCP17 - 0.893 W/m
C109 - Sr0.1
Trial 2
Temp. Response (ºC)
0.6
0.5
0.4
0.3
0.2
0.1
0
0
40
80
120
160
200
240
Time (s)

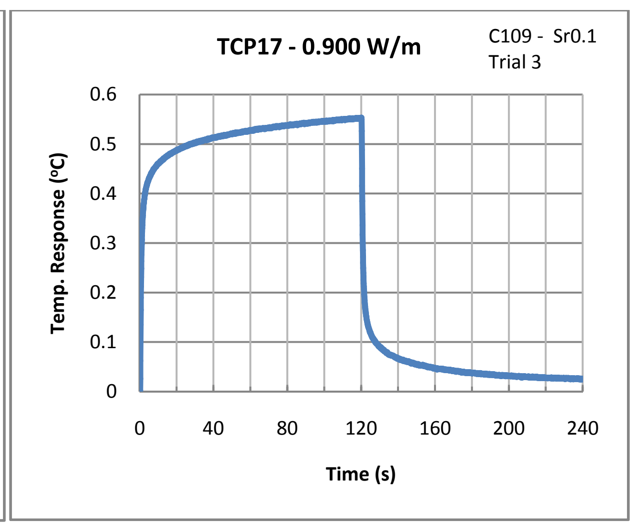
TCP17 - 0.900 W/m
C109 - Sr0.1
Trial 3
Temp. Response (ºC)
0.6
0.5
0.4
0.3
0.2
0.1
0
0
40
80
120
160
200
240
Time (s)

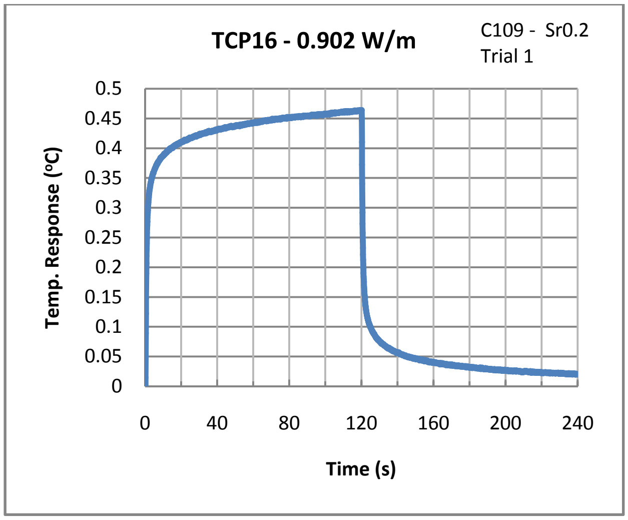
TCP16 - 0.902 W/m
C109 - Sr0.2
Trial 1
Temp. Response (ºC)
Time (s)

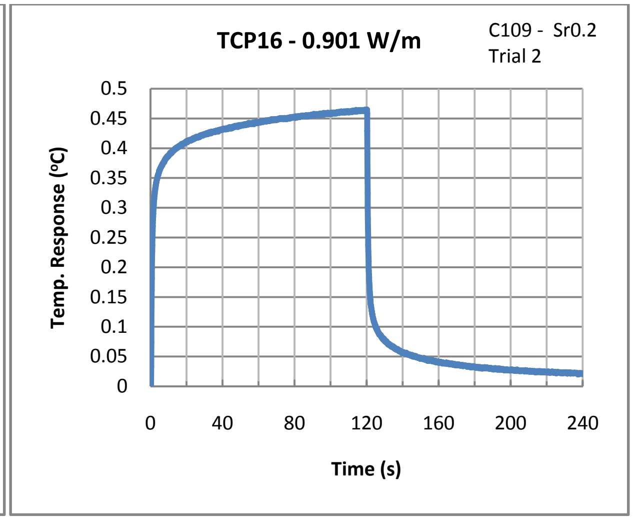
TCP16 - 0.901 W/m
C109 - Sr0.2
Trial 2
Temp. Response (ºC)
Time (s)

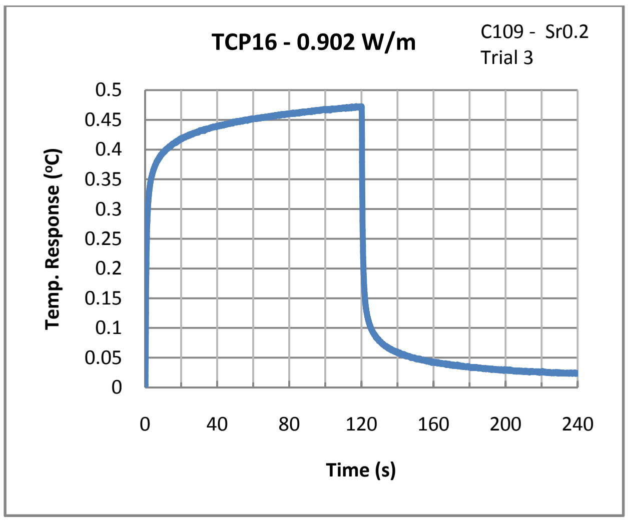
TCP16 - 0.902 W/m
C109 - Sr0.2
Trial 3
Temp. Response (ºC)
Time (s)

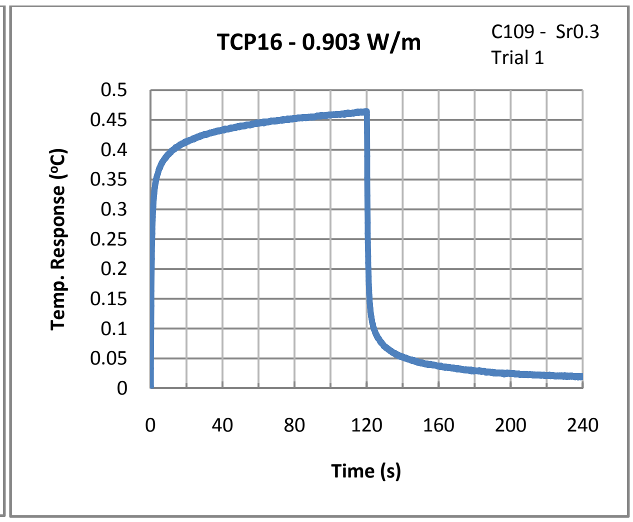
TCP16 - 0.903 W/m
C109 - Sr0.3
Trial 1
Temp. Response (ºC)
Time (s)

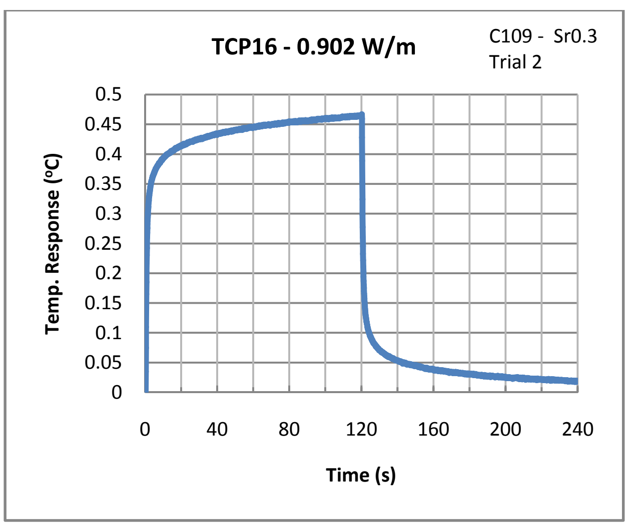
TCP16 - 0.902 W/m
C109 - Sr0.3
Trial 2
Temp. Response (ºC)
Time (s)

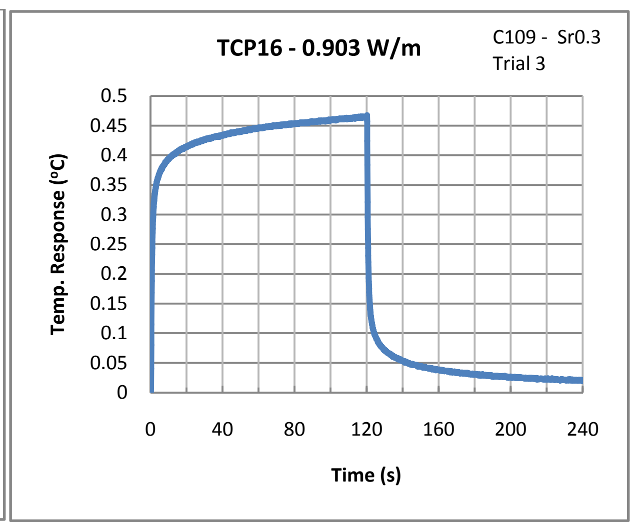
TCP16 - 0.903 W/m
C109 - Sr0.3
Trial 3
Temp. Response (ºC)
Time (s)

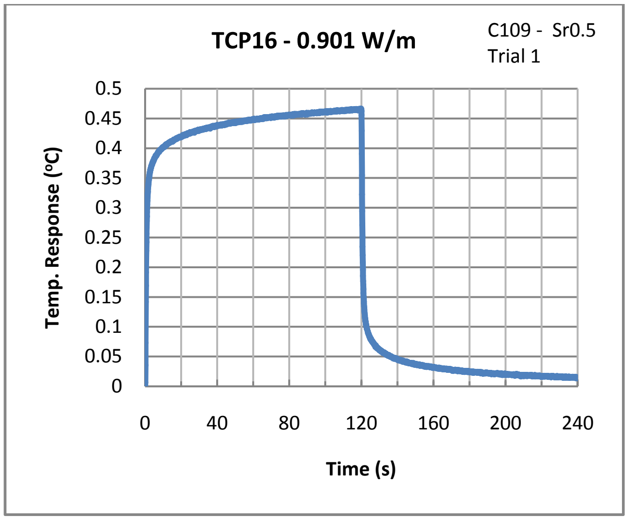
TCP16 - 0.901 W/m
C109 - Sr0.5
Trial 1
Temp. Response (ºC)
Time (s)
0.5
0.45
0.4
0.35
0.3
0.25
0.2
0.15
0.1
0.05
0
0
40
80
120
160
200
240

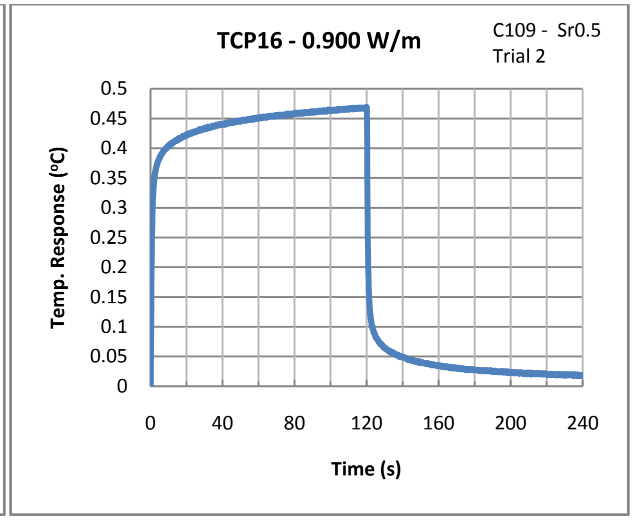
TCP16 - 0.900 W/m
C109 - Sr0.5
Trial 2
Temp. Response (ºC)
Time (s)
0.5
0.45
0.4
0.35
0.3
0.25
0.2
0.15
0.1
0.05
0
0
40
80
120
160
200
240

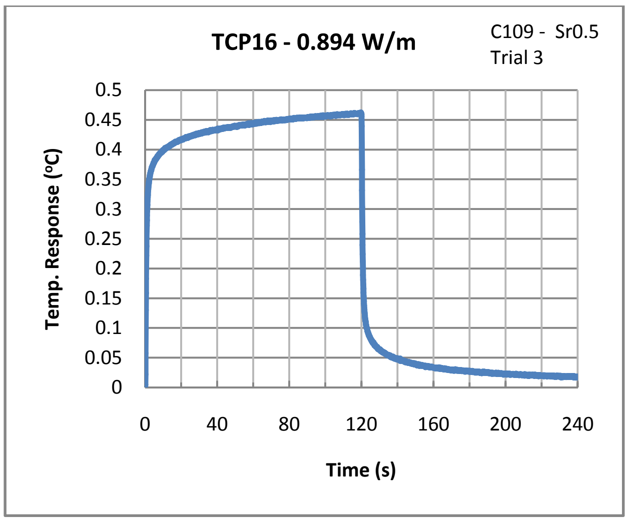
TCP16 - 0.894 W/m
C109 - Sr0.5
Trial 3
Temp. Response (ºC)
Time (s)
0.5
0.45
0.4
0.35
0.3
0.25
0.2
0.15
0.1
0.05
0
0
40
80
120
160
200
240

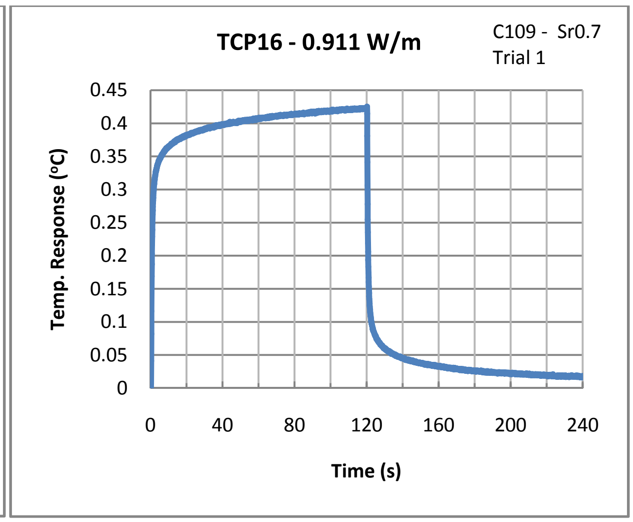
TCP16 - 0.911 W/m
C109 - Sr0.7
Trial 1
Temp. Response (ºC)
Time (s)
0.45
0.4
0.35
0.3
0.25
0.2
0.15
0.1
0.05
0
0
40
80
120
160
200
240

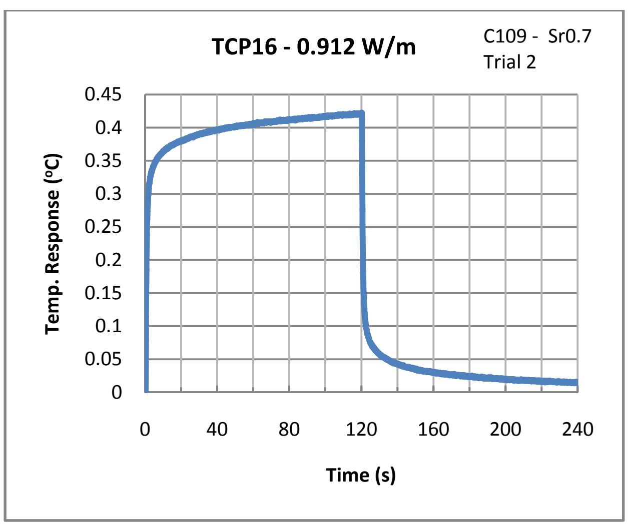
TCP16 - 0.912 W/m
C109 - Sr0.7
Trial 2
Temp. Response (ºC)
Time (s)
0.45
0.4
0.35
0.3
0.25
0.2
0.15
0.1
0.05
0
0
40
80
120
160
200
240

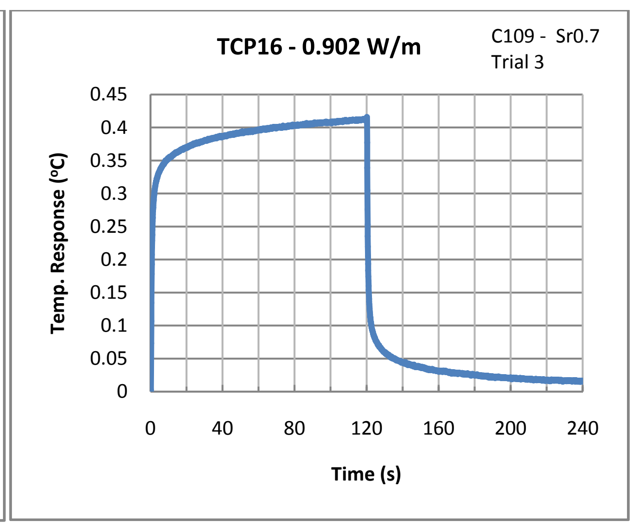
TCP16 - 0.902 W/m
C109 - Sr0.7
Trial 3
Temp. Response (ºC)
Time (s)
0.45
0.4
0.35
0.3
0.25
0.2
0.15
0.1
0.05
0
0
40
80
120
160
200
240

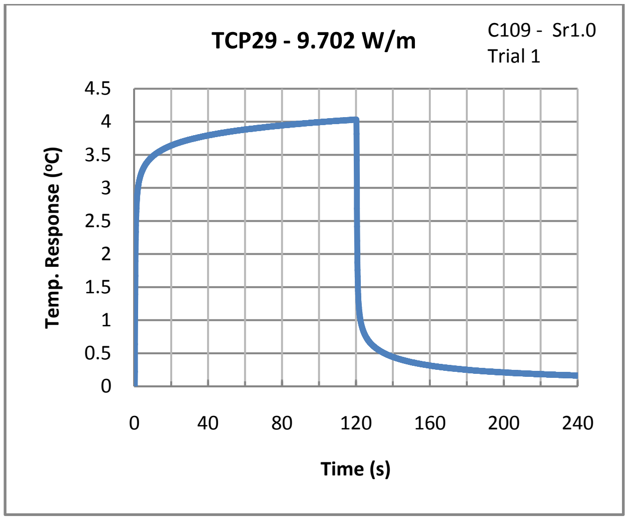
TCP29 - 9.702 W/m
C109 - Sr1.0
Trial 1
Temp. Response (ºC)
Time (s)

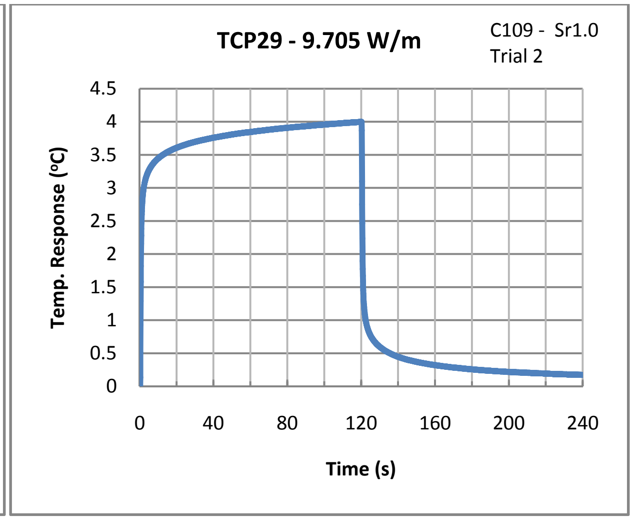
TCP29 - 9.705 W/m
C109 - Sr1.0
Trial 2
Temp. Response (ºC)
Time (s)

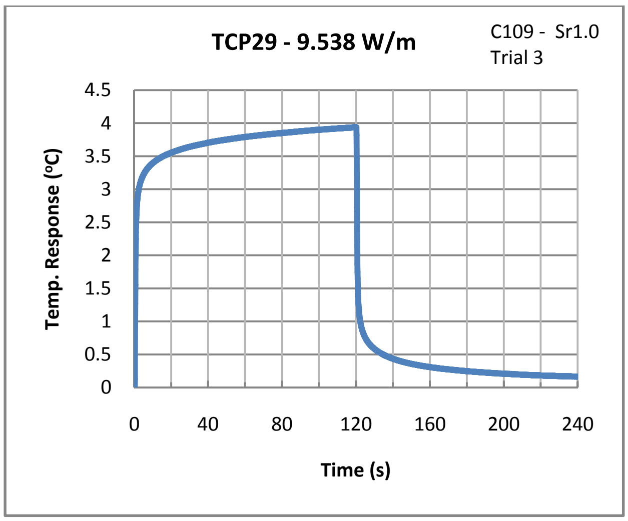
TCP29 - 9.538 W/m
C109 - Sr1.0
Trial 3
Temp. Response (ºC)
Time (s)

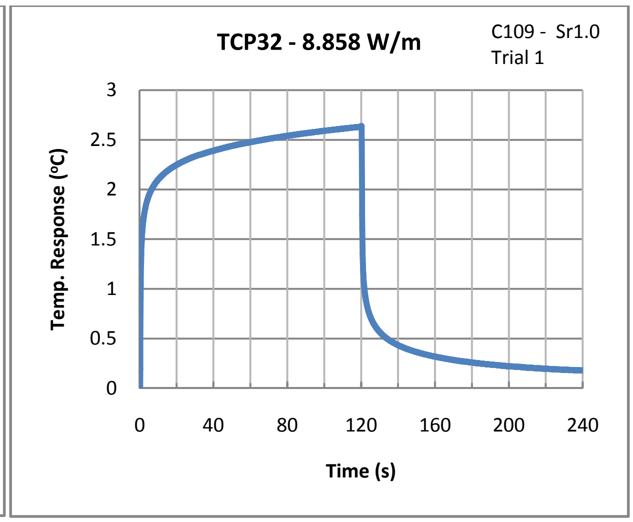
TCP32 - 8.858 W/m
C109 - Sr1.0
Trial 1
Temp. Response (ºC)
Time (s)

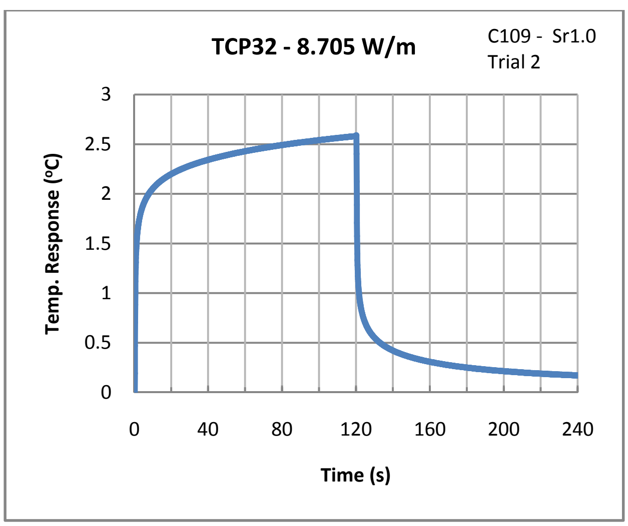
TCP32 - 8.705 W/m
C109 - Sr1.0
Trial 2
Temp. Response (ºC)
Time (s)

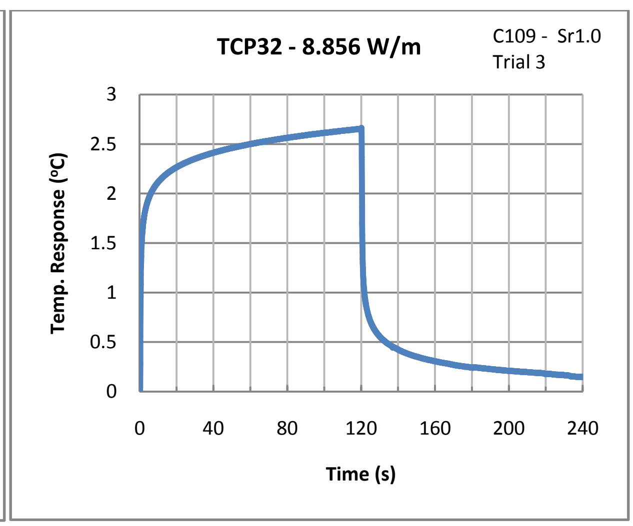
TCP32 - 8.856 W/m
C109 - Sr1.0
Trial 3
Temp. Response (ºC)
Time (s)

REFERENCES

[1]: Canadian Cancer Society's Advisory Committee on Cancer Statistics; ***Canadian Cancer Statistics 2013***; Canadian Cancer Society, Toronto, ON; 2013.

[2]: Mayo Clinic, 13400 E. Shea Blvd, Scottsdale, AZ, 85259, USA, http://www.mayoclinic.org/radiofrequency-ablation/, Aug. 5, 2013.

[3]: Z. Liu, M. Ahmed, Y. Weinstein, M. Yi, R. L. Mahajan, S. N. Goldberg; ***Characterization of the RF ablation-induced 'oven effect': The importance of background tissue thermal conductivity on tissue heating***; *Int. J. Hyperth.*, **22**(4), p. 327–342, 2006.

[4]: Faruk Aras, Vilayed Alecperov, Nursel Can, Hulya Kirkici; ***Aging of 154 kV Underground Power Cable Insulation under Combined Thermal and Electrical Stresses***; IEEE Electrical Insulation Magazine **23**(5), p. 25-33 ; 2007.

[5]: Chulho Lee, Moonseo Park, Sunhong Min, Shin-Hyung Kang, Byonghu Sohn, Hangseok Choi; ***Comparison of effective thermal conductivity in closed-loop vertical ground heat exchangers***; Applied Thermal Engineering, **31**(17-18), p. 3669-3676 ; 2011.

[6]: http://www.nist.gov/el/building_environment/history.cfm.

[7]: Robert R. Zarr, William Healy, James J. Filliben, Daniel R. Flynn; ***Design Concepts for a New Guarded Hot Plate Apparatus for Use Over an Extended Temperature Range***; Building and Fire Research Laboratory and Manufacturing Metrology Division from National Institute of Standards and Technology, Gaithersburg, MD, 20899-8632 and 20899-8220 and MetSys Corporation, Millwood, VA 22646-0317, USA, 2002.

[8]: R. E. Collins, C. A. Davis, C. J. Dey, S. J. Robinson, J. Z. Tang, G. M. Turner; ***Measurement of local heat flow in flat evacuated glazing***; Int. J. Heat Mass Transfer, **36**, p.2553-63; 1993.

[9]: J-L Vivancos, J. Soto, P. Israel, J. Ros-Lis, R. Martinez-Manez 2009; ***A New Model Based on Experimental Results for The Thermal Characterization of Bricks***; Building and Environment, **44**, p.1047-1052; 2009.

[10]: Y. A. Cengel; ***Heat and Mass Transfer - A Practical Approach, 3rd Ed.***; The McGraw-Hill Companies, Inc., 1551 Avenue of the Americas, New York, NY 10020, p.845; ISBN-13: 978-0-07-312930-3; 2003.

[11]: V. R. Tarnawski, T. Momose, W. H. Leong, G. Bovesecchi, P. Coppa; ***Thermal Conductivity of Standard Sands, Part I: Dry-State Conditions***; International Journal of Thermophysics **30**, p.949-968; 2009.

[12]: Y. Nagasaka Y, A. Nagashima; ***Absolute measurement of the thermal conductivity of electrically conducting liquids by transient hot-wire method***; J. Phys. E: Sci. Instrum. **14**, p.1435–40; 1981.

[13]: Huaqing Xie, Shuxia Cheng; ***A Fine Needle Probe for Determining The Thermal Conductivity of Penetrable Materials***; Institute of Physics Publishing, Meas. Sci. Technol. **12**, p.58-62; 2001.

[14]: W. Woodside; ***Probe for Thermal Conductivity Measurement of Dry and Moist Materials***; reprinted from ASHRAR Journal Section, National Research Council of Canada - Division of Building research; 1958.

[15]: F. C. Hooper, S. C. Chang; ***Development of The Thermal Conductivity Probe***; ASHVE Transactions, **59**, p.463-472; 1953.

[16]: H.S. Carslaw, J.C. Jaeger; ***Conduction of Heat in Solids, 2nd Ed.***; Oxford University, London; 1959.

[17]: D. A. De Vries, and A. J. Peck, ***On The Cylindrical Probe Method of Measuring Thermal Conductivity With Special Reference To Soil***; Division of Plant Industry, C.S.I.R.O, Deniliquin, N.S.W; 1957.

[18]: Faculty of Science, Building 20, Clayton Campus, Monash University, Australia, http://www.geosci.monash.edu.au/heatflow/chapter4.html, July 18, 2013.

[19]: K. L. Bristow, G. J. Kluitenberg, C. J. Goding, and T. S. Fizgerald; ***A small multi-needle probe for measuring soil thermal properties, water content and electrical conductivity***; Computer and Electronics in Agriculture, **31**, p.265-280; 2001.

[20]: M. S. Rahman; ***Food Properties Handbook***; CRC Press, Washington DC, USA, p.472; 1995.

[21]: V. R. Tarnawski, M. L. McCombie, T. Momose, I. Sakaguchi, W. H. Leong; ***Thermal COnductivity of Standard Sands. Part III. Full Range of Saturation***; Int. J. Thermophys **34**, p.1130-1147; 2013.

[22]: ASTM D5334-8: ***Standard Test Method for Determination of Thermal Conductivity of Soil and Soft Rock by Thermal Needle Probe Procedure***; 2008.

[23]: E. G. Murakami, V. E. Sweat, S. K. Sastry, and E. Kolbe; ***Analysis of various design and operating parameters of the thermal conductivity probe***; Journal of Food Engineering, **30**, p.209-225; 1996.

[24]: S. X. Cheng, Y. F. Jiang, X. G. Liang; ***A Tiny Heat Probe for Measuring Thermal Conductivities of Materials***; Meas. Sci. Technol. **5**, p.1339-1344; 1994.

[25]: Modesto Antonio Chaves, Alexsandro Oliveira de Almeida; ***Development of a Microcontrolled Instrument to Determinate Thermal Conductivity of Foods***; International Journal of Food Engineering **5**(4), p.1710-1726; 2009.

[26]: Ming Yi, H. V. Panchawagh, R. J. Podhajsky; ***Micromachined Hot-Wire Thermal Conductivity Probe for Biomedical Applications***; IEEE Transactions on Biomedical Engineering **56**(10), p.2477-2484; 2009.

[27]: X. G. Liang, X. S. Ge, Y. P. Zhang, G. J. Wang; ***A Convenient Method of Measuring The Thermal Conductivity of Biological Tissue***; Phys. Med. Biol. **36**, p.1599-1605; 1991.

[28]: J. Lund, B. Sanner, I. Rybach, R. Curtis, G. Hellstrom; ***Geothermal Heat Pumps - A World Review***; Renewable Energy World, p.218-227; 2004.

[29]: L. Sufen, Y. Shang; ***The Numerical Simulation and Experiment Study on The Coupled Thermal Conduction and Groundwater Advection Heat Transfer Process Under The Intermittent Operation of The Ground-Coupled Heat Pump System***; Asia-Pacific Power and Energy Engineering Conference (APPEEC) p.5-9; 2010.

[30]: Valentin Trillat-Berdal, Bernard Souyri, Gilbert Achard; ***Numerical Study of Ground-Coupled Heat Pump System Performance***; Ninth International IBPSA Conference, Montreal, Canada, p.1245-1252; 2005.

[31]: W. King, D. Banks, J. Findlay; ***Field Determination of Shallow Soil Thermal Conductivity Using A Short-Duration Needle Probe Test***; Quarterly Journal of Engineering Geology and Hydrogeology **45**, p.497-504; 2013.

[32]: Zhixiong Wu, Jingwen Li, Hao Zhang, Rongjin Huang, Laifeng Li; ***Study on Thermal Properties of Radiation-Resistant Epoxy Composite***; Cryogenics **52**, p.632-635; 2012.

[33]: Teka Thermophysical Instruments - Geothermal Investigation, Berlin, Germany, http://www.te-ka.de/en/tk04/thermal-conductivity-specs/probes.html, July 16, 2013.

[34]: D. Elustondo, M. P. Elustondo, and M. J. Urbicain; ***New thermal conductivity probe design based on the analysis of error sources***; Journal of Food Engineering, **35**, p.325-333; 2001.

[35]: F. C. Hooper, F. R. Lepper; ***Transient Heat Flow Apparatus for The Determination of Heating Piping and Air Conditioning***; Trans. ASHREA **56**, p.309-324; 1950.

[36]: T. L. Brandon, J. K. Mitchell; ***Factors Influencing Thermal Resistivity of Sands***; Journal of Geotechnical Enigneering **115**(12), p.1683-1698; 1989.

[37]: H. S. Radhakrishma; ***Heat Flow and Moisture Migration in Cable Backfills***; Ontario Hydro Research Quarterly **20**, p.10-20; 1968.

[38]: J. I. Adams, A. F. Baljet; ***Thermal Behavior of Cable Backfill Materials***; IEEE Transactions on Power Apparatus and Systems **PAS-87**(4), p.1149-1161; 1968.

[39]: J. H. Blackwell; ***The Axial-Flow Error In The Thermal Conductivity Probe***; Canadian Journal of Physics, **34**, p.412 – 417; 1956.

[40]: J. R. Bilskie, R. Horton, K. L. Bristow; ***Test of A Dual-Probe Heat-Pulse Method for Determining Thermal Properties of Porous Materials***; Soil Science, **163**(5), p.346-355, Williams & Wilkins; 1998.

[41]: S. Goto, O. Matsubayashi; ***Inversion of Needle-Probe Data for Sediment Thermal Properties of The Eastern Flank of The Juan de Fuca Ridge***; Journal of geophysical research **113(**B8), p.B08105; 2008.

[42]: Gang Liu, Bing C. Si, Ai X. Jiang, Bao G. Li, Tu S. Ren, Ke L. Hu; ***Probe Body and Thermal Contact Conductivity Affect Error of Heat Pulse Method Based on Infinite Line Source Approximation***; Soil Sci. Am. J., **76**, p.370-374; 2012.

[43]: V. R. Tarnawski, T. Momose, W. H. Leong; ***Thermal Conductivity of Standard Sand, Part II: Saturated Conditions***; Int. J. Thermophys **32**, p.984-1005; 2011.

[44]: Vasile Strambu; ***Influences in Thermal Conductivity Evaluation Using The Thermal Probe Method - Some Practical Aspects***; Bulletin of the Polytechnic Institute of Jassy, Construction, Architecture Section, Faculty of Civil Engineering and Building Services, Department of Civil and Industrial Engineering, 43 Dimitrie Manferon Blvd., Jassy 700050, Romania; 2003.

[45]: G. B. Asher, E. D. Sloan, M. S. Graboski; ***A Computer-Controlled Transient Needle-Probe Thermal Conductivity Instrument for Liquids***; International Journal of Thermophysics, **7**(2), p.285-294; 1986.

[46]: H. Hsieh; ***Thermal Conductivity Measurement with A Thermal Probe in The Presence of External Heat Sources***; A Master of Science thesis presented to The Faculty of The Division of Graduate Studies, Georgia Institute of Technology; 1983.

[47]: D. A. de Vries; ***A non-stationary method for determining thermal conductivity of soil in situ***; Soil Science, **73**, p.83-89; 1952.

[48]: Thermally conductive epoxy 832TC, MG Chemicals, 9347-193rd Street, Surrey, B.C., Canada, V4N 4E7, http://www.mgchemicals.com/products/protective-coatings/epoxy-potting-and-encapsulating-compounds/thermally-conductive-epoxy-832tc/; Jul. 22, 2013.

[49]: ASM Aerospace Specification Metals Inc., 2501 N.W. 34th Place #B28, Pompano Beach, FL 33069, USA, http://asm.matweb.com/search/SpecificMaterial.asp?bass num=MQ304A, Aug. 5, 2013.

[50]: R. H. Perry, C. H. Chilton; ***Chemical Engineering Handbook* (*5th Ed.*)**; McGraw-Hill, New York; 1973.

[51]: D. A. de Vries, A. I. Peck; Aust. J. Phys. **11**, p.255-271; 1958.

[52]: W. Woodside, J. B. Cliffe, Soil Sci. **87**, 78; 1958.

[53]: W. A. Slusarchuk, P. H. Fougler; in *Technical Paper No. 388*, Division of Building Research, National Research Council of Canada; 1973.

[54]: T. H. W. Baker; in DBR Paper No. 682; Division of Building Research, National Research Council of Canada; 1976.

[55]: J.V. Sengers, J.T.R. Watson; J. Phys. Chem. Ref. Data **15**, p.1291; 1986.

[56]: A.E. Wechsler, in ***Compendium of Thermophysical Property Measurement Methods, Recommended Measuring Techniques and Practices***, vol. 2, ed. by K.D. Magli´c, A. Cezairliyan,V.E. Peletsky (Plenum Press, London, 1992).

[57]: SPI Supplies/Structure Probe Inc., 569 East Gay Street, West Chester, PA, 19380, USA, http://www.2spi.com/catalog/chem/embed4d.php, Aug. 5, 2013.

[58]: Canadian Tire Corporation, 2180 Yonge Street, Toronto, ON, M4P 2V8, Canada, http://www.canadiantire.ca/AST/browse/8/KitchenBath/KitchenStorage/CanisterSets/PRD~0424648P/Magnetic+Spice+Jar.jsp?locale=en; Aug. 28, 2013.

[59]: J. H. Blackwell; ***A Transient-Flow Method for Determination of Thermal Constants of Insulating Materials in Bulk***; J. Appl. Phys., **25**, p.137-144; 1954.

[60]: O. K. Nusier, N. H. Abu-Hamdeh; ***Laboratories Techniques to Evaluate Thermal Conductivity for Some Soils***; Heat and Mass Transfer **39**(2), p.119-123; 2003.

[61]: N. H. Abu-Hamdeh; ***Soil and Water Measurement of The Thermal Conductivity of Sandy Loam and Clay Loam Soils Using Single and Dual Probes***; J. Arg. Eng. Res. **80**(2), p. 209-216; 2001.

[62]: J. P. Cull; ***Thermal Contact Resistance in Transient Conductivity Measurements***; J. Pys. E: Sci. Instrum. **11**, p. 323 - 326; 1977.

[63]: M. S. Kersten; ***Thermal Properties of Soils***; Bulletin No. 28 (University of Manitoba), p. 225; 1949.

[64]: O. T. Farouki; ***Thermal Properties of Soils***; Trans Tech Publication, Aedermannsdorf, Switzerland; 1986.

[65]: T. Bhowmick, B. R. Gupta, S. Pattanayak; ***Thermal Conductivity and Thermal Diffusivity of Silicone - Poly(Styrene Butadiene) Rubber Blends from 60 to 300 K***; Cryogenics **32**(7), p. 623-627; 1992.

[66]: From Material Data Sheets of Plastics International, 7600 Anagram Drive, Eden Prairie, MN 55344, USA, http://www.plasticsintl.com/datasheets/MACOR.pdf; Aug. 18, 2013.

[67]: S. F. Etuk, I. O. Akpabio, E. M. Udoh; ***Comparison of the Thermal Properties of Clay Samples as Potential Walling Material for Naturally Cooled Building Design***; Journal of Environmental Sciences **15**(1), p. 65-68; 2003.

[68]: Frank Bowman; ***Introduction To Bessel Functions***; Dover Publications, Inc., 180 Varick Street, New York, NY, 10014; 1958; Standard Book Number: 486-60462-4.

[69]: G. E. Roberts and H. Kaufman; ***Table of Laplace Transform***; W. B. Sauders Company, Philadelphia and London, USA; 1966. Ryerson library call #: QA 432. R6.

[70]: W. F. Waite, L. Y. Gilbert, W. J. Winters, D. H. Mason; ***Estimating Thermal Diffusivity and Specific Heat from Needle Probe Thermal Conductivity Data****;* Rev. Sci. Instruments; 77, p.044904; 2006.

[71]: Hugh W. Coleman, W. Glenn Steele; ***Experimentation and Uncertainty Analysis for Engineers, 2nd Edition***; John Wiley & Sons, USA; ISBN: 0-471-12146-0; 1999.